

## UC Irvine

### UC Irvine Electronic Theses and Dissertations

#### Title

Developing Strategies for the Synthesis of Low Valent f Element Complexes, Encapsulation of f Elements in 2.2.2-Cryptand, and Examining the Electronic Properties of Lanthanide(II) Complexes Using X-ray Photoelectron Spectroscopy

#### Permalink

<https://escholarship.org/uc/item/0x15c1jn>

#### Author

Huh, Daniel Namhyuk

#### Publication Date

2019

Peer reviewed|Thesis/dissertation

UNIVERSITY OF CALIFORNIA,  
IRVINE

**Developing Strategies for the Synthesis of Low Valent f Element Complexes, Encapsulation  
of f Elements in 2.2.2-Cryptand, and Examining the Electronic Properties of  
Lanthanide(II) Complexes Using X-ray Photoelectron Spectroscopy**

DISSERTATION

submitted in partial satisfaction of the requirements  
for the degree of

DOCTOR OF PHILOSOPHY

in Chemistry

by

Daniel N. Huh

Dissertation Committee:  
Distinguished Professor William J. Evans, Chair  
Professor Andrew S. Borovik  
Associate Professor Jenny Y. Yang

2019

Portions of Chapter 1 © 2018 American Chemical Society  
Portions of Chapter 2 © 2018 American Chemical Society  
Portions of Chapter 3 © 2018 The Royal Society of Chemistry  
Portions of Chapter 4 © 2017 The Royal Society of Chemistry  
Portions of Chapter 5 © 2018 The Royal Society of Chemistry  
Portions of Chapter 6 © 2019 American Chemical Society  
Portions of Chapter 9 © 2019 American Chemical Society  
All other materials © 2019 Daniel N. Huh

## DEDICATION

This dissertation is dedicated to my parents Kathy and James,  
and to my brother, Brian.

Thank you for your love and support.

And to all my friends who taught me that in the end  
that hard work can only be validated if there is someone there with you to celebrate it.

“Don't walk behind me; I may not lead.  
Don't walk in front of me; I may not follow.  
Just walk beside me and be my friend.”  
– Albert Camus

# TABLE OF CONTENTS

	Page
LIST OF FIGURES	v
LIST OF TABLES	xiii
ACKNOWLEDGMENTS	xv
CURRICULUM VITAE	xvii
ABSTRACT OF THE DISSERTATION	xxiii
INTRODUCTION	1
CHAPTER 1: Utility of Lithium in Rare-Earth Metal Reduction Reactions to Form Non-traditional Ln(II) Complexes and Unusual [Li(2.2.2-cryptand)] <sup>1+</sup> Cations	13
CHAPTER 2: Chelate-Free Synthesis of the U(II) Complex, [(C <sub>5</sub> H <sub>3</sub> (SiMe <sub>3</sub> ) <sub>2</sub> ) <sub>3</sub> U] <sup>1-</sup> , using Li and Cs Reductants and Comparative Studies of La(II) and Ce(II) Analogs	40
CHAPTER 3: Isolation of Reactive Ln(II) Complexes with C <sub>5</sub> H <sub>4</sub> Me (Cp <sup>Me</sup> ) Ligands Using Inverse Sandwich Counteranions: Synthesis and Structure of [(18-crown-6)K(μ-Cp <sup>Me</sup> )K(18-crown-6)][CpMe <sub>3</sub> Ln <sup>II</sup> ] (Ln = Tb, Ho)	60
CHAPTER 4: Synthesis of Rare-Earth-Metal-in-Cryptand Dications, [Ln(2.2.2-cryptand)] <sup>2+</sup> , from Sm(II), Eu(II), and Yb(II) Silyl Metallocenes (C <sub>5</sub> H <sub>4</sub> SiMe <sub>3</sub> ) <sub>2</sub> Ln(THF) <sub>2</sub>	77
CHAPTER 5: Synthesis of Uranium-in-Cryptand Complexes	93
CHAPTER 6: Facile Encapsulation of Ln(II) Ions into Cryptate Complexes from LnI <sub>2</sub> (THF) <sub>2</sub> Precursors (Ln = Sm, Eu, Yb)	108
CHAPTER 7: Isolation and Stabilization of Complexes of Ln(II) Ions in 2.2.2-Cryptand (Ln = Nd, Sm)	126
CHAPTER 8: Synthesis and Electrochemical Analysis of Complexes of U(III) Encapsulated in 2.2.2-Cryptand in Acetonitrile and Dimethylformamide	140

CHAPTER 9: Isolation of a Square Planar Th(III) Complex: Synthesis and Structure of $[\text{Th}(\text{OC}_6\text{H}_2^t\text{Bu}_{2-2,6-\text{Me}-4})_4]^{1-}$	154
CHAPTER 10: Exploring $4f^{n+1}$ vs $4f^n5d^1$ Electron Configurations for Complexes of Lanthanide(II) Ions Using X-ray Photoelectron Spectroscopy	189
APPENDIX A: Synthesis and Structural Characterization of $\{(\text{C}_5\text{H}_4\text{SiMe}_3)_2\text{Ba}(\text{THF})\}_n$ and Barium-in-2.2.2-Cryptand Complexes	206
APPENDIX B: Synthesis of $\{\text{Cs}(\text{THF})(\text{C}_5\text{H}_4\text{SiMe}_3)_3\text{Yb}\}_n$	212
APPENDIX C: Synthesis of $(\text{C}_5\text{Me}_5)_2\text{Yb}(2.2.2\text{-cryptand})$ and $[\text{Sm}_2(2.2.2\text{-cryptand})_2(\mu\text{-I})][(\text{C}_5\text{H}_4\text{SiMe}_3)_3\text{Sm}]_3$	214
APPENDIX D: Synthesis of $[\text{Cp}'_2\text{Y}(\mu\text{-OH})]_2$ and $[\text{Li}(\text{Me}_6\text{TREN})][\{\text{N}(\text{SiMe}_3)_2\}_2\text{Y}\{\text{N}(\text{SiMe}_3)_2\text{SiMe}_2\text{CH}_2\}]$	216
APPENDIX E: EPR Spectroscopy of the $(\text{C}_5\text{Me}_4\text{SiMe}_3)_2\text{YCl} + \text{KC}_8$ Reduction Product	220
APPENDIX F: List of Crystal Structures, Cell Parameters, and UCI X-ray Codes	222

## LIST OF FIGURES

		Page
Figure 1.1	ORTEP representation of [Li(crypt)][Cp'3Tb], <b>2-Tb</b> , thermal ellipsoids drawn at the 50% probability level. Hydrogen atoms are omitted for clarity.	16
Figure 1.2	Experimental X-band EPR spectra of [Li(crypt)][Cp'3Y], <b>2-Y</b> , dissolved in THF (10 mM) collected at 298 K (top; mode: perpendicular; $g_{\text{iso}} = 1.991$ ; $A_{\text{iso}} = 36.6$ G; $\nu = 9.817$ GHz; $P = 0.0203$ ; modulation amplitude = 0.902 mT) and 77 K (bottom; mode: perpendicular; $g_{\parallel} = 2.001$ , $g_{\perp} = 1.987$ ; $A_{\parallel} = 36.6$ G, $A_{\perp} = 36.6$ G; $\nu = 9.436$ GHz; $P = 0.0640$ ; modulation amplitude = 0.902 mT) and analyzed using <i>EasySpin</i> .	17
Figure 1.3	Experimental X-band EPR spectra of $[[(\text{Me}_3\text{Si})_2\text{N}]_2(\text{THF})\text{Y}]_2(\mu\text{-}\eta^2\text{:}\eta^2\text{-N}_2)]^{1-}$ in THF collected at 298 K (mode: perpendicular; $g_{\text{iso}} = 2.004$ ; $\nu = 9.817$ GHz; $P = 0.0203$ ; modulation amplitude = 0.902 mT).	20
Figure 1.4	ChemDraw representations of <b>4</b> (left) and <b>5</b> (right) depicting Li in an NO <sub>5</sub> and O <sub>6</sub> coordination environment, respectively.	21
Figure 1.5	Plot of the magnetic susceptibility (left) times temperature ( $\chi_{\text{M}}T$ ) versus temperature (K) for <b>2-Tb</b> (red circles, 0.1 T; pink circles, 0.5 T, black circles, 1 T). Solid black line corresponds to the theoretical room temperature $\chi_{\text{M}}T$ value for a coupled 4f <sup>8</sup> 5d <sup>1</sup> electronic configuration. Magnetic hysteresis measurement (right) of <b>2-Tb</b> at 2 K.	29
Figure 1.6	Plot of the magnetic susceptibility (left) times temperature ( $\chi_{\text{M}}T$ ) versus temperature (K) for <b>2-Dy</b> (green circles, 0.1 T; pink circles, 0.5 T, black circles, 1 T). Solid black line corresponds to the theoretical room temperature $\chi_{\text{M}}T$ value for a coupled 4f <sup>9</sup> 5d <sup>1</sup> electronic configuration. Magnetic hysteresis measurement (right) of <b>2-Dy</b> at 2 K.	29
Figure 1.7	Plot of the magnetic susceptibility (left) times temperature ( $\chi_{\text{M}}T$ ) versus temperature (K) for <b>2-Ho</b> (blue circles, 0.1 T; pink circles, 0.5 T, black circles, 1 T). Solid black line corresponds to the theoretical room temperature $\chi_{\text{M}}T$ value for a coupled 4f <sup>10</sup> 5d <sup>1</sup> electronic configuration. Magnetic hysteresis measurement (right) of <b>2-Ho</b> at 2 K.	30
Figure 2.1	ORTEP representation of [Li(THF) <sub>4</sub> ][Cp'' <sub>3</sub> La], <b>6-La</b> , with thermal ellipsoids drawn at the 50% probability level. Hydrogen atoms were omitted for clarity.	42

Figure 2.2	Experimental X-band EPR spectra of $[\text{Li}(\text{THF})_4][\text{Cp}^{\prime\prime}_3\text{La}]$ , <b>6-La</b> , in THF collected at 298 K (mode: perpendicular; $g_{\text{ave}} = 1.97$ ; $A_{\text{ave}} = 133.7$ G; $\nu = 9.817$ GHz; $P = 0.0203$ ; modulation amplitude = 0.902 mT).	43
Figure 2.3	UV-Vis spectrum of ~5 mM <b>6-La</b> (red) and <b>6-Ce</b> (blue) in THF.	43
Figure 2.4	ORTEP representation of $[\text{Li}(\text{THF})_4][\text{Cp}^{\prime\prime}_3\text{U}]$ , <b>6-U</b> , with thermal ellipsoids drawn at the 50% probability level. Hydrogen atoms were omitted for clarity.	45
Figure 2.5	ORTEP representation of $[\text{Cp}^{\prime\prime}\text{U}(\mu\text{-Cp}^{\prime\prime})_2\text{Cs}(\text{THF})_2]_n$ , <b>7-U</b> thermal ellipsoids drawn at the 50% probability level. Hydrogen atoms were omitted for clarity.	47
Figure 3.1	ORTEP representation of $[(18\text{-c-}6)\text{K}(\mu\text{-Cp}^{\text{Me}})\text{K}(18\text{-c-}6)][\text{Cp}^{\text{Me}}_3\text{Ho}]$ , <b>9-Ho</b> , with thermal ellipsoids drawn at the 50% probability level. Hydrogen atoms were omitted for clarity.	62
Figure 3.2	UV-visible spectra of <b>9-Ho</b> (solid) and <b>9-Er</b> (dashed) decomposition products.	63
Figure 3.3	UV-visible spectrum of <b>9-Tb</b> in THF; $\lambda_{\text{max}}$ , nm: 458, 481, 660 nm.	64
Figure 3.4	Comparison of the $[(18\text{-c-}6)\text{K}(\mu\text{-Cp}^{\text{Me}})\text{K}(18\text{-c-}6)]^{1+}$ cation in <b>9-Tb</b> (left) and $[(18\text{-c-}6)\text{K}(\mu\text{-Cp}^{\prime})\text{K}(18\text{-c-}6)]^{1+}$ in $[(18\text{-c-}6)\text{K}(\mu\text{-Cp}^{\prime})\text{K}(18\text{-c-}6)][\text{Cp}^{\prime}_3\text{Tb}]$ (right).	66
Figure 3.5	Connectivity only ORTEP representation of $[\text{K}(2.2.2\text{-cryptand})][\text{Cp}^{\text{Me}}_3\text{Dy}]$ , <b>10-Dy</b> .	67
Figure 3.6	UV-visible spectrum of a ~10 mM solution of $[\text{K}(\text{crypt})][\text{Cp}^{\text{Me}}_3\text{Dy}]$ , <b>10-Dy</b> (solid) and $[\text{K}(\text{crypt})][\text{Cp}^{\prime}_3\text{Dy}]^{25}$ (dashed) in THF.	68
Figure 4.1	ORTEP representation of $[\text{Sm}(\text{C}_{16}\text{H}_{32}\text{N}_2\text{O}_6\text{-}\kappa^2\text{O}^{\prime})\text{SmCp}^{\prime\prime}_2]$ , <b>11-Sm</b> , with the thermal ellipsoid plot drawn at 30% probability level. Hydrogen atoms are omitted for clarity.	78
Figure 4.2	ORTEP representation of $[\text{Eu}(\text{crypt})(\text{THF})][\text{Cp}^{\prime}_3\text{Eu}]_2$ , <b>12-Eu</b> thermal ellipsoids drawn at the 50% probability level. Hydrogen atoms are omitted for clarity. Distances in Å: Eu5–O1 2.656(4), Eu5–O2 2.657(4), Eu5–O3 2.632(4), Eu5–O4 2.620(3), Eu5–O5 2.657(4), Eu5–O6 2.682(4), Eu5–O7 2.567(3), Eu5–N1 2.855(5), Eu5–N2 2.871(5), average Eu–Cp' centroid 2.62.	81



Figure 4.3	ORTEP representation of [Yb(crypt)][Cp'3Yb]2, <b>13-Yb</b> thermal ellipsoids drawn at the 50% probability level. Hydrogen atoms are omitted for clarity. Distances in Å: Yb3–O1 2.508(8), Yb3–O2 2.496(6), Yb3–O3 2.444(7), Yb3–O4 2.539(5), Yb3–O5 2.506(6), Yb3–O6 2.493(6), Yb3–N1 2.634(15), Yb3–N2 2.613(10), average Yb– Cp' centroid 2.50.	83
Figure 5.1	ORTEP representation of [U(crypt)I2]I, <b>14-U</b> , with thermal ellipsoids drawn at the 50% probability level. Hydrogen atoms and three molecules of CH2Cl2 were omitted for clarity.	95
Figure 5.2	ORTEP representation of [La(crypt)Cl2]Cl, <b>15-La</b> , with thermal ellipsoids drawn at the 50% probability level. Outer sphere chloride is disordered over two positions. Hydrogen atoms were omitted for clarity.	96
Figure 5.3	ORTEP representation of [U(crypt)I(OH2)][I]2, <b>16-U</b> , with thermal ellipsoids drawn at the 50% probability level. Hydrogen atoms except those of H2O were omitted for clarity.	96
Figure 5.4	ORTEP representation of [U(crypt)I(OH2)][I][BPh4], <b>17-U</b> , with thermal ellipsoids drawn at the 50% probability level. Hydrogens except those of H2O were omitted for clarity.	97
Figure 5.5	NIR/UV-Vis of 5mM [U(crypt)I2]I, <b>14-U</b> , in DMF. Full spectrum (blue, left axis) and 20x zoom of full spectrum (red, right axis).	101
Figure 6.1	ORTEP representation of [Eu(crypt)(DMF)2][I]2, <b>18-Eu</b> , with thermal ellipsoids drawn at the 50% probability level. Hydrogen atoms were omitted for clarity. <b>18-Sm</b> is isomorphous with <b>18-Eu</b> .	110
Figure 6.2	ORTEP representation of [Yb(crypt)(DMF)][I]2, <b>19-Yb</b> , with thermal ellipsoids drawn at the 50% probability level. Hydrogen atoms were omitted for clarity.	112
Figure 6.3	ORTEP representation of [Sm(crypt)(DMF)2][BPh4]2, <b>20-Sm</b> , with thermal ellipsoids drawn at the 50% probability level and dashed lines represent hydrogen bonding. Hydrogen atoms, except for H19 and H22, were omitted for clarity.	113
Figure 6.4	UV-visible spectrum of [Sm(crypt)(DMF)][I]2, <b>18-Sm</b> , in DMF (5 mM).	118

Figure 6.5	UV-visible spectrum of [Eu(crypt)(DMF)][I] <sub>2</sub> , <b>18-Eu</b> , in DMF (5 mM).	118
Figure 6.6	UV-visible spectrum of [Yb(crypt)(DMF)][I] <sub>2</sub> , <b>19-Yb</b> , in DMF (10 mM).	118
Figure 6.7	NMR (500 MHz, DMF- <i>d</i> <sub>7</sub> ) spectra of 2.2.2-cryptand, [Sm(crypt)(DMF) <sub>2</sub> ][I] <sub>2</sub> , <b>18-Sm</b> , [Eu(crypt)(DMF)][I] <sub>2</sub> , <b>18-Eu</b> , and [Yb(crypt)(DMF)][I] <sub>2</sub> , <b>19-Yb</b> .	119
Figure 6.8	Variable temperature NMR (500 MHz, DMF- <i>d</i> <sub>7</sub> ) of [Yb(crypt)(DMF)][I] <sub>2</sub> , <b>19-Yb</b> , at temperatures of 298 K (bottom), 333 K (middle), and 373K (top) zoomed at OCH <sub>2</sub> CH <sub>2</sub> O and NCH <sub>2</sub> CH <sub>2</sub> O 2.2.2-cryptand resonances.	119
Figure 7.1	ORTEP representation of [Dy(crypt)(OTf)][OTf] <sub>2</sub> , <b>22-Dy</b> , with thermal ellipsoids drawn at the 50% probability level. Hydrogen atoms and disorder were omitted for clarity.	128
Figure 7.2	ORTEP representation of [Nd(crypt)(DMF) <sub>2</sub> ][OTf] <sub>3</sub> , <b>23-Nd</b> , with thermal ellipsoids drawn at the 50% probability level. Hydrogen atoms were omitted for clarity.	129
Figure 7.3	ORTEP representation of [Nd(crypt)(OTf) <sub>2</sub> ], <b>25-Nd</b> , with thermal ellipsoids drawn at the 50% probability level. Hydrogen atoms were omitted for clarity.	131
Figure 7.4	HOMO of [Nd(crypt)(OTf) <sub>2</sub> ], <b>25-Nd</b> , with 4f <sup>4</sup> electron configuration. DFT calculations were performed by Saswata Roy in the laboratory of Prof. Filipp Furche.	132
Figure 7.5	Simulated UV-Vis spectrum using TD-DFT and TPSSh functional. DFT calculations were performed by Saswata Roy in the laboratory of Prof. Filipp Furche.	133
Figure 8.1	ORTEP representation of [U(crypt)(MeCN)I][I] <sub>2</sub> , <b>26-U</b> , with thermal ellipsoids drawn at the 50% probability level. Hydrogen atoms were omitted for clarity.	142
Figure 8.2	ORTEP representation of [U(crypt)(OH <sub>2</sub> ) <sub>2</sub> ][I] <sub>3</sub> , <b>27-U</b> , with thermal ellipsoids drawn at the 50% probability level. Hydrogen atoms were omitted for clarity except for water.	143
Figure 8.3	ORTEP representation of [U(crypt)(DMF)(OH <sub>2</sub> )][I] <sub>3</sub> , <b>28-U</b> , and thermal ellipsoids drawn at the 50% probability level. Hydrogen atoms were omitted for clarity except for water.	143

Figure 8.4	Comparison of [U(crypt)I <sub>2</sub> ]I in DMF and tetrabutylammonium iodide (TBAI) showing that the two oxidations (*) arise from free iodide in solution (left). Variable scan rates of [U(crypt)I <sub>2</sub> ]I in DMF (500 mM TBAI) of the first oxidation event U(III) to U(IV) (E <sub>pa1</sub> ) from 10 to 500 mV/s scan rates (right).	144
Figure 8.5	DMF solution of [U(crypt)I <sub>2</sub> ]I titrated with water (full spectrum, top; zoom, inset) scanning anodically. The oxidations centered at E <sub>pa1</sub> = -0.510 V and E <sub>pa2</sub> = 0.880 V vs. Fc <sup>+0</sup> both disappear as more equivalents are added, indicating a reaction with water (either binding or reduction).	145
Figure 8.6	Variable scan rates of [U(crypt)I <sub>2</sub> ]I in MeCN scanning cathodically. Reduction and oxidation are observed at E <sub>pc1</sub> = -1.78 V and E <sub>pa1</sub> = -1.12 V (vs. Fc <sup>+/0</sup> ). Asterisks denote iodide oxidation.	146
Figure 8.7	Variable scan rates of [U(crypt)I <sub>2</sub> ]I and [CoCp <sub>2</sub> ][PF <sub>6</sub> ] in MeCN scanning cathodically. U(III)/U(II) E <sub>1/2</sub> = -1.85 V vs Fc <sup>+/0</sup> and Co(III)/Co(II) E <sub>1/2</sub> = -1.33 V vs Fc <sup>+/0</sup> .	147
Figure 9.1	ORTEP representation of [K(THF) <sub>5</sub> (Et <sub>2</sub> O)][Th(OAr') <sub>4</sub> ], <b>30-Th</b> , with side-on view and thermal ellipsoids drawn at the 50% probability level. Hydrogen atoms were omitted for clarity.	156
Figure 9.2	ORTEP representation of [Li(THF) <sub>4</sub> ][Th(OAr') <sub>4</sub> ], <b>31-Th</b> , with top view and thermal ellipsoids drawn at the 50% probability level. Hydrogen atoms were omitted for clarity.	156
Figure 9.3	Experimental X-band EPR spectra of [Th(OAr') <sub>4</sub> ] <sup>1-</sup> dissolved in THF (10 mM) collected at 298 K (left; mode: perpendicular; g <sub>iso</sub> = 1.84; ν = 9.817 GHz; P = 0.0202; modulation amplitude = 0.902 mT) and 77 K (right; mode: perpendicular; g <sub>  </sub> = 1.99, g <sub>⊥</sub> = 1.79; ν = 9.672 GHz; P = 0.0203; modulation amplitude = 0.902 mT) and analyzed using EasySpin.	158
Figure 9.4	HOMO of [Th(OAr') <sub>4</sub> ] <sup>1-</sup> plotted with an isovalue = ±0.05.	161
Figure 9.5	Example of antibonding orbitals of [Th(OAr') <sub>4</sub> ] <sup>1-</sup> (isovalue = ±0.05) involving the π orbitals on oxygen and the d <sub>xy</sub> orbital on thorium.	161

Figure 9.6	Simplified frontier molecular orbital diagram of $[\text{Th}(\text{OAr}')_4]^{1-}$ showing $\alpha$ spin orbitals with strong Th character. Red and blue levels represent computed energies of predominantly d and f orbitals, respectively; numerical values in eV are given in parentheses. The dashed blue line is the Fermi energy. Atomic orbital designations are reported in brackets whenever possible.	162
Figure 9.7	Observed UV-visible spectrum of $[\text{K}(\text{THF})_5(\text{Et}_2\text{O})][\text{Th}(\text{OAr}')_4]$ , <b>30-Th</b> , in THF (700 $\mu\text{M}$ ) (yellow) and simulated UV-visible spectra of $[\text{Th}(\text{OAr}')_4]^{1-}$ (purple) with the excitations shown as vertical lines. Calculated extinction coefficients are scaled down by a factor of 1.5.	163
Figure 9.8	Rydberg orbital 71 a (2.73 eV) plotted with isovalue = $\pm 0.02$ . The band located at 321 nm in the UV-visible spectrum results predominately from a transition out of the dz <sup>2</sup> HOMO into 71 a.	164
Figure 9.9	Space filling model for the $C_4$ structure demonstrating the eclipsed conformation of the tert-butyl groups on the aryl rings. None of the methyls are parallel to the C(ipso)-O bond.	167
Figure 9.10	Space filling model for the $S_4$ structure demonstrating the staggered conformation of the tert-butyl groups on the aryl rings. One of the methyls is parallel the C(ipso)-O bond.	167
Figure 9.11	IR spectra of $[\text{K}(\text{THF})_5(\text{Et}_2\text{O})][\text{Th}(\text{OAr}')_4]$ , <b>2</b> (top), $[\text{Li}(\text{THF})_4][\text{Th}(\text{OAr}')_4]$ , <b>3</b> (middle), and $[\text{K}(\text{crypt})][\text{Th}(\text{OAr}')_4]$ (bottom).	171
Figure 9.12	Experimental X-band EPR spectra of $[\text{Li}(\text{THF})_4][\text{Th}(\text{OAr}')_4]$ , <b>31-Th</b> , dissolved in THF (5 mM) collected at 298 K (top; mode: perpendicular; $g_{\text{iso}} = 1.84$ ; $\nu = 9.819$ GHz; $P = 0.0604$ ; modulation amplitude = 0.902 mT) and 77 K (bottom; mode: perpendicular; $g_{\parallel} = 1.99$ , $g_{\perp} = 1.79$ ; $\nu = 9.622$ GHz; $P = 0.0202$ ; modulation amplitude = 0.902 mT) and analysed using EasySpin.	172
Figure 9.13	Experimental X-band EPR spectra of $[\text{K}(\text{crypt})][\text{Th}(\text{OAr}')_4]$ dissolved in THF (5 mM) collected at 298 K (top; mode: perpendicular; $g_{\text{iso}} = 1.84$ ; $\nu = 9.796$ GHz; $P = 2.15$ mW; modulation amplitude = 0.902 mT) and 77 K (bottom; mode: perpendicular; $g_{\parallel} = 1.99$ , $g_{\perp} = 1.79$ ; $\nu = 9.434$ GHz; $P = 2.155$ mW; modulation amplitude = 0.902 mT) and analysed using EasySpin.	173
Figure 9.14	NMR (500 MHz, THF- $d_8$ ) spectra of $\text{K}[\text{Th}(\text{OAr}')_4]$ (bottom), $\text{Th}(\text{OAr}')_4$ (middle) and $\text{LiOAr}' \cdot \text{Et}_2\text{O}$ (top) at 298 K.	174

Figure 9.15	Structure of optimized anion of <b>31-Th</b> in $C_4$ symmetry.	178
Figure 9.16	Structure of optimized neutral $\text{Th}(\text{OAr}')_4$ in $S_4$ symmetry.	178
Figure 9.17	Spin density of $[\text{Th}(\text{OAr}')_4]^{1-}$ plotted with an isovalue $=\pm 0.005$	179
Figure 9.18	The simulated absorption spectrum using TD-TPSSH single- $\zeta$ (purple), TD-PBE0 single- $\zeta$ (green), and TD-PBE0 SV(P) (blue) functionals compared to the experimentally observed spectrum (orange).	179
Figure 10.1	Ball-and-stick model of single-crystal X-ray structure of $[\text{K}(\text{crypt})][(\text{C}_5\text{H}_4\text{SiMe}_3)_3\text{Ln}]$ .	190
Figure 10.2	Sm 4d XPS region of $\text{Cp}'_3\text{Sm}^{\text{III}}$ (left) and $[\text{K}(\text{crypt})][\text{Cp}'_3\text{Sm}^{\text{II}}]$ (right).	193
Figure 10.3	C 1s XPS region of $\text{Cp}'_3\text{Sm}^{\text{III}}$ (left) and $[\text{K}(\text{crypt})][\text{Cp}'_3\text{Sm}^{\text{II}}]$ (right).	194
Figure 10.4	Eu 4d XPS region of $\text{Cp}'_3\text{Eu}^{\text{III}}$ (left) and $[\text{K}(\text{crypt})][\text{Cp}'_3\text{Eu}^{\text{II}}]$ (right).	194
Figure 10.5	C 1s XPS region of $\text{Cp}'_3\text{Eu}^{\text{III}}$ (left) and $[\text{K}(\text{crypt})][\text{Cp}'_3\text{Eu}^{\text{II}}]$ (right).	196
Figure 10.6	Gd 4d XPS region of $\text{Cp}'_3\text{Gd}^{\text{III}}$ (left) and $[\text{K}(\text{crypt})][\text{Cp}'_3\text{Gd}^{\text{II}}]$ (right).	197
Figure 10.7	C 1s XPS region of $\text{Cp}'_3\text{Gd}^{\text{III}}$ (left) and $[\text{K}(\text{crypt})][\text{Cp}'_3\text{Gd}^{\text{II}}]$ (right).	197
Figure 10.8	Valence XPS region of $\text{Cp}'_3\text{Gd}^{\text{III}}$ (left) and $[\text{K}(\text{crypt})][\text{Cp}'_3\text{Gd}^{\text{II}}]$ (right).	198
Figure 10.9	Valence XPS region of $\text{KCp}'$ (left) and 2.2.2-cryptand (right).	198
Figure 10.10	Tb 4d XPS region of $\text{Cp}'_3\text{Tb}^{\text{III}}$ (left) and $[\text{K}(\text{crypt})][\text{Cp}'_3\text{Tb}^{\text{II}}]$ (right).	199
Figure 10.11	C 1s XPS region of $\text{Cp}'_3\text{Tb}^{\text{III}}$ (left) and $[\text{K}(\text{crypt})][\text{Cp}'_3\text{Tb}^{\text{II}}]$ (right).	200
Figure 10.12	The density of states in the valence region for the Gd(III) (left) and the Gd(II) (right) complexes broadened using gaussian functions with a half width at half maximum of 0.5 eV.	201
Figure 10.13	The density of states in the valence region for the Eu(III) (left) and the Eu(II) (right) complexes broadened using gaussian functions with a half width at half maximum of 0.5 eV.	202
Figure A.1	ORTEP representation of extended structure of $\{\text{Cp}'_2\text{Ba}(\text{THF})\}_n$ , with thermal ellipsoids drawn at the 50% probability level. Hydrogen atoms were omitted for clarity.	207

Figure A.2	ORTEP representation of [Ba(crypt)(DMF) <sub>2</sub> ][I] <sub>2</sub> , with thermal ellipsoids drawn at the 50% probability level. Hydrogen atoms were omitted for clarity.	207
Figure A.3	ORTEP representation of [Ba(crypt)(OTf) <sub>2</sub> ], with thermal ellipsoids drawn at the 50% probability level. Hydrogen atoms were omitted for clarity.	208
Figure B.1	ORTEP representation of {Cs(THF)Cp' <sub>3</sub> Yb} <sub>n</sub> , with thermal ellipsoids drawn at the 50% probability level. Hydrogen atoms were omitted for clarity.	212
Figure C.1	Connectivity structure of Cp* <sub>2</sub> Yb(crypt) drawn at the 50% probability level. Hydrogens have been omitted for clarity.	214
Figure C.2	Connectivity structure of [Sm <sub>2</sub> (crypt) <sub>2</sub> (μ-I)][Cp' <sub>3</sub> Sm] <sub>3</sub> drawn at the 50% probability level. Hydrogens have been omitted for clarity.	215
Figure D.1	ORTEP representation of [Cp' <sub>2</sub> Y(μ-OH)] <sub>2</sub> , thermal ellipsoids drawn at the 50% probability level. Hydrogen atoms, except for O–H hydrogens, were omitted for clarity.	216
Figure D.2	ORTEP representation of [Li(Me <sub>6</sub> TREN)][{N(SiMe <sub>3</sub> ) <sub>2</sub> } <sub>2</sub> Y{N(SiMe <sub>3</sub> ) <sub>2</sub> SiMe <sub>2</sub> CH <sub>2</sub> }], thermal ellipsoids drawn at the 50% probability level. Hydrogen atoms, except for O–H hydrogens, were omitted for clarity.	217
Figure E.1	Room temperature EPR spectrum of Cp <sup>N</sup> <sub>2</sub> YCl + KC <sub>8</sub> reduction product in toluene.	221

## LIST OF TABLES

		Page
Table 1.1	[K(crypt)][Cp'3Ln], <b>1-Ln</b> versus [Li(crypt)][Cp'3Ln], <b>2-Ln</b> comparisons of selected bond distances (Å) and bond angles (°).	18
Table 1.2	Li–O and Li–N bond distance ranges of complexes containing [Li(crypt)] <sup>1+</sup> .	21
Table 1.3	Experimental and predicted (as described in text) $\chi_M T$ products at 298 K for <b>1-Ln</b> and <b>2-Ln</b> .	23
Table 1.4	Listing of all the Li–O and Li–N distances (Å) for the [Li(crypt)][Cp'3Ln] ( <b>2-Ln</b> ), [Li(crypt)][Cp'4Tb] ( <b>4</b> ), and [Li(crypt)][(Cp'3Ho) <sub>2</sub> ( <i>u</i> -H)] ( <b>5</b> ) complexes and all currently known complexes containing [Li(crypt)] <sup>1+</sup> cations. Longer distances are highlighted in gray.	35
Table 2.1	M–centroid bond distance averages and ranges of Cp'' <sub>3</sub> M and (Cp'' <sub>3</sub> M) <sup>1-</sup> (M = La, Ce, U).	44
Table 3.1	Ln(II)–(ring centroid) distances (Å) in the [(C <sub>5</sub> H <sub>4</sub> R) <sub>3</sub> Ln] <sup>1-</sup> anions (R = Me, SiMe <sub>3</sub> ).	66
Table 5.1	Summary of bond distance ranges (Å) of compounds [U(crypt)I <sub>2</sub> ]I <b>14-U</b> , [La(crypt)Cl <sub>2</sub> ]Cl <b>15-La</b> , [U(crypt)I(OH <sub>2</sub> )] [I] <sub>2</sub> <b>16-U</b> , [U(crypt)I(OH <sub>2</sub> )] [I] [BPh <sub>4</sub> ] <b>17-U</b> , and [La(crypt)Cl(OH <sub>2</sub> )] [Cl] <sub>2</sub> . <sup>9</sup>	98
Table 6.1	Ln(II)–O(crypt) and Ln(II)–N(crypt) bond distance ranges (Å).	110
Table 8.1	U(III)-in-crypt metrical parameters of <b>26-U</b> , <b>27-U</b> , <b>28-U</b> , [U(crypt)I <sub>2</sub> ]I <b>14-U</b> , [U(crypt)I(OH <sub>2</sub> )] [I] <sub>2</sub> <b>16-U</b> , and [U(crypt)(OH <sub>2</sub> )I] [I] [BPh <sub>4</sub> ] <b>17-U</b> .	142
Table 9.1	Selected bond distances (Å) and angles (°) of [K(THF) <sub>5</sub> (Et <sub>2</sub> O)][Th <sup>III</sup> (OAr') <sub>4</sub> ], <b>30-Th</b> , [Li(THF) <sub>4</sub> ][Th <sup>III</sup> (OAr') <sub>4</sub> ], <b>31-Th</b> , [Th <sup>IV</sup> (OC <sub>6</sub> H <sub>3</sub> <sup>t</sup> Bu <sub>2-2,6</sub> ) <sub>4</sub> ], <b>32-Th</b> , and [Th <sup>IV</sup> (OC <sub>6</sub> H <sub>3</sub> Ph <sub>2-2,6</sub> ) <sub>4</sub> ], <b>33-Th</b> .	157
Table 9.2	Room temperature EPR $g_{\text{iso}}$ values and 77 K $g_{\parallel}$ and $g_{\perp}$ values of Th(III) complexes.	159

Table 9.3	Computed relative energies (kcal/mol) of the $S_4$ -symmetric minimum of <b>29-Th</b> , $C_4$ -symmetric minimum of the neutral species from <b>31-Th</b> and the $C_4$ - and $S_4$ -symmetric minima of anion of <b>31-Th</b> .	159
Table 9.4	Selected electronic excitations of $[\text{Th}(\text{OAr}')_4]^{1-}$ using PBE0 functional in the $C_2$ symmetry. Oscillator strength are in length representation.	164
Table 9.5	Select electronic excitations (with oscillator strengths larger than 0.01) of $[\text{Th}(\text{OAr}')_4]^{1-}$ using PBE0 functional in the $C_4$ symmetry using single- $\zeta$ basis sets on the ligands. Oscillator strength are in length representation.	165
Table 9.6	Select electronic excitations (with oscillator strengths larger than 0.01) of $[\text{Th}(\text{OAr}')_4]^{1-}$ using PBE0 functional in the $C_4$ symmetry using def2-SV(P) basis sets on the ligands. Oscillator strength are in length representation.	165
Table 9.7	d-Orbital splitting in square planar structure for $[\text{PtCl}_4]^{2-}$ using TPSS density functional and triple- $\zeta$ bases.	176
Table 9.8	d-Orbital splitting in square planar structure for $[\text{PdCl}_4]^{2-}$ using TPSS density functional and triple- $\zeta$ bases	177
Table 9.9	Table of bond distances and angles for $[\text{K}(\text{THF})_5(\text{Et}_2\text{O})][\text{Th}(\text{OAr}')_4]$ , <b>30-Th</b> , and $[\text{Li}(\text{THF})_4][\text{Th}(\text{OAr}')_4]$ , <b>31-Th</b> .	180
Table 9.10	Selected C...C ( $C\text{Me}_3$ ) distances of $[\text{K}(\text{THF})_5(\text{Et}_2\text{O})][\text{Th}(\text{OAr}')_4]$ , <b>30-Th</b> , and $[\text{Li}(\text{THF})_4][\text{Th}(\text{OAr}')_4]$ , <b>31-Th</b> .	181
Table 9.11	Selected H...H distances of $[\text{K}(\text{THF})_5(\text{Et}_2\text{O})][\text{Th}(\text{OAr}')_4]$ , <b>30-Th</b> , and $[\text{Li}(\text{THF})_4][\text{Th}(\text{OAr}')_4]$ , <b>31-Th</b> .	181
Table 10.1	Summary of binding energies (eV) of measured samples $\text{Cp}'_3\text{Ln}$ and $[\text{K}(\text{crypt})][\text{Cp}'_3\text{Ln}]$ ( $\text{Ln} = \text{Sm}, \text{Eu}, \text{Gd}, \text{Tb}$ ).	192
Table 10.2	Calculated binding energies (eV) of $\text{Cp}'_3\text{Gd}$ and $[\text{Cp}'_3\text{Gd}]^{1-}$ .	201



## ACKNOWLEDGEMENTS

My time spent at the University of California, Irvine has enriched my life in unimaginable ways. The completion of my doctoral studies is the embodiment of every individual who had crossed my path and contributed to my personal and intellectual growth. Obtaining a doctoral degree is by no means an individual feat, but an anthology of the many meaningful stories of collaborative pursuits of knowledge and the communal triumph for pushing the boundaries of our scientific understanding. I would like to acknowledge those who have contributed to my growth toward becoming an independent researcher during my time here.

First and foremost, I would like to thank my research mentor and friend, Bill Evans. He has taught me to approach science with gumption and conviction which in turn has generated years of exciting chemistry and fruitful collaborations in Irvine and all around the world. His teaching moments in his office, during group meetings, and manuscript writing have left a lasting impression on me which I will use as a guide during my own pursuits for knowledge in my independent career.

I would like to also express my gratitude to my committee members Andy Borovik and Jenny Yang. Your lectures, advice, and support throughout my PhD studies have guided me through my research and will remain with me as I transition into my independent career as a research chemist.

I would like to thank Joe Ziller for mentoring me during my X-ray Crystallography Fellowship, encouraging me throughout my PhD and the years of friendship. Many of my most exciting results and great laughs were had in RH 513.

To my collaborators Filipp Furche, Saswata Roy, Sree Ganesh Balasubramani, and Guo Chen, thank you for the years of fruitful research and intellectually stimulating conversations. You have shown me how powerful theoretical chemistry can be when complimented with experimental data.

Thank you to the Evans group members Ryan Langeslay, Cory Windorff, Chad Palumbo, David Woen, Monica Boshart, Megan Dumas, Sam Moehring, Austin Ryan, Tener Jenkins, Jessica White, Justin Wedal, Sierra Ciccone, Amanda Chung, Katie Harriman, Mitch Nascimento, Nick Rightmire, Feng Pan, and Song Xu. The thousands of hours spent in FRH 2022 pushing the boundaries of f element chemistry has been incredibly exciting. Thank you all for challenging my ideas to help me think deeper about the chemistry. And thank you to my colleagues and friends in the Yang, Borovik, Heyduk, and Green groups for being supportive during my PhD studies.

To my friends Austin Ryan, Jared Bruce, Devon Schatz, Drew Cunningham, Tener Jenkins, Caitlin Hanna, Kevin Garity, Jeff Barlow, Krista Fruehauf, Megan Newcomb, Jasper Liedtke, and Chris Woods, thank you for the unforgettable memories, adventures, and friendship over the years. To my friends, Emilio Mejia, Ian Mahaney, and Hannah Nicholson, thank you for making San Diego the home away from home and the amazing adventures we've taken around the world.

I would like to give special thanks to my undergraduate research mentor Chris Daley. He was the first person to inspire me to pursue a PhD in chemistry and many of the above-mentioned thanks would not have happened without his continuous support and encouragement. I would also like to thank my master's graduate research mentor Lisa Szczepura for teaching me to be determined in my research and giving me the synthetic hands to create difficult complexes.

To my parents Kathy and James and my brother Brian, thank you for your unconditional love and support you've shown me my whole life. Hearing your words of support has always warmed me and encouraged me to push onwards even when there were seemingly insurmountable obstacles. My accomplishments are very much your accomplishments.

D. N. H.

# CURRICULUM VITAE

**Daniel N. Huh**

## EDUCATION

**Ph.D. University of California: Irvine, 2019**

Principal Investigator: Prof. William J. Evans

**M.S. Illinois State University, 2015**

Principal Investigator: Prof. Lisa F. Szczepura

**B.A. University of San Diego, 2013**

Principal Investigator: Prof. Christopher J.A. Daley

## PUBLICATIONS

1. **Huh, D. N.**; Gibbons, J. B.; Haywood, R. S.; Moore, C. E.; Rheingold, A. L.; Ferguson, M. J.; Daley, C. J. A. Metal-amidato Complexes: Synthesis, Characterization, and Reactivity of a Diamidato-bis(phosphine) Nickel (II) Complex. *Inorg. Chim. Acta*, **2014**, *434*, 209-297.
2. Durham, J. L.; Wilson, W. B.; **Huh, D. N.**; McDonald, R.; Szczepura, L. F. Organometallic Rhenium(III) Chalcogenide Clusters: Coordination of *N*-Heterocyclic Carbenes. *Chem. Commun.* **2015**, *51*, 10536.
3. **Huh, D. N.**; Czer, E. T.; Cordova, K. E.; Moore, C. E.; Rheingold, A. L.; Daley, C. J. A. Metal Nitrosyl Chemistry: Interesting Nitrosylation of Ligand Framework in a Diamidato-bis(phosphine) Ruthenium(II) Complex. *Inorg. Chim. Acta* **2016**, *450*, 236-242.
4. **Huh, D. N.**; Kotyk, C. M.; Gembicky, M.; Rheingold, A. L.; Ziller, J. W.; Evans, W. J. Synthesis of Rare-Earth-Metal-in-Cryptand Dications, [Ln(2.2.2-cryptand)]<sup>2+</sup>, from Sm<sup>2+</sup>, Eu<sup>2+</sup>, and Yb<sup>2+</sup> Silyl Metallocenes (C<sub>5</sub>H<sub>4</sub>SiMe<sub>3</sub>)<sub>2</sub>Ln(THF)<sub>2</sub>. *Chem. Commun.* **2017**, *53*, 8664-8666.
5. **Huh, D. N.**; Darago, L. E.; Ziller, J. W.; Evans, W. J. Utility of Lithium in Rare-Earth Metal Reduction Reactions to Form Nontraditional Ln<sup>2+</sup> Complexes and Unusual [Li(2.2.2-cryptand)]<sup>1+</sup> Cations. *Inorg. Chem.*, **2018**, *57*, 2096-2102.

6. Woen, D. H.; **Huh, D. N.**; Ziller, J. W.; Evans, W. J. Reactivity of Ln(II) Complexes Supported by  $(C_5H_4Me)^{1-}$  Ligands with  $PhSiH_3$  and THF: Isolation of Hydride, Silyl, and Ring-Opened, Bridging Alkoxyalkyl Products. *Organometallics*, **2018**, *37*, 3055-3063.
7. **Huh, D. N.**; Ziller, J. W.; Evans, W. J. Chelate-Free Synthesis of the U(II) Complex,  $[(C_5H_3(SiMe_3)_2)_3U]^{1-}$ , using Li and Cs Reductants and Comparative Studies of La(II) and Ce(II) Analogs. *Inorg. Chem.*, **2018**, *57*, 11809-11814.
8. **Huh, D. N.**; Windorff, C. J.; Ziller, J. W.; Evans, W. J. Synthesis of Uranium-in-Cryptand Complexes. *Chem. Commun.*, **2018**, *54*, 10272-10275.
9. **Huh, D. N.**; Ziller, J. W.; Evans, W. J. Isolation of Reactive Ln(II) Complexes with  $C_5H_4Me$  ( $Cp^{Me}$ ) Ligands Using Inverse Sandwich Counteranions: Synthesis and Structure of  $[(18-crown-6)K(\mu-Cp^{Me})K(18-crown-6)][Cp^{Me}_3Ln^{II}]$  (Ln = Tb, Ho). *Dalton Trans.*, **2018**, *47*, 17285-17290.
10. Ariciu, A-M.; Woen, D. H.; **Huh, D. N.**; Nodarki, L.; Kostopoulos, A. K.; Goodwin, C. A. P.; Chilton, N. F.; McInnes, E. J. L.; Winpenny, R. E. P.; Evans, W. J.; Tuna, F. Engineering electronic structure to prolong relaxation times in molecular qubits by minimising orbital angular momentum, *Nat. Commun.*, **2019**, *10*, 1-8.
11. **Huh, D. N.**; Ziller, J. W.; Evans, W. J. Facile Encapsulation of Ln(II) Ions into Cryptate Complexes from  $LnI_2(THF)_2$  Precursors (Ln = Sm, Eu, Yb). *Inorg. Chem.*, **2019**, *589*, 9613-9617.
12. **Huh, D. N.**; Roy, S.; Ziller, J. W.; Furche, F.; Evans, W. J. Isolation of a Square Planar Th(III) Complex: Synthesis and Structure of  $[Th(OC_6H_2^tBu_{2,6}Me_4)_4]^{1-}$ . *J. Am. Chem. Soc.*, **2019**, *141*, 12458-12463.
13. Windorff, C. J.; Sperling, J. M.; Klamm, B. E.; Goodwin, C. A. P.; **Huh, D. N.**; Gaiser, A. N.; Hobart, D. E.; Kozimor, S. A.; Gaunt, A. J.; Evans, W. J.; Albrecht-Schmitt, T. E. Probing Plutonium Redox Reactivity with Cyclooctatetraene Yields Three Crystallographically-Characterizable Organoplutonium Complexes, *in preparation*.
14. **Huh, D. N.**; Bruce, J. P.; Balasubramani, S.; Ciccone, S. R.; Furche, F.; Evans, W. J.; Hemminger, J. C., Exploring  $4f^{n+1}$  vs  $4f^n5d^1$  Electron Configurations for Complexes of Lanthanide(II) Ions Using X-ray Photoelectron Spectroscopy, *in preparation*.
15. Minasian, S. G.; **Huh, D. N.**; Evans, W. J. X-Ray Absorption C K-edge Spectroscopy of  $[C_5H_4(SiMe_3)_3Ln]$  Complexes, *in preparation*.

16. **Huh, D. N.**; Barlow, J. M.; Yang, J. Y.; Evans, W. J. Stabilization of U(III) to Oxidation and Water by Encapsulation Using 2.2.2-Cryptand, *in preparation*.
17. **Huh, D. N.**; Ciccone, S. R.; Roy, S.; Ziller, J. W.; Furche, F.; Evans, W. J. Isolation and Stabilization of Ln(II) Ions into Cryptate Complexes (Ln = Nd, Sm), *in preparation*.

## ORAL PRESENTATIONS

1. **Huh, D. N.**; Daley, C. J. A.; Moore, C. E.; Rheingold, A. L. Synthesis and Characterization of Synthetic Analogue of the Distal Ni<sup>II</sup> Center of A-Cluster of Acetyl-CoA Synthase/Carbon Monoxide Dehydrogenase. Presented at University of San Diego Research Seminar. San Diego, CA, 12/21/2011.
2. **Huh, D. N.**; Daley, C. J. A.; Moore, C. E.; Rheingold, A. L. Synthesis, Characterization, and Reactivity of Diimine-bis(phosphino) Ruthenium-NO Complexes. Presented at University of California, San Diego Summer Research Conference. La Jolla, CA, 09/16/2012.
3. **Huh, D. N.** Undergraduate Research and Graduate School Opportunities. Presented at Wesleyan University, Illinois. Normal, IL, 03/25/2015.
4. **Huh, D. N.**; Szczepura, L. F. *Synthesis of Hexanuclear Rhenium(III) Clusters Containing N-Heterocyclic Carbenes Using Silver(I) Transmetalation Reagents*. Presented at Illinois State University Research Seminar. Normal, IL, 07/09/2015.
5. **Huh, D. N.**; Ziller, J. W.; Evans, W. J. *Comparison of Li with K and Na in rare-earth metal reduction chemistry: Isolation of [Li(2.2.2-cryptand)]<sup>+</sup> in unique coordination environments*. Presented at the American Chemical Society 253rd National Conference. San Francisco, CA, 04/02/2017.
6. **Huh, D. N.**; Ziller, J. W.; Evans, W. J. *Isolation of Lanthanide Cryptate Complexes by Ligand Rearrangement and Encapsulation*. Presented at the American Chemical Society 255th National Conference. New Orleans, LA, 03/21/18.
7. **Huh, D. N.**; Ziller, J. W.; Evans, W. J. *Isolation of Low Valent f-Element Complexes with Unusual Counteranions*. Presented at the University of Manchester. Manchester, England, 11/16/2018.

8. **Huh, D. N.**; Ziller, J. W.; Evans, W. J. *Importance of Counteractions in Isolating New Crystalline Examples of Complexes of f-Elements in Low Oxidation States*. Presented at the American Chemical Society 257th National Conference. Orlando, FL, 04/04/2019.
9. **Huh, D. N.**; Ziller, J. W.; Evans, W. J. *Synthesis of an unusual square planar Th(III) complex*. Presented at the American Chemical Society 258th National Conference. San Diego, CA, 08/26/2019.

## POSTER PRESENTATIONS

1. **Huh, D. N.**; Daley, C. J. A.; Moore, C. E.; Rheingold, A. L. *Synthesis, characterization, and reactivity of diamidato-bis(phosphino) nickel complexes*. Presented at the American Chemical Society 242nd National Conference. 08/30/2011.
2. **Huh, D. N.**; Daley, C. J. A.; Moore, C. E.; Rheingold, A. L. *Synthesis, characterization, and reactivity of diamidato-bis(phosphino) nickel complexes*. Presented at University of San Diego Undergraduate Research Conference 7th Annual Conference. San Diego, CA, 04/19/2012.
3. **Huh, D. N.**; Daley, C. J. A.; Moore, C. E.; Rheingold, A. L. *Synthesis, characterization, and reactivity of diimine-bis(phosphino) ruthenium-NO complexes*. Presented at the American Chemical Society Session 245th National Conference. New Orleans, LA. 04/06/2013.
4. **Huh, D. N.**; Szczepura, L. F. *Rhenium Clusters and NHCs: Use of Silver Transmetalation Reagents*. Presented at Illinois State University Summer Research Poster Session. Normal, IL. 07/24/2014.
5. **Huh, D. N.**; Szczepura, L. F. *Use of Transmetalation Reagents in the Formation of Cluster NHC Complexes*. Presented at the Heartland Local ACS Section. Peoria, IL. 10/04/2014.
6. **Huh, D. N.**; Bruce, J. P.; Hemminger, J. C.; Evans, W. J., *Exploring the Electronic Structure of Molecular Lanthanide Complexes in the +2 Oxidation State Using Photoelectron Spectroscopy*. Presented at the 65<sup>th</sup> American Vacuum Society. Long Beach, CA. 10/25/2018.

## FELLOWSHIPS AND AWARDS

Presidential Scholarship, <i>University of San Diego</i>	2009–2013
Research Excellence Award, <i>University of San Diego</i>	2013
Michael Kurz Research Fellowship, <i>Illinois State University</i>	2014
Summer Research Fellowship, <i>Illinois State University</i>	2015
UCI X-ray Crystallography Fellowship, <i>University of California: Irvine</i>	2019
Division of Inorganic Chemistry Student Travel Award, <i>American Chemical Society</i>	2019
National Security Education Center Travel Award, <i>Los Alamos National Lab</i>	2019

## OUTREACH

### **University of San Diego** **08/2010 – 05/2013**

Carson Elementary After School Science Program  
DNA extraction from fruits, solar-powered cars  
San Diego ChemExpo; chemistry demonstrations for the city of San Diego

### **University of California: Irvine** **12/2015 – 06/2018**

Laboratory demonstrations for graduating non-science major baccalaureates  
Mendez Fundamental Intermediate School; chemistry demonstrations for  
first-generation middle school students  
Julia Lathrop Intermediate School; chemistry demonstrations and explanations  
regarding cutting-edge liquid jet XPS and SEM technology

## WORK EXPERIENCE

### **Graduate Teaching Assistant, University of California: Irvine** **09/2015 – 03/2018**

General Chemistry Laboratory Instructor (CHEM 1LC, CHEM 1LD)  
Organic Chemistry Laboratory Instructor (CHEM 51LB, CHEM 51LC)  
Inorganic Chemistry Laboratory Instructor (CHEM 107L, Head TA)

### **Graduate Teaching Assistant, Illinois State University** **08/2013 – 05/2014**

Instructor for Chemistry and Society Laboratory (CHE 102)  
Teaching Assistant for General Chemistry II Laboratory (CHE 141)

**Lab Technician Assistant, University of San Diego** **09/2010 – 05/2011**

Preparation of organic chemistry teaching laboratories

Handled chemical waste for researching and teaching chemistry laboratories

**Violin Performance** **06/1995 – 08/2012**

Served as Concert Master and Soloist of *Young Professionals Orchestra* San Diego, CA

Served as Concert Master of the *University of San Diego Orchestra* San Diego, CA

Member of the *Denver Young Artists Orchestra* Denver, CO

Member of the *Denver Young Artists Symphonia* Denver, CO

Member of the *Colorado Youth Symphony Orchestra* Denver, CO

Centennial Regional Assistant Concert Master Centennial, CO

Served as Concert Master of Arapahoe High School Centennial, CO

Colorado All-State Musician



## ABSTRACT OF DISSERTATION

Developing Strategies for the Synthesis of Low Valent f Element Complexes, Encapsulation of f Elements in 2.2.2-Cryptand, and Examining the Electronic Properties of Lanthanide(II) Complexes Using X-ray Photoelectron Spectroscopy

By

Daniel N. Huh

Doctor of Philosophy in Chemistry

University of California, Irvine, 2019

Professor William J. Evans, Chair

This dissertation describes strategies for the synthesis of low valent f element complexes, isolation of f element cryptate complexes using 2.2.2-cryptand, and the analysis of the electronic structures of  $(C_5H_4SiMe_3)_3Ln$  and  $[K(2.2.2-cryptand)][(C_5H_4SiMe_3)_3Ln]$  complexes ( $Ln = Sm, Eu, Gd, Tb$ ) using X-ray photoelectron spectroscopy (XPS). The primary motivation of this research sought to expand the number of f element complexes in the +2 oxidation state by modifying counterions and ligand environments to investigate the chemical properties that help enable the isolation of these low valent ions. Several new complexes were isolated and strategies for the isolation of these ions will be discussed throughout this dissertation. In addition to developing synthetic strategies, the electronic structure of Ln(II) ions were examined using XPS to probe the electronic structure of both core electrons and valence electrons of these unusual ions with mixed-electron configurations.

In Chapter 1, lithium reduction of  $Cp'_3Ln$  ( $Cp' = C_5H_4SiMe_3$ ;  $Ln = Y, Tb, Dy, Ho$ ) under Ar in the presence of 2.2.2-cryptand (crypt) is discussed. Examples of crystallographically-characterizable Ln(II) complexes of these metals are isolable,  $[Li(crypt)][Cp'_3Ln]$ . In each complex, lithium is found in an  $N_2O_4$  donor atom coordination geometry that is unusual for the

cryptand ligand. Lithium reduction of  $\text{Cp}'_3\text{Y}$  under  $\text{N}_2$  at  $-35\text{ }^\circ\text{C}$  forms the Y(II) complex  $(\text{Cp}'_3\text{Y})^{1-}$ , which reduces dinitrogen upon warming to room temperature to generate the  $(\text{N}_2)^{2-}$  complex  $[\text{Cp}'_2\text{Y}(\text{THF})_2(\mu-\eta^2:\eta^2-\text{N}_2)]$ .

In Chapter 2, the synthetic options for generating complexes of the actinide metals in the +2 oxidation state are discussed. Reduction of  $\text{Cp}''_3\text{U}$  [ $\text{Cp}'' = \text{C}_5\text{H}_3(\text{SiMe}_3)_2$ ] and the lanthanide analogs,  $\text{Cp}''_3\text{La}$  and  $\text{Cp}''_3\text{Ce}$  with lithium in the absence of crown ether and cryptand chelates is described. In each case, crystallographically-characterizable  $[\text{Li}(\text{THF})_4][\text{Cp}''_3\text{M}]$  ( $\text{M} = \text{La}, \text{Ce}, \text{U}$ ) complexes were obtainable. Reductions using Cs were also explored and X-ray crystallography revealed the formation of an oligomeric structure,  $[\text{Cp}''\text{U}(\mu-\text{Cp}'')_2\text{Cs}(\text{THF})_2]_n$ , involving  $\text{Cp}''$  ligands that bridge  $(\text{Cp}''\text{U}^{\text{II}})^{1+}$  moieties to  $[\text{Cp}''_2\text{Cs}(\text{THF})_2]^{1-}$  units.

In Chapter 3, the synthesis of crystallographically-characterizable Ln(II) complexes of Tb and Ho by reducing  $\text{Cp}^{\text{Me}}_3\text{Ln}(\text{THF})$  ( $\text{Cp}^{\text{Me}} = \text{C}_5\text{H}_4\text{Me}$ ) with  $\text{KC}_8$  in THF in the presence of 18-crown-6 (18-c-6) is described. X-ray crystallography revealed that these complexes are isolated with a methylcyclopentadienide inverse sandwich counteranion:  $[(18\text{-c-}6)\text{K}(\mu-\text{Cp}^{\text{Me}})\text{K}(18\text{-c-}6)][\text{Cp}^{\text{Me}}_3\text{Ln}]$  ( $\text{Ln} = \text{Tb}, \text{Ho}$ ).

In Chapter 4, the reactivity of  $\text{Cp}'_2\text{Ln}(\text{THF})_2$  metallocenes with crypt to form Ln(II)-in-crypt complexes,  $[\text{Ln}(\text{crypt})(\text{THF})][\text{Cp}'_3\text{Ln}]_2$  ( $\text{Ln} = \text{Sm}, \text{Eu}$ ) and  $[\text{Yb}(\text{crypt})][\text{Cp}'_3\text{Yb}]_2$ , is discussed. In each of the complexes, a ligand rearrangement occurs to form a Ln(II) dication with two  $[\text{Cp}'_3\text{Ln}]^{1-}$  counteranions.

In Chapter 5, the facile encapsulation of U(III) and La(III) by crypt using simple starting materials is described. Addition of crypt to  $\text{UI}_3$  and  $\text{LaCl}_3$  forms the crystallographically-characterizable complexes,  $[\text{U}(\text{crypt})\text{I}_2]\text{I}$  and  $[\text{La}(\text{crypt})\text{Cl}_2]\text{Cl}$ . In the presence of water, the U(III)-aquo adducts,  $[\text{U}(\text{crypt})\text{I}(\text{OH}_2)]\text{I}]_2$  and  $[\text{UcryptI}(\text{OH}_2)]\text{I}][\text{BPh}_4]$ , can be isolated.

In Chapter 6, the reactivity of  $\text{LnI}_2(\text{THF})_2$  ( $\text{Ln} = \text{Sm}, \text{Eu}, \text{Yb}$ ) with crypt is discussed to examine if these readily accessible precursors could provide new examples of lanthanide-in-crypt complexes. The crystallographically-characterized Ln(II)-in-crypt complexes  $[\text{Ln}(\text{crypt})(\text{DMF})_2][\text{I}]_2$  ( $\text{Ln} = \text{Sm}, \text{Eu}$ ) and  $[\text{Yb}(\text{crypt})(\text{DMF})][\text{I}]_2$  were synthesized by reacting  $\text{LnI}_2(\text{THF})_2$  ( $\text{Ln} = \text{Sm}, \text{Eu}, \text{Yb}$ ) with crypt in THF and recrystallizing from DMF. Crystallographic data were also obtained on the Ln(II)-in-crypt complex  $[\text{Ln}(\text{crypt})(\text{DMF})_2][\text{BPh}_4]_2$  which was synthesized by addition of two equivalents of  $\text{NaBPh}_4$  to  $[\text{Ln}(\text{crypt})(\text{DMF})_2][\text{I}]_2$ .

In Chapter 7, the synthesis of Ln(III)-in-crypt complexes using  $\text{Ln}(\text{OTf})_3$  ( $\text{Ln} = \text{Nd}, \text{Dy}$ ) starting materials is discussed. In MeCN, the Dy(III)-in-crypt complex formed is  $[\text{Dy}(\text{crypt})(\text{OTf})][\text{OTf}]_2$  and in DMF, the Nd(III)-in-crypt complex formed is  $[\text{Nd}(\text{crypt})(\text{DMF})_2][\text{OTf}]_3$ . A Nd(III)-in-crypt complex,  $[\text{Nd}(\text{crypt})(\text{OTf})_2][\text{OTf}]$ , can also be formed in THF and subsequently reduced using  $\text{KC}_8$  to form the Nd(II)-in-crypt complex  $[\text{Nd}(\text{crypt})(\text{OTf})_2]$ .

In Chapter 8, the electrochemical properties of U(III)-in-crypt complex  $[\text{U}(\text{crypt})\text{I}_2]$  were examined in DMF and MeCN to determine the oxidative stability offered by crypt as a ligand. Cyclic-voltammetry revealed a U(IV)/U(III) quasi-reversible redox couple of  $-0.55$  V (vs  $\text{Fc}^{+/0}$ ). In the presence of  $[\text{CoCp}_2][\text{PF}_6]$  in MeCN, a reversible U(III)/U(II) redox couple of  $-1.84$  V (vs  $\text{Fc}^{+/0}$ ) was observed. U(III)-in-crypt complexes were also found to be robust to water. Additional examples of a U(III)-in-crypt complex with a DMF, MeCN and water adducts have also been crystallographically-characterized.

In Chapter 9, reduction of  $\text{Th}(\text{OC}_6\text{H}_2^t\text{Bu}_2\text{-2,6-Me-4})_4$  using either  $\text{KC}_8$  or Li in THF forming crystallographically-characterizable Th(III) complexes in the salts

$[\text{K}(\text{THF})_5(\text{Et}_2\text{O})][\text{Th}(\text{OC}_6\text{H}_2^t\text{Bu}_{2-2,6-\text{Me}-4})_4]$  and  $[\text{Li}(\text{THF})_4][\text{Th}(\text{OC}_6\text{H}_2^t\text{Bu}_{2-2,6-\text{Me}-4})_4]$  is discussed. In each structure the four aryloxo ligands are arranged in a square planar geometry, the first example of this coordination mode for an f element complex. The Th(III) ion and four oxygen donor atoms are coplanar to within 0.05 Å. EPR spectroscopy reveals an axial signal consistent with a metal-based radical in a planar complex. DFT calculations yield a  $C_4$ -symmetric structure which accommodates a low-lying SOMO of  $6d_{z^2}$  character with 7s Rydberg admixture.

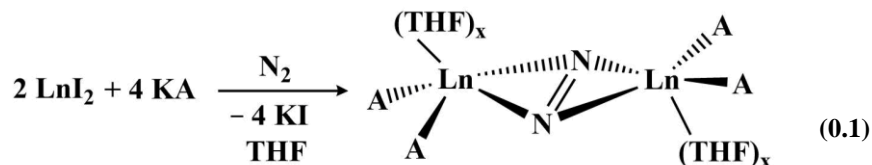
In Chapter 10, using X-ray photoelectron spectroscopy (XPS) and density functional theory (DFT) calculations are discussed to evaluate the electronic structure of molecular Ln(II) complexes  $[\text{Cp}'_3\text{Ln}]^{1-}$  ( $\text{Cp}' = \text{C}_5\text{H}_4\text{SiMe}_3$ ; Ln = Sm, Eu, Gd, Tb) formed by reduction of the Ln(III) precursors,  $\text{Cp}'_3\text{Ln}$ . DFT calculations suggest that Eu(II) has a  $4f^7$  and Gd(II) has a  $4f^75d^1$  electron configuration, whereas Tb(II) could not be unambiguously assigned due to its possible multiconfigurational ground state.

## INTRODUCTION

Metal oxidation states are fundamental to understanding electron movement in chemical redox reactions. Physical properties of metal ions and the chemical transformations they carry out inherently hinge on accessing different metal oxidation states. Understanding their role in chemical reactions could aid in harnessing their chemical potential. Transition metal ions have many accessible oxidation states and have been exploited for a vast variety of applications. However, f elements are far more limited to accessing oxidation states compared to transition metals.

**Rare-Earth Metals.** The most common oxidation state for rare-earth metals is the +3 oxidation state followed by the +2 (Nd, Sm, Eu, Dy, Tm, Yb)<sup>1-7</sup> and +4 (Ce,<sup>8</sup> Tb<sup>9-10</sup>) oxidation states. Molecular lanthanides in the +2 oxidation states for Sm, Eu, and Yb were known since 1906<sup>1-4</sup> and it was not until the late 1990s and early 2000s when the first examples of Nd(II),<sup>5</sup> Dy(II),<sup>6</sup> and Tm(II)<sup>7</sup> were isolated. Extending the +2 oxidation state to the rest of the lanthanide series to form isolable molecular complexes was thought to be difficult since the calculated potentials to reduce  $4f^n$  Ln(III) ions to  $4f^{n+1}$  Ln(II) ions were too large for syntheses in organic solvents.<sup>11</sup>

Reactions of  $\text{LnI}_2$  (Ln = Nd, Dy, Tm) with  $\text{N}_2$  in the presence of amide, aryloxide, and cyclopentadienide salts were examined which resulted in the isolation of bimetallic Ln(III) complexes bridged by a reduced dinitrogen moiety ( $\text{N}=\text{N}$ )<sup>2-</sup>, eq 0.1.<sup>12-14</sup> These reactions helped establish that the reduction of  $\text{N}_2$  originated from Ln(II). Additional synthetic routes to

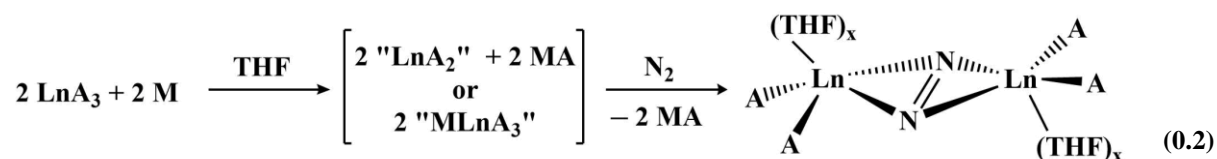


**Ln = Nd, Dy, Tm**

**A = amide, aryloxy, cyclopentadienide**

**x = 0-2**

bridging  $(\text{N}=\text{N})^{2-}$  products were explored using Ln(III) (Ln = Nd, Dy, Tm)<sup>15-16</sup> precursors in the presence of an alkali metal reducing agent, eq 0.2. In this reaction, the Ln(III) ion presumably



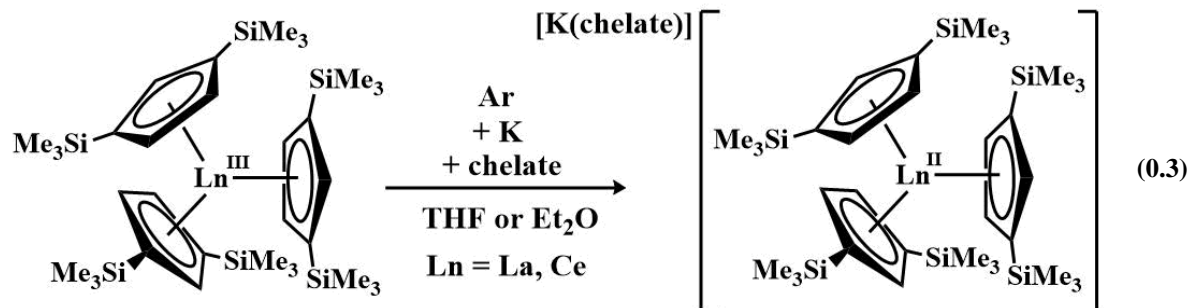
**Ln = Y, La, Ce, Pr, Nd, Gd, Tb, Dy, Ho, Er, Tm, Lu**

**A = amide, aryloxy, cyclopentadienide**

**M = K, KC<sub>8</sub>, Na; x = 0-2**

becomes reduced to form a transient Ln(II) ion which proceeds to reduce  $\text{N}_2$  to form a  $(\text{N}=\text{N})^{2-}$  product. Surprisingly, other rare-earth metals that were not known in the +2 oxidation state could also access this reactivity and form additional examples of the bimetallic Ln(III) bridged  $(\text{N}=\text{N})^{2-}$  products for Ln = Y, La, Ce, Pr, Gd, Tb, Ho, Er, and Lu.<sup>15-18</sup> This raised the question whether other rare-earth metals not previously known in the +2 oxidation state could be observed or even isolated.

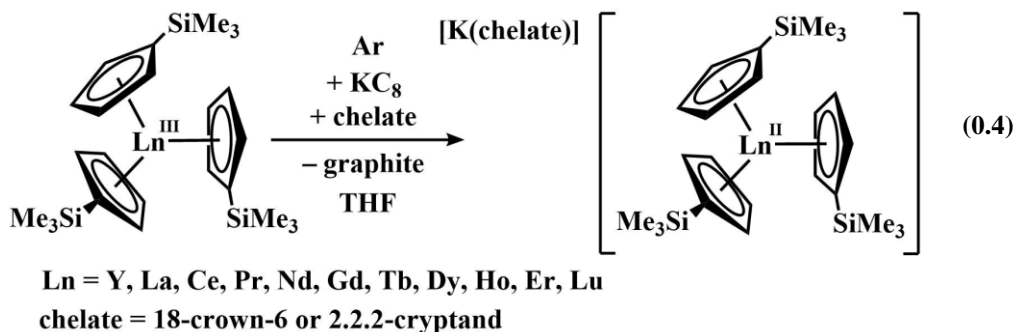
It was not until 2008 that Lappert and coworkers isolated the first examples of a La(II) and a Ce(II) complex,  $[\text{K}(\text{chelate})][\text{Cp}''_3\text{La}^{\text{II}}]$  and  $[\text{K}(18\text{-crown-6})][\text{Cp}''_3\text{Ce}^{\text{II}}] \cdot [\text{Cp}''_3\text{Ce}^{\text{III}}]$  [chelate = 18-crown-6, 2.2.2-cryptand;  $\text{Cp}'' = \text{C}_5\text{H}_3(\text{SiMe}_3)_2$ ], by reducing  $\text{Cp}''_3\text{Ln}$  (Ln = La, Ce) using potassium metal in the presence of a chelating agent in an argon atmosphere, eq 0.3.<sup>19</sup> This result



chelate = 18-crown-6 or 2.2.2-cryptand

suggested that other rare-earth metals in the +2 oxidation state could be isolated despite their large calculated Ln(III) to Ln(II) reduction potentials.<sup>11</sup>

In 2011, reduction of  $\text{Y}[\text{N}(\text{SiMe}_3)_2]_3$  under an argon atmosphere provided EPR evidence of a Y(II) in solution.<sup>20</sup> Later that year, the first example of a Y(II) was isolated in a similar manner to eq 0.3, but instead of using Cp'', the smaller Cp' (Cp' = C<sub>5</sub>H<sub>4</sub>SiMe<sub>3</sub>) ligand was used, eq 0.4.<sup>21</sup>



Soon after, the entire lanthanide series was isolated in the +2 oxidation state using the Cp' ligand with the exception of Pm due to its radioactivity.<sup>22-23</sup> These results not only demonstrated that Ln(II) are accessible for the entire series, but that the steric bulk of the ligand is important in the isolation of lanthanides in the +2 oxidation state. Complexes of  $[\text{Cp}''_3\text{Ln}]^{1-}$  can be isolated for the larger Ln = La, Ce, Pr, and Nd<sup>19, 24</sup>

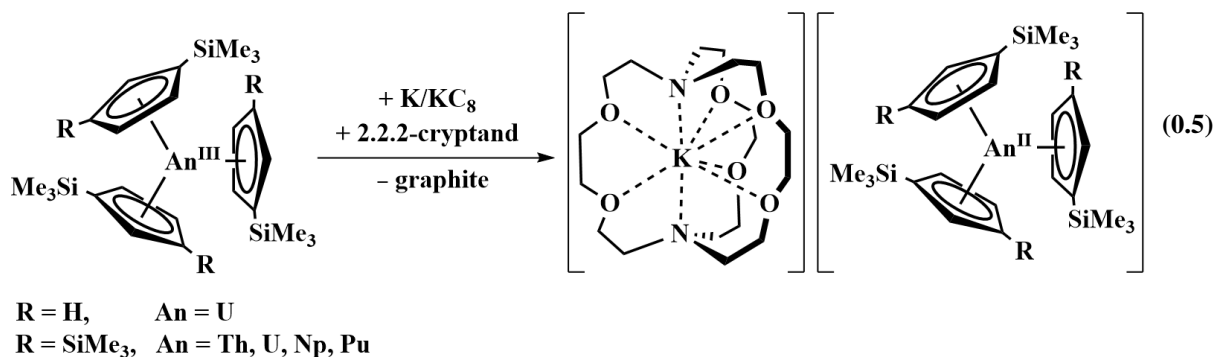
The metrical parameters of the Cp<sub>3</sub>Ln precursor and the [Cp<sub>3</sub>Ln]<sup>1-</sup> reduction product revealed that the Ln–Cp' centroid distance is longer in the Ln(II) complexes as is expected for metals with lower oxidation states. The complexes Sm, Eu, Tm, and Yb have a difference of 0.1-0.2 Å in Ln–Cp' centroid distance.<sup>25</sup> However, for Ln = Y, La, Ce, Pr, Nd, Gd, Tb, Dy, Ho, Er, and Lu, the differences in Ln–Cp' centroid distances are 0.027-0.031 Å.<sup>22, 25</sup> This unexpected small change in distance was attributed to the difference in electron configuration upon reduction. The electron configurations for +2 ions of Ln = Sm, Eu, Tm, and Yb, are 4f<sup>n+1</sup> which was identified by DFT and UV-vis studies. For Ln = Y, La, Ce, Pr, Nd, Gd, Tb, Dy, Ho, Er, and Lu, the electron configurations were found to be a 4f<sup>n</sup>5d<sup>1</sup> (4d<sup>1</sup> for Y) where the additional electron populates an essentially non-bonding d<sub>z2</sub> orbital instead of an f orbital. Additionally, Nd(II) and Dy(II), which were previously identified to have a 4f<sup>n+1</sup> electron configuration, have a 4f<sup>n</sup>5d<sup>1</sup> electron configuration in the [Cp<sub>3</sub>Ln]<sup>1-</sup> complexes thus demonstrating the variable nature of Nd and Dy.<sup>25</sup> Since the initial isolation of these the first Ln(II) ions, the first crystallographically-characterizable Sc(II)<sup>26</sup> complex was isolated using [N(SiMe<sub>3</sub>)<sub>2</sub>]<sup>1-</sup>. Additional examples of Ln(II) complexes have been reported using various cyclopentadienyl analogs such as (C<sub>5</sub>Me<sub>4</sub>H)<sup>1-</sup>,<sup>27</sup> [C<sub>5</sub>H<sub>2</sub>(CMe<sub>3</sub>)<sub>3</sub>]<sup>1-</sup>,<sup>28</sup> [C<sub>5</sub>H<sub>4</sub>(CMe<sub>3</sub>)]<sup>1-</sup>,<sup>29</sup> and (C<sub>5</sub>H<sub>4</sub>Me)<sup>1-</sup><sup>30</sup> as well as [N(SiMe<sub>3</sub>)<sub>2</sub>]<sup>1-</sup>,<sup>31</sup> [OC<sub>6</sub>H<sub>2</sub>(CMe<sub>3</sub>)<sub>2-2,6-Me-4</sub>]<sup>1-</sup>,<sup>32</sup> and the tris(aryloxy)mesitylene, [(<sup>Ad,Me</sup>ArO)<sub>3</sub>mes]<sup>1-</sup>.<sup>33-34</sup>

**Actinides.** Unlike the lanthanide series, actinides have a rich number of available oxidation states.<sup>35</sup> Molecular examples of actinides in the +2 oxidation state, however, are much more limited. Prior to the discovery of [Cp<sub>3</sub>Ln]<sup>1-</sup> complexes, molecular examples of actinides in the +2 oxidation state were not known. Using similar strategies for the isolation of Ln(II) ions as described in eq 0.4, the first example of U(II) was isolated by reducing Cp<sub>3</sub>U with potassium



graphite ( $\text{KC}_8$ ) in the presence of 2.2.2-cryptand (crypt) to form  $[\text{K}(\text{crypt})][\text{Cp}'_3\text{U}]$ , eq 0.5.<sup>36</sup>

Similarly to the the  $4f^n5d^1$  Ln(II) ions, the electron configuration of this U(II) ion was assigned



as  $5f^36d^1$  by DFT calculations. Additional examples of U(II) were later isolated using the bulkier  $\text{Cp}''$  to form  $[\text{M}(\text{chelate})][\text{Cp}''_3\text{U}]$  ( $\text{M} = \text{Na, K}$ ; chelate = 12-crown-4, 18-crown-6, 2.2.2-cryptand).<sup>37</sup>

Using the techniques described in eq 0.4 and 0.5, the first Th(II) was also isolated by reducing the Th(III)  $6d^1$  complex  $\text{Cp}''_3\text{Th}$ <sup>38</sup> with  $\text{KC}_8$  in the presence of a chelating agent.<sup>39</sup> Unlike the Ln(II) and U(II) examples, the electron configuration of this Th(II) complex was assigned as a diamagnetic  $6d^2$  ion. Both DFT and NMR corroborate this assignment. Inspired by these results, molecular examples of Np(II)<sup>40</sup> and Pu(II)<sup>41</sup> were also isolated using similar methods described in eq 0.5.

**Dissertation Outline.** In Chapter 1, lithium reduction of  $\text{Cp}'_3\text{Ln}$  ( $\text{Cp}' = \text{C}_5\text{H}_4\text{SiMe}_3$ ; Ln = Y, Tb, Dy, Ho) under Ar in the presence of 2.2.2-cryptand (crypt) is discussed. Examples of crystallographically-characterizable Ln(II) complexes of these metals are isolable,  $[\text{Li}(\text{crypt})][\text{Cp}'_3\text{Ln}]$ . In each complex, lithium is found in an  $\text{N}_2\text{O}_4$  donor atom coordination geometry that is unusual for the cryptand ligand. The Dy and Ho complexes have exceptionally high single-ion magnetic moments, 11.35 and 11.67  $\mu_B$ , respectively, and are consistent with  $4f^n5d^1$  electron configurations. Lithium reduction of  $\text{Cp}'_3\text{Y}$  under  $\text{N}_2$  at  $-35^\circ\text{C}$  forms the Y(II)

complex  $(\text{Cp}'_3\text{Y})^{1-}$ , which reduces dinitrogen upon warming to room temperature to generate the  $(\text{N}_2)^{2-}$  complex  $[\text{Cp}'_2\text{Y}(\text{THF})_2(\mu-\eta^2:\eta^2-\text{N}_2)]$ .

In Chapter 2, the synthetic options for generating complexes of the actinide metals in the +2 oxidation state are discussed. Reduction of  $\text{Cp}''_3\text{U}$  [ $\text{Cp}'' = \text{C}_5\text{H}_3(\text{SiMe}_3)_2$ ] and the lanthanide analogs,  $\text{Cp}''_3\text{La}$  and  $\text{Cp}''_3\text{Ce}$  with lithium in the absence of crown ether and cryptand chelates is described. In each case, crystallographically-characterizable  $[\text{Li}(\text{THF})_4][\text{Cp}''_3\text{M}]$  ( $\text{M} = \text{La}, \text{Ce}, \text{U}$ ) complexes were obtainable, *i.e.* chelating agents are not necessary to sequester the lithium counteranion to form isolable crystalline M(II) products. Reductions using Cs were also explored and X-ray crystallography revealed the formation of an oligomeric structure,  $[\text{Cp}''\text{U}(\mu-\text{Cp}'')_2\text{Cs}(\text{THF})_2]_n$ , involving  $\text{Cp}''$  ligands that bridge  $(\text{Cp}''\text{U}^{\text{II}})^{1+}$  moieties to  $[\text{Cp}''_2\text{Cs}(\text{THF})_2]^{1-}$  units.

In Chapter 3, the synthesis of crystallographically-characterizable Ln(II) complexes of Tb and Ho by reducing  $\text{Cp}^{\text{Me}}_3\text{Ln}(\text{THF})$  ( $\text{Cp}^{\text{Me}} = \text{C}_5\text{H}_4\text{Me}$ ) with  $\text{KC}_8$  in THF in the presence of 18-crown-6 (18-c-6) is described. X-ray crystallography revealed that these complexes are isolated with a methylcyclopentadienide inverse sandwich counteranion:  $[(18\text{-c-}6)\text{K}(\mu-\text{Cp}^{\text{Me}})\text{K}(18\text{-c-}6)][\text{Cp}^{\text{Me}}_3\text{Ln}]$  ( $\text{Ln} = \text{Tb}, \text{Ho}$ ).

In Chapter 4, the reactivity of  $\text{Cp}'_2\text{Ln}(\text{THF})_2$  metallocenes with crypt to form Ln(II)-in-crypt complexes,  $[\text{Ln}(\text{crypt})(\text{THF})][\text{Cp}'_3\text{Ln}]_2$  ( $\text{Ln} = \text{Sm}, \text{Eu}$ ) and  $[\text{Yb}(\text{crypt})][\text{Cp}'_3\text{Yb}]_2$ , is discussed. In each of the complexes, a ligand rearrangement occurs to form a Ln(II) dication with two  $[\text{Cp}'_3\text{Ln}]^{1-}$  counteranions.

In Chapter 5, the facile encapsulation of U(III) and La(III) by crypt using simple starting materials is described. Addition of crypt to  $\text{UI}_3$  and  $\text{LaCl}_3$  forms the crystallographically-

characterizable complexes,  $[\text{U}(\text{crypt})\text{I}_2]\text{I}$  and  $[\text{La}(\text{crypt})\text{Cl}_2]\text{Cl}$ . In the presence of water, the U(III)-aquo adducts,  $[\text{U}(\text{crypt})\text{I}(\text{OH}_2)][\text{I}]_2$  and  $[\text{U}(\text{crypt})\text{I}(\text{OH}_2)][\text{I}][\text{BPh}_4]$ , can be isolated.

In Chapter 6, the reactivity of  $\text{LnI}_2(\text{THF})_2$  ( $\text{Ln} = \text{Sm}, \text{Eu}, \text{Yb}$ ) with crypt is discussed to examine if these readily accessible precursors could provide new examples of lanthanide-in-crypt complexes. The crystallographically-characterized Ln(II)-in-crypt complexes  $[\text{Ln}(\text{crypt})(\text{DMF})_2][\text{I}]_2$  ( $\text{Ln} = \text{Sm}, \text{Eu}$ ) and  $[\text{Yb}(\text{crypt})(\text{DMF})][\text{I}]_2$  were synthesized by reacting  $\text{LnI}_2(\text{THF})_2$  ( $\text{Ln} = \text{Sm}, \text{Eu}, \text{Yb}$ ) with crypt in THF and recrystallizing from DMF. Crystallographic data were also obtained on the Ln(II)-in-crypt complex  $[\text{Ln}(\text{crypt})(\text{DMF})_2][\text{BPh}_4]_2$  which was synthesized by addition of two equivalents of  $\text{NaBPh}_4$  to  $[\text{Ln}(\text{crypt})(\text{DMF})_2][\text{I}]_2$ .

In Chapter 7, the synthesis of Ln(III)-in-crypt complexes using  $\text{Ln}(\text{OTf})_3$  ( $\text{Ln} = \text{Nd}, \text{Dy}$ ) starting materials is discussed. In MeCN, the Dy(III)-in-crypt complex formed is  $[\text{Dy}(\text{crypt})(\text{OTf})][\text{OTf}]_2$  and in DMF, the Nd(III)-in-crypt complex formed is  $[\text{Nd}(\text{crypt})(\text{DMF})_2][\text{OTf}]_3$ . A Nd(III)-in-crypt complex,  $[\text{Nd}(\text{crypt})(\text{OTf})_2][\text{OTf}]$ , can also be formed in THF and subsequently reduced using  $\text{KC}_8$  to form the Nd(II)-in-crypt complex  $[\text{Nd}(\text{crypt})(\text{OTf})_2]$ .

In Chapter 8, the electrochemical properties of U(III)-in-crypt complex  $[\text{U}(\text{crypt})\text{I}_2]\text{I}$  were examined in DMF and MeCN to determine the oxidative stability offered by crypt as a ligand. Cyclic-voltammetry revealed a U(IV)/U(III) quasi-reversible redox couple of  $-0.55 \text{ V}$  (vs  $\text{Fc}^{+/0}$ ). In the presence of  $[\text{CoCp}_2][\text{PF}_6]$  in MeCN, a reversible U(III)/U(II) redox couple of  $-1.84 \text{ V}$  (vs  $\text{Fc}^{+/0}$ ) was observed. U(III)-in-crypt complexes were also found to be robust to water. Additional examples of a U(III)-in-crypt complex with a DMF, MeCN and water adducts have also been crystallographically-characterized.

In Chapter 9, reduction of  $\text{Th}(\text{OC}_6\text{H}_2^t\text{Bu}_{2,6}\text{-Me-4})_4$  using either  $\text{KC}_8$  or  $\text{Li}$  in THF forming crystallographically-characterizable Th(III) complexes in the salts  $[\text{K}(\text{THF})_5(\text{Et}_2\text{O})][\text{Th}(\text{OC}_6\text{H}_2^t\text{Bu}_{2,6}\text{-Me-4})_4]$  and  $[\text{Li}(\text{THF})_4][\text{Th}(\text{OC}_6\text{H}_2^t\text{Bu}_{2,6}\text{-Me-4})_4]$  is discussed. In each structure the four aryloxy ligands are arranged in a square planar geometry, the first example of this coordination mode for an f element complex. The Th(III) ion and four oxygen donor atoms are coplanar to within 0.05 Å with O–Th–O angles of 89.27(8) to 92.02(8)° between cis ligands. The ligands have Th–O–C(ipso) angles of 173.9(2) to 178.6(4)° and the aryl rings make angles of 58.5 to 65.1° with the  $\text{ThO}_4$  plane. The effect of the eight tert-butyl substituents in generating the unusual structure through packing and/or dispersion forces is discussed. EPR spectroscopy reveals an axial signal consistent with a metal-based radical in a planar complex. DFT calculations yield a  $C_4$ -symmetric structure which accommodates a low-lying SOMO of  $6dz^2$  character with 7s Rydberg admixture.

In Chapter 10, the use of X-ray photoelectron spectroscopy (XPS) and density functional theory (DFT) calculations are discussed to evaluate the electronic structure of molecular Ln(II) complexes  $[\text{Cp}'_3\text{Ln}]^{1-}$  ( $\text{Cp}' = \text{C}_5\text{H}_4\text{SiMe}_3$ ; Ln = Sm, Eu, Gd, Tb) formed by reduction of the Ln(III) precursors,  $\text{Cp}'_3\text{Ln}$ . The complexes contain  $4f^5$  Sm(III) and  $4f^6$  Eu(III) ions would be expected to make  $4f^6$  Sm(II) and  $4f^7$  Eu(II) products upon reduction. Structural, spectroscopic, and magnetic data suggest this is true for Sm and Eu, but for Gd and Tb, the Ln(II) ions have  $4f^95d^1$  ions. DFT calculations suggest that Eu(II) has a  $4f^7$  and Gd(II) has a  $4f^75d^1$  electron configuration, whereas Tb(II) could not be unambiguously assigned due to its possible multiconfigurational ground state.

## References

- (1) Atwood, D. A., *The rare earth elements: fundamentals and applications*. John Wiley & Sons: 2013.
- (2) Matignon, C.; Cazes, E., Le chlorure samareux. *Ann. Chim. Phys.* **1906**, *8*, 417-426.
- (3) Jantsch, G.; Grubitsch, H.; Hoffmann, F.; Alber, H., Zur Kenntnis der Halogenide der seltenen Erden. Über die Jodide der Ceriterdenelemente und die Neubestimmung der Schmelzpunkte der Chloride. *Z. Anorg. Allg. Chem.* **1929**, *185* (1), 49-64.
- (4) Klemm, W.; Bommer, H., Contribution to the knowledge of the rare earths. *Z. Anorg. Allg. Chem.* **1937**, *231*, 138-171.
- (5) Bochkarev, M. N.; Fedushkin, I. L.; Dechert, S.; Fagin, A. A.; Schumann, H., [NdI<sub>2</sub>(THF)<sub>5</sub>], the First Crystallographically Authenticated Neodymium(II) Complex. *Angew. Chem. Int. Ed.* **2001**, *40* (17), 3176-3178.
- (6) Evans, W. J.; Allen, N. T.; Ziller, J. W., The Availability of Dysprosium Diiodide as a Powerful Reducing Agent in Organic Synthesis: Reactivity Studies and Structural Analysis of DyI<sub>2</sub>(DME)<sub>3</sub> and Its Naphthalene Reduction Product. *J. Am. Chem. Soc.* **2000**, *122* (47), 11749-11750.
- (7) Bochkarev, M. N.; Fedushkin, I. L.; Fagin, A. A.; Petrovskaya, T. V.; Ziller, J. W.; Broomhall-Dillard, R. N.; Evans, W. J., Synthesis and structure of the first molecular thulium(II) complex: [TmI<sub>2</sub>(MeOCH<sub>2</sub>CH<sub>2</sub>OMe)<sub>3</sub>]. *Angew. Chem. Int. Ed.* **1997**, *36* (1-2), 133-135.
- (8) Piro, N. A.; Robinson, J. R.; Walsh, P. J.; Schelter, E. J., The electrochemical behavior of cerium(III/IV) complexes: Thermodynamics, kinetics and applications in synthesis. *Coord. Chem. Rev.* **2014**, *260*, 21-36.
- (9) Palumbo, C. T.; Zivkovic, I.; Scopelliti, R.; Mazzanti, M., Molecular Complex of Tb in the +4 Oxidation State. *J. Am. Chem. Soc.* **2019**, *141* (25), 9827-9831.
- (10) Rice, N. T.; Popov, I. A.; Russo, D. R.; Bacsa, J.; Batista, E. R.; Yang, P.; Telser, J.; La Pierre, H. S., Design, Isolation, and Spectroscopic Analysis of a Tetravalent Terbium Complex. *J. Am. Chem. Soc.* **2019**, *141* (33), 13222-13233.
- (11) Morss, L. R., Thermochemical properties of yttrium, lanthanum, and the lanthanide elements and ions. *Chem. Rev.* **1976**, *76* (6), 827-841.
- (12) Evans, W. J.; Zucchi, G.; Ziller, J. W., Dinitrogen Reduction by Tm(II), Dy(II), and Nd(II) with Simple Amide and Aryloxide Ligands. *J. Am. Chem. Soc.* **2003**, *125* (1), 10-11.
- (13) Evans, W. J.; Allen, N. T.; Ziller, J. W., Expanding Divalent Organolanthanide Chemistry: The First Organothulium(II) Complex and the In Situ Organodysprosium(II) Reduction of Dinitrogen. *Angew. Chem. Int. Ed.* **2002**, *41* (2), 359-361.

- (14) Evans, W. J.; Allen, N. T.; Ziller, J. W., Facile Dinitrogen Reduction via Organometallic Tm(II) Chemistry. *J. Am. Chem. Soc.* **2001**, *123* (32), 7927-7928.
- (15) Evans, W. J.; Lee, D. S.; Ziller, J. W., Reduction of Dinitrogen to Planar Bimetallic  $M_2(\mu-\eta^2:\eta^2-N_2)$  Complexes of Y, Ho, Tm, and Lu Using the K/Ln[N(SiMe<sub>3</sub>)<sub>2</sub>]<sub>3</sub> Reduction System. *J. Am. Chem. Soc.* **2004**, *126* (2), 454-455.
- (16) Evans, W. J.; Lee, D. S.; Rego, D. B.; Perotti, J. M.; Kozimor, S. A.; Moore, E. K.; Ziller, J. W., Expanding Dinitrogen Reduction Chemistry to Trivalent Lanthanides via the LnZ<sub>3</sub>/Alkali Metal Reduction System: Evaluation of the Generality of Forming Ln<sub>2</sub> ( $\mu-\eta^2:\eta^2-N_2$ ) Complexes via LnZ<sub>3</sub>/K. *J. Am. Chem. Soc.* **2004**, *126* (44), 14574-14582.
- (17) Evans, W. J.; Lee, D. S.; Lie, C.; Ziller, J. W., Expanding the LnZ<sub>3</sub>/Alkali-Metal Reduction System to Organometallic and Heteroleptic Precursors: Formation of Dinitrogen Derivatives of Lanthanum. *Angew. Chem. Int. Ed.* **2004**, *43* (41), 5517-5519.
- (18) Evans, W. J.; Rego, D. B.; Ziller, J. W., Synthesis, structure, and <sup>15</sup>N NMR studies of paramagnetic lanthanide complexes obtained by reduction of dinitrogen. *Inorg. Chem.* **2006**, *45* (26), 10790-10798.
- (19) Hitchcock, P. B.; Lappert, M. F.; Maron, L.; Protchenko, A. V., Lanthanum Does Form Stable Molecular Compounds in the +2 Oxidation State. *Angew. Chem. Int. Ed.* **2008**, *47* (8), 1488-1491.
- (20) Fang, M.; Lee, D. S.; Ziller, J. W.; Doedens, R. J.; Bates, J. E.; Furche, F.; Evans, W. J., Synthesis of the (N<sub>2</sub>)<sup>3-</sup> Radical from Y<sup>2+</sup> and Its Protonolysis Reactivity To Form (N<sub>2</sub>H<sub>2</sub>)<sup>2-</sup> via the Y[N(SiMe<sub>3</sub>)<sub>2</sub>]<sub>3</sub>/KC<sub>8</sub> Reduction System. *J. Am. Chem. Soc.* **2011**, *133* (11), 3784-3787.
- (21) MacDonald, M. R.; Ziller, J. W.; Evans, W. J., Synthesis of a Crystalline Molecular Complex of Y<sup>2+</sup>, [(18-crown-6)K][(C<sub>5</sub>H<sub>4</sub>SiMe<sub>3</sub>)<sub>3</sub>Y]. *J. Am. Chem. Soc.* **2011**, *133* (40), 15914-15917.
- (22) MacDonald, M. R.; Bates, J. E.; Ziller, J. W.; Furche, F.; Evans, W. J., Completing the Series of +2 Ions for the Lanthanide Elements: Synthesis of Molecular Complexes of Pr<sup>2+</sup>, Gd<sup>2+</sup>, Tb<sup>2+</sup>, and Lu<sup>2+</sup>. *J. Am. Chem. Soc.* **2013**, *135* (26), 9857-9868.
- (23) MacDonald, M. R.; Bates, J. E.; Fieser, M. E.; Ziller, J. W.; Furche, F.; Evans, W. J., Expanding Rare-Earth Oxidation State Chemistry to Molecular Complexes of Holmium(II) and Erbium(II). *J. Am. Chem. Soc.* **2012**, *134* (20), 8420-8423.
- (24) Palumbo, C. T.; Darago, L. E.; Windorff, C. J.; Ziller, J. W.; Evans, W. J., Trimethylsilyl versus Bis(trimethylsilyl) Substitution in Tris(cyclopentadienyl) Complexes of La, Ce, and Pr: Comparison of Structure, Magnetic Properties, and Reactivity. *Organometallics* **2018**, *37* (6), 900-905.

- (25) Fieser, M. E.; MacDonald, M. R.; Krull, B. T.; Bates, J. E.; Ziller, J. W.; Furche, F.; Evans, W. J., Structural, Spectroscopic, and Theoretical Comparison of Traditional vs Recently Discovered Ln<sup>2+</sup> Ions in the [K(2.2.2-cryptand)][(C<sub>5</sub>H<sub>4</sub>SiMe<sub>3</sub>)<sub>3</sub>Ln] Complexes: The Variable Nature of Dy<sup>2+</sup> and Nd<sup>2+</sup>. *J. Am. Chem. Soc.* **2015**, *137* (1), 369-382.
- (26) Woen, D. H.; Chen, G. P.; Ziller, J. W.; Boyle, T. J.; Furche, F.; Evans, W. J., Solution Synthesis, Structure, and CO<sub>2</sub> Reduction Reactivity of a Scandium(II) Complex, {Sc[N(SiMe<sub>3</sub>)<sub>2</sub>]<sub>3</sub>}<sup>-</sup>. *Angew. Chem. Int. Ed.* **2017**, *56* (8), 2050-2053.
- (27) Jenkins, T. F.; Woen, D. H.; Mohanam, L. N.; Ziller, J. W.; Furche, F.; Evans, W. J., Tetramethylcyclopentadienyl Ligands Allow Isolation of Ln(II) Ions across the Lanthanide Series in [K(2.2.2-cryptand)][(C<sub>5</sub>Me<sub>4</sub>H)<sub>3</sub>Ln] Complexes. *Organometallics* **2018**, *37* (21), 3863-3873.
- (28) Jaroschik, F.; Momin, A.; Nief, F.; Le Goff, X.-F.; Deacon, G. B.; Junk, P. C., Dinitrogen Reduction and C-H Activation by the Divalent Organoneodymium Complex [(C<sub>5</sub>H<sub>2</sub><sup>1</sup>Bu<sub>3</sub>)<sub>2</sub>Nd(μ-I)K([18]crown-6)]. *Angew. Chem. Int. Ed.* **2009**, *48* (6), 1117-1121.
- (29) Angadol, M. A.; Woen, D. H.; Windorff, C. J.; Ziller, J. W.; Evans, W. J., tert-Butyl(cyclopentadienyl) Ligands Will Stabilize Nontraditional +2 Rare-Earth Metal Ions. *Organometallics* **2019**, *38* (5), 1151-1158.
- (30) Huh, D. N.; Ziller, J. W.; Evans, W. J., Isolation of reactive Ln(II) complexes with C<sub>5</sub>H<sub>4</sub>Me ligands (Cp<sup>Me</sup>) using inverse sandwich counteranions: synthesis and structure of [(18-crown-6)K(μ-Cp<sup>Me</sup>)K(18-crown-6)][Cp<sup>Me</sup><sub>3</sub>Ln<sup>II</sup>] (Ln = Tb, Ho). *Dalton Transactions* **2018**, *47* (48), 17285-17290.
- (31) Ryan, A. J.; Darago, L. E.; Balasubramani, S. G.; Chen, G. P.; Ziller, J. W.; Furche, F.; Long, J. R.; Evans, W. J., Synthesis, Structure, and Magnetism of Tris(amide) [Ln{N(SiMe<sub>3</sub>)<sub>2</sub>]<sub>3</sub>]<sup>-</sup> Complexes of the Non-traditional +2 Lanthanide Ions. *Chem. Eur. J.* **2018**, *24* (30), 7702-7709.
- (32) Moehring, S. A.; Beltrán-Leiva, M. J.; Páez-Hernández, D.; Arratia-Pérez, R.; Ziller, J. W.; Evans, W. J., Rare-Earth Metal(II) Aryloxides: Structure, Synthesis, and EPR Spectroscopy of [K(2.2.2-cryptand)][Sc(OC<sub>6</sub>H<sub>2</sub><sup>4</sup>Bu<sub>2</sub>-2,6-Me-4)<sub>3</sub>]. *Chem. Eur. J.* **2018**, *24* (68), 18059-18067.
- (33) Fieser, M. E.; Palumbo, C. T.; La Pierre, H. S.; Halter, D. P.; Voora, V. K.; Ziller, J. W.; Furche, F.; Meyer, K.; Evans, W. J., Comparisons of lanthanide/actinide +2 ions in a tris(aryloxide)arene coordination environment. *Chem. Sci.* **2017**, *8* (11), 7424-7433.
- (34) Palumbo, C. T.; Halter, D. P.; Voora, V. K.; Chen, G. P.; Chan, A. K.; Fieser, M. E.; Ziller, J. W.; Hieringer, W.; Furche, F.; Meyer, K.; Evans, W. J., Metal versus Ligand Reduction in Ln<sup>3+</sup> Complexes of a Mesitylene-Anchored Tris(Aryloxide) Ligand. *Inorg. Chem.* **2018**, *57* (5), 2823-2833.
- (35) Morss, L. R.; Edelstein, N. M.; Fuger, J.; Katz, J. J.; Morss, L., *The chemistry of the actinide and transactinide elements*. Springer: 2006; Vol. 1.

- (36) MacDonald, M. R.; Fieser, M. E.; Bates, J. E.; Ziller, J. W.; Furche, F.; Evans, W. J., Identification of the +2 Oxidation State for Uranium in a Crystalline Molecular Complex, [K(2.2.2-Cryptand)][(C<sub>5</sub>H<sub>4</sub>SiMe<sub>3</sub>)<sub>3</sub>U]. *J. Am. Chem. Soc.* **2013**, *135* (36), 13310-13313.
- (37) Windorff, C. J.; MacDonald, M. R.; Meihaus, K. R.; Ziller, J. W.; Long, J. R.; Evans, W. J., Expanding the Chemistry of Molecular U<sup>2+</sup> Complexes: Synthesis, Characterization, and Reactivity of the {[C<sub>5</sub>H<sub>3</sub>(SiMe<sub>3</sub>)<sub>2</sub>]<sub>3</sub>U}<sup>-</sup> Anion. *Chem. Eur. J.* **2016**, *22* (2), 772-782.
- (38) Blake, P. C.; Edelstein, N. M.; Hitchcock, P. B.; Kot, W. K.; Lappert, M. F.; Shalimoff, G. V.; Tian, S., Synthesis, properties and structures of the tris (cyclopentadienyl) thorium (III) complexes [Th{ $\eta^5$ -C<sub>5</sub>H<sub>3</sub>(SiMe<sub>2</sub>R)<sub>2-1,3</sub>}]<sub>3</sub>(R= Me or <sup>t</sup>Bu). *J. Organomet. Chem.* **2001**, *636*, 124-129.
- (39) Langeslay, R. R.; Fieser, M. E.; Ziller, J. W.; Furche, F.; Evans, W. J., Synthesis, structure, and reactivity of crystalline molecular complexes of the {[C<sub>5</sub>H<sub>3</sub>(SiMe<sub>3</sub>)<sub>2</sub>]<sub>3</sub>Th}<sup>1-</sup> anion containing thorium in the formal +2 oxidation state. *Chem. Sci.* **2015**, *6* (1), 517-521.
- (40) Sü, J.; Windorff, C. J.; Batista, E. R.; Evans, W. J.; Gaunt, A. J.; Janicke, M. T.; Kozimor, S. A.; Scott, B. L.; Woen, D. H.; Yang, P., Identification of the Formal +2 Oxidation State of Neptunium: Synthesis and Structural Characterization of {Np<sup>II</sup>[C<sub>5</sub>H<sub>3</sub>(SiMe<sub>3</sub>)<sub>2</sub>]<sub>3</sub>}<sup>1-</sup>. *J. Am. Chem. Soc.* **2018**, *140* (24), 7425-7428.
- (41) Windorff, C. J.; Chen, G. P.; Cross, J. N.; Evans, W. J.; Furche, F.; Gaunt, A. J.; Janicke, M. T.; Kozimor, S. A.; Scott, B. L., Identification of the Formal +2 Oxidation State of Plutonium: Synthesis and Characterization of {Pu<sup>II</sup>[C<sub>5</sub>H<sub>3</sub>(SiMe<sub>3</sub>)<sub>2</sub>]<sub>3</sub>}<sup>-</sup>. *J. Am. Chem. Soc.* **2017**, *139* (11), 3970-3973.

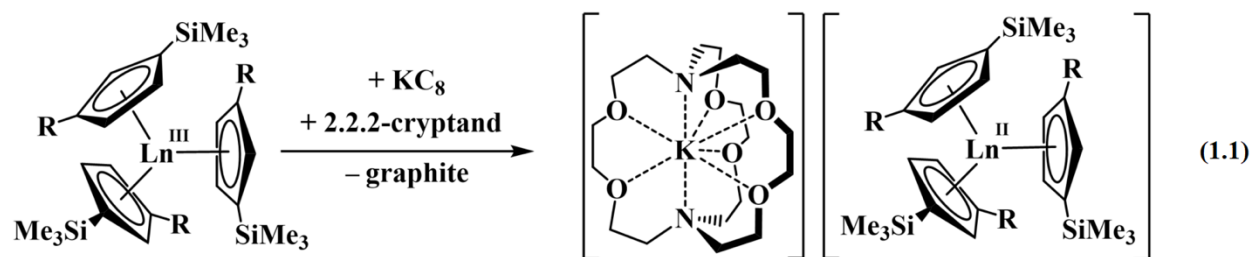


## CHAPTER 1

### Utility of Lithium in Rare-Earth Metal Reduction Reactions to Form Non-traditional Ln(II) Complexes and Unusual [Li(2.2.2-cryptand)]<sup>1+</sup> Cations

#### Introduction\*

The discovery of new oxidation states for the rare-earth metals Y, La, Ce, Pr, Gd, Tb, Ho, Er, and Lu via LnA<sub>3</sub>/M reactions (Ln = rare-earth metal; A = anion; M = alkali metal), eq 1.1,<sup>1-4</sup> initially involved potassium almost exclusively as the alkali metal reductant. Sodium was



R = H, Ln = Y, La, Ce, Pr, Nd, Gd, Tb, Dy, Ho, Er, and Lu

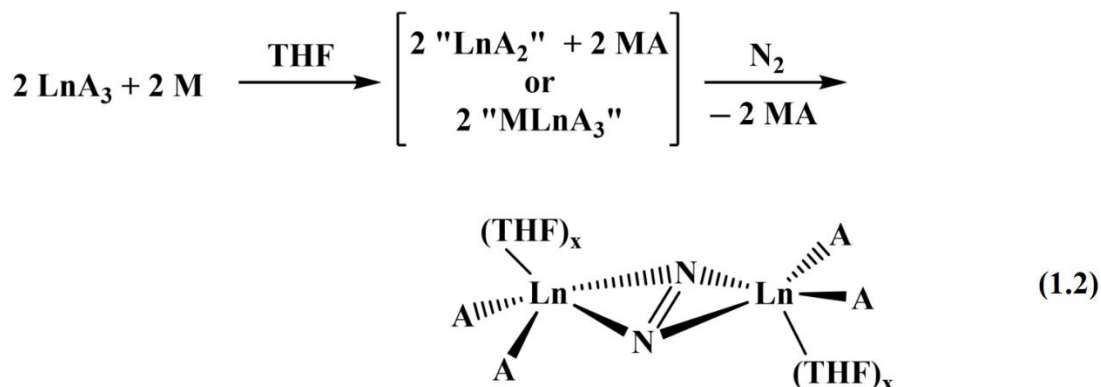
R = SiMe<sub>3</sub>, Ln = La and Ce

used successfully as a reductant with Cp'<sub>3</sub>Y<sup>5</sup> (Cp' = C<sub>5</sub>H<sub>4</sub>SiMe<sub>3</sub>) and the uranium complex, Cp''<sub>3</sub>U<sup>6</sup> (Cp'' = C<sub>5</sub>H<sub>3</sub>(SiMe<sub>3</sub>)<sub>2</sub>). While lithium was used by Lappert and co-workers to examine reduction of Cp''<sub>3</sub>Ln complexes (Ln = La, Ce, Pr) in dimethoxyethane (DME), these reactions produced only the Ln<sup>3+</sup> methoxide products, [Cp''<sub>2</sub>Ln(OMe)]<sub>2</sub> and Cp''<sub>2</sub>Nd(OMe)<sub>2</sub>Li(DME).<sup>7</sup> The reductions of complexes of C<sub>5</sub>H<sub>3</sub>(CMe<sub>3</sub>)<sub>2</sub> (Cp<sup>tt</sup>)<sup>7, 8</sup> and C<sub>5</sub>H<sub>2</sub>(CMe<sub>3</sub>)<sub>3</sub> (Cp<sup>ttt</sup>)<sup>9, 10</sup> and complexes of the tris(aryloxy) mesitylene ligand, ((<sup>Ad,Me</sup>ArO)<sub>3</sub>mes)<sup>3-, 11</sup> using K were also reported in the literature.

Lithium was not used in the Evans laboratory for LnA<sub>3</sub>/M rare-earth metal reduction

\*Portions of this chapter have been published: Huh, D. N.; Darago, L. E.; Ziller, J. W.; Evans, W. J. Utility of Lithium in Rare-Earth Metal Reduction Reactions to Form Nontraditional Ln<sup>2+</sup> Complexes and Unusual [Li(2.2.2-cryptand)]<sup>1+</sup> Cations. *Inorg. Chem.*, **2018**, 57, 2096-2102. DOI: 10.1021/acs.inorgchem.7b03000

since these were originally developed to isolate reduced dinitrogen complexes with rare-earth reactions metals, eq 1.2. As lithium can reduce N<sub>2</sub> on its own, it was to ensure that the N<sub>2</sub> reduction was caused by the rare-earth metal complex.<sup>7, 12, 13</sup> However, there is no reason to avoid lithium in reactions to form Ln(II) complexes since reductions are performed under Ar.



**Ln = Sc, Y, La, Ce, Pr, Nd, Gd, Tb, Dy, Ho, Er, Tm, Lu**

**A = N(SiMe<sub>3</sub>)<sub>2</sub>, OC<sub>6</sub>H<sub>3</sub><sup>t</sup>Bu<sub>2-2,6</sub>, C<sub>5</sub>Me<sub>5</sub>, C<sub>5</sub>Me<sub>4</sub>H, C<sub>5</sub>H<sub>4</sub>SiMe<sub>3</sub>, C<sub>5</sub>H<sub>2</sub><sup>t</sup>Bu<sub>3</sub>**

**M = K, KC<sub>8</sub>, Na; x = 0-2**

Accordingly, lithium has been examined as a reductant in LnA<sub>3</sub>/M reactions to determine if it offers any advantages over sodium or potassium in eq 1.1 and 1.2. Due to its small size, lithium has the capacity to become incorporated into organometallic complexes by coordinating to cyclopentadienyl, amide, or aryloxy ligands.<sup>14-16</sup> This could produce complexes with different reactivity compared to the [K(crypt)][Cp'<sub>3</sub>Ln], **1-Ln**, and [K(crypt)][Cp''<sub>3</sub>Ln] series of complexes in eq 1.1, which are typically isolated with [alkali metal (chelate)]<sup>1+</sup> counter-cations. To explore these options, reductions with lithium were examined both in the presence and the absence of chelators.

The lithium salts of the (Cp'<sub>3</sub>Ln)<sup>1-</sup> anions were of further interest as complexes containing non-traditional divalent lanthanide ions with unusual electron configurations. In previous potassium-based reductions of the 4f<sup>n</sup> Ln<sup>3+</sup> complexes, Cp'<sub>3</sub>Ln, the [K(crypt)][Cp'<sub>3</sub>Ln],

**1-Ln**, the series was produced with Ln = La, Ce, Pr, Nd, Gd, Tb, Dy, Ho, Er, and Lu. These complexes had properties consistent with  $4f^n5d^1$  electron configurations rather than the  $4f^{n+1}$  electron configurations found in the past for traditional Ln(II) ions of Ln = Eu, Yb, Sm, and Tm. Magnetic studies of the Dy(II) and Ho(II) complexes showed high single-ion magnetic moments, 11.35 and 11.41  $\mu_B$ , for [K(crypt)][Cp<sub>3</sub>Dy] (**1-Dy**) and [K(crypt)][Cp<sub>3</sub>Ho] (**1-Ho**), respectively.<sup>17</sup> It was of interest here to determine if similar electron configurations, and thereby similarly high single-ion magnetic moments, could be observed upon altering the counter-cation of **1-Ln**.

## Results and Discussion

**Synthesis of Ln(II) Complexes.** The Cp<sub>3</sub>Ln complexes (Ln = Y, Tb, Dy, and Ho) are reduced by lithium under argon at -35 °C in the presence of 2.2.2-cryptand (crypt) in Et<sub>2</sub>O to form Y(II), Tb(II), Dy(II), and Ho(II) complexes, [Li(crypt)][Cp<sub>3</sub>Ln], **2-Ln**, according to eq 1.3. As found for the **1-Ln** complexes, the products of these reactions must be isolated within minutes, since the solutions become colorless with longer reaction times. The specific decomposition pathways were not identified in these cases, but they could involve degradation of the solvent<sup>7</sup> or the chelate.<sup>21</sup> Reductions using Li in the presence of 12-crown-4 also yielded dark maroon solutions, but reduction products could not be isolated due to rapid decomposition even at -35 °C. Single crystals of each complex were identified by X-ray diffraction, Figure 1.1. Crystalline yields of **2-Ln** were lower than for the **1-Ln** complexes due to the high solubility of **2-Ln** in Et<sub>2</sub>O. Reductions can also be performed in THF, but this solvent was avoided due to greater solubility of the reduction products.

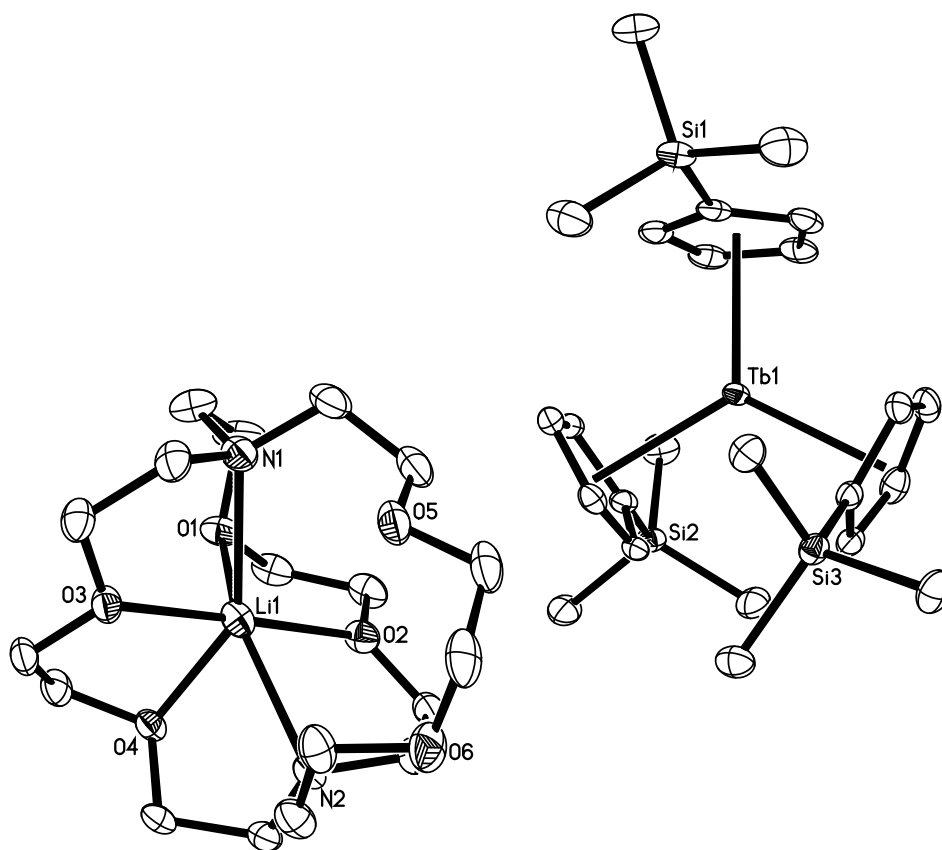
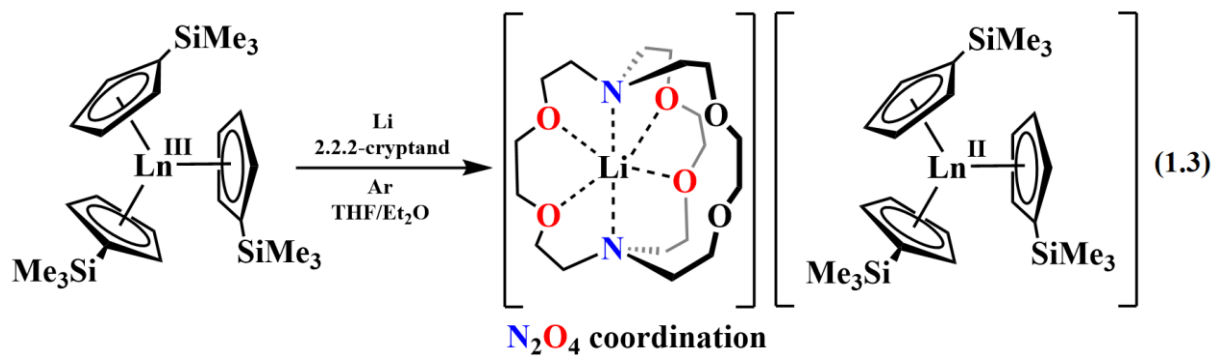


**Figure 1.1.** ORTEP representation of  $[\text{Li}(\text{crypt})][\text{Cp}'_3\text{Tb}]$ , **2-Tb**, thermal ellipsoids drawn at the 50% probability level. Hydrogen atoms are omitted for clarity.

Each complex has the intense maroon color previously observed for the **1-Ln**<sup>3, 4</sup> and  $[\text{K}(18\text{-crown-6})][\text{Cp}'_3\text{Ln}]$  complexes.<sup>2, 3, 18</sup> The EPR spectra of **2-Y**, Figure 1.2, match those of

the previously-reported **1-Y** and [K(18-crown-6)][Cp<sub>3</sub>Y].<sup>2, 3</sup> The  $g = 1.991$  and  $A = 36.6$  G at 298 K arising from the  $I = 1/2$  nucleus of <sup>89</sup>Y are indistinguishable from those of **1-Y**.

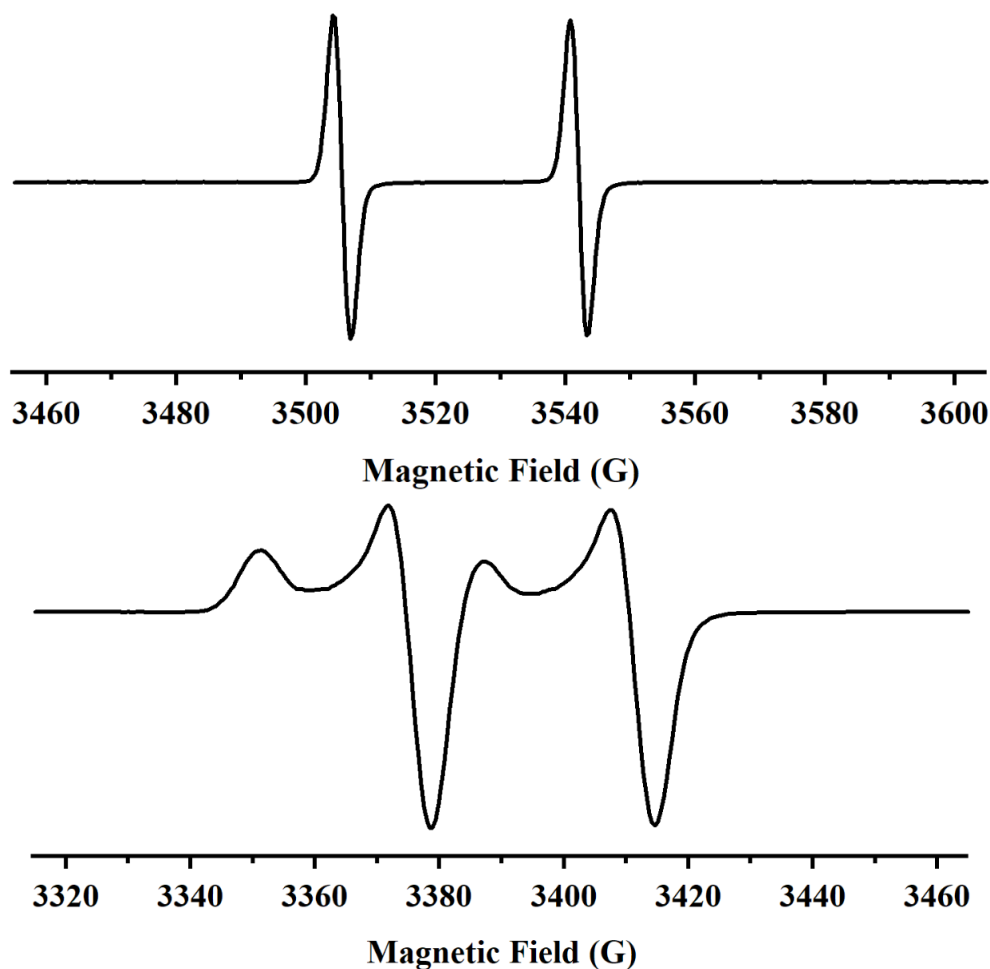


**Figure 1.2.** Experimental X-band EPR spectra of [Li(crypt)][Cp<sub>3</sub>Y], **2-Y**, dissolved in THF (10 mM) collected at 298 K (top; mode: perpendicular;  $g_{\text{iso}} = 1.991$ ;  $A_{\text{iso}} = 36.6$  G;  $\nu = 9.817$  GHz;  $P = 0.0203$ ; modulation amplitude = 0.902 mT) and 77 K (bottom; mode: perpendicular;  $g_{\parallel} = 2.001$ ,  $g_{\perp} = 1.987$ ;  $A_{\parallel} = 36.6$  G,  $A_{\perp} = 36.6$  G;  $\nu = 9.436$  GHz;  $P = 0.0640$ ; modulation amplitude = 0.902 mT) and analyzed using *EasySpin*.<sup>22</sup>

The X-ray crystal structures of **2-Ln** contain (Cp<sub>3</sub>Ln)<sup>1-</sup> anions with a trigonal arrangement of the three cyclopentadienyl ring centroids. Structural parameters are

indistinguishable from those of **1-Ln** (Table 1.1). However, the structures of the [Li(crypt)]<sup>1+</sup> cations are more unusual.

**Table 1.1.** [K(crypt)][Cp'<sub>3</sub>Ln], **1-Ln** versus [Li(crypt)][Cp'<sub>3</sub>Ln], **2-Ln** comparisons of selected bond distances (Å) and bond angles (°).

	Ln–centroid Ave (Å)	Ln–C Range (Å)	centroid–Ln–centroid range (°)	centroid–Ln–centroid ave (°)
<b>1-Y</b>	2.436(6)	2.680(2)-2.750(2)	118.18-122.48	120.0(23)
<b>2-Y</b>	2.438(14)	2.683(3)-2.755(4)	118.35-122.46	120.0(17)
<b>1-Tb</b>	2.454(5)	2.699(2)-2.766(2)	118.26-123.14	120.0(22)
<b>2-Tb</b>	2.455(12)	2.699(2)-2.770(2)	118.38-122.48	120.0(18)
<b>1-Dy</b>	2.443(7)	2.686(3)-2.755(3)	118.29-123.16	120.0(22)
<b>2-Dy</b>	2.445(12)	2.700(4)-2.755(5)	118.27-122.49	120.0(18)
<b>1-Ho</b>	2.426(5)	2.678(2)-2.745(2)	118.25-123.14	120.0(22)
<b>2-Ho</b>	2.425(13)	2.674(3)-2.741(4)	118.38-122.4	120.0(17)

**Reduction Under Dinitrogen.** When the reduction of Cp'<sub>3</sub>Y using Li is conducted under N<sub>2</sub> at –35 °C, the EPR spectrum is identical to the spectrum of the [M(crypt)][Cp'<sub>3</sub>Y] (M = Li, K) complexes isolated from reactions under argon. This was of considerable interest since many LnA<sub>3</sub>/M reductions (A = anion, M = alkali metal) under N<sub>2</sub> form reduced dinitrogen complexes rather than isolable Ln(II) products, particularly with A = N(SiMe<sub>3</sub>)<sub>2</sub>, eq 1.2.<sup>7, 12, 13, 23-27</sup> When the Cp'<sub>3</sub>Y/Li reaction under N<sub>2</sub> warms to room temperature over 15 min, the previously reported complex [Cp'<sub>2</sub>(THF)Y]<sub>2</sub>(μ-η<sup>2</sup>:η<sup>2</sup>-N<sub>2</sub>), **3**,<sup>2</sup> is isolated in 39% yield and was identified by <sup>1</sup>H NMR

spectroscopy.<sup>2</sup> The dark Cp'<sub>3</sub>Y/Li solutions generated under N<sub>2</sub> at -35 °C convert to the green **3** at similar rates whether crypt is present or not.<sup>27</sup>

These syntheses of **3** contrast with the Cp'<sub>3</sub>Y/K reaction under N<sub>2</sub> at room temperature which gives some EPR active products rather than purely the diamagnetic (N=N)<sup>2-</sup> complex, **3**.<sup>28</sup> The Cp'<sub>3</sub>Y/K reaction under N<sub>2</sub> exhibited a 16-line EPR spectrum that was not easily modeled. Reinvestigation of the reduction of Cp'<sub>3</sub>Y with K under N<sub>2</sub> revealed that it will form **3**, but only at -78 °C. These reactions emphasize the importance of both temperature and alkali metal in LnA<sub>3</sub>/M/substrate reactions. The specific A ligand in these reactions is also important. For example, reduction of (C<sub>5</sub>Me<sub>4</sub>H)<sub>3</sub>Y with K at room temperature forms the reduced dinitrogen complex, [(C<sub>5</sub>Me<sub>4</sub>H)<sub>2</sub>Y(THF)]<sub>2</sub>(μ-η<sup>2</sup>:η<sup>2</sup>-N<sub>2</sub>),<sup>23</sup> but it has not yet been possible to isolate the divalent complex, [(C<sub>5</sub>Me<sub>4</sub>H)<sub>3</sub>Y]<sup>1-</sup>. Furthermore, the use of lithium in the reduction of amide analogues of Cp'<sub>3</sub>Y, namely Y[N(SiMe<sub>3</sub>)<sub>2</sub>]<sub>3</sub>, revealed that under N<sub>2</sub> in THF at room temperature, both in the presence and absence of crypt, orange solutions are formed with EPR spectra Figure 1.3 identical to the previously reported (N<sub>2</sub>)<sup>3-</sup> complex,

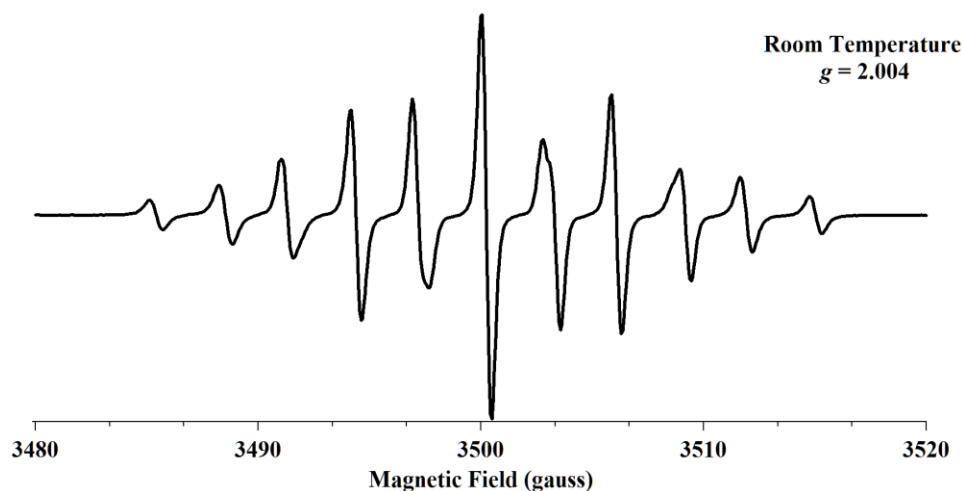


**Figure 1.3.** Experimental X-band EPR spectra of [{}[(Me<sub>3</sub>Si)<sub>2</sub>N]<sub>2</sub>(THF)Y]<sub>2</sub>(μ-η<sup>2</sup>:η<sup>2</sup>-N<sub>2</sub>)]<sup>1-</sup> in THF collected at 298 K (mode: perpendicular;  $g_{\text{iso}} = 2.004$ ;  $\nu = 9.817$  GHz;  $P = 0.0203$ ; modulation amplitude = 0.902 mT).

[K(THF)<sub>6</sub>]{[(Me<sub>3</sub>Si)<sub>2</sub>N]<sub>2</sub>(THF)Y}<sub>2</sub>(μ-η<sup>2</sup>:η<sup>2</sup>-N<sub>2</sub>).<sup>24</sup> Analysis of the orange product by <sup>1</sup>H NMR spectroscopy revealed the presence of the (N<sub>2</sub>)<sup>2-</sup> product {[(Me<sub>3</sub>Si)<sub>2</sub>N]<sub>2</sub>(THF)Y}<sub>2</sub>(μ-η<sup>2</sup>:η<sup>2</sup>-N<sub>2</sub>).<sup>27</sup>  
<sup>29</sup> Mixtures of the (N<sub>2</sub>)<sup>3-</sup> and (N<sub>2</sub>)<sup>2-</sup> products had previously been observed.<sup>19</sup>

**Unusual Structures of the Li(crypt)<sup>1+</sup> Cations.** Although the anions in **2-Ln** are not unusual, the cations contain a rare coordination environment for lithium in crypt: the metal is coordinated with an N<sub>2</sub>O<sub>4</sub> donor atom set. Usually, lithium has a NO<sub>5</sub> donor atom set in [Li(crypt)]<sup>1+</sup> cations.<sup>30-34</sup> Only one previous example of N<sub>2</sub>O<sub>4</sub> coordination has been reported in the literature.<sup>35</sup>

Lithium salts were also explored in ligand displacement reactions between lithium naphthalenide and Cp'<sub>3</sub>Tb and Cp'<sub>3</sub>Ho to determine the accessibility of compounds like [Cp'<sub>2</sub>Ln(η<sup>4</sup>-C<sub>10</sub>H<sub>8</sub>)]<sup>1-</sup>.<sup>36</sup> The naphthalenide products were not isolated, but these reactions gave crystals of two products, [Li(crypt)][Cp'<sub>4</sub>Tb], **4**, and [Li(crypt)][(Cp'<sub>3</sub>Ho)<sub>2</sub>(μ-H)], **5** (Figure 1.4), respectively, which are include here since few [Li(crypt)]<sup>1+</sup> salts have been crystallographically characterized. (Cp'<sub>4</sub>Ln)<sup>1-</sup> complexes are frequent by-products in rare-earth reduction reactions.<sup>36</sup> Hydrides are also observed by-products in rare-earth reduction systems.<sup>37</sup> Complex **4** has Li in an NO<sub>5</sub> coordination environment and **5** contains the first example of Li in an O<sub>6</sub> coordination environment in crypt, Figure 1.4.

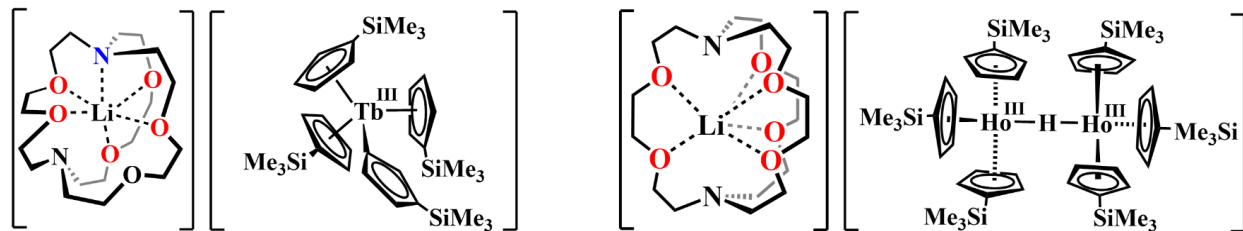


**Figure 1.4.** ChemDraw representations of **4** (left) and **5** (right) depicting Li in an NO<sub>5</sub> and O<sub>6</sub> coordination environment, respectively.



A full listing of all the Li–O and Li–N distances for the **2-Ln** complexes as well as all currently known complexes containing [Li(crypt)]<sup>1+</sup> cations is given in Table 1.4 of the *Structural Details* section of Chapter 1. The eight distances in these complexes span a wide range, but they fall into two sets, one group of six with short distances in a similar range and two distances that are more than 0.5 Å longer with most in the 3–5 Å range. For comparison, Table 1.2 lists the range of distances to the set of six donor atoms that have the shorter distances. The average Li–N and Li–O bond distances for the **2-Ln** complexes are similar to those reported for

**Table 1.2.** Li–O and Li–N bond distance ranges of complexes containing [Li(crypt)]<sup>1+</sup>.

Compound	Li–O (Å)	Li–N (Å)	N <sub>x</sub> O <sub>y</sub>
	<b>This Study</b>		
<b>2-Y</b>	2.061(7)-2.150(6)	2.437(7)-2.499(6)	N <sub>2</sub> O <sub>4</sub>
<b>2-Tb</b>	2.068(5)-2.159(4)	2.456(5)-2.474(4)	N <sub>2</sub> O <sub>4</sub>
<b>2-Dy</b>	2.06(1)-2.161(8)	2.44(1)-2.478(9)	N <sub>2</sub> O <sub>4</sub>
<b>2-Ho</b>	2.057(8)-2.158(7)	2.450(9)-2.485(8)	N <sub>2</sub> O <sub>4</sub>
<b>4</b>	2.082(6)-2.186(6)	2.233(4)	NO <sub>5</sub>
<b>5</b>	2.317(1)	--	O <sub>6</sub>
	<b>Previous Studies</b>		
[Li(crypt)] <sub>2</sub> [LiF <sub>2</sub> B(C <sub>2</sub> O <sub>4</sub> )] <sup>35</sup>	2.001(3)-2.187(4)	2.400(5)-2.443(4)	N <sub>2</sub> O <sub>4</sub>
	2.105(5)-2.405(3)	2.548(4)	NO <sub>5</sub>
[Li(crypt)][ClO <sub>4</sub> ] <sup>31</sup>	2.072(3)-2.497(3)	2.681(3)	NO <sub>5</sub>
[Li(crypt)] <sub>2</sub> [PtP <sub>4</sub> ] <sup>32</sup>	2.042(9)-2.64(1)	2.24(1)	NO <sub>5</sub>
	2.104(9)-2.617(9)	2.230(9)	NO <sub>5</sub>
[Li(crypt)][C <sub>5</sub> PMePh <sub>3</sub> ] <sup>34</sup>	2.093(8)-2.242(8)	2.244(8)	NO <sub>5</sub>
[Li(crypt)][C <sub>5</sub> P <sup>t</sup> BuPh <sub>3</sub> ] <sup>34</sup>	2.081(3)-2.246(3)	2.254(3)	NO <sub>5</sub>
[Li(crypt)][CoAlN <sub>2</sub> ] <sup>30</sup>	2.09(1)-2.425(7)	2.554(6)	NO <sub>5</sub>

[Li(crypt)]<sub>2</sub>[LiF<sub>2</sub>B(C<sub>2</sub>O<sub>4</sub>)], which contains one [Li(crypt)]<sup>1+</sup> cation with an N<sub>2</sub>O<sub>4</sub> donor atom set and the other with an NO<sub>5</sub> donor atom set.<sup>35</sup> Bond distances for previously reported complexes with the NO<sub>5</sub> donor atom set show large variability ranging from 2.042(9)-2.64(1) Å for Li–O and 2.230(9)-2.681(3) Å for Li–N. In contrast, as shown with **2-Ln**, the N<sub>2</sub>O<sub>4</sub> coordination sets

display rather similar distances from one compound to another. The bond distances in the NO<sub>5</sub> coordination environment in **4** fall into the broad range of previously observed values of NO<sub>5</sub>-coordinated complexes. The unique example of O<sub>6</sub> coordination observed in **5** is, interestingly, predicted to be the most stable coordination geometry for [Li(crypt)]<sup>1+</sup> by density functional calculations.<sup>31</sup>

**Magnetic Susceptibility Studies.** While the magnetic moments of traditional divalent 4f<sup>n+1</sup> ions can be predicted from the standard  $\mu_{\text{eff}} = g[J(J+1)]^{1/2}$  formula, in the case of the non-traditional divalent 4f<sup>n</sup>5d<sup>1</sup> ions, two models have been proposed by the group of Jeffery Long at UC Berkeley to describe the magnetic interaction of the 4f and 5d electrons.<sup>17, 38</sup> A “coupled model” assumes that spin-spin coupling is stronger than *L-S* coupling such that an overall spin of  $S_{\text{TOTAL}} = S_{4f} + 1/2$  is present, which couples to the orbital angular momentum, *L*, of the 4f electrons to produce a new *J* value, for which an expected magnetic moment can be calculated. An “uncoupled model” assumes that *L-S* coupling of the 4f electrons is much stronger than coupling of the 5d and 4f electrons. In this model, a predicted  $\chi_{\text{M}}T$  arises from the sum of the  $\chi_{\text{M}}T$  value expected for the 5d electron (*S* = 1/2) plus that calculated from the *J* value determined from *L-S* coupling of the 4f electrons. Magnetic measurements of the new lithium salts described here were used to further evaluate the ability of these models to assign electron configurations consistent with crystallographic, spectroscopic, and magnetic data.

Table 1.3 shows the magnetic data for the **2-Ln** complexes collected by Lucy E. Darago in the laboratory of Professor Jeffery R. Long at the University of California, Berkeley, along with data on the **1-Ln** series.<sup>17</sup> Calculated  $\chi_{\text{M}}T$  values for 4f<sup>n+1</sup> configurations as well as for the two models of the 4f<sup>n</sup>5d<sup>1</sup> configurations are also included.<sup>17</sup>

**Table 1.3.** Experimental and predicted (as described in text)  $\chi_{MT}$  products at 298 K for **1-Ln** and **2-Ln**.

	Exp. $\mu_{\text{eff}}^{\text{a}}$	Exp. $\chi_{MT}^{\text{b}}$	$\chi_{MT}$ ( $4f^n5d^1$ ) coupled	$\chi_{MT}$ ( $4f^n5d^1$ ) uncoupled	$\chi_{MT}$ ( $4f^{n+1}$ )
<b>1-Tb</b> <sup>17</sup>	10.48	13.73	14.42	12.20	14.13
<b>2-Tb</b>	10.58	13.99			
<b>1-Dy</b> <sup>17</sup>	11.35	16.10	17.01	14.51	14.07
<b>2-Dy</b>	11.35	16.10			
<b>1-Ho</b> <sup>17</sup>	11.41	16.26	16.9	14.45	11.48
<b>2-Ho</b>	11.67	17.01			

<sup>a</sup> Units of  $\mu_{\text{B}}$

<sup>b</sup> All  $\chi_{MT}$  data are reported in units of  $\text{emu} \cdot \text{K} / \text{mol}$  and were collected under a field of 0.1 T.

Complex **2-Tb** exhibits a  $\chi_{MT}$  product of  $13.99 \text{ emu K} \cdot \text{mol}^{-1}$  at 300 K, under an applied dc magnetic field of 0.1 T. This experimental room-temperature  $\chi_{MT}$  product is somewhat lower than the expected value of  $14.42 \text{ emu K} \cdot \text{mol}^{-1}$  for a Tb(II) ion with a coupled  $4f^85d^1$  electronic configuration. An “uncoupled”  $4f^85d^1$  configuration is unlikely given that its predicted  $\chi_{MT}$  product is substantially lower than that observed, while the crystallographic data are inconsistent with a  $4f^9$  traditional divalent assignment. The slightly lower-than-expected  $\chi_{MT}$  product may be attributed to strong crystal field splitting enforced by the cyclopentadienyl ligands, leading to incomplete population of the ground  $m_J$  manifold state even at room temperature. A similar  $\chi_{MT}$  product was observed for  $[\text{K}(\text{crypt})][\text{Cp}'_3\text{Tb}]$ , **1-Tb**.

Similar to **2-Tb**, complex **2-Dy** exhibits a room-temperature  $\chi_{MT}$  product of  $16.10 \text{ emu K} \cdot \text{mol}^{-1}$  under an applied dc magnetic field of 0.1 T, somewhat lower than the expected value of  $17.01 \text{ emu K} \cdot \text{mol}^{-1}$  for a Dy(II) ion with a coupled  $4f^95d^1$  electronic configuration. However, it is identical to that of the complex  $[\text{K}(\text{crypt})][\text{Cp}'_3\text{Dy}]$ , **1-Dy**, and, again, a coupled  $4f^95d^1$

electron configuration assignment is favored. The possibility of a multiconfigurational ground state may also be considered given the small energy difference between  $4f^{10}$  and  $4f^95d^1$  configurations anticipated for the Dy(II) ion.<sup>4</sup> The holmium complex, **2-Ho**, exhibits a  $\chi_{MT}$  product of  $17.01 \text{ emu K} \cdot \text{mol}^{-1}$  at 300 K, under an applied dc magnetic field of 0.1 T, in good agreement with the expected value of  $16.9 \text{ emu K} \cdot \text{mol}^{-1}$  for a Ho(II) ion with a coupled  $4f^{10}5d^1$  electronic configuration, and again consistent with the value observed for [K(crypt)][Cp'<sub>3</sub>Ho], **1-Ho**.

The  $11.35$  and  $11.67 \mu_B$  magnetic moments of **2-Dy** and **2-Ho** are additional examples of the large magnetic moments that can arise from the  $4f^n5d^1$  configurations of the Ln(II) ions in complexes such as **1-Ln** and **2-Ln**. These complexes can display such high magnetic moments due to the large sum of their  $S$  and  $L$  values, which results in a large ground state,  $J$ . Prior to the discovery of **1-Dy** and **1-Ho**, the highest magnetic moments observable for monometallic complexes arose from  $4f^9$  and  $4f^{10}$  configurations, with calculated values of  $10.60$  and  $10.63 \mu_B$ , respectively.<sup>39</sup> Complexes **2-Dy** and **2-Ho** demonstrate that the results of **1-Dy** and **1-Ho** can be extended to other systems, in this case, those with lithium counter-cations.

## Conclusion

Lithium has proven to be as effective as potassium in reducing Cp'<sub>3</sub>Ln complexes in the presence of 2.2.2-cryptand to form crystallographically-characterizable complexes, [Li(crypt)][Cp'<sub>3</sub>Ln], **2-Ln**, of Dy(II) as well as of the non-traditional Y(II), Tb(II), and Ho(II) ions. Complexes of the three later-lanthanide ions provide new examples on which to evaluate magnetic models for 4f-5d electron interactions in  $4f^n5d^1$  ions, and the Ho and Dy complexes provide new examples of single-ion magnetic moments over  $11 \mu_B$ .<sup>39</sup> Dy(II) and Ho(II) have magnetic ground states,  $J$ , that arise from their combined  $S$  and  $L$  values. The ions Dy(II) and

Ho(II) have the highest sums of  $S$  and  $L$  possible across both trivalent and non-traditional divalent lanthanide electron configurations, thereby yielding the highest possible magnetic moments according to the formula:  $\mu_{\text{eff}} = g[J(J+1)]^{1/2}$ . The  $(\text{Cp}'_3\text{Ln})^{1-}$  anions crystallize with  $[\text{Li}(\text{crypt})]^{1+}$  cations that display unusual  $\text{N}_2\text{O}_4$  donor atom coordination geometries. The first example of an  $\text{O}_6$  donor atom set in a  $[\text{Li}(\text{crypt})]^{1+}$  cation was also identifiable through these studies, found in the complex  $[\text{Li}(\text{crypt})][(\text{Cp}'_3\text{Ho})_2(\mu\text{-H})]$ , **5**. Comparison of reductions of  $\text{Cp}'_3\text{Y}$  with Li versus K under  $\text{N}_2$  show the importance of the specific alkali metal reductant and the temperature in generating reduced dinitrogen complexes.

### Experimental Details

All syntheses and manipulations described below were conducted under  $\text{N}_2$  or Ar with rigorous exclusion of air and water using glovebox, Schlenk-line, and high-vacuum-line techniques. All  $\text{Cp}'_3\text{Ln}$  ( $\text{Ln} = \text{Y},^2 \text{Tb},^3 \text{Dy},^4 \text{Ho}^{18}$ ) materials were prepared according to previously published literature. 2.2.2-Cryptand (4,7,13,16,21,24-hexaoxa-1,10-diazabicyclo[8.8.8]hexacosane, Aldrich) was placed under vacuum ( $10^{-3}$  Torr) for 12 h before use. Li metal (99+%) was purchased as granules from Strem and used as received.  $\text{Li}(\text{C}_{10}\text{H}_8)^{19}$  and  $[\text{Li}(18\text{-crown-6})(\text{THF}_2)][\text{C}_{14}\text{H}_{10}]^{20}$  were prepared according to the literature. Solvents were sparged with UHP Ar and dried over columns containing Q-5 and molecular sieves. Benzene- $d_6$  was dried over sodium-potassium alloy, degassed using three freeze-pump-thaw cycles, and vacuum transferred before use.  $^1\text{H}$  (500 MHz) NMR spectra were obtained on a Bruker GN500 or CRYO500 MHz spectrometer at 25 °C in benzene- $d_6$  unless otherwise stated. IR samples were prepared as KBr pellets on a Varian 1000 FT-IR or a Jasco FT/IR-4700 spectrometer. Elemental analyses were performed on a PerkinElmer series II 2400 CHNS analyzer. Electron

paramagnetic resonance spectra were collected using a Bruker EMX spectrometer equipped with an ER041XG microwave bridge in THF at 298 and 77 K.

**[Li(crypt)][Cp<sub>3</sub>Y], 2-Y.** In an argon-filled glovebox, a cold (−35 °C) yellow solution of Cp<sub>3</sub>Y (200 mg, 0.400 mmol) and 2.2.2-cryptand (150 mg, 0.40 mmol) in Et<sub>2</sub>O (3 mL) was added to a flask containing a smear of lithium metal. A dark maroon solution immediately formed. This solution was stirred for 15 min and filtered to remove excess lithium metal. The filtered solution was placed in a freezer at −35 °C. After 1 d, X-ray quality maroon crystals of **2-Y** were isolated and washed with cold Et<sub>2</sub>O (−35 °C) (102 mg, 28%). Crystalline yields are low due to the high solubility of these complexes. IR: 3078w, 3060w, 2947s, 2919m, 2884s, 2814m, 1477w, 1444w, 1399w, 1360m, 1354m, 1296m, 1256m, 1241s, 1175s, 1133s, 1105s, 1078s, 1057m, 1038s, 1006w, 981w, 951m, 931m, 923m, 906m, 833s, 767m, 750s, 684w, 679m, 642w, 629m cm<sup>−1</sup>. Anal. Calcd for C<sub>42</sub>H<sub>75</sub>LiN<sub>2</sub>O<sub>6</sub>Si<sub>3</sub>Y: C, 57.05; H, 8.55; N, 3.17. Found: C, 57.11; H, 8.92; N, 2.95.

**[Li(crypt)][Cp<sub>3</sub>Tb], 2-Tb.** As described for **2-Y**, a yellow solution of Cp<sub>3</sub>Tb (200 mg, 0.350 mmol) and 2.2.2-cryptand (132 mg, 0.35 mmol) added to excess Li produced a dark maroon solution. A solution of **2-Tb** in Et<sub>2</sub>O produced X-ray quality maroon crystals (102 mg, 31%). IR: 3080w, 3065w, 2949s, 2922m, 2883s, 2854m, 2818w, 1479w, 1470m, 1451m, 1435m, 1402w, 1375w, 1360m, 1302m, 1292m, 1238s, 1194w, 1175s, 1128m, 1111s, 1103s, 1080m, 1072m, 1038m, 945w, 930w, 924w, 903m, 831s, 806m, 762w, 745s, 679w, 629m cm<sup>−1</sup>. Anal. Calcd for C<sub>42</sub>H<sub>75</sub>LiN<sub>2</sub>O<sub>6</sub>Si<sub>3</sub>Tb: C, 52.87; H, 7.92.; N, 2.94. Found: C, 52.51; H, 7.75; N, 2.91.

**[Li(2.2.2-cryptand)][Cp<sub>3</sub>Dy], 2-Dy.** As described for **2-Y**, reaction of a yellow solution of Cp<sub>3</sub>Dy (200 mg, 0.35 mmol) and 2.2.2-cryptand (131 mg, 0.35 mmol) with excess Li

produced a dark maroon solution. A solution of **2-Dy** in Et<sub>2</sub>O produced X-ray quality maroon crystals (120 mg, 36%). IR: 3081w, 3052w, 2948s, 2924m, 2883s, 2814m, 2759w, 2730w, 1477w, 1459w, 1451m, 1446m, 1435m, 1399w, 1360m, 1301m, 1292m, 1269w, 1237s, 1196w, 1176s, 1132s, 1096s, 1079s, 1036s, 1010w, 1004w, 947m, 929m, 921m, 902s, 833s, 266m, 750s, 737s, 727s, 679m, 631m, 625m, 605w, 604w cm<sup>-1</sup>. Anal. Calcd for C<sub>42</sub>H<sub>75</sub>LiN<sub>2</sub>O<sub>6</sub>Si<sub>3</sub>Dy: C, 52.67; H, 7.89; N, 2.92. Found: C, 52.16; H, 7.76; N, 2.85.

**[Li(2.2.2-cryptand)][Cp'3Ho], 2-Ho.** As described for **2-Y**, addition of a yellow solution of Cp'3Ho (200 mg, 0.350 mmol) and 2.2.2-cryptand (131 mg, 0.35 mmol) to excess Li produced a dark maroon solution. A solution of **2-Ho** in Et<sub>2</sub>O produced X-ray quality maroon crystals (123 mg, 37%). IR: 3081w, 3060w, 2948s, 2923m, 2884s, 2816m 2757w, 2730w, 1477w, 1456w, 1445w, 1398w, 1361m, 1355m, 1310w, 1294m, 1255m, 1239s, 1176s, 1132s, 1105s, 1179s, 1038s, 1006w, 950m, 930m, 922w, 906m, 903m, 831s, 768m, 751s, 683w, 641w, 631m cm<sup>-1</sup>. Anal. Calcd for C<sub>42</sub>H<sub>75</sub>LiN<sub>2</sub>O<sub>6</sub>Si<sub>3</sub>Ho: C, 52.54; H, 7.87; N, 2.92. Found: C, 51.94; H, 7.84; N, 3.17.

**[Cp'2(THF)Y]<sub>2</sub>(μ-η<sup>2</sup>:η<sup>2</sup>-N<sub>2</sub>), 3.** This synthesis is an improved version of a previously published procedure.<sup>2</sup> An H-shaped tube (two 20 cm vertical tubes with 2 cm diameter connected at the center by a 15 cm horizontal tube with a 2 cm diameter containing a frit in the center) under N<sub>2</sub> was charged with THF (10 mL) on one side and Cp'3Y (200 mg, 0.399 mmol) with excess pinched Li pellets (8 mg, 1.2 mmol) on the other. THF was condensed onto the solids using a -78 °C dry ice bath. A dark purple solution immediately formed and was stirred for 1 h at -78 °C. The purple solution remains stable up to -35 °C, but warming to room temperature resulted in a light green solution. The H-tube was taken into an N<sub>2</sub> glovebox and the green solution was decanted from unreacted Li. Addition of hexanes (5 mL) formed a green

precipitate. Solvent was removed *in vacuo* and the solids were washed with hexanes yielding a light green powder, **3** (141 mg, 39%), identified by  $^1\text{H}$  NMR spectroscopy.<sup>2</sup>  $^1\text{H}$  NMR ( $\text{C}_6\text{D}_6$ ):  $\delta$  6.20 (t,  $\text{C}_5\text{H}_4\text{SiMe}_3$ , 8H), 5.94 (t,  $\text{C}_5\text{H}_4\text{SiMe}_3$ , 8H), 0.49 (s,  $\text{C}_5\text{H}_4\text{SiMe}_3$ , 36H). Full characterization of this complex is in the literature.<sup>2</sup>

**Magnetic Measurements.** Magnetic susceptibility data were obtained by SQUID magnetometry. Samples were prepared by adding crystalline powder of **2-Tb** (14.7 mg), **2-Dy** (15.1 mg), or **2-Ho** (13.4 mg) to a 5 mm inner diameter quartz tube containing a raised quartz platform. Solid eicosane was added to cover the sample to prevent crystallite torquing and provide good thermal contact between the sample and the cryostat. The tubes were fitted with Teflon sealable adapters, evacuated on a Schlenk line, and flame-sealed under static vacuum. Following flame sealing, the solid eicosane was melted in a water bath held at 40 °C. Magnetic susceptibility measurements were performed using a Quantum Design MPMS XL SQUID magnetometer. Dc magnetic susceptibility measurements were collected in the temperature range 2 – 300 K under applied magnetic fields of 0.1, 0.5, and 1 T. Diamagnetic corrections were applied to the data using Pascal's constants to give  $\chi_{\text{D}} = -0.00056909$  emu/mol (**2-Tb**),  $\chi_{\text{D}} = -0.00056909$  emu/mol (**2-Dy**),  $\chi_{\text{D}} = -0.00056909$  emu/mol (**2-Ho**), and  $\chi_{\text{D}} = -0.00024036$  emu/mol (eicosane).



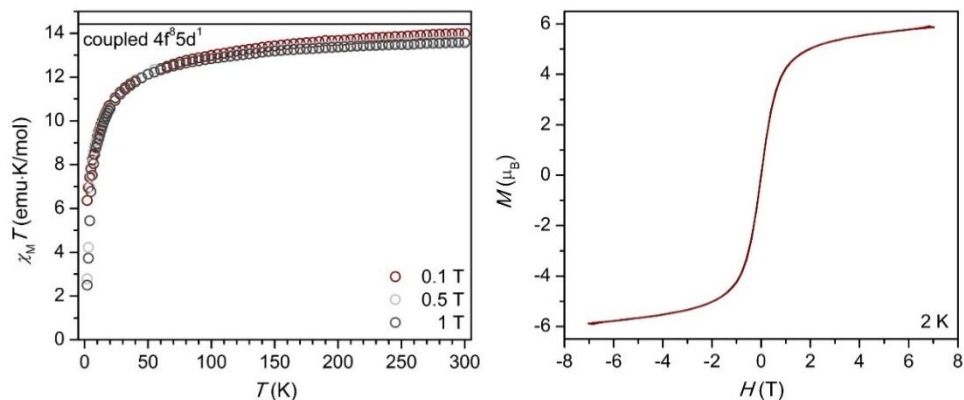


**Figure 1.5.** Plot of the magnetic susceptibility (left) times temperature ( $\chi_M T$ ) versus temperature (K) for **2-Tb** (red circles, 0.1 T; pink circles, 0.5 T, black circles, 1 T). Solid black line corresponds to the theoretical room temperature  $\chi_M T$  value for a coupled  $4f^8 5d^1$  electronic configuration. Magnetic hysteresis measurement (right) of **2-Tb** at 2 K.

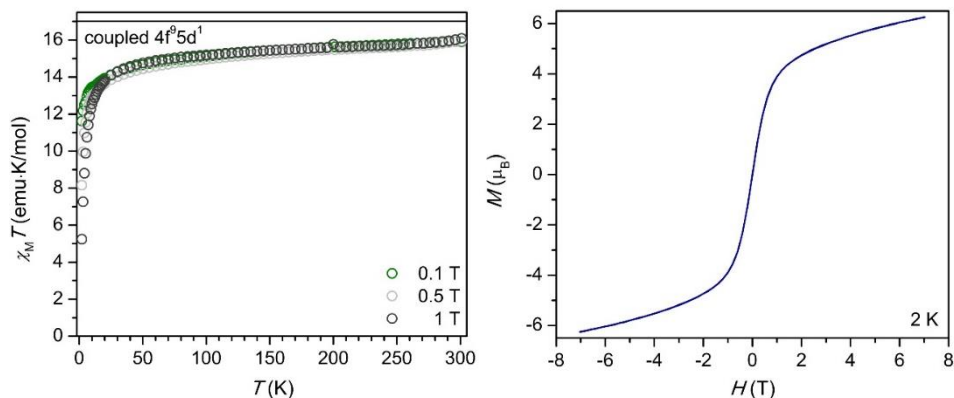


**Figure 1.6.** Plot of the magnetic susceptibility (left) times temperature ( $\chi_M T$ ) versus temperature (K) for **2-Dy** (green circles, 0.1 T; pink circles, 0.5 T, black circles, 1 T). Solid black line corresponds to the theoretical room temperature  $\chi_M T$  value for a coupled  $4f^9 5d^1$  electronic configuration. Magnetic hysteresis measurement (right) of **2-Dy** at 2 K.

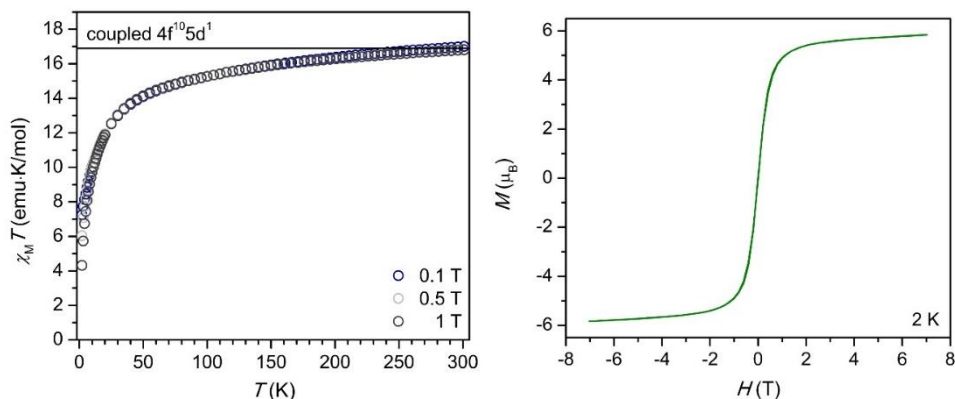


**Figure 1.7.** Plot of the magnetic susceptibility (left) times temperature ( $\chi_M T$ ) versus temperature (K) for **2-Ho** (blue circles, 0.1 T; pink circles, 0.5 T, black circles, 1 T). Solid black line corresponds to the theoretical room temperature  $\chi_M T$  value for a coupled  $4f^{10}5d^1$  electronic configuration. Magnetic hysteresis measurement (right) of **2-Ho** at 2 K.

**Comments on Magnetic Data of 2-Tb, 2-Dy, and 2-Ho.** Ac magnetic susceptibility measurements on **2-Tb**, **2-Dy**, and **2-Ho** collected at 2 K from 1 – 1500 Hz and under applied dc magnetic fields of 0-0.4 T did not reveal any out of-phase peaks, indicating an absence of slow magnetic relaxation behavior. The saturation magnetizations at 2 K and 7 T for **2-Tb**, **2-Dy**, and **2-Ho**, respectively, are  $5.87 \mu_B$ ,  $5.84 \mu_B$ , and  $6.25 \mu_B$ .

## Structural Details

**X-ray Data Collection, Structure Solution and Refinement for 2-Y, [Li(crypt)][Cp'3Y].** A purple crystal of approximate dimensions 0.169 x 0.322 x 0.440 mm was mounted in a cryoloop and transferred to a Bruker SMART APEX II diffractometer. The APEX2<sup>40</sup> program package was used to determine the unit-cell parameters and for data collection (20 sec/frame scan time for a sphere of diffraction data). The raw frame data was processed using SAINT<sup>41</sup> and SADABS<sup>42</sup> to yield the reflection data file. Subsequent calculations were carried out using the SHELXTL<sup>43</sup> program. There were no systematic absences nor any diffraction symmetry other than the Friedel condition. The centrosymmetric

triclinic space group  $P\bar{1}$  was assigned and later determined to be correct. The structure was solved using the coordinates of the isomorphous terbium complex and refined on  $F^2$  by full-matrix least-squares techniques. The analytical scattering factors<sup>44</sup> for neutral atoms were used throughout the analysis. Hydrogen atoms were included using a riding model. At convergence,  $wR2 = 0.1321$  and  $Goof = 0.980$  for 505 variables refined against 11220 data ( $0.80\text{\AA}$ ),  $R1 = 0.0525$  for those 7702 data with  $I > 2.0\sigma(I)$ . Based on the isomorphous terbium complex and from residual peaks observed in the difference-Fourier map, it appeared that tetrahydrofuran and diethylether solvent molecules were present. Suitable models for the disordered solvents were unsatisfactory so the SQUEEZE<sup>46a</sup> routine in the PLATON<sup>46b</sup> program package was used to account for the electrons in the solvent accessible voids.

**X-ray Data Collection, Structure Solution and Refinement for 2-Tb, [Li(crypt)][Cp'3Tb].** A purple crystal of approximate dimensions 0.268 x 0.275 x 0.335 mm was mounted on a glass fiber and transferred to a Bruker SMART APEX II diffractometer. The APEX2<sup>40</sup> program package was used to determine the unit-cell parameters and for data collection (20 sec/frame scan time for a sphere of diffraction data). The raw frame data was processed using SAINT<sup>41</sup> and SADABS<sup>42</sup> to yield the reflection data file. Subsequent calculations were carried out using the SHELXTL<sup>43</sup> program. There were no systematic absences nor any diffraction symmetry other than the Friedel condition. The centrosymmetric triclinic space group  $P\bar{1}$  was assigned and later determined to be correct. The structure was solved by dual space methods and refined on  $F^2$  by full-matrix least-squares techniques. The analytical scattering factors<sup>44</sup> for neutral atoms were used throughout the analysis. Hydrogen atoms were included using a riding model. There were tetrahydrofuran and diethylether solvent molecules present. One solvent void was included as a composition of  $\frac{1}{2}$  tetrahydrofuran and  $\frac{1}{2}$

diethylether. The other void contained a disordered diethylether located about an inversion center. Solvent molecules were included using partial site-occupancy-factors and isotropic thermal parameters. At convergence,  $wR2 = 0.0693$  and  $Goof = 1.072$  for 569 variables refined against 13425 data ( $0.73\text{\AA}$ ),  $R1 = 0.0262$  for those 12489 data with  $I > 2.0\sigma(I)$ .

**X-ray Data Collection, Structure Solution and Refinement for 2-Dy, [Li(crypt)][Cp'3Dy].** A purple crystal of approximate dimensions  $0.170 \times 0.176 \times 0.243$  mm was mounted on a glass fiber and transferred to a Bruker SMART APEX II diffractometer. The APEX2<sup>40</sup> program package was used to determine the unit-cell parameters and for data collection (20 sec/frame scan time for a sphere of diffraction data). The raw frame data was processed using SAINT<sup>41</sup> and SADABS<sup>42</sup> to yield the reflection data file. Subsequent calculations were carried out using the SHELXTL<sup>43</sup> program. There were no systematic absences nor any diffraction symmetry other than the Friedel condition. The centrosymmetric triclinic space group  $P\bar{1}$  was assigned and later determined to be correct. The structure was solved using the coordinates of the isomorphous terbium complex and refined on  $F^2$  by full-matrix least-squares techniques. The analytical scattering factors<sup>44</sup> for neutral atoms were used throughout the analysis. Hydrogen atoms were included using a riding model. At convergence,  $wR2 = 0.1199$  and  $Goof = 0.990$  for 505 variables refined against 13127 data ( $0.75\text{\AA}$ ),  $R1 = 0.0477$  for those 9880 data with  $I > 2.0\sigma(I)$ .

Based on the isomorphous terbium complex and from residual peaks observed in the difference-Fourier map, it appeared that tetrahydrofuran and diethylether solvent molecules were present. Suitable models for the disordered solvents were unsatisfactory so the SQUEEZE<sup>46a</sup> routine in the PLATON<sup>46b</sup> program package was used to account for the electrons in the solvent accessible voids.

**X-ray Data Collection, Structure Solution and Refinement for 2-Ho, [Li(crypt)][Cp'3Ho].** A purple crystal of approximate dimensions 0.171 x 0.176 x 0.337 mm was mounted in a cryoloop and transferred to a Bruker SMART APEX II diffractometer. The APEX2<sup>40</sup> program package was used to determine the unit-cell parameters and for data collection (30 sec/frame scan time for a sphere of diffraction data). The raw frame data was processed using SAINT<sup>41</sup> and SADABS<sup>42</sup> to yield the reflection data file. Subsequent calculations were carried out using the SHELXTL<sup>43</sup> program. There were no systematic absences nor any diffraction symmetry other than the Friedel condition. The centrosymmetric triclinic space group  $P\bar{1}$  was assigned and later determined to be correct. The structure was solved using the coordinates of the isomorphous terbium complex and refined on  $F^2$  by full-matrix least-squares techniques. The analytical scattering factors<sup>44</sup> for neutral atoms were used throughout the analysis. Hydrogen atoms were included using a riding model. At convergence,  $wR2 = 0.0858$  and  $Goof = 1.000$  for 505 variables refined against 11160 data (0.80Å),  $R1 = 0.0371$  for those 9028 data with  $I > 2.0\sigma(I)$ . Based on the isomorphous terbium complex and from residual peaks observed in the difference-Fourier map, it appeared that tetrahydrofuran and diethylether solvent molecules were present. Suitable models for the disordered solvents were unsatisfactory so the SQUEEZE<sup>46a</sup> routine in the PLATON<sup>46b</sup> program package was used to account for the electrons in the solvent accessible voids.

**X-ray Data Collection, Structure Solution and Refinement for 4, [Li(crypt)][Cp'4Tb].** A blue crystal of approximate dimensions 0.220 x 0.338 x 0.419 mm was mounted in a cryoloop and transferred to a Bruker SMART APEX II diffractometer. The APEX2<sup>40</sup> program package was used to determine the unit-cell parameters and for data collection (15 sec/frame scan time for a sphere of diffraction data). The raw frame data was

processed using SAINT<sup>41</sup> and SADABS<sup>42</sup> to yield the reflection data file. Subsequent calculations were carried out using the SHELXTL<sup>43</sup> program. There were no systematic absences nor any diffraction symmetry other than the Friedel condition. The centrosymmetric triclinic space group  $P\bar{1}$  was assigned and later determined to be correct. The structure was solved by direct methods and refined on  $F^2$  by full-matrix least-squares techniques. The analytical scattering factors<sup>44</sup> for neutral atoms were used throughout the analysis. H(26A) was located from a difference-Fourier map and refined (x,y,z, riding  $U_{iso}$ ). All remaining hydrogen atoms were included using a riding model. At convergence,  $wR2 = 0.0722$  and  $Goof = 1.049$  for 592 variables refined against 13743 data ( $0.73\text{\AA}$ ),  $R1 = 0.0281$  for those 12535 data with  $I > 2.0\sigma(I)$ .

**X-ray Data Collection, Structure Solution and Refinement for 5, [Li(crypt)][(Cp'zHo)2 $\mu$ -H].** A brown crystal of approximate dimensions 0.260 x 0.339 x 0.400 mm was mounted in a cryoloop and transferred to a Bruker SMART APEX II diffractometer. The APEX2<sup>40</sup> program package was used to determine the unit-cell parameters and for data collection (20 sec/frame scan time for a hemisphere of diffraction data). The raw frame data was processed using SAINT<sup>41</sup> and SADABS<sup>42</sup> to yield the reflection data file. Subsequent calculations were carried out using the SHELXTL<sup>43</sup> program. The systematic absences were consistent with the cubic space group  $P4_132$  that was later determined to be correct. The structure was solved by dual space methods and refined on  $F^2$  by full-matrix least-squares techniques. The analytical scattering factors<sup>44</sup> for neutral atoms were used throughout the analysis. Hydrogen atoms located from a difference-map and refined (xyz and  $U_{iso}$ ). The molecule and counter-ion were located on sites of 32 symmetry. Least-squares analysis yielded  $wR2 = 0.0324$  and  $Goof = 1.054$  for 203 variables refined against 3591 data ( $0.78\text{\AA}$ ),  $R1 =$

0.0132 for those 3435 data with  $I > 2.0\sigma(I)$ . The absolute structure was assigned by refinement of the Flack parameter<sup>45</sup>. There were residuals present in the final difference-Fourier map. The SQUEEZE<sup>46a</sup> routine in the PLATON<sup>46b</sup> program package was used to account for the electrons in the solvent accessible voids.

**Table 1.4.** Listing of all the Li–O and Li–N distances (Å) for the [Li(crypt)][Cp'3Ln] (**2-Ln**), [Li(crypt)][Cp'4Tb] (**4**), and [Li(crypt)][(Cp'3Ho)<sub>2</sub>(*u*-H)] (**5**) complexes and all currently known complexes containing [Li(crypt)]<sup>1+</sup> cations. Longer distances are highlighted in gray.

<b>This Work</b>	O1	O2	O3	O4	O5	O6	N1	N2	N <sub>x</sub> O <sub>y</sub>
[Li(crypt)][Cp'3Y]	2.128	2.061	2.078	2.150	3.810	4.652	2.437	2.499	N <sub>2</sub> O <sub>4</sub>
[Li(crypt)][Cp'3Tb]	2.122	2.068	2.068	2.159	3.786	4.658	2.474	2.456	N <sub>2</sub> O <sub>4</sub>
[Li(crypt)][Cp'3Dy]	2.140	2.080	2.058	2.161	3.802	4.645	2.444	2.478	N <sub>2</sub> O <sub>4</sub>
[Li(crypt)][Cp'3Ho]	2.114	2.057	2.073	2.158	3.807	4.644	2.450	2.485	N <sub>2</sub> O <sub>4</sub>
[Li(crypt)][Cp'4Tb]	2.186	2.082	2.161	2.110	2.103	4.465	2.233	3.551	NO <sub>5</sub>
[Li(crypt)][(Cp'3Ho) <sub>2</sub> ( <i>u</i> -H)]	2.317	2.317	2.317	2.317	2.317	2.317	2.846	2.846	O <sub>6</sub>
<b>Other Work</b>									
[Li(crypt)][ClO <sub>4</sub> ] <sup>31</sup>	2.326	2.265	2.076	2.933	2.497	2.072	2.681	3.030	NO <sub>5</sub>
[Li(crypt)] <sub>2</sub> [PtP <sub>4</sub> ] <sup>32</sup>	2.140	2.133	4.387	2.638	2.155	2.042	2.238	3.568	NO <sub>5</sub>
	2.104	2.175	3.694	2.617	2.180	2.126	2.230	3.616	NO <sub>5</sub>
[Li(crypt)][C <sub>5</sub> P(Ph <sub>3</sub> )]THF <sup>34</sup>	2.148	2.115	2.093	2.242	2.197	4.414	2.244	3.489	NO <sub>5</sub>
[Li(crypt)][C <sub>5</sub> P(Ph <sub>3</sub> )] <sup>34</sup>	2.246	2.083	2.181	2.108	2.081	4.397	2.254	3.478	NO <sub>5</sub>
[Li(crypt)][CoAlN <sub>2</sub> ] <sup>30</sup>	2.114	2.425	2.091	3.928	2.151	2.215	3.264	2.554	NO <sub>5</sub>
[Li(crypt)] <sub>2</sub> [Liboro(oxalates)] <sup>35</sup>	2.157	2.025	2.001	2.187	4.561	3.957	2.400	2.443	N <sub>2</sub> O <sub>4</sub>
	2.346	2.339	2.405	2.175	2.105	2.946	2.548	3.005	NO <sub>5</sub>

## References

- (1) Hitchcock, P. B.; Lappert, M. F.; Maron, L.; Protchenko, A. V. Lanthanum Does Form Stable Molecular Compounds in the +2 Oxidation State. *Angew.Chem. Int. Ed.* **2008**, *47*, 1488-1491.
- (2) MacDonald, M. R.; Ziller, J. W.; Evans, W. J. Synthesis of a Crystalline Molecular Complex of Y<sup>2+</sup>, [(18-crown-6)K][(C<sub>5</sub>H<sub>4</sub>SiMe<sub>3</sub>)<sub>3</sub>Y]. *J. Am. Chem. Soc.* **2011**, *133*, 15914-15917.
- (3) MacDonald, M. R.; Bates, J. E.; Ziller, J. W.; Furche, F.; Evans, W. J. Completing the Series of +2 Ions for the Lanthanide Elements: Synthesis of Molecular Complexes of Pr<sup>2+</sup>, Gd<sup>2+</sup>, Tb<sup>2+</sup>, and Lu<sup>2+</sup>. *J. Am. Chem. Soc.* **2013**, *135*, 9857-9868.
- (4) Fieser, M. E.; MacDonald, M. R.; Krull, B. T.; Bates, J. E.; Ziller, J. W.; Furche, F.; Evans, W. J. Structural, Spectroscopic, and Theoretical Comparison of Traditional vs Recently

Discovered Ln<sup>2+</sup> Ions in the [K(2.2.2-cryptand)][(C<sub>5</sub>H<sub>4</sub>SiMe<sub>3</sub>)<sub>3</sub>Ln] Complexes: The Variable Nature of Dy<sup>2+</sup> and Nd<sup>2+</sup>. *J. Am. Chem. Soc.* **2015**, *137*, 369-382.

(5) Fieser, M. E. Dissertation. Spectroscopic and Computational Analysis of Rare Earth and Actinide Complexes In Unusual Coordination Environments and Oxidation States. University of California, Irvine, 2015.

(6) Windorff, C. J.; MacDonald, M. R.; Meihaus, K. R.; Ziller, J. W.; Long, J. R.; Evans, W. J. Expanding the Chemistry of Molecular U<sup>2+</sup> Complexes: Synthesis, Characterization, and Reactivity of the {[C<sub>5</sub>H<sub>3</sub>(SiMe<sub>3</sub>)<sub>2</sub>]<sub>3</sub>U}<sup>-</sup> Anion. *Chemistry – A European Journal* **2016**, *22*, 772-782.

(7) Gun'ko, Y. K.; Hitchcock, P. B.; Lappert, M. F. Activation of a C-O bond by reaction of a tris(cyclopentadienyl)lanthanide complex with an alkali metal in dimethoxyethane (DME); crystal structures of [Nd{η-C<sub>5</sub>H<sub>3</sub>(SiMe<sub>3</sub>)<sub>2-1,3</sub>}<sub>2</sub>(μ-OMe)<sub>2</sub>Li(DME)] and [{Ce(η-C<sub>5</sub>H<sub>3</sub><sup>t</sup>Bu<sub>2-1,3</sub>)<sub>2</sub>(μ-OMe)}<sub>2</sub>]. *J. Organomet. Chem.* **1995**, *499*, 213-219.

(8) Cassani, M. C.; Duncalf, D. J.; Lappert, M. F. The First Example of a Crystalline Subvalent Organolanthanum Complex: [K([18]crown-6)- (η<sup>2</sup>-C<sub>6</sub>H<sub>6</sub>)<sub>2</sub>][(LaCp<sup>t</sup>)<sub>2</sub>(μ-η<sup>6</sup>:η<sup>6</sup>-C<sub>6</sub>H<sub>6</sub>)]•2C<sub>6</sub>H<sub>6</sub> (Cp<sup>t</sup> = η<sup>5</sup>-C<sub>5</sub>H<sub>3</sub>Bu<sup>t</sup><sub>2-1,3</sub>). *J. Am. Chem. Soc.* **1998**, *120*, 12958-12959.

(9) Jaroschik, F.; Nief, F.; Le Goff, X.-F.; Ricard, L. Isolation of Stable Organodysprosium(II) Complexes by Chemical Reduction of Dysprosium(III) Precursors. *Organometallics* **2007**, *26*, 1123-1125.

(10) Jaroschik, F.; Momin, A.; Nief, F.; Le Goff, X.-F.; Deacon, G. B.; Junk, P. C. Dinitrogen Reduction and C-H Activation by the Divalent Organoneodymium Complex [(C<sub>5</sub>H<sub>2</sub><sup>t</sup>Bu<sub>3</sub>)<sub>2</sub>Nd(μ-I)K([18]crown-6)]. *Angew. Chem.* **2009**, *121*, 1137-1141.

(11) Fieser, M. E.; Palumbo, C. T.; La Pierre, H. S.; Halter, D. P.; Voora, V. K.; Ziller, J. W.; Furche, F.; Meyer, K.; Evans, W. J. Comparisons of lanthanide/actinide +2 ions in a tris(aryloxy)arene coordination environment. *Chemical Science* **2017**, *8*, 7424-7433.

(12) Evans, W. J.; Dominguez, R.; Levan, K. R.; Doedens, R. J. Synthesis and X-ray crystal structure of a dialkyldicyclopentadienylyttrium complex: {(C<sub>5</sub>H<sub>5</sub>)<sub>2</sub>Y[CH<sub>2</sub>Si(CH<sub>3</sub>)<sub>3</sub>]<sub>2</sub>Li<sub>2</sub>(CH<sub>3</sub>OCH<sub>2</sub>CH<sub>2</sub>OCH<sub>3</sub>)<sub>2</sub>(C<sub>4</sub>H<sub>8</sub>O<sub>2</sub>)}. *Organometallics* **1985**, *4*, 1836-1841.

(13) Lappert, M. F.; Singh, A.; Engelhardt, L. M.; White, A. H. X-ray structure of a derivative of the “simplest metallocene: Cyclopentadienyllithium”, [Li{η-C<sub>5</sub>H<sub>4</sub>(SiMe<sub>3</sub>)}{NMe<sub>2</sub>(CH<sub>2</sub>)<sub>2</sub>NMe<sub>2</sub>}] (i.e., LiCp'(TMEDA)). *J. Organomet. Chem.* **1984**, *262*, 271-278.

(14) Zheng, P.; Hong, J.; Liu, R.; Zhang, Z.; Pang, Z.; Weng, L.; Zhou, X. Synthesis and Reactivities of Guanidinate Dianion Complexes of Heterobimetallic Lanthanide–Lithium Cp<sub>2</sub>Ln[(CyN)<sub>2</sub>CNPh]Li(THF)<sub>3</sub>. *Organometallics* **2010**, *29*, 1284-1289.



- (15) Lu, X.-H.; Ma, M.-T.; Yao, Y.-M.; Zhang, Y.; Shen, Q. Controlled synthesis of lanthanide–lithium inverse crown ether complexes. *Inorg. Chem. Commun.* **2010**, *13*, 1566-1568.
- (16) Qian, C.; Zhang, X.; Zhang, Y.; Shen, Q. Heterobimetallic complexes of lanthanide and lithium metals with dianionic guanidinate ligands: Syntheses, structures and catalytic activity for amidation of aldehydes with amines. *J. Organomet. Chem.* **2010**, *695*, 747-752.
- (17) Meihaus, K. R.; Fieser, M. E.; Corbey, J. F.; Evans, W. J.; Long, J. R. Record High Single-Ion Magnetic Moments Through  $4f^n5d^1$  Electron Configurations in the Divalent Lanthanide Complexes  $[(C_5H_4SiMe_3)_3Ln]^-$ . *J. Am. Chem. Soc.* **2015**, *137*, 9855-60.
- (18) MacDonald, M. R.; Bates, J. E.; Fieser, M. E.; Ziller, J. W.; Furche, F.; Evans, W. J. Expanding Rare-Earth Oxidation State Chemistry to Molecular Complexes of Holmium(II) and Erbium(II). *J. Am. Chem. Soc.* **2012**, *134*, 8420-8423.
- (19) Screttas, C. G.; Micha-Screttas, M. Single-titration method for the determination of lithium naphthalenide in tetrahydrofuran. *J. Organomet. Chem.* **1983**, *252*, 263-265.
- (20) Castillo, M.; Metta-Magaña, A. J.; Fortier, S. Isolation of gravimetrically quantifiable alkali metal arenides using 18-crown-6. *New J. Chem.* **2016**, *40*, 1923-1926.
- (21) Huh, D. N.; Kotyk, C. M.; Gembicky, M.; Rheingold, A. L.; Ziller, J. W.; Evans, W. J. Synthesis of rare-earth-metal-in-cryptand dications,  $[Ln(2.2.2\text{-cryptand})]^{2+}$ , from  $Sm^{2+}$ ,  $Eu^{2+}$ , and  $Yb^{2+}$  silyl metallocenes  $(C_5H_4SiMe_3)_2Ln(THF)_2$ . *Chem. Commun.* **2017**, *53*, 8664-8666.
- (22) Stoll, S.; Schweiger, A. EasySpin, a comprehensive software package for spectral simulation and analysis in EPR. *J. Magn. Reson.* **2006**, *128*, 42-55.
- (23) Lorenz, S. E.; Schmiede, B. M.; Lee, D. S.; Ziller, J. W.; Evans, W. J. Synthesis and Reactivity of Bis(tetramethylcyclopentadienyl) Yttrium Metallocenes Including the Reduction of  $Me_3SiN_3$  to  $[(Me_3Si)_2N]^-$  with  $[(C_5Me_4H)_2Y(THF)]_2(\mu-\eta^2:\eta^2-N_2)$ . *Inorg. Chem.* **2010**, *49*, 6655-6663.
- (24) Evans, W. J.; Fang, M.; Zucchi, G.; Furche, F.; Ziller, J. W.; Hoekstra, R. M.; Zink, J. I. Isolation of Dysprosium and Yttrium Complexes of a Three-Electron Reduction Product in the Activation of Dinitrogen, the  $(N_2)^{3-}$  Radical. *J. Am. Chem. Soc.* **2009**, *131*, 11195-11202.
- (25) Evans, W. J.; Lee, D. S.; Rego, D. B.; Perotti, J. M.; Kozimor, S. A.; Moore, E. K.; Ziller, J. W. Expanding Dinitrogen Reduction Chemistry to Trivalent Lanthanides via the  $LnZ_3$ /Alkali Metal Reduction System: Evaluation of the Generality of Forming  $Ln_2(\mu-\eta^2:\eta^2-N_2)$  Complexes via  $LnZ_3/K$ . *J. Am. Chem. Soc.* **2004**, *126*, 14574-14582.
- (26) Evans, W. J.; Lee, D. S.; Ziller, J. W. Reduction of Dinitrogen to Planar Bimetallic  $M_2(\mu-\eta^2:\eta^2-N_2)$  Complexes of Y, Ho, Tm, and Lu Using the  $K/Ln[N(SiMe_3)_2]_3$  Reduction System. *J. Am. Chem. Soc.* **2004**, *126*, 454-455.

- (27) Fieser, M. E.; Woen, D. H.; Corbey, J. F.; Mueller, T. J.; Ziller, J. W.; Evans, W. J. Raman spectroscopy of the N-N bond in rare earth dinitrogen complexes. *Dalton Trans.* **2016**, 45, 14634-14644.
- (28) MacDonald, M. R. Dissertation. Expanding the Redox Chemistry of Yttrium, the Lanthanides, and Uranium through Synthesis and Reactivity of Bis-, Tris-, and Tetrakis-(Trimethylsilylcyclopentadienyl) Complexes. University of California, Irvine, 2013.
- (29) Fang, M.; Lee, D. S.; Ziller, J. W.; Doedens, R. J.; Bates, J. E.; Furche, F.; Evans, W. J. Synthesis of the  $(N_2)^{3-}$  Radical from  $Y^{2+}$  and Its Protonolysis Reactivity To Form  $(N_2H_2)^{2-}$  via the  $Y[N(SiMe_3)_2]_3/KC_8$  Reduction System. *J. Am. Chem. Soc.* **2011**, 133, 3784-3787.
- (30) Rudd, P. A.; Planas, N.; Bill, E.; Gagliardi, L.; Lu, C. C. Dinitrogen Activation at Iron and Cobalt Metallaluminatranes. *Eur. J. Inorg. Chem.* **2013**, 2013, 3898-3906.
- (31) Guzei, I. A.; Spencer, L. C.; Su, J. W.; Burnette, R. R. Low-temperature enantiotropic  $k_2$  phase transition in the ionic 222-cryptand complex with  $LiClO_4$ . *Acta Cryst.* **2007**, 63, 93-100.
- (32) Tirla, C.; Mézailles, N.; Ricard, L.; Mathey, F.; Le Floch, P. Dianionic Platinadiphospholene Complexes. *Inorg. Chem.* **2002**, 41, 6032-6037.
- (33) Olsher, U.; Izatt, R. M.; Bradshaw, J. S.; Dalley, N. K. Coordination chemistry of lithium ion: a crystal and molecular structure review. *Chem. Rev.* **1991**, 91, 137-164.
- (34) Moores, A.; Ricard, L.; Le Floch, P.; Mézailles, N. First X-ray Crystal Study and DFT Calculations of Anionic  $\lambda^4$ -Phosphinines. *Organometallics* **2003**, 22, 1960-1966.
- (35) Han, S.-D.; Allen, J. L.; Jónsson, E.; Johansson, P.; McOwen, D. W.; Boyle, P. D.; Henderson, W. A. Solvate Structures and Computational/Spectroscopic Characterization of Lithium Difluoro(oxalato)borate ( $LiDFOB$ ) Electrolytes. *J. Phys. Chem. C* **2013**, 117, 5521-5531.
- (36) Kotyk, C. M.; MacDonald, M. R.; Ziller, J. W.; Evans, W. J. Reactivity of the  $Ln^{2+}$  Complexes  $[K(2.2.2\text{-cryptand})][(C_5H_4SiMe_3)_3Ln]$ : Reduction of Naphthalene and Biphenyl. *Organometallics* **2015**, 34, 2287-2295.
- (37) Gun'ko, Y. K.; Hitchcock, P. B.; Lappert, M. F. Nonclassical Organolanthanoid Metal Chemistry:  $[K([18\text{-crown-6})(\eta^2\text{-PhMe})_2]X$  ( $X = [(LnCp^t)_2(\mu\text{-H})]$ ,  $[(LnCp''_2)_2(\mu\text{-}\eta^6\text{-PhMe})]$ ) from  $[LnCp^x_3]$ , K, and [18]-crown-6 in Toluene ( $Ln = La, Ce$ ;  $Cp^t = \eta^5\text{-C}_5\text{H}_4\text{SiMe}_2\text{Bu}^t$ ;  $Cp'' = \eta^5\text{-C}_5\text{H}_3(\text{SiMe}_3)_2\text{-1,3}$ ). *Organometallics* **2000**, 19, 2832-2834.
- (38) Anderson, D. M.; Cloke, F. G. N.; Cox, P. A.; Edelstein, N.; Green, J. C.; Pang, T.; Sameh, A. A.; Shalimoff, G. On the stability and bonding in bis( $\eta$ -arene)lanthanide complexes. *J. Chem. Soc., Chem. Commun.* **1989**, 53-55.

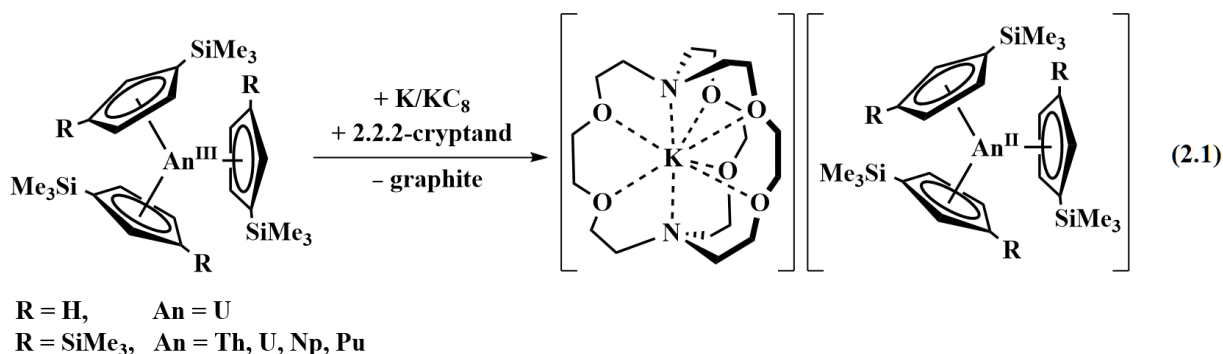
- (39) Jiang, S.-D.; Wang, B.-W.; Gao, S. In *Molecular Nanomagnets and Related Phenomena*; Gao, S., Ed.; Springer Berlin Heidelberg: Berlin, Heidelberg, 2015; pp 111-141.
- (40) APEX2 Version 2014.11-0, Bruker AXS, Inc.; Madison, WI 2014.
- (41) SAINT Version 8.34a, Bruker AXS, Inc.; Madison, WI 2013.
- (42) Sheldrick, G. M. SADABS, Version 2014/5, Bruker AXS, Inc.; Madison, WI 2014.
- (43) Sheldrick, G. M. SHELXTL, Version 2014/7, Bruker AXS, Inc.; Madison, WI 2014.
- (44) International Tables for Crystallography 1992, Vol. C., Dordrecht: Kluwer Academic Publishers.
- (45) Parsons, S., Flack, H. D., Wagner, T. Use of intensity quotients and differences in absolute structure refinement. *Acta Cryst.* **2013**, B69, 249-259.
- (46) (a) Spek, A.L. PLATON SQUEEZE: a tool for the calculation of the disordered solvent contribution to the calculated structure factors. *Acta Cryst.* **2015**, C71, 9-19., (b) Spek, A. L. Structure validation in chemical crystallography. *Acta. Cryst.* **2009**, D65, 148-155

## CHAPTER 2

### Chelate-Free Synthesis of the U(II) Complex, $[(C_5H_3(SiMe_3)_2)_3U]^{1-}$ , using Li and Cs Reductants and Comparative Studies of La(II) and Ce(II) Analogs

#### Introduction\*

One of the fundamental properties of any element is the range of oxidation states accessible for molecular chemistry. The range of oxidation states accessible to the actinide metals was expanded by the discovery of the first crystalline molecular examples of complexes containing the Th(II),<sup>1</sup> U(II),<sup>2-4</sup> Pu(II),<sup>5</sup> and Np(II)<sup>6</sup> ions as well as solution reductive chemistry consistent with Np(II).<sup>7</sup> Many of these complexes were obtained by reduction of tris(silyl-substituted)cyclopentadienyl actinide complexes,  $Cp''_3An$  [ $An = Th, U, Pu, Np$ ;  $Cp'' = C_5H_3(SiMe_3)_2$ ] and  $Cp'_3U$  ( $Cp' = C_5H_4SiMe_3$ ), with potassium in the presence of a chelate, 2.2.2-cryptand (crypt), generating  $[K(crypt)][Cp''_3An]$  and  $[K(crypt)][Cp'_3U]$ , eq 2.1.



A U(II) complex was also synthesized by reduction of the U(III) tris(aryloxy)mesitylene ligated complex,  $[(^{Ad,Me}ArO)_3mes]U$ , again with potassium in the presence of crypt<sup>3</sup>. However, Meyer and coworkers have also shown the reversible U(III)/U(II) electrochemical reduction

\*Portions of this chapter have been published: Huh, D. N.; Ziller, J. W.; Evans, W. J. Chelate-Free Synthesis of the U(II) Complex,  $[(C_5H_3(SiMe_3)_2)_3U]^{1-}$ , using Li and Cs Reductants and Comparative Studies of La(II) and Ce(II) Analogs. *Inorg. Chem.*, **2018**, 57, 11809-11814. DOI: 10.1021/acs.inorgchem.8b01966

without the support of  $[\text{K}(\text{crypt})]^{1+}$  in solution.<sup>8</sup> The  $(\text{Cp}''_3\text{U})^{1-}$  anion in eq 2.1 was also isolated in crystalline form by reduction with potassium and sodium in the presence of crown ethers, *i.e.*, as salts of  $[\text{K}(\text{18-crown-6})(\text{THF})_2]^{1+}$ ,  $[\text{Na}(\text{18-crown-6})(\text{THF})_2]^{1+}$ , and  $[\text{Na}(\text{12-crown-4})_2]^{1+}$ .<sup>4</sup>

In general, it had been assumed that the crypt and crown chelates add stability to these highly reactive An(II) complexes by sequestering the alkali metal cations which aids in the isolation of crystalline products. These chelates were also used to make analogous lanthanide complexes,  $[\text{M}(\text{chelate})][\text{Cp}^x_3\text{Ln}]$  where  $\text{M} = \text{Li}, \text{Na}, \text{K}$ ;<sup>9, 10</sup> chelate = 2.2.2-cryptand, 18-crown-6;  $\text{Cp}^x = \text{Cp}'$ ,<sup>9-13</sup>  $\text{Cp}''$ ,<sup>14</sup>  $\text{C}_5\text{H}_3(\text{CMe}_3)_2$ ,<sup>15, 16</sup> and  $\text{C}_5\text{H}_2(\text{CMe}_3)_3$ ,<sup>17, 18</sup>;  $\text{Ln} = \text{lanthanide and yttrium}$ .

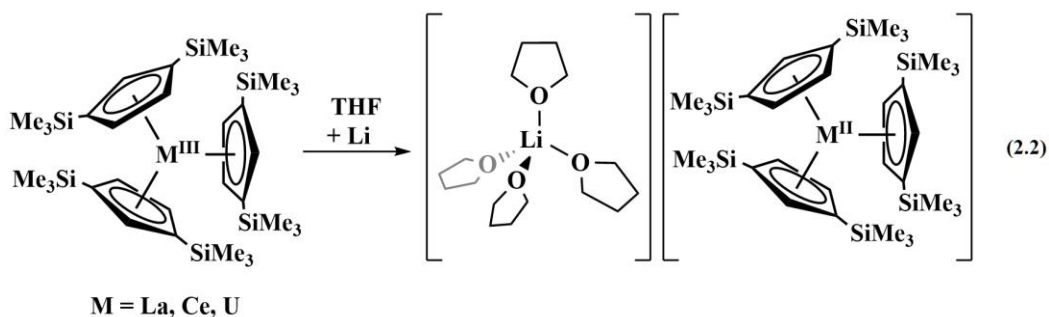
The synthesis of An(II) complexes of the transuranic metals, *e.g.* Np, Pu, and Am, is challenging due to the radioactivity of these elements. The reactions generally are conducted on a small scale for both logistical and safety reasons. Since some of these elements are available in only small amounts, it is desirable to minimize the number of experiments conducted and to optimize the reaction conditions. Success in the synthesis of  $[\text{K}(\text{2.2.2-cryptand})][\text{Cp}''_3\text{Pu}]^5$  was aided by prior examination of analogous lanthanide reactions with the larger lanthanides, La and Ce, that have radial sizes similar to those of the actinides.<sup>19</sup>

One goal of this research was to develop new options for synthesizing complexes of An(II) ions particularly using alkali metals other than the common Na and K and exploring reactions in which the alkali metal chelate is not present. It was found that Li could be a viable reducing agent for the formation of Ln(II) complexes.<sup>13</sup> Here, it is discussed how lithium can also be used to make isolable U(II) complexes *in the absence of a chelate*. The chelate-free reaction was first investigated with the uranium mimics, La and Ce, and these complexes are also described here. The efficacy of the largest non-radioactive alkali metal, cesium, was also evaluated in the absence of chelates. Color changes consistent with reduction are observed in

these cases and a crystallographically-characterizable product was isolated as a polymeric U(II) complex.

## Results and Discussion

**The Actinide Mimics, La and Ce.**  $\text{Cp}''_3\text{La}$  and  $\text{Cp}''_3\text{Ce}$  are reduced by lithium in the absence of a chelating agent in THF to form the La(II) and Ce(II) complexes,  $[\text{Li}(\text{THF})_4][\text{Cp}''_3\text{La}]$ , **6-La**, and  $[\text{Li}(\text{THF})_4][\text{Cp}''_3\text{Ce}]$ , **6-Ce**, respectively, eq 2.2. Each complex has an intense maroon



color as was previously observed for the  $[\text{K}(\text{crypt})]^{1+}$  salts of the La(II) and Ce(II) complexes,  $[\text{K}(\text{crypt})][\text{Cp}'_3\text{Ln}]^{10}$  and  $[\text{K}(\text{crypt})][\text{Cp}''_3\text{Ln}]$ .<sup>10, 14</sup> Both **6-La** and **6-Ce** were identified by X-ray crystallography, Figure 2.1, and are isomorphous.

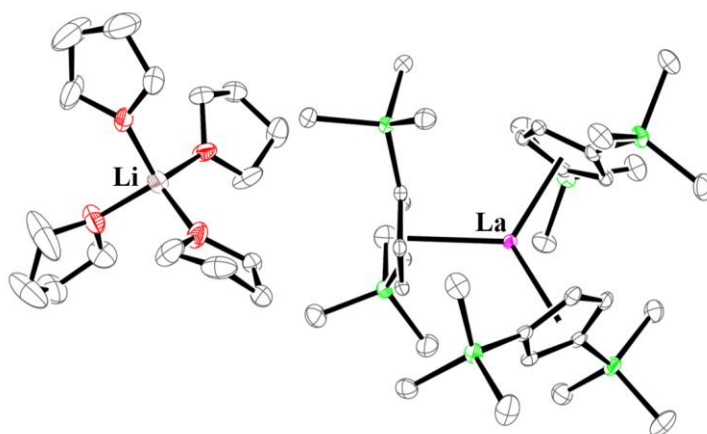


**Figure 2.1.** ORTEP representation of  $[\text{Li}(\text{THF})_4][\text{Cp}''_3\text{La}]$ , **6-La**, with thermal ellipsoids drawn at the 50% probability level. Hydrogen atoms were omitted for clarity.

The EPR spectrum of **6-La** in THF is identical to the previously reported eight line spectra of [K(18-crown-6)][Cp<sup>''</sup><sub>3</sub>La] and [K(2.2.2-cryptand)][Cp<sup>''</sup><sub>3</sub>La]<sup>14</sup> with  $g_{\text{ave}} = 1.97$  and  $A_{\text{ave}} = 133.7$  G arising from the  $I = 7/2$  nucleus of <sup>139</sup>La, Figure 2.2. The UV-Vis spectra of **6-La** and **6-Ce** are also similar to those of [K(crypt)][Cp<sup>''</sup><sub>3</sub>Ln],<sup>14, 25</sup> Figure 2.3.

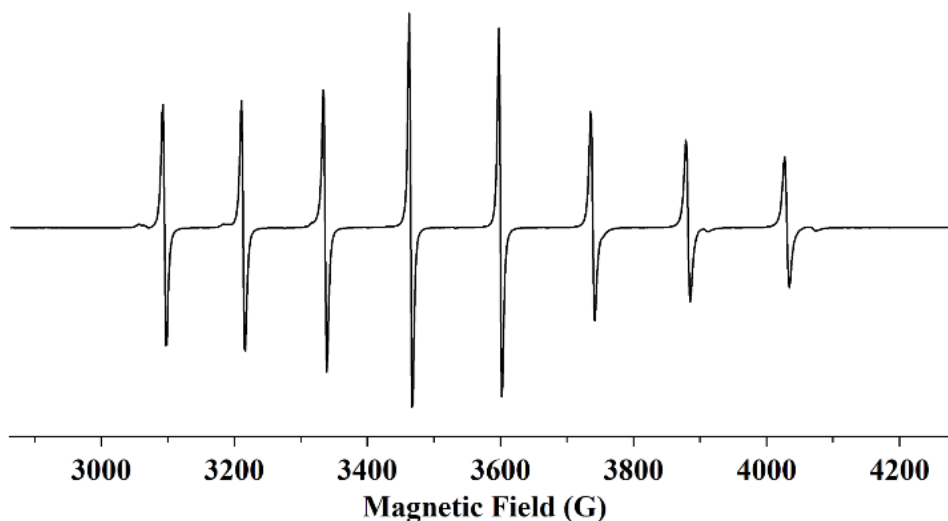


**Figure 2.2.** Experimental X-band EPR spectra of [Li(THF)<sub>4</sub>][Cp<sup>''</sup><sub>3</sub>La], **6-La**, in THF collected at 298 K (mode: perpendicular;  $g_{\text{ave}} = 1.97$ ;  $A_{\text{ave}} = 133.7$  G;  $\nu = 9.817$  GHz;  $P = 0.0203$ ; modulation amplitude = 0.902 mT).

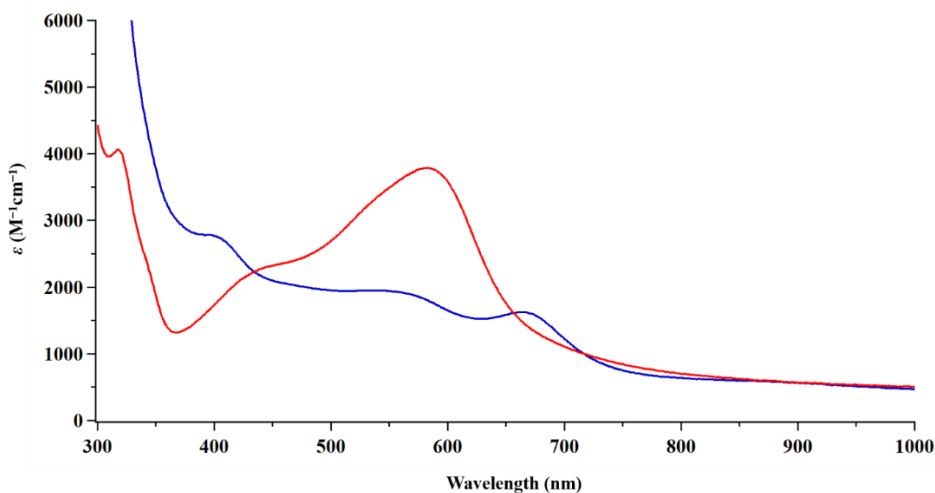


**Figure 2.3.** UV-Vis spectrum of ~5 mM **6-La** (red) and **6-Ce** (blue) in THF.

In both **6-La** and **6-Ce**, the  $[\text{Li}(\text{THF})_4]^{1+}$  cation is well-separated from the  $(\text{Cp}''_3\text{Ln})^{1-}$  anion. The metrical parameters of the  $(\text{Cp}''_3\text{Ln})^{1-}$  anions are nearly identical to those of the anions in  $[\text{K}(\text{crypt})][\text{Cp}''_3\text{Ln}]^{14}$  and  $[\text{K}(18\text{-crown-6})][\text{Cp}''_3\text{Ln}]^{14}$  Table 2.1. The Ln-centroid distances of **6-Ln** are only 0.02-0.03 Å larger than those in the  $\text{Cp}''_3\text{Ln}$  precursors, Table 2.1, which is characteristic of  $4f^n5d^1$  electron configurations of Ln(II) ions as previously noted.<sup>26,27</sup>

**Table 2.1.** M-centroid bond distance averages and ranges of  $\text{Cp}''_3\text{M}$  and  $(\text{Cp}''_3\text{M})^{1-}$

(M = La, Ce, U).

	Average (Å)	Range (Å)
$\text{Cp}''_3\text{La}^{26}$	2.60(1)	2.586-2.615
$[\text{K}(\text{crypt})][\text{Cp}''_3\text{La}]^{14}$	2.62(2)	2.606-2.642
$[\text{K}(18\text{-crown-6})][\text{Cp}''_3\text{La}]^{14}$	2.63(2)	2.629-2.634
<b>6-La</b>	2.63(1)	2.608-2.638
$\text{Cp}''_3\text{Ce}^{27}$	2.57(2)	2.542-2.579
$[\text{K}(18\text{-crown-6})][\text{Cp}''_3\text{Ce}^{\text{III}}][\text{Cp}''_3\text{Ce}^{\text{II}}]^{14}$	2.569(3)	2.565-2.572
$[\text{K}(18\text{-crown-6})][\text{Cp}''_3\text{Ce}^{\text{III}}][\text{Cp}''_3\text{Ce}^{\text{II}}]^{14}$	2.600(3)	2.596-2.603
<b>6-Ce</b>	2.60(1)	2.577-2.607
$\text{Cp}''_3\text{U}^{28}$	2.54(2)	2.507-2.561
<b>6-U</b>	2.56(1)	2.541-2.566

The  $[\text{Li}(\text{THF})_4]^{1+}$  cations in **1-La** and **1-Ce** have Li-O bond distances ranging from 1.900(4) to 1.953(4) Å. These are in the range of previously reported structures of salts containing the  $[\text{Li}(\text{THF})_4]^{1+}$  cation.<sup>29-32</sup>

**A Chelate-Free U(II) Complex.** The successful chelate-free reductions of  $\text{Cp}''_3\text{La}$  and  $\text{Cp}''_3\text{Ce}$  complexes encouraged the examination of the  $\text{Cp}''_3\text{U}$  analog since the radial size of 6-coordinate U(III) is 1.025 Å versus 1.032 and 1.010 Å for La(III) and Ce(III), respectively.<sup>33</sup>



The analogous reaction of  $\text{Cp}''_3\text{U}$  with a lithium smear in THF followed by the crystallization methods used for **6-Ln**, yielded crystals of  $[\text{Li}(\text{THF})_4][\text{Cp}''_3\text{U}]$ , **6-U**, in 45-50% yield according to eq 2.2. The  $^1\text{H}$  NMR spectrum of **6-U** revealed  $\text{Cp}''$  signals for  $\text{C}_5\text{H}_3(\text{SiMe}_3)_2$  at  $\delta -5$  ppm and for  $\text{C}_5\text{H}_3(\text{SiMe}_3)_2$  at  $\delta 13$  and  $-11$  ppm (in a 1:2 ratio) which is similar to the spectra of the previously published complexes  $[\text{M}(18\text{-crown-6})][\text{Cp}''_3\text{U}]$  ( $\text{M} = \text{Na}, \text{K}$ ) and  $[\text{Na}(12\text{-crown-4})_2][\text{Cp}''_3\text{U}]$ , *e.g.* for the latter compound,  $\text{C}_5\text{H}_3(\text{SiMe}_3)_2$  at  $\delta -4$  ppm and  $\text{C}_5\text{H}_3(\text{SiMe}_3)_2$  at 11 and  $-12$  ppm.<sup>4</sup> Resonances could not be found using  $^{29}\text{Si}$  NMR spectroscopy in the  $\delta +100$  to  $-500$  ppm region despite previous reports of  $^{29}\text{Si}$  resonances for  $(\text{Cp}'_3\text{U}^{\text{II}})^{1-}$  and  $(\text{Cp}''_3\text{U}^{\text{II}})^{1-}$ .<sup>4, 21</sup> **6-U** was also identified by X-ray crystallography and is isomorphous with **6-Ln**, Figure 2.4.

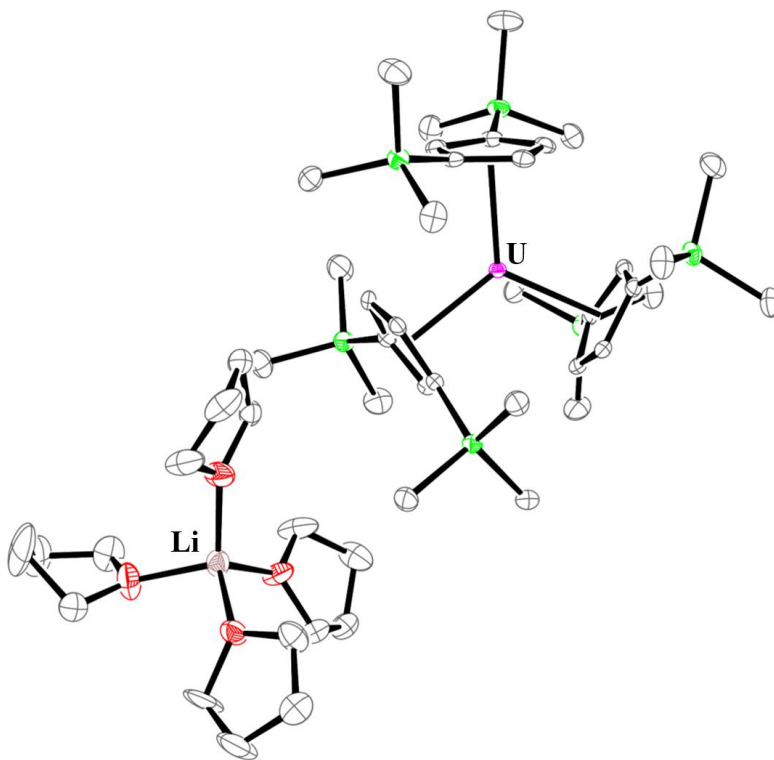


**Figure 2.4.** ORTEP representation of  $[\text{Li}(\text{THF})_4][\text{Cp}''_3\text{U}]$ , **6-U**, with thermal ellipsoids drawn at the 50% probability level. Hydrogen atoms were omitted for clarity.

In contrast to the crystal structures of  $[M(18\text{-crown-}6)[Cp''_3U]$  ( $M = Na, K$ ) and  $[Na(12\text{-crown-}4)_2][Cp''_3U]$ ,<sup>4</sup> which did not provide good crystallographic data due to disorder, **6-U** provides good data for structural comparison in Table 2.1.<sup>2</sup>

**Chelate-Free Cs Reductions.** Reduction of  $Cp''_3La$ ,  $Cp''_3Ce$ , and  $Cp''_3U$  with Cs metal also forms dark maroon solutions as observed in Li and K reductions. However, when Cs is the reductant, crystalline products were isolated only for La(II) and U(II) and the complexes,  $[Cp''M(\mu\text{-}Cp'')_2Cs(THF)_2]_n$ , **7-M**,  $M = La, U$ , eq 2.3, Figure 2.5, were identified by X-ray diffraction. The EPR spectrum of **7-La** in THF was identical to that of **6-La**, Figure 2.2.

X-ray crystallography revealed polymeric structures for these complexes with a repeating unit of  $[Cp''M(\mu\text{-}Cp'')_2Cs(THF)_2]_n$ , Figure 2.5. Unlike the **6-M** complexes ( $M = La, Ce, \text{ and } U$ ), which have well separated  $[Li(THF)_4]^{1+}$  cations, the  $[(THF)_2Cs]^{1+}$  cation bridges through two  $(\mu\text{-}Cp'')^{1-}$  rings to  $(Cp''M)^{1+}$  moieties thereby forming a bent metallocene cesium unit,  $[Cp''_2Cs(THF)_2]^{1-}$ . The structures of **7-La** and **7-U** are isomorphous. Although good crystallographic data were obtainable for **7-U**, the data on **7-La** were not of sufficient quality for detailed metrical analysis.

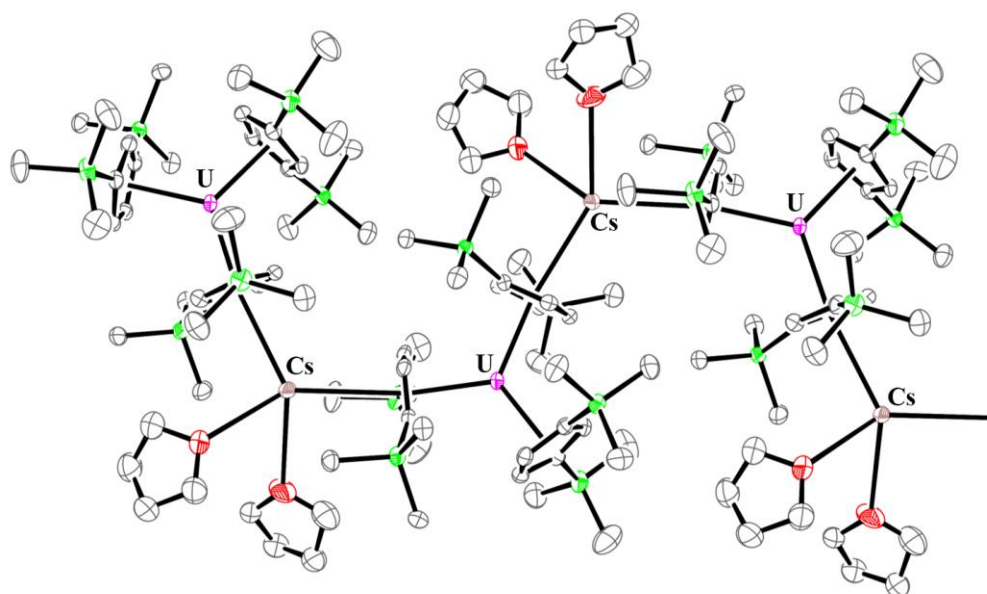
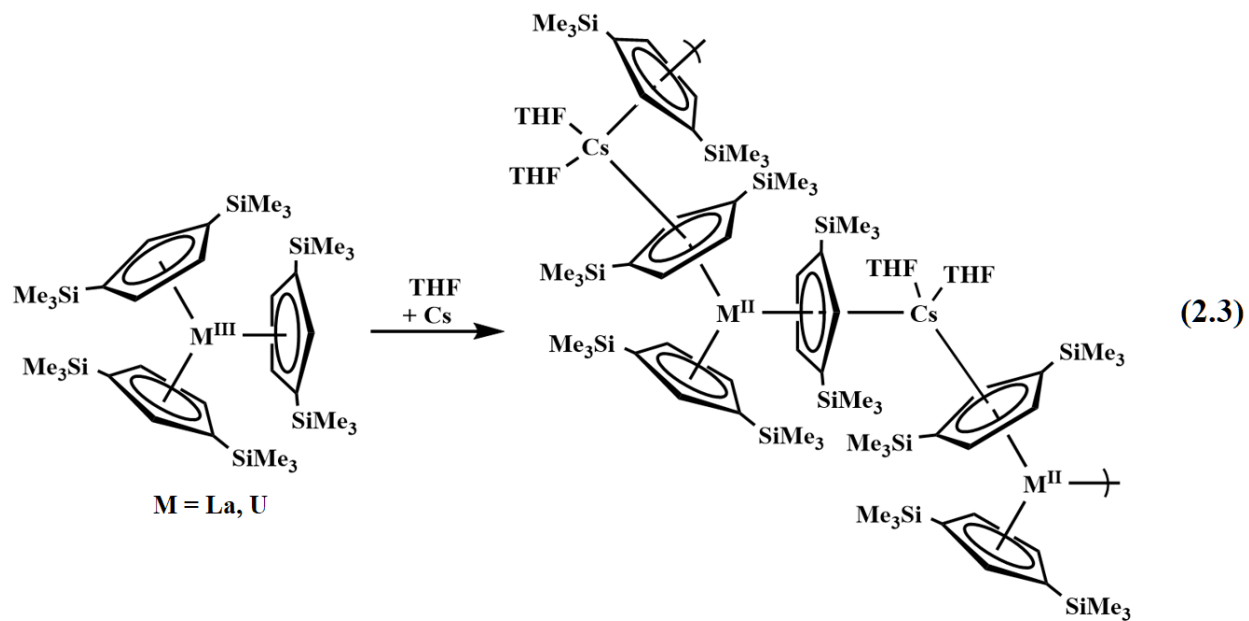


**Figure 2.5.** ORTEP representation of  $[\text{Cp}^*\text{U}(\mu\text{-Cp}^*)_2\text{Cs}(\text{THF})_2]_n$ , 7-U thermal ellipsoids drawn at the 50% probability level. Hydrogen atoms were omitted for clarity.

The 2.532 Å U–(terminal Cp'' ring centroid) distance in **7-U** is shorter than the 2.570 and 2.578 Å U–(bridging Cp'' ring centroid) distances as is typical for terminal vs bridging ligands. These distances are similar to the 2.541 to 2.566 Å range of U–(Cp'' ring centroid) distances in [Li(THF)<sub>4</sub>][Cp''<sub>3</sub>U], **6-U**. In contrast, the two Cs–(bridging Cp'' ring centroid) distances, 3.278 and 3.435 Å, vary significantly. The smaller value is similar to the Cs–(cyclopentadiene) distances reported in  $\{[(\text{Me}_3\text{Si})_2\text{NCs}]_2 \cdot [(\text{C}_5\text{H}_5)_2\text{Fe}]0.5 \cdot (\text{C}_6\text{H}_5\text{Me})\}_n$ , 3.396 Å, which contain Cs–( $\mu$ -C<sub>5</sub>H<sub>5</sub>)–Fe<sup>3+</sup> linkages and [(THF)<sub>2</sub>Cs( $\mu_3$ -O)<sub>3</sub>{[Ti(C<sub>5</sub>Me<sub>5</sub>)]<sub>3</sub>( $\mu_3$ -CCH<sub>2</sub>)}],<sup>35</sup> 3.337 Å, which has Cs–( $\mu$ -C<sub>5</sub>Me<sub>5</sub>)–Ti connections. The 3.081(7)-3.119(8) Å Cs–O<sub>THF</sub> distances of **2-U** are similar to the Cs–O<sub>THF</sub> distances in [(THF)<sub>2</sub>Cs( $\mu_3$ -O)<sub>3</sub>{[Ti(C<sub>5</sub>Me<sub>5</sub>)]<sub>3</sub>( $\mu_3$ -CCH<sub>2</sub>)}], 3.034(9)-3.06(1) Å. It is interesting that the comparison of **6-U** and **7-U** shows that the U–centroid distances apparently are unaffected by the proximity of the cesium ions.

**Chelate Free M(II) Complexes.** The synthesis of chelate-free M(II) complexes, [Li(THF)<sub>4</sub>][Cp''<sub>3</sub>M], **6-M**, with M = La, Ce, and U demonstrates that the tris(cyclopentadienyl) M(II) anions, [(C<sub>5</sub>R<sub>5</sub>)<sub>3</sub>M]<sup>1-</sup> do not necessarily require chelated alkali metal counterions to be isolated in crystalline form suitable for X-ray analysis. Whatever stability for the complex or the crystal structure that is provided by the [K(crypt)]<sup>1+</sup> cation, it is not a rigid requirement for forming tris(cyclopentadienyl) M(II) complexes. The **6-M** complexes are not more stable than their chelated analogs, but it is clear that the chelate is not always necessary to obtain crystals.

Analogous reductions of the Cp'<sub>3</sub>Ln (Cp' = C<sub>5</sub>H<sub>4</sub>SiMe<sub>3</sub>) complexes of the less sterically demanding mono-silylcyclopentadienyl ligand using Li or Cs without a chelating agent also provided dark maroon solutions indicative of Ln(II) formation. However, the reduction products could not be isolated even at –35 °C, as the dark maroon solutions decompose to colorless solutions within hours. This is consistent with previous studies that show that

[K(crypt)][Cp''<sub>3</sub>Ln] (Ln = La, Ce, Pr, Nd) complexes are more stable than their Cp' analogs.<sup>25</sup> The steric protection offered by the bulkier (Cp''<sub>3</sub>)<sup>3-</sup> ligand set is likely to be responsible for the increased stability of the **6-M** complexes versus the Cp'<sub>3</sub>Ln reduction products.

In the case of chelate-free lithium reactions, it was possible that the lithium would coordinate to the "backside" of the cyclopentadienyl ligand away from the f element metal as has been found in other rare-earth metal organometallic complexes, *e.g.* {(C<sub>5</sub>H<sub>5</sub>)<sub>2</sub>Y(CH<sub>2</sub>SiMe<sub>3</sub>)<sub>2</sub>}Li<sub>2</sub>(1,4-dioxane)(DME)<sub>2</sub><sup>36</sup> and as is observed in the [K(18-crown-6)[Cp'<sub>3</sub>Ln] structures of Ln = Y,<sup>12</sup> Ho, and Er,<sup>9</sup> which have the cation oriented toward one of the Cp' rings. Lithium coordination to the rings was not observed, however, in these reactions which form [Li(THF)<sub>4</sub>]<sup>1+</sup> salts, **6-M**. The [Li(THF)<sub>4</sub>]<sup>1+</sup> cation is a well-known entity, so formation of this species is not unusual, but it had been expected that Li would interact with the cyclopentadienyl ligands.

In contrast, it was not expected that the large Cs<sup>1+</sup> ion would coordinate to the backside of cyclopentadienyl ligands particularly since there are few Cs-(bridging cyclopentadienyl)-(metal) complexes in the literature. Two rare examples involving Cs-( $\mu$ -C<sub>5</sub>H<sub>5</sub>)-Fe<sup>34</sup> and Cs-( $\mu$ -C<sub>5</sub>Me<sub>5</sub>)-Ti<sup>35</sup> linkages are mentioned above. Since two Cp'' rings coordinate to each cesium in the **7-M** complexes, they are essentially bent cesium metallocenes. This is a known, but rare, class of metallocenes with [PPh<sub>4</sub>][Cp<sub>3</sub>Cs<sub>2</sub>] as an example.<sup>37</sup> Chelate-free reductions of Cp''<sub>3</sub>Ln using potassium and rubidium metal have also yielded dark maroon solutions similar to the chelate-free reduction of Li and Cs. However, the reduction products were not isolable.

## Conclusion

New options for isolating actinide complexes of +2 ions have been defined by showing that Li can reduce Cp''<sub>3</sub>U in the *absence* of a chelating reagent to form the crystallographically-characterizable product, [Li(THF)<sub>4</sub>][Cp''<sub>3</sub>U]. This shows that Li can be used for such reductions and alkali metal chelating reagents are not necessary. The lanthanide metals that mimic actinides in size, La and Ce, behave similarly. Investigations of Cs reductions show that chelates are also not required to isolate crystals with this alkali metal reductant. In the cesium case, the cesium cation binds to two cyclopentadienyl ligands to create a polymer containing both (Cp''<sub>3</sub>U)<sup>1-</sup> moieties and (Cp''<sub>2</sub>Cs)<sup>1-</sup> metallocene components. In cases in which it is optimum to make an extended structure, Cs without a chelating agent could be the favorable reducing reagent.

## Experimental

All syntheses and manipulations described below were conducted under Ar with rigorous exclusion of air and water using glovebox, Schlenk-line, and high-vacuum-line techniques. All Cp''<sub>3</sub>M (M = La,<sup>20</sup> Ce,<sup>15</sup> U<sup>21</sup>) materials were prepared according to previously published literature. Solvents were sparged with UHP Ar and dried over columns containing Q-5 and molecular sieves. THF-*d*<sub>8</sub> was dried over sodium–potassium alloy, degassed using three freeze-pump-thaw cycles, and vacuum transferred before use. <sup>1</sup>H (500 MHz) NMR spectra were obtained on a Bruker GN500 MHz or Bruker CRYO600 MHz spectrometer at 25 °C in THF-*d*<sub>8</sub>. IR samples were prepared as KBr pellets on a Jasco FT/IR-4700 spectrometer. UV–vis spectra were collected in THF at 298 K using a Varian Cary 60 Scan UV–vis spectrophotometer. Elemental analyses were performed on a PerkinElmer series II 2400 CHNS analyzer. Electron paramagnetic resonance spectra were collected using a Bruker EMX spectrometer equipped with

an ER041XG microwave bridge in THF at 298 K and the magnetic field was calibrated with DPPH ( $g = 2.0036$ ).

**[Li(THF)<sub>4</sub>][Cp\*<sub>3</sub>La], 6-La.** In a glovebox, addition of a colorless solution of Cp\*<sub>3</sub>La (50 mg, 0.065 mmol) in THF to excess Li smear produced a dark purple solution. The mixture was stirred for 15 min at room temperature. The solution was then layered into a vial containing hexanes and placed in a  $-35^{\circ}$  C freezer. After 1 d, X-ray quality dark purple crystals of **6-La** were isolated (52 mg, 75%). Evans method (THF, 298 K):  $1.6 \mu_B$ . IR: 3074w, 2953s, 2894s, 1435m, 1402w, 1319w, 1250s, 1207w, 1175w, 1120m, 1078s, 1043m, 967m, 924m, 752m, 734m, 688m, 638s. UV-vis (THF)  $\lambda_{\max}$  nm ( $\epsilon$ ,  $M^{-1}cm^{-1}$ ): 318 (4100), 430 (2200 shoulder), 531 (3200 shoulder), 582 (3800). Anal. Calcd for desolvated C<sub>33</sub>H<sub>63</sub>Si<sub>6</sub>LiLa C, 51.19; H, 8.20. Found: C, 50.38; H, 8.34. Elemental analysis was complicated by incomplete combustion which has been observed before for silyl lanthanide complexes.<sup>22-24</sup> However, the C:H ratio found by elemental analysis, 33:65.1, matches the calculated.

**[Li(THF)<sub>4</sub>][Cp\*<sub>3</sub>Ce], 6-Ce.** As described for **6-La**, Cp\*<sub>3</sub>Ce (50 mg, 0.065 mmol) was treated in THF using excess Li smear and a dark purple solution was produced. After recrystallization, X-ray quality dark purple crystals of **6-Ce** were isolated (51 mg, 74%). Evans method (THF, 298 K):  $2.5 \mu_B$ . IR: 3080w, 3044w, 2982m, 2951s, 2886s, 1677w, 1545w, 1445m, 1436m, 1401m, 1365w, 1343w, 1314m, 1293w, 1247s, 1203m, 1175w, 1142w, 1128w, 1115w, 1078s, 1053m, 1042s, 990w, 974w, 961w, 941w, 923s, 885m, 832s, 806m, 775m, 750s, 686m, 677m, 635s, 624m. UV-vis (THF)  $\lambda_{\max}$  nm ( $\epsilon$ ,  $M^{-1}cm^{-1}$ ): 400 (2800), 543 (2000), 667 (1600). Anal. Calcd for the partially desolvated complex, [Li(THF)<sub>2</sub>][Cp\*<sub>3</sub>Ce], C<sub>41</sub>H<sub>79</sub>O<sub>4</sub>Si<sub>6</sub>LiCe: C, 53.55; H, 8.66. Found: C, 52.60; H, 8.94.

**[Li(THF)<sub>4</sub>][Cp<sup>'''</sup><sub>3</sub>U], 6-U.** As described for **6-La**, Cp<sup>'''</sup><sub>3</sub>U (100 mg, 0.115 mmol) was reduced in THF using excess Li smear producing a dark purple solution. After recrystallization, X-ray quality dark purple crystals of **6-U** were isolated (61 mg, 45%). <sup>1</sup>H NMR (THF-*d*<sub>8</sub>): δ 13.04 (s, C<sub>5</sub>H<sub>3</sub>(SiMe<sub>3</sub>)<sub>2</sub>, 3H), 3.62 (m, C<sub>4</sub>H<sub>8</sub>O, 16H), 1.78 (m, C<sub>4</sub>H<sub>8</sub>O, 16H), -5.36 (s, C<sub>5</sub>H<sub>3</sub>(SiMe<sub>3</sub>)<sub>2</sub>, 54H), -10.98 (s, C<sub>5</sub>H<sub>3</sub>(SiMe<sub>3</sub>)<sub>2</sub>, 6H). Evans method (THF, 298 K): 2.7 μ<sub>B</sub>. IR: 3084w, 3054w, 3037w, 2980m, 2953s, 2891s, 1676w, 1545w, 1444m, 1435m, 1402m, 1365w, 1342w, 1315m, 1292w, 1248s, 1201m, 1185w, 1175w, 1132w, 1120w, 1077s, 1042s, 967m, 921s, 882m, 833s, 771m, 750s, 687m, 634s. Calcd for the partially desolvated complex, [Li(THF)<sub>2</sub>][Cp<sup>'''</sup><sub>3</sub>U], C<sub>41</sub>H<sub>79</sub>O<sub>4</sub>Si<sub>6</sub>LiU: C, 48.40; H, 7.83. Found: C, 48.11; H, 7.84.

**[Cp<sup>'''</sup>La(μ-Cp<sup>'''</sup>)<sub>2</sub>Cs(THF)<sub>2</sub>]<sub>n</sub>, 7-La.** Addition of a colorless solution of Cp<sup>'''</sup><sub>3</sub>La (50 mg, 0.065 mmol) in THF (1 mL) to excess Cs smear produced a dark purple solution. This was stirred for 15 min at room temperature and then layered into a vial containing hexanes for crystallization. After 3 d, X-ray quality dark purple crystals of **7-La** were isolated (23 mg, 34%). Crystalline yields are low due to the high solubility of these complexes.

**[Cp<sup>'''</sup>U(μ-Cp<sup>'''</sup>)<sub>2</sub>Cs(THF)<sub>2</sub>]<sub>n</sub>, 7-U.** As described for **7-La**, Cp<sup>'''</sup><sub>3</sub>U (30 mg, 0.035 mmol) in THF (1 mL) to excess Cs smear produced a dark purple solution. This was stirred for 15 min at room temperature and then layered into a vial containing hexanes for crystallization. After 5 d, X-ray quality dark purple crystals of **7-U** were isolated (10 mg, 25%). Incomplete combustion<sup>22-24</sup> was observed for **7-U**. Calcd for C<sub>41</sub>H<sub>79</sub>O<sub>2</sub>Si<sub>6</sub>CsU: C, 43.06; H, 6.96. Found: C, 34.00; H, 4.97.

## Structural Details

**X-ray Data Collection, Structure Solution and Refinement for [Li(THF)<sub>4</sub>][Cp<sup>'''</sup><sub>3</sub>La], 6-La.** A black crystal of approximate dimensions 0.156 x 0.234 x 0.359 mm was mounted in a



cryoloop and transferred to a Bruker SMART APEX II diffractometer. The APEX2<sup>38</sup> program package was used to determine the unit-cell parameters and for data collection (20 sec/frame scan time for a sphere of diffraction data). The raw frame data was processed using SAINT<sup>39</sup> and SADABS<sup>40</sup> to yield the reflection data file. Subsequent calculations were carried out using the SHELXTL<sup>41</sup> program. The diffraction symmetry was  $2/m$  and the systematic absences were consistent with the monoclinic space group  $P2_1/c$  that was later determined to be correct. The structure was solved by dual space methods and refined on  $F^2$  by full-matrix least-squares techniques. The analytical scattering factors<sup>42</sup> for neutral atoms were used throughout the analysis. Hydrogen atoms were included using a riding model. Several atoms were disordered and included using multiple components with partial site-occupancy-factors. Least-squares analysis yielded  $wR2 = 0.0588$  and  $Goof = 1.040$  for 602 variables refined against 14165 data ( $0.76 \text{ \AA}$ ),  $R1 = 0.0244$  for those 12687 data with  $I > 2.0\sigma(I)$ .

**X-ray Data Collection, Structure Solution and Refinement for  $[\text{Li}(\text{THF})_4][\text{Cp}''_3\text{Ce}]$ , **6-Ce**.** A black crystal of approximate dimensions  $0.198 \times 0.314 \times 0.358 \text{ mm}$  was mounted in a cryoloop and transferred to a Bruker SMART APEX II diffractometer. The APEX2<sup>38</sup> program package was used to determine the unit-cell parameters and for data collection (30 sec/frame scan time for a sphere of diffraction data). The raw frame data was processed using SAINT<sup>39</sup> and SADABS<sup>40</sup> to yield the reflection data file. Subsequent calculations were carried out using the SHELXTL<sup>41</sup> program. The diffraction symmetry was  $2/m$  and the systematic absences were consistent with the monoclinic space group  $P2_1/c$  that was later determined to be correct. The structure was solved by dual space methods and refined on  $F^2$  by full-matrix least-squares techniques. The analytical scattering factors<sup>42</sup> for neutral atoms were used throughout the analysis. Hydrogen atoms were included using a riding model. Disordered atoms were included

using multiple components with partial site-occupancy-factors. Least-squares analysis yielded  $wR2 = 0.0658$  and  $Goof = 1.044$  for 603 variables refined against 14032 data (0.76 Å),  $R1 = 0.0289$  for those 11847 data with  $I > 2.0\sigma(I)$ .

**X-ray Data Collection, Structure Solution and Refinement for [Li(THF)<sub>4</sub>][Cp''<sub>3</sub>U], 6-U.** A black crystal of approximate dimensions 0.130 x 0.137 x 0.215 mm was mounted in a cryoloop and transferred to a Bruker SMART APEX II diffractometer. The APEX2<sup>38</sup> program package was used to determine the unit-cell parameters and for data collection (60 sec/frame scan time for a sphere of diffraction data). The raw frame data was processed using SAINT<sup>39</sup> and SADABS<sup>40</sup> to yield the reflection data file. Subsequent calculations were carried out using the SHELXTL<sup>41</sup> program. The diffraction symmetry was  $2/m$  and the systematic absences were consistent with the monoclinic space group  $P2_1/c$  that was later determined to be correct. The structure was solved by dual space methods and refined on  $F^2$  by full-matrix least-squares techniques. The analytical scattering factors<sup>42</sup> for neutral atoms were used throughout the analysis. Hydrogen atoms were included using a riding model. Disordered atoms were included using multiple components with partial site-occupancy-factors. Least-squares analysis yielded  $wR2 = 0.0575$  and  $Goof = 1.039$  for 603 variables refined against 14000 data (0.76 Å),  $R1 = 0.0262$  for those 12016 data with  $I > 2.0\sigma(I)$ .

**X-ray Data Collection, Structure Solution and Refinement for [Cp''U( $\mu$ -Cp'')<sub>2</sub>Cs(THF)<sub>2</sub>]<sub>n</sub>, 7-U.** A purple crystal of approximate dimensions 0.197 x 0.224 x 0.406 mm was mounted in a cryoloop and transferred to a Bruker SMART APEX II diffractometer. The APEX2<sup>38</sup> program package was used to determine the unit-cell parameters and for data collection (60 sec/frame scan time for a sphere of diffraction data). The raw frame data was processed using SAINT<sup>39</sup> and SADABS<sup>40</sup> to yield the reflection data file. Subsequent

calculations were carried out using the SHELXTL<sup>41</sup> program. The diffraction symmetry was  $2/m$  and the systematic absences were consistent with the monoclinic space groups  $P2_1$  and  $P2_1/m$ . It was later determined that space group  $P2_1$  was correct. The structure was solved by dual space methods and refined on  $F^2$  by full-matrix least-squares techniques. The analytical scattering factors<sup>42</sup> for neutral atoms were used throughout the analysis. Hydrogen atoms were included using a riding model. The complex was polymeric. Least-squares analysis yielded  $wR2 = 0.0808$  and  $Goof = 1.056$  for 478 variables refined against 12181 data (0.76 Å),  $R1 = 0.0352$  for those 11335 data with  $I > 2.0\sigma(I)$ . The absolute structure was assigned by refinement of the Flack<sup>43</sup> parameter.

## References

- (1) Langeslay, R. R.; Fieser, M. E.; Ziller, J. W.; Furche, F.; Evans, W. J. Synthesis, structure, and reactivity of crystalline molecular complexes of the  $\{[C_5H_3(SiMe_3)_2]_3Th\}^{1-}$  anion containing thorium in the formal +2 oxidation state. *Chem. Sci.* **2015**, *6*, 517-521.
- (2) MacDonald, M. R.; Fieser, M. E.; Bates, J. E.; Ziller, J. W.; Furche, F.; Evans, W. J. Identification of the +2 Oxidation State for Uranium in a Crystalline Molecular Complex,  $[K(2.2.2-Cryptand)][(C_5H_4SiMe_3)_3U]$ . *J. Am. Chem. Soc.* **2013**, *135*, 13310-13313.
- (3) La Pierre, H. S.; Scheurer, A.; Heinemann, F. W.; Hieringer, W.; Meyer, K. Synthesis and Characterization of a Uranium(II) Monoarene Complex Supported by  $\delta$  Backbonding. *Angew. Chem., Int. Ed.* **2014**, *53*, 7158-7162.
- (4) Windorff, C. J.; MacDonald, M. R.; Meihaus, K. R.; Ziller, J. W.; Long, J. R.; Evans, W. J. Expanding the Chemistry of Molecular  $U^{2+}$  Complexes: Synthesis, Characterization, and Reactivity of the  $\{[C_5H_3(SiMe_3)_2]_3U\}^-$  Anion. *Chem. Eur. J.* **2016**, *22*, 772-782.
- (5) Windorff, C. J.; Chen, G. P.; Cross, J. N.; Evans, W. J.; Furche, F.; Gaunt, A. J.; Janicke, M. T.; Kozimor, S. A.; Scott, B. L. Identification of the Formal +2 Oxidation State of Plutonium: Synthesis and Characterization of  $\{Pu^{II}[C_5H_3(SiMe_3)_2]_3\}^-$ . *J. Am. Chem. Soc.* **2017**, *139*, 3970-3973.
- (6) Su, J.; Windorff, C. J.; Batista, E. R.; Evans, W. J.; Gaunt, A. J.; Janicke, M. T.; Kozimor, S. A.; Scott, B. L.; Woen, D. H.; Yang, P. Identification of the Formal +2 Oxidation State of Neptunium: Synthesis and Structural Characterization of  $\{Np^{II}[C_5H_3(SiMe_3)_2]_3\}^{1-}$ . *J. Am. Chem. Soc.* **2018**, *140*, 7425-7428.

- (7) Dutkiewicz, M. S.; Apostolidis, C.; Walter, O.; Arnold, P. L. Reduction chemistry of neptunium cyclopentadienide complexes: from structure to understanding. *Chem. Sci.* **2017**, *8*, 2553-2561.
- (8) La Pierre, H. S.; Kameo, H.; Halter, D. P.; Heinemann, F. W.; Meyer, K. Coordination and Redox Isomerization in the Reduction of a Uranium(III) Monoarene Complex. *Angew. Chem., Int. Ed.* **2014**, *53*, 7154-7157.
- (9) MacDonald, M. R.; Bates, J. E.; Fieser, M. E.; Ziller, J. W.; Furche, F.; Evans, W. J. Expanding Rare-Earth Oxidation State Chemistry to Molecular Complexes of Holmium(II) and Erbium(II). *J. Am. Chem. Soc.* **2012**, *134*, 8420-8423.
- (10) MacDonald, M. R.; Bates, J. E.; Ziller, J. W.; Furche, F.; Evans, W. J. Completing the Series of +2 Ions for the Lanthanide Elements: Synthesis of Molecular Complexes of Pr<sup>2+</sup>, Gd<sup>2+</sup>, Tb<sup>2+</sup>, and Lu<sup>2+</sup>. *J. Am. Chem. Soc.* **2013**, *135*, 9857-9868.
- (11) Fieser, M. E. Spectroscopic and Computational Analysis of Rare Earth and Actinide Complexes In Unusual Coordination Environments and Oxidation States. *Ph.D. Dissertation*, University of California, Irvine, 2015.
- (12) MacDonald, M. R.; Ziller, J. W.; Evans, W. J. Synthesis of a Crystalline Molecular Complex of Y<sup>2+</sup>, [(18-crown-6)K][(C<sub>5</sub>H<sub>4</sub>SiMe<sub>3</sub>)<sub>3</sub>Y]. *J. Am. Chem. Soc.* **2011**, *133*, 15914-15917.
- (13) Huh, D. N.; Darago, L. E.; Ziller, J. W.; Evans, W. J. Utility of Lithium in Rare-Earth Metal Reduction Reactions to Form Nontraditional Ln<sup>2+</sup> Complexes and Unusual [Li(2.2.2-cryptand)]<sup>1+</sup> Cations. *Inorg. Chem.* **2018**, *57*, 2096-2102.
- (14) Hitchcock, P. B.; Lappert, M. F.; Maron, L.; Protchenko, A. V. Lanthanum Does Form Stable Molecular Compounds in the +2 Oxidation State. *Angew. Chem., Int. Ed.* **2008**, *47*, 1488-1491.
- (15) Gun'ko, Y. K.; Hitchcock, P. B.; Lappert, M. F. Activation of a C-O bond by reaction of a tris(cyclopentadienyl)lanthanide complex with an alkali metal in dimethoxyethane (DME); crystal structures of [Ndη-C<sub>5</sub>H<sub>3</sub>(SiMe<sub>3</sub>)<sub>2</sub>-1,3<sub>2</sub>(μ-OMe)<sub>2</sub>Li(DME)] and [{Ce(η-C<sub>5</sub>H<sub>3</sub><sup>t</sup>Bu<sub>2</sub>-1,3)<sub>2</sub>(μ-OMe)<sub>2</sub>}. *J. Organomet. Chem.* **1995**, *499*, 213-219.
- (16) Cassani, M. C.; Duncalf, D. J.; Lappert, M. F. The First Example of a Crystalline Subvalent Organolanthanum Complex: [K([18]crown-6)-(η<sup>2</sup>-C<sub>6</sub>H<sub>6</sub>)<sub>2</sub>][(LaCp<sup>t</sup>)<sub>2</sub>(μ-η<sup>6</sup>:η<sup>6</sup>-C<sub>6</sub>H<sub>6</sub>)]•2C<sub>6</sub>H<sub>6</sub> (Cp<sup>t</sup> = η<sup>5</sup>-C<sub>5</sub>H<sub>3</sub>Bu<sup>t</sup><sub>2</sub>-1,3). *J. Am. Chem. Soc.* **1998**, *120*, 12958-12959.
- (17) Jaroschik, F.; Nief, F.; Le Goff, X.-F.; Ricard, L. Isolation of Stable Organodysprosium(II) Complexes by Chemical Reduction of Dysprosium(III) Precursors. *Organometallics* **2007**, *26*, 1123-1125.

- (18) Jaroschik, F.; Momin, A.; Nief, F.; Le Goff, X.-F.; Deacon, G. B.; Junk, P. C. Dinitrogen Reduction and C-H Activation by the Divalent Organoneodymium Complex [(C<sub>5</sub>H<sub>2</sub><sup>t</sup>Bu<sub>3</sub>)<sub>2</sub>Nd(μ-I)K([18]crown-6)]. *Angew. Chem., Int. Ed.* **2009**, *48*, 1117-1121.
- (19) Windorff, C. J.; Dumas, M. T.; Ziller, J. W.; Gaunt, A. J.; Kozimor, S. A.; Evans, W. J. Small-Scale Metal-Based Syntheses of Lanthanide Iodide, Amide, and Cyclopentadienyl Complexes as Analogues for Transuranic Reactions. *Inorg. Chem.* **2017**, *56*, 11981-11989.
- (20) Cassani, M. C.; Gun'ko, Y. K.; Hitchcock, P. B.; Lappert, M. F.; Laschi, F. Synthesis and Characterization of Organolanthanidocene(III) (Ln = La, Ce, Pr, Nd) Complexes Containing the 1,4-Cyclohexa-2,5-dienyl Ligand (Benzene 1,4-Dianion): Structures of [K([18]-crown-6)][Ln{η<sup>5</sup>-C<sub>5</sub>H<sub>3</sub>(SiMe<sub>3</sub>)<sub>2-1,3</sub>}<sub>2</sub>(C<sub>6</sub>H<sub>6</sub>)] [Cp'' = η<sup>5</sup>-C<sub>5</sub>H<sub>3</sub>(SiMe<sub>3</sub>)<sub>2-1,3</sub>; Ln = La, Ce, Nd]. *Organometallics* **1999**, *18*, 5539-5547.
- (21) Windorff, C. J.; Evans, W. J. <sup>29</sup>Si NMR Spectra of Silicon-Containing Uranium Complexes. *Organometallics* **2014**, *33*, 3786-3791.
- (22) Chilton, N. F.; Goodwin, C. A. P.; Mills, D. P.; Winpenny, R. E. P. The first near-linear bis(amide) f-block complex: a blueprint for a high temperature single molecule magnet. *Chem. Commun.* **2015**, *51*, 101-103.
- (23) Goodwin, C. A. P.; Chilton, N. F.; Vettese, G. F.; Moreno Pineda, E.; Crowe, I. F.; Ziller, J. W.; Winpenny, R. E. P.; Evans, W. J.; Mills, D. P. Physicochemical Properties of Near-Linear Lanthanide(II) Bis(silylamide) Complexes (Ln = Sm, Eu, Tm, Yb). *Inorg. Chem.* **2016**, *55*, 10057-10067.
- (24) Goodwin, C. A. P.; Joslin, K. C.; Lockyer, S. J.; Formanuk, A.; Morris, G. A.; Ortu, F.; Vitorica-Yrezabal, I. J.; Mills, D. P. Homoleptic Trigonal Planar Lanthanide Complexes Stabilized by Superbulky Silylamide Ligands. *Organometallics* **2015**, *34*, 2314-2325.
- (25) Palumbo, C. T.; Darago, L. E.; Windorff, C. J.; Ziller, J. W.; Evans, W. J. Trimethylsilyl versus Bis(trimethylsilyl) Substitution in Tris(cyclopentadienyl) Complexes of La, Ce, and Pr: Comparison of Structure, Magnetic Properties, and Reactivity. *Organometallics* **2018**, *37*, 900-905.
- (26) Xie, Z.; Chui, K.; Liu, Z.; Xue, F.; Zhang, Z.; Mak, T. C. W.; Sun, J. Systematic studies on the reactions of lanthanide trichlorides with Na[1,3-bis(trimethylsilyl) cyclopentadienyl]. Crystal structures of [1,3-(Me<sub>3</sub>Si)<sub>2</sub>C<sub>5</sub>H<sub>3</sub>]<sub>3</sub>Ln (Ln = La, Nd, Gd, Dy). *J. Organomet. Chem.* **1997**, *549*, 239-244.
- (27) Stults, S. D.; Andersen, R. A.; Zalkin, A. Structural studies on cyclopentadienyl compounds of trivalent cerium: tetrameric (MeC<sub>5</sub>H<sub>4</sub>)<sub>3</sub>Ce and monomeric (Me<sub>3</sub>SiC<sub>5</sub>H<sub>4</sub>)<sub>3</sub>Ce and [(Me<sub>3</sub>Si)<sub>2</sub>C<sub>5</sub>H<sub>3</sub>]<sub>3</sub>Ce and their coordination chemistry. *Organometallics* **1990**, *9*, 115-122.

- (28) Conejo, M. d. M.; Parry, J. S.; Carmona, E.; Schultz, M.; Brenmann, J. G.; Beshouri, S. M.; Andersen, R. A.; Rogers, R. D.; Coles, S.; Hursthouse, M. B. Carbon Monoxide and Isocyanide Complexes of Trivalent Uranium Metallocenes. *Chem. Eur. J.* **1999**, *5*, 3000-3009.
- (29) Lyubov, D. M.; Cherkasov, A. V.; Fukin, G. K.; Lyssenko, K. A.; Rychagova, E. A.; Ketkov, S. Y.; Trifonov, A. A. Rare-earth metal-mediated PhC≡N insertion into N,N-bis(trimethylsilyl)naphthalene-1,8-diamido dianion - a synthetic approach to complexes coordinated by ansa-bridged amido-amidinato ligand. *Dalton Trans.* **2018**, *47*, 438-451.
- (30) Gowda, A. S.; Petersen, J. L.; Milsmann, C. Redox Chemistry of Bis(pyrrolyl)pyridine Chromium and Molybdenum Complexes: An Experimental and Density Functional Theoretical Study. *Inorg. Chem.* **2018**, *57*, 1919-1934.
- (31) McLellan, R.; Uzelac, M.; Kennedy, A. R.; Hevia, E.; Mulvey, R. E. LiTMP Trans-Metal-Trapping of Fluorinated Aromatic Molecules: A Comparative Study of Aluminum and Gallium Carbanion Traps. *Angew. Chem., Int. Ed.* **2017**, *56*, 9566-9570.
- (32) Motolko, K. S. A.; Emslie, D. J. H.; Britten, J. F. Rigid NON-donor pincer ligand complexes of lutetium and lanthanum: synthesis and hydroamination catalysis. *RSC Advances* **2017**, *7*, 27938-27945.
- (33) Shannon, R. Revised effective ionic radii and systematic studies of interatomic distances in halides and chalcogenides. *Acta Crystallogr.* **1976**, *32*, 751-767.
- (34) Morris, J. J.; Noll, B. C.; Honeyman, G. W.; O'Hara, C. T.; Kennedy, A. R.; Mulvey, R. E.; Henderson, K. W. Organometallic Polymers Assembled from Cation- $\pi$  Interactions: Use of Ferrocene as a Ditopic Linker Within the Homologous Series  $\{[(\text{Me}_3\text{Si})_2\text{NM}]_2(\text{Cp}_2\text{Fe})\}_\infty$  (M=Na, K, Rb, Cs; Cp = cyclopentadienyl). *Chem. Eur. J.* **2007**, *13*, 4418-4432.
- (35) Gonzalez-del Moral, O.; Martin, A.; Mena, M.; Morales-Varela, M. d. C.; Santamaria, C. Hydrocarbon species  $\mu_3\text{-CCH}_2^-$ ,  $\mu_3\text{-CCH}_3$  and  $\mu\text{-CHCH}_3$  supported on  $\text{Ti}_3\text{O}_3$ . *Chem. Commun.* **2005**, 3682-3684.
- (36) Evans, W. J.; Dominguez, R.; Levan, K. R.; Doedens, R. J. Synthesis and X-ray crystal structure of a dialkyldicyclopentadienylyttrium complex:  $\{(\text{C}_5\text{H}_5)_2\text{Y}[\text{CH}_2\text{Si}(\text{CH}_3)_3]_2\}_2\text{Li}_2(\text{CH}_3\text{OCH}_2\text{CH}_2\text{OCH}_3)_2(\text{C}_4\text{H}_8\text{O}_2)$ . *Organometallics* **1985**, *4*, 1836-1841.
- (37) Harder, S.; Prosenc, M. H. The Heaviest Alkali Metallocene: Structure of an Anionic Cesocene Triple-Decker. *Angew. Chem., Int. Ed.* **1996**, *35*, 97-99.
- (38) APEX2 Version 2014.11-0, Bruker AXS, Inc.; Madison, WI 2014.
- (39) SAINT Version 8.34a, Bruker AXS, Inc.; Madison, WI 2013.
- (40) Sheldrick, G. M. SADABS, Version 2014/5, Bruker AXS, Inc.; Madison, WI 2014.

- (41) Sheldrick, G. M. SHELXTL, Version 2014/7, Bruker AXS, Inc.; Madison, WI 2014.
- (42) International Tables for Crystallography 1992, Vol. C., Dordrecht: Kluwer Academic Publishers.
- (43) Parsons, S., Flack, H. D., Wagner, T. Use of intensity quotients and differences in absolute structure refinement. *Acta Cryst.* **2013**, B69, 249-259.

## CHAPTER 3

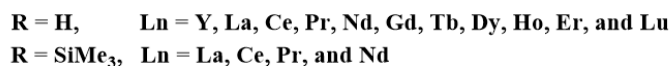
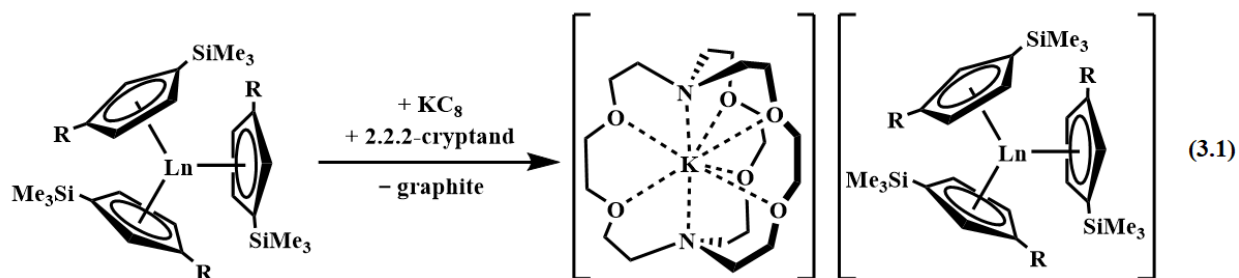
### Isolation of Reactive Ln(II) Complexes with C<sub>5</sub>H<sub>4</sub>Me (Cp<sup>Me</sup>) Ligands Using

#### Inverse Sandwich Counteranions: Synthesis and Structure of



#### Introduction\*

As previously described in Chapter 1, the discovery of oxidation states for the rare-earth metals Y, La, Ce, Pr, Gd, Tb, Ho, Er, and Lu by LnA<sub>3</sub>/M reduction reactions initially involved almost exclusively silyl-substituted cyclopentadienyl ligands C<sub>5</sub>H<sub>4</sub>SiMe<sub>3</sub> (Cp') and C<sub>5</sub>H<sub>3</sub>(SiMe<sub>3</sub>)<sub>2</sub> (Cp''), eq 3.1.<sup>1-8</sup> It was thought that the cyclopentadienyl ligands containing silyl groups were



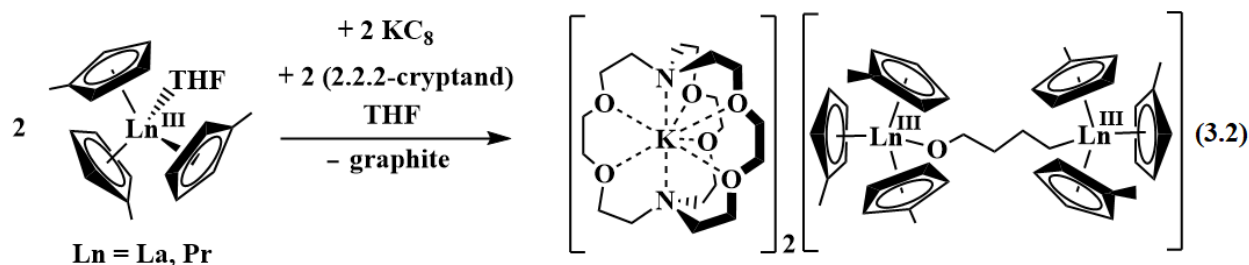
optimum because the silyl groups provided the “right” balance of electronic and steric stabilization.<sup>7</sup> EPR studies of reduction reactions of the yttrium complexes (C<sub>5</sub>H<sub>5</sub>)<sub>3</sub>Y, (C<sub>5</sub>H<sub>4</sub>Me)<sub>3</sub>Y, (C<sub>5</sub>Me<sub>4</sub>H)<sub>3</sub>Y, and Y(NR<sub>2</sub>)<sub>3</sub> (R = SiMe<sub>3</sub>) were consistent with this trend.<sup>9,10</sup> In each case, an EPR spectrum characteristic of Y(II) was observed, but the complexes proved to have

\*Portions of this chapter have been published: Huh, D. N.; Ziller, J. W.; Evans, W. J. Isolation of Reactive Ln(II) Complexes with C<sub>5</sub>H<sub>4</sub>Me (Cp<sup>Me</sup>) Ligands Using Inverse Sandwich Counteranions: Synthesis and Structure of [(18-crown-6)K(μ-Cp<sup>Me</sup>)K(18-crown-6)][Cp<sup>Me</sup><sub>3</sub>Ln<sup>II</sup>] (Ln = Tb, Ho). *Dalton Trans.*, **2018**, 47, 17285-17290. DOI: 10.1039/C8DT03890B



only transient stability and were not crystallographically-characterizable.<sup>9, 10</sup>

Studies have shown one reason that the reduction of  $\text{Cp}^{\text{Me}}_3\text{Ln}$  ( $\text{Cp}^{\text{Me}} = \text{C}_5\text{H}_4\text{Me}$ ) complexes does not give isolable Ln(II) complexes: for the large metals, La and Pr, reduction of  $\text{Cp}^{\text{Me}}_3\text{Ln}(\text{THF})$ , **8-Ln**, forms solutions that ring-open THF to form  $(\text{OCH}_2\text{CH}_2\text{CH}_2\text{CH}_2)^{2-}$  dianions, eq 3.2.<sup>11</sup> Spectroscopic evidence was also obtained for ring opening of THF in the  $\text{Cp}^{\text{Me}}_3\text{Y/K}$  reaction.



Historically, it has been found that yttrium exhibits similar chemistry to the late lanthanide metals of similar size, *e.g.* holmium and erbium.<sup>2, 4, 12</sup> Hence, it would be expected that the  $(\text{Cp}^{\text{Me}}_3)^{3-}$  ligand set would not support Ln(II) complexes for these metals. However, studies of the reduction of  $\text{Ln}(\text{NR}_2)_3$  complexes ( $\text{R} = \text{SiMe}_3$ ) showed that the late lanthanides,<sup>13</sup> as well as scandium,<sup>14</sup> can differ from yttrium<sup>10</sup> in the +2 oxidation state chemistry. Accordingly, the reduction chemistry of  $\text{Cp}^{\text{Me}}_3\text{Ln}$  with late lanthanides was investigated. Described in this Chapter is the surprising result that crystallographically-characterizable complexes of the late lanthanides in the +2 oxidation state could be isolated with the  $(\text{Cp}^{\text{Me}}_3)^{3-}$  ligand set and that a cyclopentadienyl inverse sandwich complex,  $[(18\text{-crown-6})\text{K}(\mu\text{-Cp}^{\text{Me}})\text{K}(18\text{-crown-6})]^{1+}$ , is an effective countercation for their isolation.

## Results and Discussion

Reductions of  $\text{Cp}^{\text{Me}}_3\text{Ln}(\text{THF})$ , **8-Ln** ( $\text{Ln} = \text{Tb}, \text{Ho}, \text{Er}$ ), using  $\text{KC}_8$  in the presence of 18-crown-6 (18-c-6) yield black solutions at  $-35^\circ\text{C}$  that retain their color for at least 3 days at low

temperature and provide isolable black solids. Crystals suitable for single-crystal X-ray diffraction were isolated and structurally characterized as  $[(18-c-6)K(\mu-Cp^{Me})K(18-c-6)][Cp^{Me}_3Ln]$ , **9-Ln** (Ln = Tb and Ho), Figure 3.1. The unit cell of **9-Er** matched that of **9-Tb** and **9-Ho**. However, due to rapid decomposition of the crystal upon transferring from the sample vial to the diffractometer, suitable data could not be collected for X-ray crystallography.

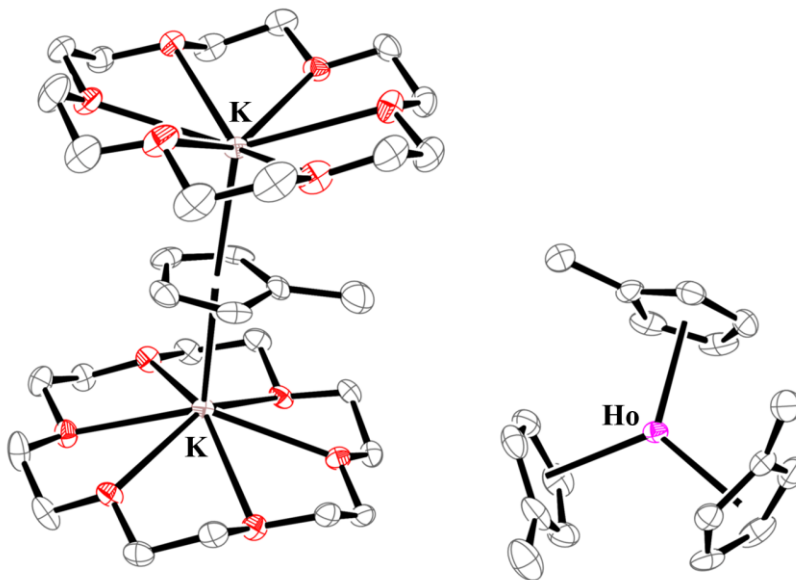
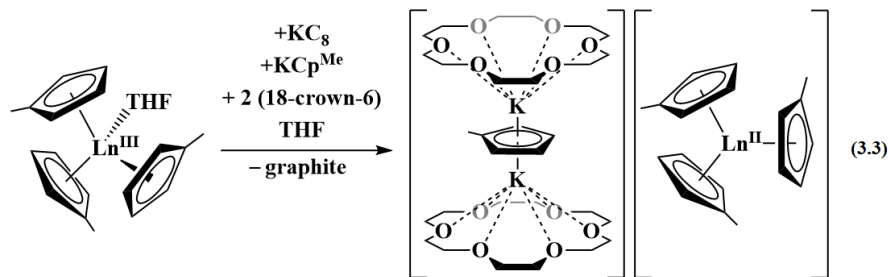


**Figure 3.1.** ORTEP representation of  $[(18-c-6)K(\mu-Cp^{Me})K(18-c-6)][Cp^{Me}_3Ho]$ , **9-Ho**, with thermal ellipsoids drawn at the 50% probability level. Hydrogen atoms were omitted for clarity.

The X-ray crystal structure of **9-Ln** showed that it contained an extra equivalent of  $(Cp^{Me})^{1-}$  which bridges two  $[K(18-c-6)]^{1+}$  units to generate an inverse sandwich complex,  $[(18-c-6)K(\mu-Cp^{Me})K(18-c-6)]^{1+}$ , as the counteranion. In subsequent syntheses of **9-Ln**, an extra equivalent of  $KCp^{Me}$  was added to improve the yield, eq 3.3. It appears that this counteranion is particularly effective in allowing isolation of these new Ln(II) complexes.



Several inverse sandwich complexes of this type have been reported with the unsubstituted  $(C_5H_5)^{1-}$  anion, *i.e.* the  $[(18-c-6)K(\mu-C_5H_5)K(18-c-6)]^{1+}$  cation,<sup>15-22</sup> but only two examples with substituted-cyclopentadienyl rings are in the literature, one with a  $(Cp')^{1-}$  anion bridge ( $Cp' = C_5H_4SiMe_3$ )<sup>3</sup> and one with a  $(C_5H_4CMe_3)^{1-}$  anion bridge.<sup>23</sup> Of these two substituted examples, crystallographically-determined metrical parameters were reported only for the  $Cp'$  complex,  $[(18-c-6)K(\mu-Cp')K(18-c-6)][Cp'_3Tb]$ .<sup>3</sup>

Although crystals of two examples of **9-Ln** could be isolated and characterized by X-ray diffraction, further characterization such as elemental analysis was challenging because the complexes decompose within seconds at temperatures above  $-35$  °C. Magnetic measurements of **9-Ln** are also difficult to obtain due to their inevitable contamination of Ln(III) from rapid decomposition. Attempts to obtain UV-visible spectra of **9-Ho** and **9-Er** showed significant decomposition with sharp absorbances characteristic of Ho(III) and Er(III) complexes, Figure 3.2.

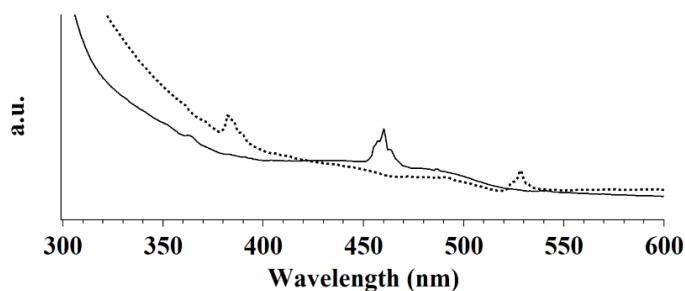


**Figure 3.2.** UV-visible spectra of **9-Ho** (solid) and **9-Er** (dashed) decomposition products at room temperature.

However, the spectra also contained broad features at 490 nm and 493 nm, respectively. These broad absorbances are similar to the most intense absorptions in [K(18-c-6)][Cp'3Ho]<sup>2</sup> of 507 nm, [K(18-c-6)][Cp'3Er]<sup>2</sup> of 510 nm, [K(crypt)][Cp'3Ho]<sup>3</sup> of 499 nm, and [K(crypt)][Cp'3Er]<sup>3</sup> of 502 nm. Complex **9-Tb** did survive long enough to provide a UV-visible spectrum absent of sharp Tb(III) features that contained broad absorptions at 458 nm and 660 nm, Figure 3.3, similar

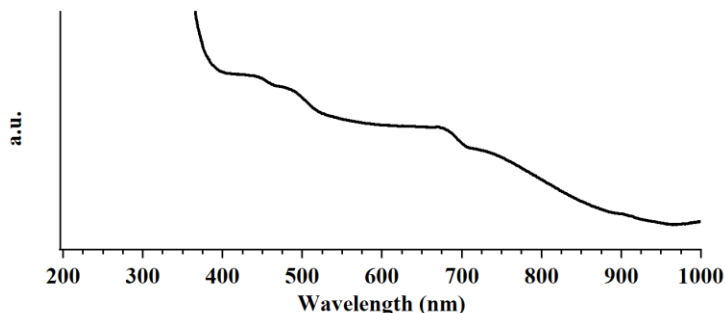


**Figure 3.3.** UV-visible spectrum of **9-Tb** in room temperature THF;  $\lambda_{\text{max}}$ , nm: 458, 481, 660 nm.

to those previously reported for [K(18-c-6)][Cp'3Tb] of 446 nm and 650 nm and [K(crypt)][Cp'3Tb] of 464 nm and 635 nm.<sup>3</sup> Each of the latter complexes was characterized as containing a Tb(II) ion with a 4f<sup>8</sup>5d<sup>1</sup> electron configuration.<sup>24</sup>

The crystallographic data on complexes of Ln(II) ions normally allows evaluation of the electron configuration since a characteristic of 4f<sup>n</sup>5d<sup>1</sup> Ln(II) complexes vs 4f<sup>n+1</sup> Ln(II) compounds is that the former complexes have metal–ligand bond distances only slightly larger than their Ln(III) analogs, within 0.02-0.05 Å.<sup>3, 25</sup> In contrast, traditional 4f<sup>n+1</sup> Ln(II) complexes have metal–ligand distances 0.1-0.2 Å larger than their Ln(III) counterparts.<sup>25</sup> This comparison cannot be made directly with **9-Ln**, since the X-ray crystal structures of Cp<sup>Me</sup><sub>3</sub>Ln for Tb and Ho are unknown. Structural data have been reported on the Cp<sup>Me</sup><sub>3</sub>Ln complexes of Ln = La,<sup>26</sup> Ce,<sup>27</sup> Pr,<sup>28</sup> and Nd,<sup>29</sup> but they crystallize in oligomeric forms with a higher coordination number for the

metal. The structures of  $\text{Cp}^{\text{Me}}_3\text{Ln}(\text{THF})$  ( $\text{Ln} = \text{Y},^9 \text{Sm},^{30} \text{Dy},^{31}$ ) are not appropriate for this analysis because the coordination number in these complexes is larger due to the THF.

The structure of unsolvated monomeric  $\text{Cp}^{\text{Me}}_3\text{Yb}^{32}$  is known, however, and will be used for comparison. The range of  $\text{Yb}-\text{Cp}^{\text{Me}}$  ring centroid distances is 2.29-2.38 Å and the average is 2.35 Å. Since the Shannon radii<sup>33</sup> of  $\text{Tb}(\text{III})$  and  $\text{Ho}(\text{III})$  are 0.055 and 0.033 Å larger than that of  $\text{Yb}(\text{III})$ , the predicted  $\text{Tb}(\text{III})-\text{Cp}^{\text{Me}}$  and  $\text{Ho}(\text{III})-\text{Cp}^{\text{Me}}$  average distances in " $\text{Cp}^{\text{Me}}_3\text{Ln}$ " are 2.405 and 2.383 Å, respectively. These are similar to  $\text{Tb}(\text{III})-\text{Cp}'$  and  $\text{Ho}(\text{III})-\text{Cp}'$  distances, 2.423 and 2.394 Å, in  $\text{Cp}'_3\text{Ln}$  complexes ( $\text{Cp}' = \text{C}_5\text{H}_4\text{SiMe}_3$ ). The observed  $\text{Ln}(\text{III})-\text{Cp}^{\text{Me}}$  distances of **9-Tb** and **9-Ho**, 2.456 and 2.432 Å, are about 0.05 Å larger than the estimates for the " $\text{Cp}^{\text{Me}}_3\text{Ln}$ " analogs. This is slightly larger than the difference found for the  $\text{Cp}' 4f^{n+1}$  series, but much less than the difference found for  $4f^{n+1} \text{Ln}(\text{II})$  ions.

The metrical parameters of the  $(\text{Cp}^{\text{Me}}_3\text{Ln})^{1-}$  anions in **8-Ln** can be further compared with those of the previously reported  $(\text{Cp}'_3\text{Ln})^{1-}$  complexes, Table 3.1. This table shows that the metal–ring centroid distances for **9-Ln** are very close to those of previously reported  $(\text{Cp}'_3\text{Ln})^{1-}$  anions,<sup>2, 3, 34</sup> which are only slightly larger than those of  $\text{Cp}'_3\text{Ln}$ . All of these metrical data are consistent with the presence of  $4f^n 5d^1$  electron configurations for **9-Tb** and **9-Ho**.

The metrical parameters of the  $[(18\text{-c-6})\text{K}(\mu\text{-Cp}^{\text{Me}})\text{K}(18\text{-c-6})]^{1+}$  inverse cyclopentadienyl sandwich cations in **9-Tb** and **9-Ho**, Figure 3.4, are similar. The  $\text{K}-\text{Cp}^{\text{Me}}$  centroid distances for **9-Ln** range from 2.848-2.860 Å and the  $\text{K}-(\text{Cp}^{\text{Me}} \text{ ring centroid})-\text{K}$  bond angles in the cations approach linearity, 177.2° and 177.1°, respectively. These metrical parameters are similar to previously reported unsubstituted-cyclopentadienyl  $[(18\text{-c-6})\text{K}(\mu\text{-C}_5\text{H}_5)\text{K}(18\text{-c-6})]^{1+}$  inverse sandwich complexes.<sup>15-20, 22</sup> The  $\text{K}-\text{C}_5\text{H}_5$  ring centroid distances in those compounds range from 2.812-2.894 Å and the  $\text{K}-(\text{C}_5\text{H}_5 \text{ ring centroid})-\text{K}$  angles vary from 171.5-179.2°. In contrast, in

**Table 3.1.** Ln(II)–(ring centroid) distances (Å) in the  $[(C_5H_4R)_3Ln]^{1-}$  anions (R = Me, SiMe<sub>3</sub>).

	Ln–cnt range (Å)	Ln–cnt average (Å)
<b>9-Tb</b>	2.451-2.463	2.456
$[K_2(18-c-6)_2(\mu-Cp')][Cp'_3Tb]^3$	2.446-2.464	2.454
$[K(18-c-6)][Cp'_3Tb]^3$	2.441-2.453	2.446
$[K(crypt)][Cp'_3Tb]^3$	2.448-2.461	2.454
$[Li(crypt)][Cp'_3Tb]^{34}$	2.441-2.472	2.455
<b>9-Ho</b>	2.430-2.435	2.432
$[K(18-c-6)][Cp'_3Ho]^2$	2.417-2.432	2.423
$[K(crypt)][Cp'_3Ho]^2$	2.420-2.433	2.426
$[Li(crypt)][Cp'_3Ho]^{34}$	2.409-2.440	2.425

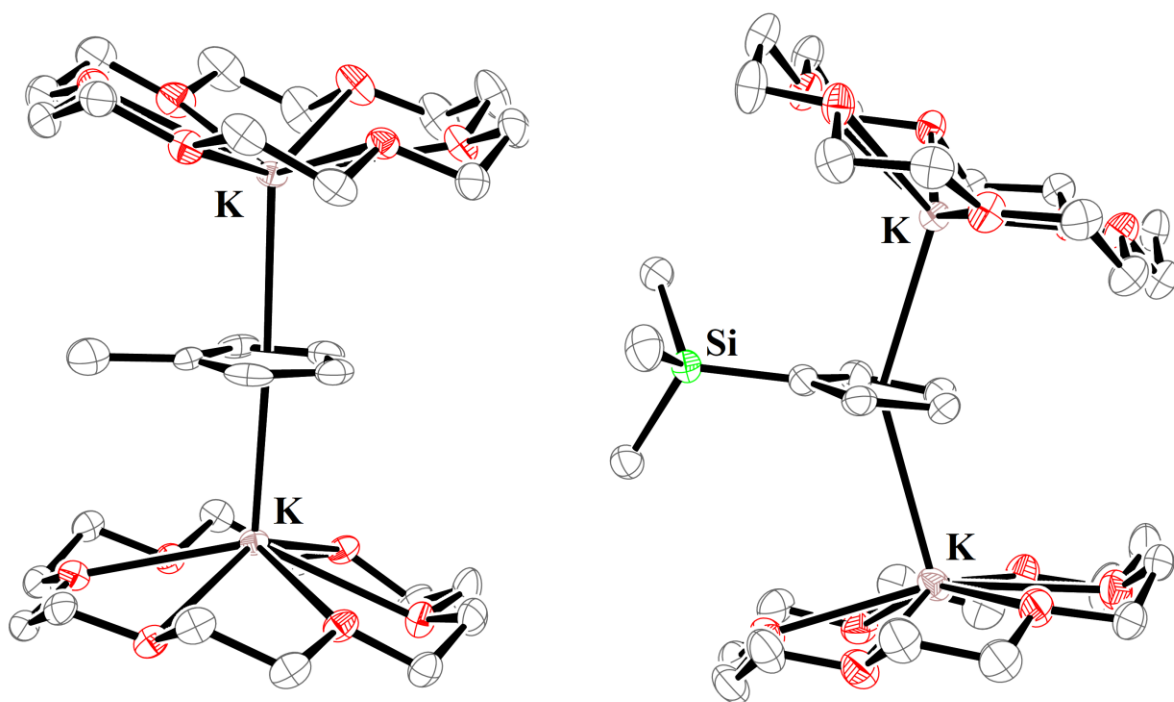


**Figure 3.4.** Comparison of the  $[(18-c-6)K(\mu-Cp^{Me})K(18-c-6)]^{1+}$  cation in **9-Tb** (left) and  $[(18-c-6)K(\mu-Cp')K(18-c-6)]^{1+}$  in  $[(18-c-6)K(\mu-Cp')K(18-c-6)][Cp'_3Tb]^3$  (right).

the Cp' inverse sandwich cation in  $[(18-c-6)K(\mu-Cp')K(18-c-6)][Cp'_3Tb]$ ,<sup>3</sup> the K–(Cp' ring centroid)–K angle is significantly bent:  $147.5^\circ$ , Figure 3.4. The steric bulk provided by the silyl substituent on the  $(Cp')^{1-}$  ligand evidently causes the K–Cp'–K angle to bend.

Attempts to reduce  $Cp^{Me}_3Ln(THF)$ , **8-Ln**, complexes in the presence of 2.2.2-cryptand (crypt), a chelating agent commonly used with potassium as the reductant, eq 3.1, gave dark colored solutions. Although crystalline products could be isolated for Ln = Tb, Ho and Er with crypt, these were not suitable for single crystal X-ray diffraction. This was further complicated by the fast decomposition at temperatures above  $-35^\circ C$ . However, reduction of **7-Dy** in THF using  $KC_8$  and crypt at  $-35^\circ C$  yielded a black solution similar to the previously reported reductions of **7-Ln** that persisted for days at this temperature. This allowed the isolation of  $[K(crypt)][Cp^{Me}_3Dy]$ , **10-Dy**, eq 3.4. Although crystals suitable for single-crystal X-ray crystallography were obtained, Figure 3.5, they were not of sufficient quality to provide useful

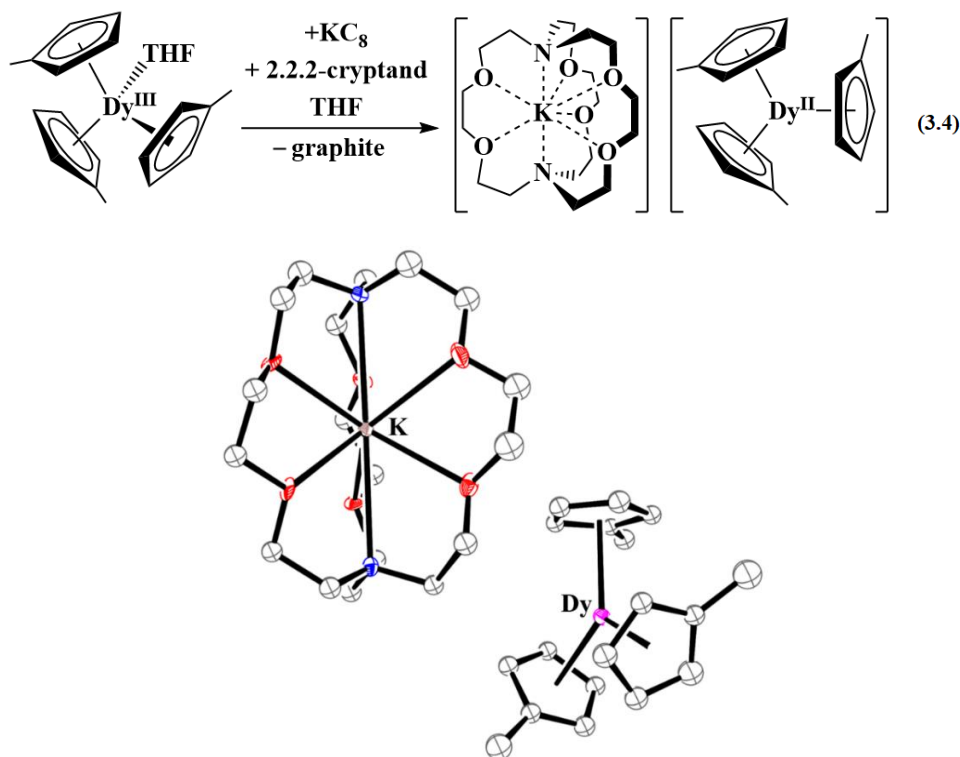


**Figure 3.5.** Connectivity only ORTEP representation of  $[K(2.2.2-cryptand)][Cp^{Me}_3Dy]$ , **10-Dy**.

metrical parameters with which to evaluate the presence of either a  $4f^{10}$  or  $4f^9 5d^1$  configuration.

Another characteristic of complexes of  $4f^n 5d^1$  Ln(II) ions is UV-visible spectra with large extinction coefficients compared to  $4f^{n+1}$  Ln(II) complexes. The UV-visible spectrum of **10-Dy**, Figure 3.6, contained broad absorbances at 424 and 674 nm with  $\epsilon = 2100$  and  $1200 \text{ M}^{-1}\text{cm}^{-1}$ , respectively, that were similar to those in the UV-visible spectrum of  $[\text{K}(\text{crypt})][\text{Cp}'_3\text{Dy}]$ ,<sup>25</sup> which has broad absorptions at 483 and 644 nm with  $\epsilon = 3400$  and  $1000 \text{ M}^{-1}\text{cm}^{-1}$ , respectively. Hence, by this metric, **10-Dy** appears to contain a  $4f^9 5d^1$  ion.

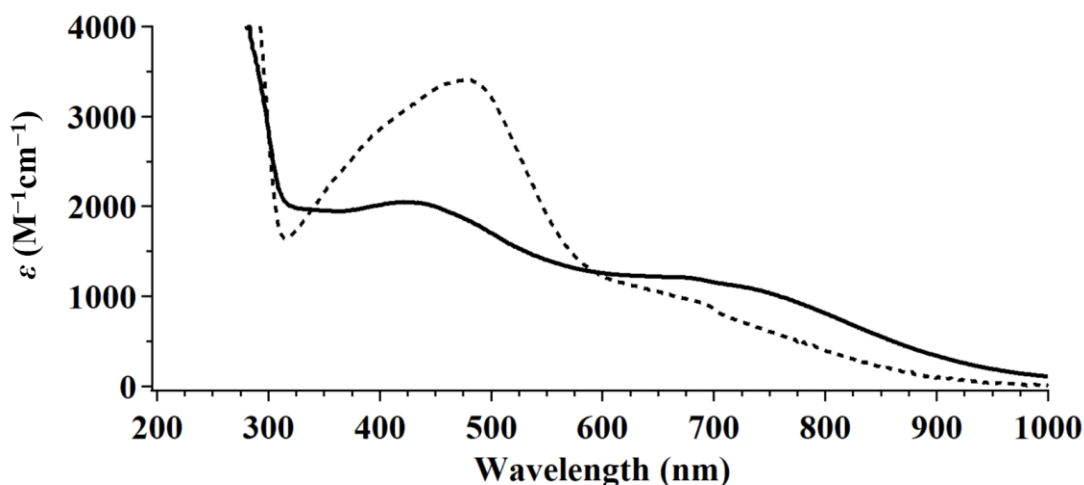


**Figure 3.6.** UV-visible spectrum of a  $\sim 10$  mM solution of  $[\text{K}(\text{crypt})][\text{Cp}^{\text{Me}}_3\text{Dy}]$ , **10-Dy** (solid) and  $[\text{K}(\text{crypt})][\text{Cp}'_3\text{Dy}]$ <sup>25</sup> (dashed) in THF.

The isolation of **9-Ln** for Ln = Tb and Ho provides another example in which the divalent late lanthanides are not like divalent yttrium. The solutions obtained by reduction of  $\text{Cp}^{\text{Me}}_3\text{Ln}$  clearly have greater stability than the product of  $\text{Cp}^{\text{Me}}_3\text{Y}$  reduction. Dissimilar chemistry for yttrium versus the late lanthanides has now been observed in reductions of  $\text{Ln}(\text{NR}_2)_3$  (R =  $\text{SiMe}_3$ ),<sup>13</sup>  $(\text{C}_5\text{Me}_4\text{H})_3\text{Ln}$ ,<sup>35</sup> and  $\text{Cp}^{\text{Me}}_3\text{Ln}$ . The origin of this difference is not known, but it is clear that the connection of yttrium with the late lanthanides so common for Y(III) complexes should



not be expected to necessarily apply for Y(II) species. It is possible that this is a 4d vs 5d effect which is sometimes seen in transition metal chemistry, *e.g.* in the differences between Pd and Pt.<sup>36, 37</sup>

Since the  $(\text{Cp}^{\text{Me}}_3\text{Ln})^{1-}$  anions were isolable with an inverse cyclopentadienyl sandwich counteraction, these results show yet another variation in the importance of the counteraction in isolating Ln(II) complexes. Attempts to crystallize  $(\text{Cp}^{\text{Me}}_3\text{Ln})^{1-}$  anions with  $[\text{K}(\text{crypt})]^{1+}$  did not provide suitable crystals for X-ray crystallography. The inverse cyclopentadienyl sandwich counteraction, however, allowed for facile crystallization and crystals were suitable for X-ray crystallography. Crystallographically-characterizable salts obtained from rare-earth metal reduction reactions with 18-c-6 as the chelator have been found with the following types of counteractions:  $[\text{K}(\text{crown})]^{1+, 2-4, 38}$   $[\text{K}(\text{crown})(\text{Et}_2\text{O})]^{1+}$ ,  $[\text{K}(\text{crown})(\text{THF})_2]^{1+}$ ,<sup>39-42</sup>  $\{[\text{K}(\text{crown})(\text{Et}_2\text{O})]_2\}^{2+}$ ,<sup>39</sup>  $\{[\text{K}(\text{crown})(\text{Et}_2\text{O})][\text{K}(\text{crown})]\}^{2+}$ ,<sup>43</sup> and  $[\text{K}_2(\text{crown})_3]^{2+}$ .<sup>39</sup> In each case, it appears that just one of these variations is the optimum counteraction for the anion involved, but the reason for the exact pairing is not known. It appears that much remains to be learned about matching cation and anion in these reduction reactions.<sup>44</sup> The presence of the 18-c-6 chelator may assist in rapid crystallization which is desirable for the isolation of reactive complexes.

## Conclusion

It was a surprise that Ln(II) complexes supported by  $\text{Cp}^{\text{Me}}$  ligands,  $[(18\text{-c-6})\text{K}(\mu\text{-Cp}^{\text{Me}})\text{K}(18\text{-c-6})][\text{Cp}^{\text{Me}}_3\text{Ln}]$ , **9-Ln**, could be isolated for the smaller lanthanides, Tb and Ho. This contrasts with the larger metals, La and Pr, that reductively ring-open THF and with the 4d metal, yttrium, that has in the past been used as a mimic of the late small lanthanides but does not form a stable **9-Y** analog. The isolation of these complexes as salts of the inverse sandwich

cation,  $[(18\text{-c-}6)\text{K}(\mu\text{-Cp}^{\text{Me}})\text{K}(18\text{-c-}6)]^{1+}$ , demonstrates another possibility for 18-c-6 to chelate potassium. This also allowed for the facile crystallization with  $(\text{Cp}^{\text{Me}}_3\text{Ln})^{1-}$  anions to form additional crystallographically-characterized examples of Tb and Ho in the +2 oxidation state.

## Experimental

All syntheses and manipulations described below were conducted under Ar with rigorous exclusion of air and water using glovebox, Schlenk-line, and high-vacuum-line techniques.  $\text{Cp}^{\text{Me}}_3\text{Ln}(\text{THF})$  (Ln = Tb, Dy, Ho, Er)<sup>31</sup>,  $\text{KCp}^{\text{Me}}$ ,<sup>45</sup> and  $\text{KC}_8$ <sup>46</sup> were prepared according to previously published literature. 2.2.2-Cryptand (4,7,13,16,21,24-hexaoxa-1,10-diazabicyclo[8.8.8]hexacosane, Aldrich) was placed under vacuum (10–3 Torr) for 12 h before use. 18-crown-6 purchased from Alfa Aesar was sublimed prior to use. THF and hexanes were sparged with UHP Ar and dried over columns containing Q-5 and molecular sieves. UV-vis spectra were collected on a Cary-60. IR samples were prepared as KBr pellets on a Jasco FT/IR-4700 spectrometer. The thermal instability of the complexes did not allow elemental analytical data to be collected.

**$[(18\text{-c-}6)\text{K}(\mu\text{-Cp}^{\text{Me}})\text{K}(18\text{-c-}6)][\text{Cp}^{\text{Me}}_3\text{Tb}]$ , 9-Tb.** In an argon-filled box, a colorless solution of  $\text{Cp}^{\text{Me}}_3\text{Tb}(\text{THF})$  (50 mg, 0.11 mmol), 18-crown-6 (57 mg, 0.21 mmol) and  $\text{KCp}^{\text{Me}}$  (13 mg, 11 mmol) in THF (2 mL) as well as a vial containing  $\text{KC}_8$  (22 mg, 0.16 mmol) were cooled to  $-35\text{ }^\circ\text{C}$ . The THF solution was transferred to the vial of  $\text{KC}_8$  and vigorously swirled forming a black mixture. The black mixture was immediately filtered and layered into cold ( $-35\text{ }^\circ\text{C}$ ) hexanes and placed in a  $-35\text{ }^\circ\text{C}$  freezer. After 1 d, X-ray quality crystals were isolated (73 mg, 63 %). IR: 3087w, 3059w, 3040m, 2947m, 2892s, 2859s, 2824m, 2792w, 2743w, 2707w, 2687w, 1979w, 1634m, 1618m, 1471m, 1452m, 1432w, 1405w, 1350s, 1283m, 1248m, 1109s, 1059w, 1030w, 1019w. UV-vis (THF)  $\lambda_{\text{max}}$  nm: 458, 660.

**[(18-c-6)K( $\mu$ -Cp<sup>Me</sup>)K(18-c-6)][Cp<sup>Me</sup><sub>3</sub>Ho], 9-Ho.** As described for **9-Tb**, Cp<sup>Me</sup><sub>3</sub>Ho(THF) (50 mg, mmol), 18-crown-6 (55 mg, 0.21 mmol) and KCp<sup>Me</sup> (12 mg, 0.11 mmol) was reduced in THF using KC<sub>8</sub> (22 mg, 0.16 mmol) which produced a black solution. Black single crystals of **9-Ho** were grown from THF/hexanes after 1 d (23 mg, 20 %). IR: 3070m, 3046m, 2948m, 2912s, 2895s, 2858s, 2824m, 2794w, 2743w, 2710w, 2687w, 2173w, 1975w, 1601w, 1490w, 1471m, 1452m, 1407w, 1383w, 1351s, 1283m, 1249m, 1111s, 1046w, 1031w, 1019w. UV-vis (THF)  $\lambda_{\max}$  nm: 490.

**[(18-c-6)K( $\mu$ -Cp<sup>Me</sup>)K(18-c-6)][Cp<sup>Me</sup><sub>3</sub>Er], 2-Er.** As described for **9-Tb**, Cp<sup>Me</sup><sub>3</sub>Er(THF) (50 mg, 0.11 mmol), 18-crown-6 (55 mg, 0.21 mmol) and KCp<sup>Me</sup> (12 mg, 0.11 mmol) treated in THF with KC<sub>8</sub> (21 mg, 0.16 mmol) which produced a black solution. Black crystals of **9-Er** were grown from THF/hexanes after 1 d (18 mg, 16 %). IR: 3083m, 3063m, 3046m, 2946s, 2911s, 2889s, 2857s, 2824s, 2795m, 2744m, 2711w, 2688w, 2173w, 1977w, 1572w, 1492w, 1471s, 1452s, 1433m, 1406w, 1351s, 1283m, 1249s, 1236m, 1110s, 1058m, 1046m, 1031m, 1019w. UV-vis (THF)  $\lambda_{\max}$  nm: 493.

**[K(crypt)][Cp<sup>Me</sup><sub>3</sub>Dy], 10-Dy.** In an argon-filled box, a colorless solution of Cp<sup>Me</sup><sub>3</sub>Dy(THF) (45 mg, 0.10 mmol) and 2.2.2-cryptand (39 mg, 0.10 mmol) in THF (2 mL) as well as a vial containing KC<sub>8</sub> (19 mg, 0.14 mmol) were cooled to -35 °C. The THF solution was transferred to the vial of KC<sub>8</sub> and vigorously swirled forming a black mixture. The black mixture was immediately filtered and layered into cold (-35 °C) hexanes and placed in a -35 °C freezer. After 1 d, X-ray quality crystals were isolated (40 mg, 51 %). IR: 3077w, 3059w, 3036w, 2956s, 2882s, 2817s, 2757m, 2727m, 1476m, 1457m, 1443m, 1410w, 1353s, 1296m, 1259m, 1236w, 1173w, 1132s, 1102s, 1178s, 1056m, 1031m. UV-vis (THF)  $\lambda_{\max}$  nm ( $\epsilon$ , M<sup>-1</sup>cm<sup>-1</sup>): 424 (2050), 674 (1200), 728 (1100 shoulder).

## Structural Details

**X-ray Data Collection, Structure Solution and Refinement for [(18-c-6)K( $\mu$ -Cp<sup>Me</sup>)K(18-c-6)][Cp<sup>Me</sup><sub>3</sub>Tb], 9-Tb.** A black crystal of approximate dimensions 0.100 x 0.136 x 0.335 mm was mounted in a cryoloop and transferred to a Bruker SMART APEX II diffractometer. The APEX2<sup>47</sup> program package was used to determine the unit-cell parameters and for data collection (120 sec/frame scan time for a sphere of diffraction data). The raw frame data was processed using SAINT<sup>48</sup> and SADABS<sup>49</sup> to yield the reflection data file. Subsequent calculations were carried out using the SHELXTL<sup>50</sup> program. The diffraction symmetry was  $2/m$  and the systematic absences were consistent with the monoclinic space group  $P2_1/c$  that was later determined to be correct. The structure was solved by dual space methods and refined on  $F^2$  by full-matrix least-squares techniques. The analytical scattering factors<sup>51</sup> for neutral atoms were used throughout the analysis. Hydrogen atoms were included using a riding model. There were three molecules of tetrahydrofuran solvent present. One solvent molecule was disordered and included using multiple components, partial site-occupancy-factors, geometric constraints and equivalent anisotropic thermal parameters. Least-squares analysis yielded  $wR2 = 0.0959$  and  $Goof = 1.046$  for 680 variables refined against 12924 data ( $0.80 \text{ \AA}$ ),  $R1 = 0.0389$  for those 10335 data with  $I > 2.0\sigma(I)$ .

**X-ray Data Collection, Structure Solution and Refinement for [(18-c-6)K( $\mu$ -Cp<sup>Me</sup>)K(18-c-6)][Cp<sup>Me</sup><sub>3</sub>Ho], 9-Ho.** A black crystal of approximate dimensions 0.060 x 0.116 x 0.452 mm was mounted in a cryoloop and transferred to a Bruker SMART APEX II diffractometer. The APEX2<sup>47</sup> program package was used to determine the unit-cell parameters and for data collection (120 sec/frame scan time for a sphere of diffraction data). The raw frame data was processed using SAINT<sup>48</sup> and SADABS<sup>49</sup> to yield the reflection data file. Subsequent

calculations were carried out using the SHELXTL<sup>50</sup> program. The diffraction symmetry was  $2/m$  and the systematic absences were consistent with the monoclinic space group  $P2_1/c$  that was later determined to be correct. The structure was solved by dual space methods and refined on  $F^2$  by full-matrix least-squares techniques. The analytical scattering factors<sup>51</sup> for neutral atoms were used throughout the analysis. Hydrogen atoms were included using a riding model. There were three molecules of tetrahydrofuran solvent present. One solvent molecule was disordered and included using multiple components, partial site-occupancy-factors, geometric constraints and equivalent anisotropic thermal parameters. Least-squares analysis yielded  $wR2 = 0.0995$  and  $Goof = 1.022$  for 680 variables refined against 12898 data ( $0.80 \text{ \AA}$ ),  $R1 = 0.0398$  for those 9972 data with  $I > 2.0\sigma(I)$ .

## References

- (1) Hitchcock, P. B.; Lappert, M. F.; Maron, L.; Protchenko, A. V. *Angew. Chem. Int. Ed.*, **2008**, *47*, 1488-1491.
- (2) MacDonald, M. R.; Bates, J. E.; Fieser, M. E.; Ziller, J. W.; Furche, F.; Evans, W. J. *J. Am. Chem. Soc.*, **2012**, *134*, 8420-8423.
- (3) MacDonald, M. R.; Bates, J. E.; Ziller, J. W.; Furche, F.; Evans, W. J. *J. Am. Chem. Soc.*, **2013**, *135*, 9857-9868.
- (4) MacDonald, M. R.; Ziller, J. W.; Evans, W. J. *J. Am. Chem. Soc.*, **2011**, *133*, 15914-15917.
- (5) Palumbo, C. T.; Darago, L. E.; Windorff, C. J.; Ziller, J. W.; Evans, W. J. *Organometallics*, **2018**, *37*, 900-905.
- (6) Examples with other ligands such as  $C_5H_3(CMe_3)_2$  ( $Cp^{tt}$ ),<sup>7</sup>  $C_5H_2(CMe_3)_3$  ( $Cp^{ttt}$ ),<sup>8</sup> and the tris(aryloxy) mesitylene ligand,  $((^{Ad, Me}ArO)_3mes)^{3-}$ , are also known: Fieser, M. E.; Palumbo, C. T.; La Pierre, H. S.; Halter, D. P.; Voora, V. K.; Ziller, J. W.; Furche, F.; Meyer, K.; Evans, W. J. *Chem. Sci.*, **2017**, *8*, 7424-7433.
- (7) Cassani, M. C.; Duncalf, D. J.; Lappert, M. F. *J. Am. Chem. Soc.*, **1998**, *120*, 12958-12959.

- (8) Jaroschik, F.; Nief, F.; Le Goff, X.-F.; Ricard, L. *Organometallics*, **2007**, *26*, 1123-1125.  
Jaroschik, F.; Momin, A.; Nief, F.; Le Goff, X.-F.; Deacon, G. B.; Junk, P. C. *Angew. Chem. Int. Ed.*, **2009**, *48*, 1117-1121.
- (9) Corbey, J. F.; Woen, D. H.; Palumbo, C. T.; Fieser, M. E.; Ziller, J. W.; Furche, F.; Evans, W. J. *Organometallics*, **2015**, *34*, 3909-3921.
- (10) Fang, M.; Lee, D. S.; Ziller, J. W.; Doedens, R. J.; Bates, J. E.; Furche, F.; Evans, W. J. *J. Am. Chem. Soc.*, **2011**, *133*, 3784-3787.
- (11) Woen, D. H.; Huh, D. N.; Ziller, J. W.; Evans, W. J. *Organometallics*, **2018**, *37*, 3055-3063.
- (12) Holton, J.; Lappert, M. F.; Ballard, D. G. H.; Pearce, R.; Atwood, J. L.; Hunter, W. E. *J. Chem. Soc., Chem. Commun.*, **1976**, 480-481.
- (13) Ryan, A. J.; Darago, L. E.; Balasubramani, S. G.; Chen, G. P.; Ziller, J. W.; Furche, F.; Long J. R.; Evans, W. J. *Chem. Eur. J.*, **2018**, *24*, 7702-7709.
- (14) Woen, D. H.; Chen, G. P.; Ziller, J. W.; Boyle, T. J.; Furche, F.; Evans, W. J. *Angew. Chem. Int. Ed.*, **2017**, *56*, 2050-2053.
- (15) Zitz, R.; Arp, H.; Hlina, J.; Walewska, M.; Marschner, C.; Szilvási, T.; Blom, B.; Baumgartner, J. *Inorg. Chem.*, **2015**, *54*, 3306-3315.
- (16) Brennessel, W. W.; Ellis, J. E. *Inorg. Chem.*, **2012**, *51*, 9076-9094.
- (17) Benda, C. B.; Wang, J.-Q.; Wahl, B.; Fässler, T. F. *Eur. J. Inorg. Chem.*, **2011**, 4262-4269.
- (18) Benda, C. B.; Waibel, M.; Fässler, T. F. *Angew. Chem. Int. Ed.*, **2015**, *54*, 522-526.
- (19) Wang, J.-Q.; Fassler, T. F. *Z. Naturforsch., B: Chem. Sci.*, **2009**, *64*, 985.
- (20) Sanger, I.; Kuckmann, T. I.; Dornhaus, F.; Bolte, M.; Wagner, M.; Lerner, H.-W. *Dalton Trans.*, **2012**, *41*, 6671-6676.
- (21) Zirngast, M.; Florke, U.; Baumgartner, J.; Marschner, C. *Chem. Commun.*, **2009**, 5538-5540.
- (22) Arp, H.; Zirngast, M.; Marschner, C.; Baumgartner, J.; Rasmussen, K.; Zark, P.; Müller, T. *Organometallics*, **2012**, *31*, 4309-4319.
- (23) Berthet, J.-C.; Villiers, C.; Le Maréchal, J.-F.; Delavaux-Nicot, B.; Lance, M.; Nierlich, M.; Vigner, J.; Ephritikhine, M. *J. Organomet. Chem.*, **1992**, *440*, 53-65.

- (24) Meihaus, K. R.; Fieser, M. E.; Corbey, J. F.; Evans, W. J.; Long, J. R. *J. Am. Chem. Soc.*, **2015**, *137*, 9855-9860.
- (25) Fieser, M. E.; MacDonald, M. R.; Krull, B. T.; Bates, J. E.; Ziller, J. W.; Furche, F.; Evans, W. J. *J. Am. Chem. Soc.*, **2015**, *137*, 369-382.
- (26) Xie, Z.; Hahn, F. E.; Qian, C. *J. Organomet. Chem.*, **1991**, *414*, C12-C14.
- (27) Stults, S. D.; Andersen, R. A.; Zalkin, A. *Organometallics*, **1990**, *9*, 115-122.
- (28) Zhou, X.-G.; Huang, Z.-E.; Cai, R.-F.; Yu, S.-N.; Huang, X.-Y. *Chin. J. Struct. Chem.*, **1997**, *16*, 384.
- (29) Burns, J. H.; Baldwin, W. H.; Fink, F. H. *Inorg. Chem.*, **1974**, *13*, 1916-1920.
- (30) Liu, T. *Kristallografiya*, **2002**, *47*, 470.
- (31) Fieser, M. E.; Woen, D. H.; Corbey, J. F.; Mueller, T. J.; Ziller, J. W.; Evans, W. J. *Dalton Trans.*, **2016**, *45*, 14634-14644.
- (32) Hammel, A.; Schwarz, W.; Weidlein, J. *J. Organomet. Chem.*, **1989**, *363*, C29-C35.
- (33) Shannon, R. *Acta Crystallographica Section A*, **1976**, *32*, 751-767.
- (34) Huh, D. N.; Darago, L. E.; Ziller, J. W.; Evans, W. J. *Inorg. Chem.*, **2018**, *57*, 2096-2102.
- (35) Jenkins, T. F.; Woen, D. H.; Mohanam, L. N.; Ziller, J. W.; Furche, F.; Evans, W. J. *Organometallics*, **2018**, *37*, 3863-3873.
- (36) Shimazaki, Y.; Stack, T. D. P.; Storr, T. *Inorg. Chem.*, **2009**, *48*, 8383-8392.
- (37) Leconte, N.; Moutet, J.; Constantin, T.; Molton, F.; Philouze, C.; Thomas, F. *Eur. J. Inorg. Chem.*, **2018**, 1752-1761.
- (38) Jaroschik, F.; Momin, A.; Nief, F.; Le Goff, X.-F.; Deacon, G. B.; Junk, P. C. *Angew. Chem. Int. Ed.*, **2009**, *48*, 1117-1121.
- (39) Fang, M.; Farnaby, J. H.; Ziller, J. W.; Bates, J. E.; Furche, F.; Evans, W. J. *J. Am. Chem. Soc.*, **2012**, *134*, 6064-6067.
- (40) Rinehart, J. D.; Fang, M.; Evans, W. J.; Long, J. R. *J. Am. Chem. Soc.*, **2011**, *133*, 14236-14239.
- (41) Fang, M.; Bates, J. E.; Lorenz, S. E.; Lee, D. S.; Rego, D. B.; Ziller, J. W.; Furche, F.; Evans, W. J. *Inorg. Chem.*, **2011**, *50*, 1459-1469.

- (42) Rinehart, J. D.; Fang, M.; Evans, W. J.; Long, J. R. *Nature Chemistry*, **2011**, *3*, 538.
- (43) Woen, D. H.; Chen, G. P.; Ziller, J. W.; Boyle, T. J.; Furche, F.; Evans, W. J. *J. Am. Chem. Soc.*, **2017**, *139*, 14861-14864.
- (44) Mingos, P. M. D.; Rohl, A. L. *Inorg. Chem.*, **1991**, *30*, 3769-3771.
- (45) Reynolds, L. T.; Wilkinson, G. J. *Inorg. Nucl. Chem.*, **1959**, *9*, 86-92.
- (46) Bergbreiter, D. E.; Killough, J. M. *J. Am. Chem. Soc.*, **1978**, *100*, 2126-2134.
- (47) APEX2 Version 2014.11-0, Bruker AXS, Inc.; Madison, WI 2014.
- (48) SAINT Version 8.34a, Bruker AXS, Inc.; Madison, WI 2013.
- (49) Sheldrick, G. M. SADABS, Version 2014/5, Bruker AXS, Inc.; Madison, WI 2014.
- (50) Sheldrick, G. M. SHELXTL, Version 2014/7, Bruker AXS, Inc.; Madison, WI 2014.
- (51) International Tables for Crystallography 1992, Vol. C., Dordrecht: Kluwer Academic Publishers.

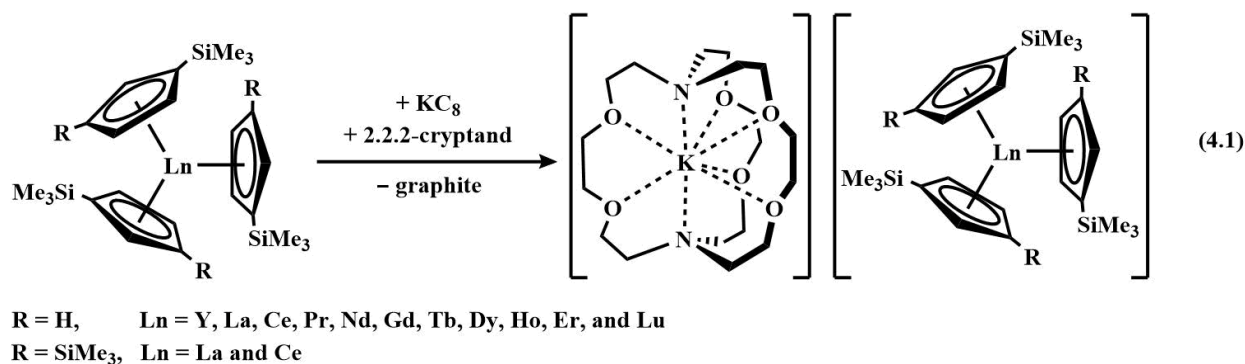


## CHAPTER 4

### Synthesis of Rare-Earth-Metal-in-Cryptand Dications, $[\text{Ln}(2.2.2\text{-cryptand})]^{2+}$ , from $\text{Sm}(\text{II})$ , $\text{Eu}(\text{II})$ , and $\text{Yb}(\text{II})$ Silyl Metallocenes $(\text{C}_5\text{H}_4\text{SiMe}_3)_2\text{Ln}(\text{THF})_2$

#### Introduction\*

As described in Chapter 1, studies of reductive rare-earth metal chemistry have shown that the +2 oxidation state is available for all of the rare-earth metals (except Pm, which was not studied due to its radioactivity) as soluble molecular complexes,  $[\text{K}(\text{crypt})][\text{Cp}'_3\text{Ln}]$  ( $\text{Cp}' = \text{C}_5\text{H}_4\text{SiMe}_3$ ).<sup>1-4</sup> Rare-earth metals Eu, Yb, Sm, Tm, Dy, and Nd were thought to be capable of forming isolable +2 complexes based on the calculated redox potentials for the reduction of  $4f^n \text{Ln}(\text{III})$  ions to  $4f^{n+1} \text{Ln}(\text{II})$  species.<sup>5-6</sup> The new Ln(II) ions were obtained according to eq 4.1 in tris(cyclopentadienyl) ligand environments



that had low lying  $d_{z^2}$  orbitals such that  $4f^n 5d^1$  ground states became available via reduction of a  $4f^n \text{Ln}(\text{III})$  ion with potassium.<sup>1-6</sup>

A natural extension of the discovery of new +2 oxidation states is the pursuit of molecular complexes of lanthanide metals ions in the +1 oxidation state. Ln(I) ions are known in

\*Portions of this chapter have been published: Huh, D. N.; Kotyk, C. M.; Gembicky, M.; Rheingold, A. L.; Ziller, J. W.; Evans, W. J. Synthesis of Rare-Earth-Metal-in-Cryptand Dications,  $[\text{Ln}(2.2.2\text{-cryptand})]^{2+}$ , from  $\text{Sm}^{2+}$ ,  $\text{Eu}^{2+}$ , and  $\text{Yb}^{2+}$  Silyl Metallocenes  $(\text{C}_5\text{H}_4\text{SiMe}_3)_2\text{Ln}(\text{THF})_2$ . *Chem. Commun.* **2017**, *53*, 8664-8666. DOI: 10.1039/C7CC04396A

the gas phase for all lanthanides,<sup>7</sup> molecular complexes of Sc(I) ions have been isolated and crystallographically characterized,<sup>8-9</sup> and spectroscopic evidence for Sm<sup>1+</sup> in the solid state has been reported.<sup>10</sup> In addition, Ln(C<sub>6</sub>H<sub>3</sub><sup>t</sup>Bu<sub>3</sub>-1,3,5)<sub>2</sub> complexes have been isolated for Ln = Nd, Tb, Dy, Ho, Er, and Lu that have the formal oxidation state of zero.<sup>11</sup> Sm(I) is an attractive target since it could have a half-filled shell 4f<sup>7</sup> electron configuration. In attempts to isolate Ln<sup>1+</sup> ions, silylcyclopentadienyl ligands were chosen since they are known to stabilize low oxidation state Ln(II) ions.<sup>1, 3-6, 12</sup>

Previous work by Dr. Christopher M. Kotyk demonstrated that reduction of dark green Cp<sup>''</sup><sub>2</sub>Sm(THF) with KC<sub>8</sub> in the presence of crypt immediately formed a dark brown product that was characterized by X-ray crystallography as the bimetallic, mixed-ligand, metallocene/opened-crypt Sm(II) complex, [Sm(C<sub>16</sub>H<sub>32</sub>N<sub>2</sub>O<sub>6</sub>-κ<sup>2</sup>O:κ<sup>2</sup>O')SmCp<sup>''</sup><sub>2</sub>], **11-Sm**, Figure 4.1, eq 4.2. The

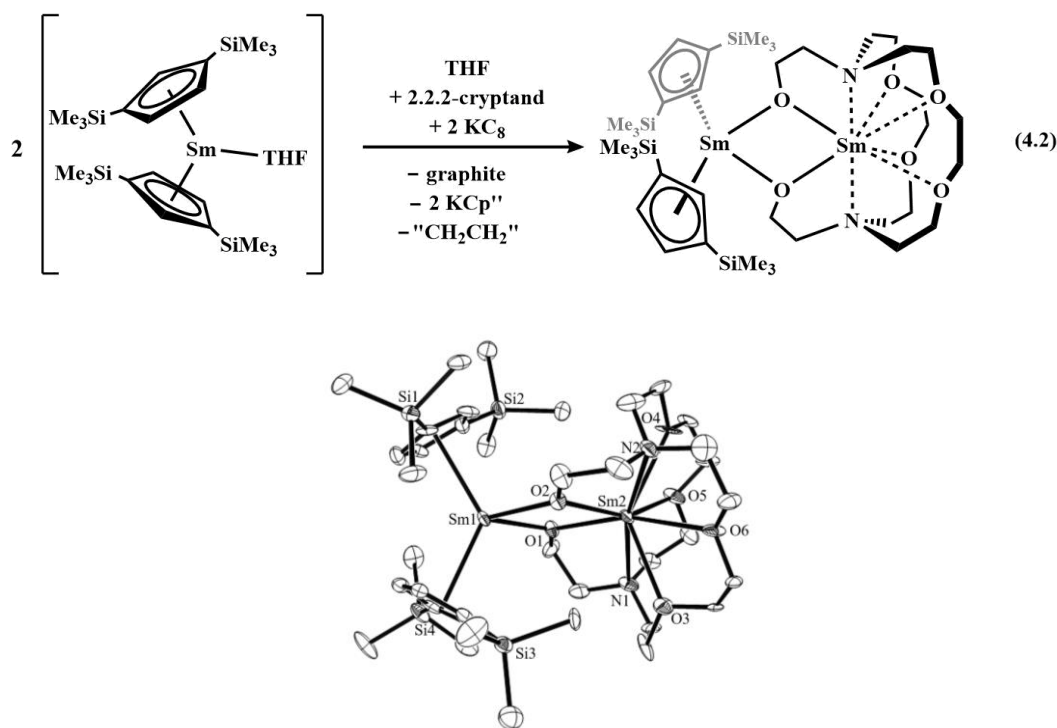


**Figure 4.1.** ORTEP representation of [Sm(C<sub>16</sub>H<sub>32</sub>N<sub>2</sub>O<sub>6</sub>-κ<sup>2</sup>O:κ<sup>2</sup>O')SmCp<sup>''</sup><sub>2</sub>], **11-Sm**, with the thermal ellipsoid plot drawn at 30% probability level. Hydrogen atoms are omitted for clarity.

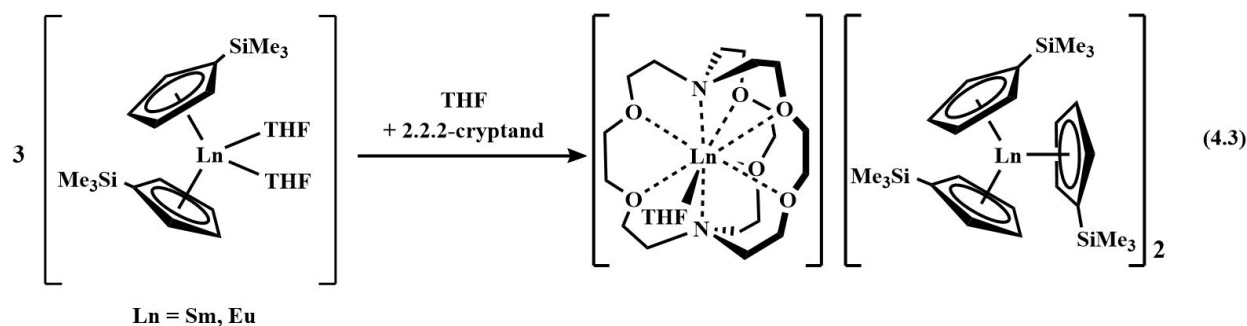
product is highly unusual in that one Sm(II) ion has lost both cyclopentadienyl ligands and resides inside a modified cryptand ligand that has lost a “CH<sub>2</sub>CH<sub>2</sub>” bridge.<sup>13</sup> Many reports of C–O bond cleavage under reducing conditions are in the literature.<sup>14-20</sup> The resulting crypt fragment is formally a dianion, (C<sub>16</sub>H<sub>32</sub>N<sub>2</sub>O<sub>6</sub>)<sup>2-</sup> containing two anionic alkoxide functionalities. These coordinate to a SmCp''<sub>2</sub> moiety, which effectively replaces the “CH<sub>2</sub>CH<sub>2</sub>” bridge to complete the cryptand structure. Unfortunately, the X-ray data on **11-Sm** were sufficient for a connectivity-only structure and detailed bond distance analysis is not possible.

This chapter describes reactions of crypt alone with Ln(II) metallocenes which were examined to obtain background information on the **11-Sm** reduction product. Crystallographic data were obtainable with Cp'<sub>2</sub>Ln(THF)<sub>2</sub> (Ln = Sm, Eu, Yb) that provided a general synthesis of Ln(II)-in-crypt dications with ligand redistribution counteranions, [Cp'<sub>3</sub>Ln]<sup>1-</sup>.

## Results and Discussion

To investigate the unusual result in eq 4.2, the reactivity of Ln(II) silyl metallocenes with the crypt ligand alone was studied as a control reaction. Since reactions of crypt with Cp''<sub>2</sub>Sm(THF)<sup>13</sup> did not give tractable products, the reactivity of the less soluble Cp' analog was studied.

The Cp'<sub>2</sub>Ln(THF)<sub>2</sub> complexes (Ln = Sm,<sup>4</sup> Eu<sup>15</sup>) react in THF with crypt in the absence of a reductant within two minutes to form new examples of dark purple Sm(II)-in-crypt and dark red Eu(II)-in-crypt complexes, [Ln(crypt)(THF)][Cp'<sub>3</sub>Ln]<sub>2</sub>, **12-Ln**, isolated in 50% (Sm) and 67% (Eu) yields. As shown in eq 4.3, a ligand rearrangement occurs that generates two [Cp'<sub>3</sub>Ln]<sup>1-</sup> anions.



and a  $[\text{Ln}(\text{crypt})(\text{THF})]^{2+}$  counteranion in the complexes  $[\text{Ln}(\text{crypt})(\text{THF})][\text{Cp}'_3\text{Ln}]_2$ , **12-Ln**, Figure 4.2. This reaction is reminiscent of the ligand rearrangement reported by Lappert and coworkers in which unsolvated  $\text{Cp}''_2\text{Sm}$  reacts with 18-crown-6 (18-c-6) in benzene to form a monocyclopentadienyl crown cation complex of a tris(cyclopentadienyl) anion,  $[\text{Sm}(18\text{-c-}6)\text{Cp}''][\text{Cp}''_3\text{Sm}]$ .<sup>21</sup>

The  $[\text{Ln}(\text{crypt})(\text{THF})]^{2+}$  dication in **12-Ln** is unusual in two respects: it is a rare case of a Ln(II) ion in a crypt and a rare case of any lanthanide ion in a crypt without an additional anionic ligand. Several examples of Ln(III) ions in crypt have been reported including the X-ray crystal structures of  $[\text{Ln}(\text{NO}_3)_5(\text{OH}_2)][\text{Ln}(\text{crypt})(\text{NO}_3)]$  (Ln = Nd, Sm, Eu),<sup>22-24</sup>  $[\text{La}(\text{crypt})(\text{OH}_2)\text{Cl}](\text{Cl})_2$ ,<sup>25</sup>  $[\text{La}(\text{crypt})(\text{OTf})(\text{DMF})_2](\text{OTf})_2$ ,<sup>25</sup> and  $[\text{Eu}(\text{crypt})(\text{ClO}_4)](\text{ClO}_4)_2$ .<sup>26</sup> In each of these cases, there is an anionic ligand binding the lanthanide in addition to crypt. Ln(II) ions have not been reported in crypt, but the structure of Eu(II) in a fluorobenzocryptand, [5,6-(4-fluorobenzo)-4,7,13,16,21,24-hexaoxa-1,10-diazabicyclo[8.8.8]hexacos-5-ene],  $\text{Eu}(\text{fluorobenzocrypt})\text{Cl}]\text{Cl}$ , is known.<sup>27</sup> As in all other cases, there is one anionic ligand bound to the metal in addition to this cryptand. The metrical parameters in  $[\text{Eu}(\text{crypt})(\text{THF})][\text{Cp}'_3\text{Eu}]_2$ , **12-Eu**, will be discussed in detail, since the crystallographic data on **12-Sm** were sufficient for connectivity only. The bond distances and angles in the  $[\text{Cp}'_3\text{Eu}]^{1-}$  counter-anions in **12-Eu** are the same as those of  $[\text{K}(\text{crypt})][\text{Cp}'_3\text{Eu}]^3$  within the error limits.

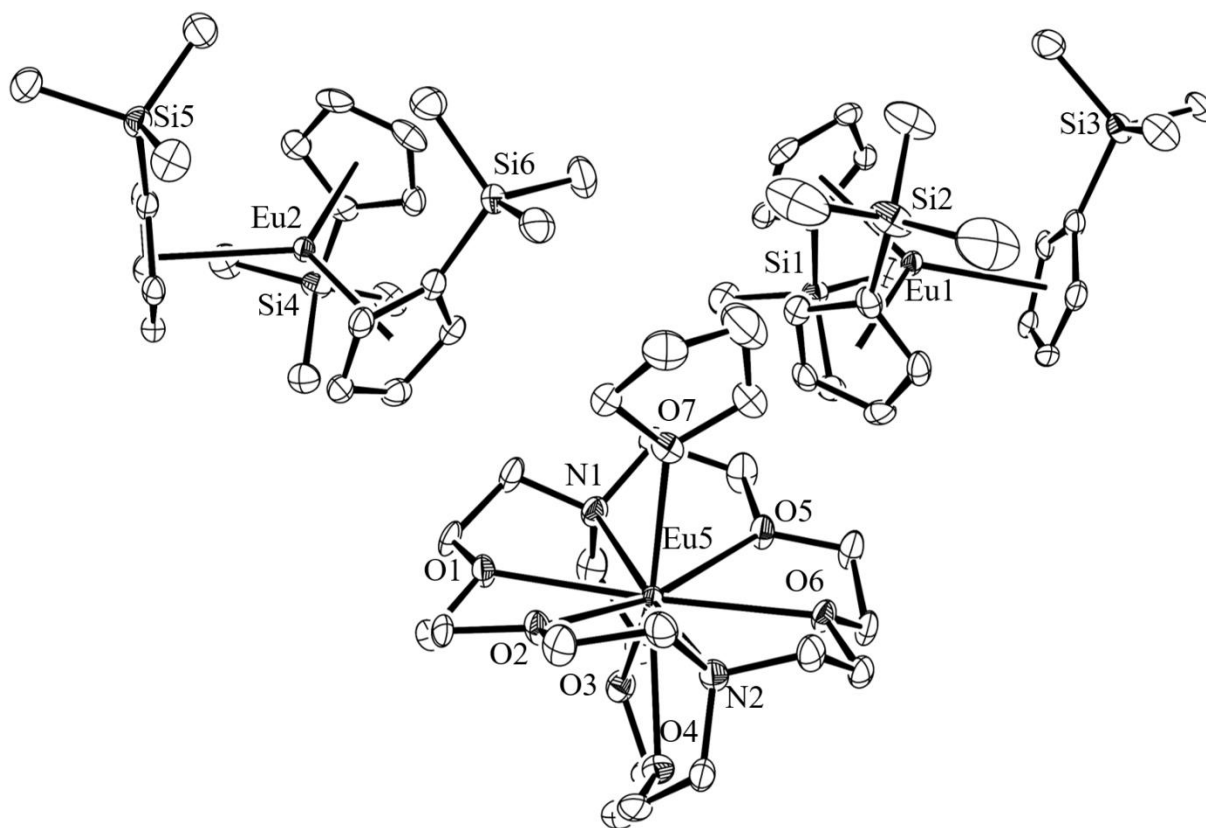
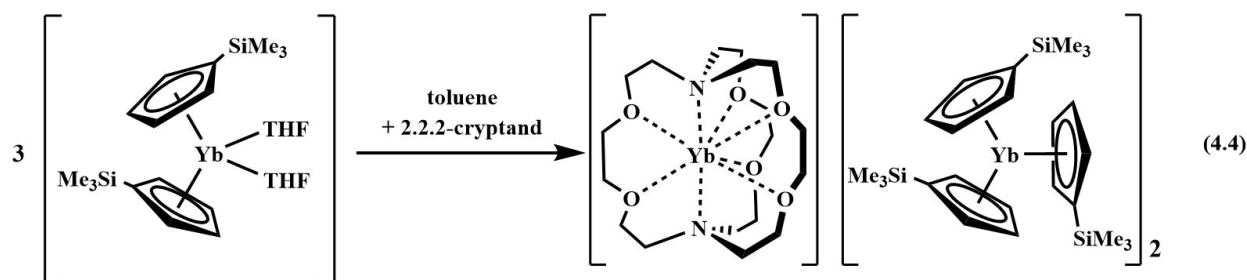


**Figure 4.2.** ORTEP representation of  $[\text{Eu}(\text{crypt})(\text{THF})][\text{Cp}'_3\text{Eu}]_2$ , **12-Eu** thermal ellipsoids drawn at the 50% probability level. Hydrogen atoms are omitted for clarity. Distances in Å: Eu5–O1 2.656(4), Eu5–O2 2.657(4), Eu5–O3 2.632(4), Eu5–O4 2.620(3), Eu5–O5 2.657(4), Eu5–O6 2.682(4), Eu5–O7 2.567(3), Eu5–N1 2.855(5), Eu5–N2 2.871(5), average Eu–Cp' centroid 2.62.

The nine-coordinate encapsulated Eu(II) ion has an irregular geometry that can roughly be described as a hexagonal pyramid that has the THF oxygen, O7, in the axial position and O3 and O4 below the “plane” of O1, O2, O5, O6, N1 and N2 donor atoms. The latter six atoms and Eu5 are only co-planar to within 0.19 Å. The 174° N–Eu–N angle in the cation of **12-Eu** is within the range of angles of 169.26 to 178.72° observed in the five Ln(III) crypt structures listed above. The Eu–O<sub>THF</sub> distance 2.568(3) Å in **12-Eu** is consistent with that in

$[(C_5Me_5)Eu(THF)]_2[C_8H_4(Si^iPr_3)_2]$ , 2.555(5) Å.<sup>13, 28</sup> The Eu–O<sub>crypt</sub> distances in **12-Eu** range from 2.620(3) to 2.681(4) Å and the Eu–N<sub>crypt</sub> lengths vary from 2.849(5) to 2.870(5) Å. Previously isolated Eu(III) cryptates were reported to have shorter bond distances as expected for the smaller +3 ion<sup>29</sup>:  $[Eu(crypt)(ClO_4)](ClO_4)_2$ , Eu–O<sub>crypt</sub> 2.44(4) to 2.52(3) Å and Eu–N<sub>crypt</sub> 2.64(3) to 2.70(5) Å;  $[Eu(NO_3)_5(OH_2)][Eu(crypt)(NO_3)]$ , Eu–O<sub>crypt</sub> 2.440(3) to 2.563(4) Å and Eu–N<sub>crypt</sub> 2.747(5) to 2.7776(6) Å.<sup>23, 26</sup>



In the case of the smaller metal, ytterbium, a Ln(II)-in-crypt dication was obtained that has no coordinated THF. Purple  $Cp'_2Yb(THF)_2$  reacts with crypt in toluene to form green  $[Yb(crypt)][Cp'_3Yb]_2$ , **13-Yb**, in 18% yield, eq 4.4. The complex **13-Yb** is the first example of ytterbium in a cryptand. As in the anion of **12-Eu**, the  $[Cp'_3Yb]^{1-}$  anion bond distances in **13-Yb** are equivalent to those of the previously reported  $[K(crypt)][Cp'_3Yb]$ .<sup>3</sup> The coordination geometry of the encapsulated Yb(II) is also irregular, but it can be approximated by a bicapped distorted octahedron with the nitrogen atoms in capping vertices. The Yb–O<sub>crypt</sub> and Yb–N<sub>crypt</sub> average distances are 0.15 to 0.16 Å shorter than those in **12-Eu**, which is similar to the difference in ionic radii of 0.16 Å for nine-coordinate Eu(II) and eight-coordinate Yb(II) ions.<sup>29</sup>

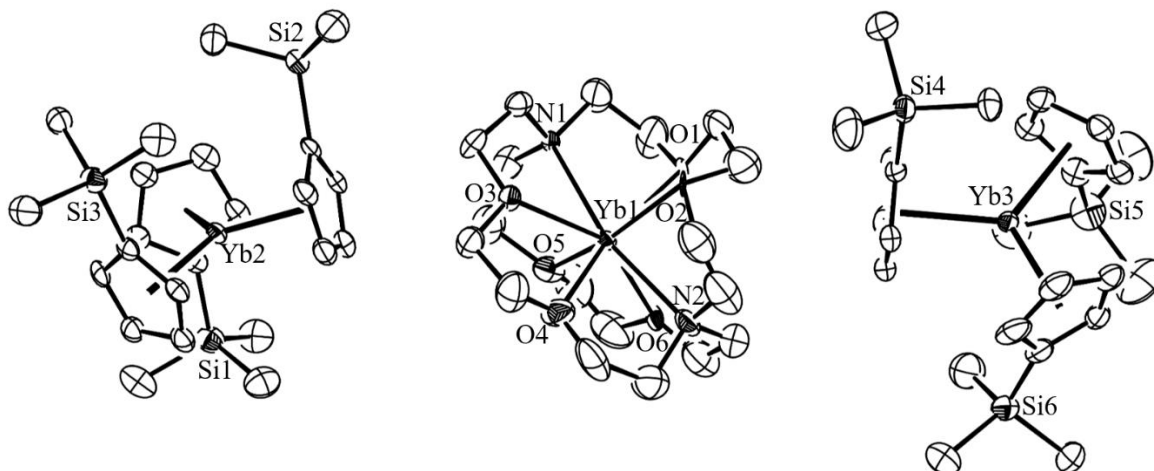


**Figure 4.3.** ORTEP representation of  $[\text{Yb}(\text{crypt})][\text{Cp}'_3\text{Yb}]_2$ , **13-Yb** thermal ellipsoids drawn at the 50% probability level. Hydrogen atoms are omitted for clarity. Distances in Å: Yb3–O1 2.508(8), Yb3–O2 2.496(6), Yb3–O3 2.444(7), Yb3–O4 2.539(5), Yb3–O5 2.506(6), Yb3–O6 2.493(6), Yb3–N1 2.634(15), Yb3–N2 2.613(10), average Yb–Cp' centroid 2.50.

## Conclusions

The facile ligand distribution in eq 4.3 and 4.4 was not expected. It was thought that Ln(II) ions would prefer anionic cyclopentadienyl ligands to the neutral ligand environment of the  $[\text{Ln}(\text{crypt})(\text{THF})]^{2+}$  or  $[\text{Ln}(\text{crypt})]^{2+}$  dications. Formation of the  $[\text{Cp}'_3\text{Ln}]^{1-}$  counteranions is also unusual since  $(\text{Cp}')^{1-}$  loss from these anions appears to be facile in some cases.<sup>2</sup> The transformation in eq 4.2 is even more unusual. It is not known if this involves a Sm(I) intermediate or if traditional Sm(II) reaction pathways can lead to such species. The Ln(II) cryptate cations are interesting in reduction chemistry since Allen and coworkers have found that Eu(II) is stabilized with respect to oxidation when encapsulated in cryptates.<sup>30-31</sup> Hence, these complexes may be good precursors to Ln(I) species.

## Experimental

All syntheses and manipulations described below were conducted under nitrogen or argon with rigorous exclusion of air and water using glovebox, Schlenk-line, and high-vacuum techniques.  $\text{KC}_8$ ,<sup>32</sup>  $\text{Cp}'_2\text{Ln}(\text{THF})_2$  ( $\text{Ln} = \text{Sm}, \text{Eu}, \text{Yb}$ ),<sup>33</sup> and  $\text{Cp}''_2\text{Sm}(\text{THF})$ <sup>34</sup> were prepared according to previously published literature. 2.2.2-Cryptand (4,7,13,16,21,24-hexaoxa-1,10-diazabicyclo[8.8.8]hexacosane, Aldrich) was placed under vacuum ( $10^{-3}$  Torr) for 12 h before use. Solvents were sparged with UHP argon and dried over columns containing Q-5 and molecular sieves.  $^1\text{H}$  NMR (500 MHz) and  $^{13}\text{C}$  NMR (125 MHz) spectra were obtained on a Bruker GN500 or CRYO500 MHz spectrometer at 298 K. IR samples were prepared as KBr pellets on a Varian 1000 FT-IR system. Elemental analyses were performed on a PerkinElmer series II 2400 CHNS analyzer.

**[Sm(C<sub>16</sub>H<sub>32</sub>N<sub>2</sub>O<sub>6</sub>-κ<sup>2</sup>O:κ<sup>2</sup>O')SmCp''<sub>2</sub>], 11-Sm.**  $\text{KC}_8$  (28 mg, 0.21 mmol) was added to a dark green solution of  $\text{Cp}''_2\text{Sm}(\text{THF})$  (75 mg, 0.12 mmol) and 2.2.2-cryptand (66 mg, 0.18 mmol) stirred in THF (1.5 mL). After 5 min, the brown solution was filtered, layered into  $\text{Et}_2\text{O}$ , and placed in a  $-35$  °C freezer. After 2 d, X-ray quality dark brown crystals of the product were isolated.

**[Sm(crypt)(THF)][Cp'<sub>3</sub>Sm]<sub>2</sub>, 12-Sm.** Addition of THF (3 mL) to a mixture of purple  $\text{Cp}'_2\text{Sm}(\text{THF})_2$  (50 mg, 0.088 mmol) and 2.2.2-cryptand (11 mg, 0.029 mmol) formed a dark purple solution. The mixture was stirred for 2 h and placed in a  $-35$  °C freezer in a vial within a vial containing pentane for vapor diffusion crystallization. After 2 d, X-ray quality dark purple crystals of **2-Sm** were isolated (30mg, 0.018 mmol, 50%). IR: 3064s, 2947s, 2887s, 2697w, 2345w, 1665w, 1595w, 1560w, 1476m, 1458m, 1439s, 1397m, 1354s, 1306m, 1275m, 1257s, 1242s, 1182s, 1109s, 1085s, 1063s, 1038s, 953s, 903s, 827s, 741s, 679m, 638m, 626m  $\text{cm}^{-1}$ .



Anal. Calcd for [Sm(crypt)(THF)][Cp'3Sm]2 C, 48.82; H, 7.08; N, 1.62. Found: C, 42.11; H, 6.09; N, 1.66. Elemental analysis was complicated by incomplete combustion which has been observed before for silyl lanthanide complexes.<sup>35-37</sup> However, the CHN ratios found by elemental analysis, 70:123.6:2.4, match that calculated: C<sub>70</sub>H<sub>122</sub>N<sub>2</sub>.

**[Eu(crypt)(THF)][Cp'3Eu]2, 12-Eu.** As described for **2-Sm**, an orange THF solution of Cp'2Eu(THF)<sub>2</sub> (50 mg, 0.088 mmol) was reacted with 2.2.2-cryptand (11 mg, 0.029 mmol). Upon addition of 2.2.2-cryptand, the solution immediately formed a dark red solution. The dark red solution was placed in a vial within a vial containing pentane for vapor diffusion. After 4 d, dark red X-ray quality crystals were formed. (34 mg, 0.020 mmol, 67%). IR: 3065s, 2949s, 2889s, 2749w, 2697w, 2654w, 2607w, 2540w, 2486w, 2465w, 2407w, 2347w, 2257w, 2160w, 2087w, 1919w, 1869w, 1665w, 1595w, 1560w, 1553w, 1476m, 1458m, 1438s, 1397m, 1354s, 1306m, 1292m, 1277m, 1242s, 1182s, 1189s, 1109s, 1086s, 1065s, 1038s, 955s, 903s, 829s, 744s, 679m, 638m, 627m cm<sup>-1</sup>. Anal. Calcd for [Eu(crypt)(THF)][Cp'3Eu]2: C, 48.68; H, 7.06; N, 1.62. Found: C, 46.18; H, 6.61; N, 1.54 Elemental analysis was complicated by incomplete combustion which has been observed before for silyl lanthanide complexes.<sup>35-37</sup> However, the CHN ratios found by elemental analysis, 70:119.3:2.0, match that calculated: C<sub>70</sub>H<sub>122</sub>N<sub>2</sub>.

**[Yb(crypt)][Cp'3Yb]2, 13-Yb.** A solution of Cp'2Yb(THF)<sub>2</sub> (103 mg, 0.17 mmol) in toluene (50 mL) was added dropwise to a solution of 2.2.2-cryptand (22 mg, 0.058 mmol) in toluene (3 mL) which formed a light green solution. The mixture was stirred for 2 h and the solution was filtered from an insoluble green precipitate. Toluene was removed from the filtrate *in vacuo* and Et<sub>2</sub>O (*ca.* 3 mL) was added. Microcrystals formed at -35° C after 2 d (18 mg, 0.010 mmol, 18%). Light green X-ray quality crystals were obtained by placing a concentrated

solution of the product in toluene at  $-35\text{ }^{\circ}\text{C}$  after 1 d.  $^1\text{H}$  NMR ( $\text{C}_6\text{D}_6$ ):  $\delta$  6.67 (s,  $\text{C}_5\text{H}_4\text{SiMe}_3$ , 12H), 6.46 (s,  $\text{C}_5\text{H}_4\text{SiMe}_3$ , 12H),  $-0.11$  (s,  $\text{C}_5\text{H}_4\text{SiMe}_3$ , 54H).  $^{13}\text{C}$  NMR ( $\text{C}_6\text{D}_6$ ):  $\delta$  133.4 ( $\text{C}_5\text{H}_4\text{SiMe}_3$ ), 130.6 ( $\text{C}_5\text{H}_4\text{SiMe}_3$ ), 127.6 ( $\text{C}_5\text{H}_4\text{SiMe}_3$ ),  $-2.08$  ( $\text{C}_5\text{H}_4\text{SiMe}_3$ ). IR: 3068m, 2947s, 2886m, 2824s, 2762w, 2731w, 2697w, 2085w, 1958w, 1919w, 1560w, 1479m, 1456m, 1446s, 1439s, 1416w, 1398w, 1381w, 1360s, 1354s, 1302s, 1260s, 1240s, 1182s, 1134s, 1105s, 1082s, 1055w, 1036s, 951s, 934s, 905s, 831s, 748s, 741s, 687m, 679m, 664w, 638m, 629m  $\text{cm}^{-1}$ .

### Structural Details

**X-ray Data Collection, Structure Solution and Refinement for 11-Sm,  $[\text{Sm}(\text{C}_{16}\text{H}_{32}\text{N}_2\text{O}_6\text{-}\kappa^2\text{O}:\kappa^2\text{O}')\text{SmCp}''_2]$ .** A black crystal of approximate dimensions 0.225 x 0.281 x 0.330 mm was mounted on a glass fiber and transferred to a Bruker SMART APEX II diffractometer. The APEX2<sup>38</sup> program package was used to determine the unit-cell parameters and for data collection (60 sec/frame scan time for a sphere of diffraction data). The raw frame data was processed using SAINT<sup>39</sup> and SADABS<sup>40</sup> to yield the reflection data file. Subsequent calculations were carried out using the SHELXTL<sup>41</sup> program. The diffraction symmetry was  $2/m$  and the systematic absences were consistent with the monoclinic space groups  $Cc$  and  $C2/c$ . It was later determined that space group  $Cc$  was correct. The structure was solved by direct methods and refined on  $F^2$  by full-matrix least-squares techniques. The analytical scattering factors<sup>42</sup> for neutral atoms were used throughout the analysis. Hydrogen atoms were included using a riding model. There were two molecules of the formula-unit and two molecules of tetrahydrofuran solvent present. Several atoms were disordered and included using multiple components with partial site-occupancy-factors. Least-squares yielded  $wR2 = 0.2105$  and  $\text{Goof} = 1.114$  for 787 variables refined against 25579 data ( $0.74\text{\AA}$ ),  $R1 = 0.0861$  for those 22978 data with  $I > 2.0\sigma(I)$ . The structure was refined as a two-component inversion twin. There were

several high residuals present in the final difference-Fourier map. It was not possible to determine the nature of the residuals although it was probable that additional tetrahydrofuran solvent was present. The SQUEEZE<sup>43a</sup> routine in the PLATON<sup>43b</sup> program package was used to account for the electrons in the solvent accessible voids.

**X-ray Data Collection, Structure Solution and Refinement for 12-Eu, [Eu(crypt)(THF)][Cp'3Eu]2.** An orange crystal of approximate dimensions 0.060 x 0.085 x 0.140 mm was mounted in a cryoloop. Data were collected on a Bruker Kappa four-circle micro-focus rotating anode diffractometer system equipped with an APEX II CCD detector. The APEX3<sup>38</sup> program package was used to determine the unit-cell parameters and for data collection (3 sec/frame scan time). The raw frame data was processed using SAINT<sup>39</sup> and SADABS<sup>40</sup> to yield the reflection data file. Subsequent calculations were carried out using the SHELXTL<sup>41</sup> program. There were no systematic absences nor any diffraction symmetry other than the Friedel condition. The centrosymmetric triclinic space group  $P\bar{1}$  was assigned and later determined to be correct. The structure was solved by dual space methods and refined on  $F^2$  by full-matrix least-squares techniques. The analytical scattering factors<sup>42</sup> for neutral atoms were used throughout the analysis. Hydrogen atoms were included using a riding model. Disordered atoms were included using multiple components with partial site-occupancy factors. There were two formula-units present ( $Z=4$ ) and four molecules of tetrahydrofuran solvent present per formula-unit. At convergence,  $wR2 = 0.0937$  and  $Goof = 1.015$  for 1985 variables refined against 37495 data ( $0.82\text{\AA}$ ),  $R1 = 0.0402$  for those 26135 data with  $I > 2.0\sigma(I)$ .

**X-ray Data Collection, Structure Solution and Refinement for 12-Sm, [Sm(crypt)(THF)][Cp'3Sm]2.** A violet crystal of approximate dimensions 0.130 x 0.130 x 0.141 mm was mounted in a cryoloop and transferred to a Bruker SMART APEX II

diffractometer. The APEX2<sup>38</sup> program package was used to determine the unit-cell parameters and for data collection (30 sec/frame scan time for a sphere of diffraction data). The raw frame data was processed using SAINT<sup>39</sup> and SADABS<sup>40</sup> to yield the reflection data file. Subsequent calculations were carried out using the SHELXTL<sup>41</sup> program. There were no systematic absences nor any diffraction symmetry other than the Friedel condition. The centrosymmetric triclinic space group  $P\bar{1}$  was assigned and later determined to be correct. The structure was solved using the coordinates of the europium analogue and refined on  $F^2$  by full-matrix least-squares techniques. The analytical scattering factors<sup>42</sup> for neutral atoms were used throughout the analysis. Hydrogen atoms were included using a riding model. Disordered atoms were included using multiple components with partial site-occupancy factors. There were two formula-units present ( $Z=4$ ) and four molecules of tetrahydrofuran solvent present per formula-unit. Least-squares analysis yielded  $wR2 = 0.1442$  and  $Goof = 0.941$  for 1975 variables refined against 37384 data ( $0.82\text{\AA}$ ),  $R1 = 0.0674$  for those 17221 data with  $I > 2.0\sigma(I)$ .

**X-ray Data Collection, Structure Solution and Refinement for 13-Yb, [Yb(crypt)][Cp'<sub>3</sub>Yb]<sub>2</sub>.** A green crystal of approximate dimensions 0.151 x 0.172 x 0.474 mm was mounted in a cryoloop and transferred to a Bruker SMART APEX II diffractometer. The APEX2<sup>38</sup> program package was used to determine the unit-cell parameters and for data collection (30 sec/frame scan time for a sphere of diffraction data). The raw frame data was processed using SAINT<sup>39</sup> and SADABS<sup>40</sup> to yield the reflection data file. Subsequent calculations were carried out using the SHELXTL<sup>41</sup> program. The diffraction symmetry was  $2/m$  and the systematic absences were consistent with the monoclinic space group  $P2_1/c$  that was later determined to be correct. The structure was solved by dual space methods and refined on  $F^2$  by full-matrix least-squares techniques. The analytical scattering factors<sup>42</sup> for neutral atoms were

used throughout the analysis. Hydrogen atoms were included using a riding model. Disordered atoms were included using partial site-occupancy-factors and isotropic thermal parameters. There were three molecules of toluene solvent present. Two of the toluene molecules were refined as rigid groups. At convergence,  $wR2 = 0.0968$  and  $Goof = 1.048$  for 792 variables refined against 24068 data ( $0.73 \text{ \AA}$ ),  $R1 = 0.0409$  for those 19184 data with  $I > 2.0\sigma(I)$ .

## References

- (1) Hitchcock, P. B.; Lappert, M. F.; Maron, L.; Protchenko, A. V., Lanthanum Does Form Stable Molecular Compounds in the +2 Oxidation State. *Angew. Chem. Int. Ed.* **2008**, *47* (8), 1488-1491.
- (2) MacDonald, M. R.; Ziller, J. W.; Evans, W. J., Synthesis of a Crystalline Molecular Complex of  $Y^{2+}$ , [(18-crown-6)K][(C<sub>5</sub>H<sub>4</sub>SiMe<sub>3</sub>)<sub>3</sub>Y]. *J. Am. Chem. Soc.* **2011**, *133* (40), 15914-15917.
- (3) Fieser, M. E.; MacDonald, M. R.; Krull, B. T.; Bates, J. E.; Ziller, J. W.; Furche, F.; Evans, W. J., Structural, Spectroscopic, and Theoretical Comparison of Traditional vs Recently Discovered Ln<sup>2+</sup> Ions in the [K(2.2.2-cryptand)][(C<sub>5</sub>H<sub>4</sub>SiMe<sub>3</sub>)<sub>3</sub>Ln] Complexes: The Variable Nature of Dy<sup>2+</sup> and Nd<sup>2+</sup>. *J. Am. Chem. Soc.* **2015**, *137* (1), 369-382.
- (4) MacDonald, M. R.; Bates, J. E.; Ziller, J. W.; Furche, F.; Evans, W. J., Completing the Series of +2 Ions for the Lanthanide Elements: Synthesis of Molecular Complexes of Pr<sup>2+</sup>, Gd<sup>2+</sup>, Tb<sup>2+</sup>, and Lu<sup>2+</sup>. *J. Am. Chem. Soc.* **2013**, *135* (26), 9857-9868.
- (5) Evans, W. J., Tutorial on the Role of Cyclopentadienyl Ligands in the Discovery of Molecular Complexes of the Rare-Earth and Actinide Metals in New Oxidation States. *Organometallics* **2016**, *35* (18), 3088-3100.
- (6) Woen, D. H.; Evans, W. J., Chapter 293 - Expanding the + 2 Oxidation State of the Rare-Earth Metals, Uranium, and Thorium in Molecular Complexes. In *Handbook on the Physics and Chemistry of Rare Earths*, Jean-Claude, G. B.; Vitalij, K. P., Eds. Elsevier: 2016; Vol. Volume 50, pp 337-394.
- (7) Dorenbos, P.,  $f \rightarrow d$  transition energies of divalent lanthanides in inorganic compounds. *J. Phys.: Condens. Matter* **2003**, *15* (3), 575.
- (8) Clentsmith, G. K. B.; Cloke, F. G. N.; Green, J. C.; Hanks, J.; Hitchcock, P. B.; Nixon, J. F., Stabilization of Low-Oxidation-State Early Transition-Metal Complexes Bearing 1,2,4-Triphosphacyclopentadienyl Ligands: Structure of [{Sc(P<sub>3</sub>C<sub>2</sub><sup>t</sup>Bu<sub>2</sub>)<sub>2</sub>]<sub>2</sub>]; Sc<sup>II</sup> or Mixed Oxidation State? *Angew. Chem. Int. Ed.* **2003**, *42* (9), 1038-1041.

- (9) Neculai, A.-M.; Cummins, C. C.; Neculai, D.; Roesky, H. W.; Bunkóczi, G.; Walfort, B.; Stalke, D., Elucidation of a Sc(I) Complex by DFT Calculations and Reactivity Studies. *Inorg. Chem.* **2003**, *42* (26), 8803-8810.
- (10) Fong, F. K.; Cape, J. A.; Wong, E. Y., Monovalent Samarium in Potassium Chloride. *Phys. Rev.* **1966**, *151* (1), 299-303.
- (11) Anderson, D. M.; Cloke, F. G. N.; Cox, P. A.; Edelstein, N.; Green, J. C.; Pang, T.; Sameh, A. A.; Shalimoff, G., On the stability and bonding in bis( $\eta$ -arene)lanthanide complexes. *J. Chem. Soc., Chem. Commun.* **1989**, (1), 53-55.
- (12) MacDonald, M. R.; Fieser, M. E.; Bates, J. E.; Ziller, J. W.; Furche, F.; Evans, W. J., Identification of the +2 Oxidation State for Uranium in a Crystalline Molecular Complex, [K(2.2.2-Cryptand)][(C<sub>5</sub>H<sub>4</sub>SiMe<sub>3</sub>)<sub>3</sub>U]. *J. Am. Chem. Soc.* **2013**, *135* (36), 13310-13313.
- (13) Evans, W. J.; Kociok-Köhn, G.; Foster, S. E.; Ziller, J. W.; Doedens, R. J., Synthesis and structure of mono-THF solvates of bis(cyclopentadienyl)samarium(II) complexes: (C<sub>5</sub>Me<sub>5</sub>)<sub>2</sub>Sm(THF) and [C<sub>5</sub>H<sub>2</sub>(SiMe<sub>3</sub>)<sub>3</sub>][C<sub>5</sub>H<sub>3</sub>(SiMe<sub>3</sub>)<sub>2</sub>]Sm(THF). *J. Organomet. Chem.* **1993**, *444* (1), 61-66.
- (14) Kim, J.; Ichimura, A. S.; Huang, R. H.; Redko, M.; Phillips, R. C.; Jackson, J. E.; Dye, J. L., Crystalline Salts of Na- and K- (Alkalides) that Are Stable at Room Temperature. *J. Am. Chem. Soc.* **1999**, *121* (45), 10666-10667.
- (15) Cauliez, P. M.; Jackson, J. E.; Dye, J. L., An unusual reduction of ethylene occurring during the thermal decomposition of alkalides and electrides. *Tetrahedron Lett.* **1991**, *32* (38), 5039-5042.
- (16) Gun'ko, Y. K.; Hitchcock, P. B.; Lappert, M. F., Activation of a C-O bond by reaction of a tris(cyclopentadienyl)lanthanide complex with an alkali metal in dimethoxyethane (DME); crystal structures of [Nd $\eta$ -C<sub>5</sub>H<sub>3</sub>(SiMe<sub>3</sub>)<sub>2-1,3</sub> 2( $\mu$ -OMe)<sub>2</sub>Li(DME)] and [{Ce( $\eta$ -C<sub>5</sub>H<sub>3</sub>tBu<sub>2-1,3</sub>)<sub>2</sub>( $\mu$ -OMe)<sub>2</sub>]. *J. Organomet. Chem.* **1995**, *499* (1), 213-219.
- (17) Duncalf, D. J.; Hitchcock, P. B.; Lawless, G. A., Synthesis and characterisation of iodo functionalised ytterbium(II) and ytterbium(III) alkoxides. *Chem. Commun.* **1996**, (2), 269-271.
- (18) Cristina Cassani, M.; F. Lappert, M.; Laschi, F., First identification by EPR spectra of lanthanum(ii) organometallic intermediates (and E<sub>1/2</sub> for La<sup>3+</sup> --> La<sup>2+</sup>) in the C-O bond activation of dimethoxyethane. *Chem. Commun.* **1997**, (16), 1563-1564.
- (19) Arnold, P. L.; Liddle, S. T., Deprotonation of N-Heterocyclic Carbenes to Afford Heterobimetallic Organolanthanide Complexes. *Organometallics* **2006**, *25* (6), 1485-1491.
- (20) Deacon, G. B.; Junk, P. C.; Moxey, G. J., Reactivity of Lanthanoid Aryloxy Complexes: Isolation of a 1,2-Dimethoxyethane Cleavage Product. *Z. Anorg. Allg. Chem.* **2008**, *634* (15), 2789-2792.

- (21) K. Gun'ko, Y.; B. Hitchcock, P.; F. Lappert, M., Displacement of a cyclopentadienyl ligand by a crown ether from a lanthanocene(II) [LnCp<sup>''</sup>]<sub>2</sub>]; crystal structures of the first cationic lanthanoid(II) complexes, [SmCp<sup>''</sup>([18]-crown-6)][SmCp<sup>''</sup>]<sub>3</sub> · 0.5C<sub>6</sub>H<sub>6</sub> and [YbCp<sup>''</sup>([18]-crown-6)][Cp<sup>''</sup>]<sub>3</sub> · 3C<sub>6</sub>H<sub>6</sub> [Cp<sup>''</sup> = η<sup>5</sup>-C<sub>5</sub>H<sub>3</sub>(SiMe<sub>3</sub>)<sub>2-1,3</sub>]. *Chem. Commun.* **1998**, (17), 1843-1844.
- (22) Benetollo, F.; Bombieri, G.; Cassol, A.; De Paoli, G.; Legendziewicz, J., Coordination chemistry of lanthanides with cryptands. An X-ray and spectroscopic study of the complex Nd<sub>2</sub>(NO<sub>3</sub>)<sub>6</sub> [C<sub>18</sub>H<sub>36</sub>O<sub>6</sub>N<sub>2</sub>] · H<sub>2</sub>O. *Inorg. Chim. Acta* **1985**, *110* (1), 7-13.
- (23) Yang, G.; Liu, S.; Jin, Z., Coordination chemistry and structure characterization of C<sub>18</sub>H<sub>36</sub>O<sub>6</sub>N<sub>2</sub>Eu<sub>2</sub>(NO<sub>3</sub>)<sub>6</sub> · H<sub>2</sub>O. *Inorg. Chim. Acta* **1987**, *131* (1), 125-128.
- (24) Burns, J. H., Crystal and molecular structure of a cryptate complex of samarium: C<sub>18</sub>H<sub>36</sub>O<sub>6</sub>N<sub>2</sub>Sm<sub>2</sub>(NO<sub>3</sub>)<sub>6</sub> · H<sub>2</sub>O. *Inorg. Chem.* **1979**, *18* (11), 3044-3047.
- (25) Mao, J.; Jin, Z., Synthesis and structure characterization of lanthanum [2,2,2]cryptates, [LaCl[2,2,2](H<sub>2</sub>O)]Cl<sub>2</sub> · H<sub>2</sub>O and [La(CF<sub>3</sub>SO<sub>3</sub>)[2,2,2](DMF)](CF<sub>3</sub>SO<sub>3</sub>)<sub>2</sub>. *Polyhedron* **1994**, *13* (2), 319-323.
- (26) Ciampolini, M.; Dapporto, P.; Nardi, N., Structure and properties of some lanthanoid(III) perchlorates with the cryptand 4,7,13,16,21,24-hexaoxa-1,10-diazabicyclo[8.8.8]hexacosane. *J. Chem. Soc. Dalton Trans.* **1979**, (6), 974-977.
- (27) Ekanger, L. A.; Polin, L. A.; Shen, Y.; Haacke, E. M.; Martin, P. D.; Allen, M. J., A Eu(II)-Containing Cryptate as a Redox Sensor in Magnetic Resonance Imaging of Living Tissue. *Angew. Chem. Int. Ed.* **2015**, *54* (48), 14398-14401.
- (28) Summerscales, O. T.; Jones, S. C.; Cloke, F. G. N.; Hitchcock, P. B., Anti-Bimetallic Complexes of Divalent Lanthanides with Silylated Pentalene and Cyclooctatetraenyl Bridging Ligands as Molecular Models for Lanthanide-Based Polymers. *Organometallics* **2009**, *28* (20), 5896-5908.
- (29) Shannon, R., Revised effective ionic radii and systematic studies of interatomic distances in halides and chalcogenides. *Acta Crystallographica Section A* **1976**, *32* (5), 751-767.
- (30) Gamage, N.-D. H.; Mei, Y.; Garcia, J.; Allen, M. J., Oxidatively Stable, Aqueous Europium(II) Complexes through Steric and Electronic Manipulation of Cryptand Coordination Chemistry. *Angew. Chem. Int. Ed.* **2010**, *49* (47), 8923-8925.
- (31) Yee, E. L.; Gansow, O. A.; Weaver, M. J., Electrochemical studies of europium and ytterbium cryptate formation in aqueous solution. Effects of varying the metal oxidation state upon cryptate thermodynamics and kinetics. *J. Am. Chem. Soc.* **1980**, *102* (7), 2278-2285.
- (32) Bergbreiter, D. E.; Killough, J. M., *J. Am. Chem. Soc.* **1978**, *100*, 2126-2134.
- (33) Fieser, M. E.; MacDonald, M. R.; Krull, B. T.; Bates, J. E.; Ziller, J. W.; Furche, F.; Evans, W. J., *J. Am. Chem. Soc.* **2015**, *137*, 369-382.

- (34) Evans, W. J.; Kociok-Köhn, G.; Foster, S. E.; Ziller, J. W.; Doedens, R. J., *J. Organomet. Chem.* **1993**, *444*, 61-66.
- (35) Chilton, N. F.; Goodwin, C. A. P.; Mills, D. P.; Winpenny, R. E. P., *Chem. Commun.* **2015**, *51*, 101-103.
- (36) Goodwin, C. A. P.; Chilton, N. F.; Vettese, G. F.; Moreno Pineda, E.; Crowe, I. F.; Ziller, J. W.; Winpenny, R. E. P.; Evans, W. J.; Mills, D. P., *Inorg. Chem.* **2016**, *55*, 10057-10067.
- (37) Goodwin, C. A. P.; Joslin, K. C.; Lockyer, S. J.; Formanuk, A.; Morris, G. A.; Ortu, F.; Vitorica-Yrezabal, I. J.; Mills, D. P., *Organometallics* **2015**, *34*, 2314-2325.
- (38) APEX2 Version 2014.11-0, Bruker AXS, Inc.; Madison, WI 2014.
- (39) SAINT Version 8.34a, Bruker AXS, Inc.; Madison, WI 2013.
- (40) Sheldrick, G. M. SADABS, Version 2014/5, Bruker AXS, Inc.; Madison, WI 2014.
- (41) Sheldrick, G. M. SHELXTL, Version 2014/7, Bruker AXS, Inc.; Madison, WI 2014.
- (42) International Tables for Crystallography 1992, Vol. C., Dordrecht: Kluwer Academic Publishers.
- (43) (a) Spek, A.L. SQUEEZE, *Acta Cryst.* 2015, *C71*, 9-19., (b) Spek, A. L. PLATON, *Acta. Cryst.* 2009, *D65*, 148-155



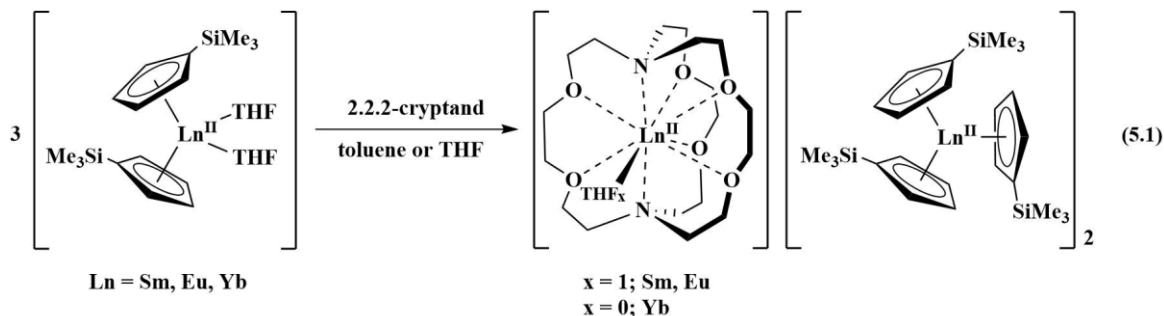
## CHAPTER 5

### Synthesis of Uranium-in-Cryptand Complexes

#### Introduction\*

Development of new ligand systems is critical to advancing the chemistry of any metal. This Chapter describes the first crystallographic confirmation of uranium encapsulated within the 2.2.2-cryptand (crypt) ligand. Since the crypt ligand has been known for decades,<sup>1,2</sup> it was quite surprising that it had not been used extensively with actinides. Numerous studies have been published on crypt, but most focus on alkali and alkaline-earth metals.<sup>1-4</sup> Lanthanide crypt complexes have been reported as early as 1980 in solution<sup>5</sup> and several crystal structures have been subsequently reported.<sup>6-10</sup> Complexes of lanthanide ions encapsulated in ligands that are variations of crypt are also known.<sup>11, 12</sup> With uranium, there are reports on the spectroscopy and elemental analysis of U(IV) and uranyl cryptand complexes dating back to 1976,<sup>13-16</sup> but no X-ray crystal structures of uranium crypt complexes were reported prior to this research.

The investigation of U-in-crypt complexes was stimulated by the discovery that Sm(II), Eu(II), and Yb(II) can be readily encapsulated into crypt from metallocene precursors according to eq 5.1.<sup>17</sup> It was sought to determine if facile encapsulation of actinides into crypt was possible



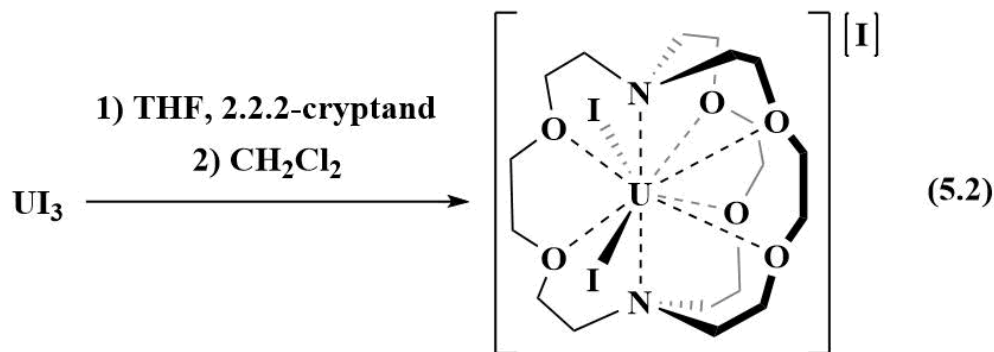
\*Portions of this chapter have been published: Huh, D. N.; Windorff, C. J.; Ziller, J. W.; Evans, W. J. Synthesis of Uranium-in-Cryptand Complexes. *Chem. Commun.*, **2018**, 54. 10272-10275. DOI: 10.1039/C8CC05341C

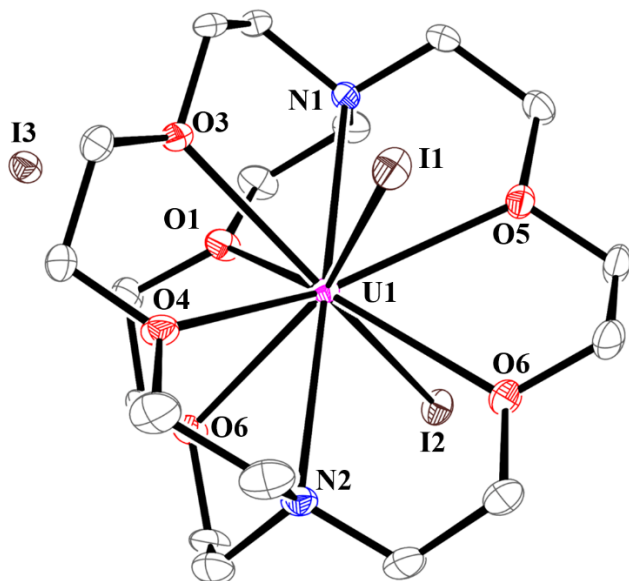
in toluene or THF and could also lead to crystallographically-characterizable compounds. This would not only establish this special coordination environment for these f block metals, but it could also be valuable in manipulating the redox chemistry for these elements. Lower oxidation states of the lanthanides have been shown to be stabilized by the crypt ligand.<sup>5, 18</sup> Hence metal-in-cryptand complexes are attractive precursors for generating low oxidation states of the rare-earth and actinide metals.<sup>19-26</sup>

## Results and Discussion

To probe the generality of incorporating f elements into the crypt ligand shown in eq 5.1, simple halides of uranium and lanthanum, a rare-earth metal of similar size, were treated with crypt. The first crystallographically-characterized actinide-in-cryptand and an analogous lanthanum-in-cryptand complex are herein described. In all the examples described below, there are two additional coordination sites accessible to the metal. This has allowed isolation of aquo complexes of U(III),<sup>27-30</sup> an ion that under other conditions can readily reduce water.<sup>31-35</sup>

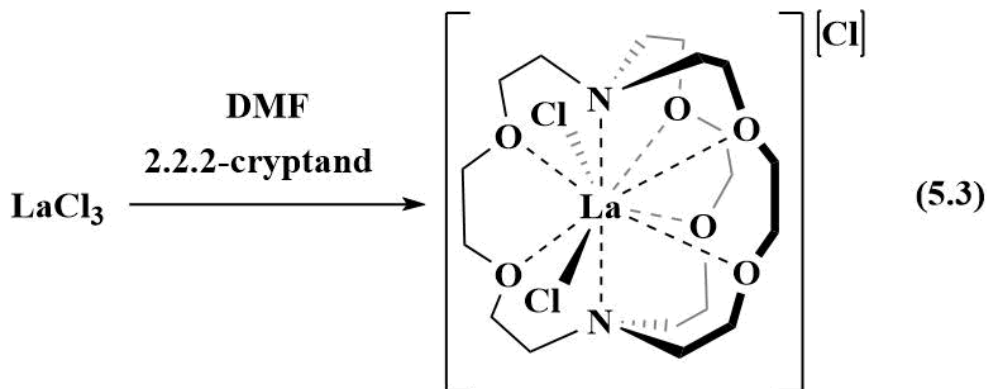
Addition of a blue THF solution of  $UI_3$  to a colorless THF solution of 2.2.2-cryptand (crypt) immediately forms a brown/green precipitate that is soluble in  $CH_2Cl_2$ . Recrystallization from  $CH_2Cl_2/Et_2O$  generates dichroic brown/green crystals of  $[U(crypt)_2I]I$ , **14-U**, eq 5.2. As shown in Figure 5.1, two iodides are coordinated to the U(III) ion in the crypt and one iodide is outer sphere.





**Figure 5.1.** ORTEP representation of  $[\text{U}(\text{crypt})\text{I}_2]\text{I}$ , **14-U**, with thermal ellipsoids drawn at the 50% probability level. Hydrogen atoms and three molecules of  $\text{CH}_2\text{Cl}_2$  were omitted for clarity.

An analogous reaction was conducted with  $\text{LaCl}_3$  since the larger rare-earth metals are often used as mimics for the actinides<sup>36</sup> and it was of interest to see if the reaction was also applicable to 4f metals. Treatment of  $\text{LaCl}_3$  with crypt in dimethylformamide (DMF) led to the insertion of La(III) into the crypt forming  $[\text{La}(\text{crypt})\text{Cl}_2]\text{Cl}$ , **15-La**, Figure 5.2, as shown in eq 5.3.



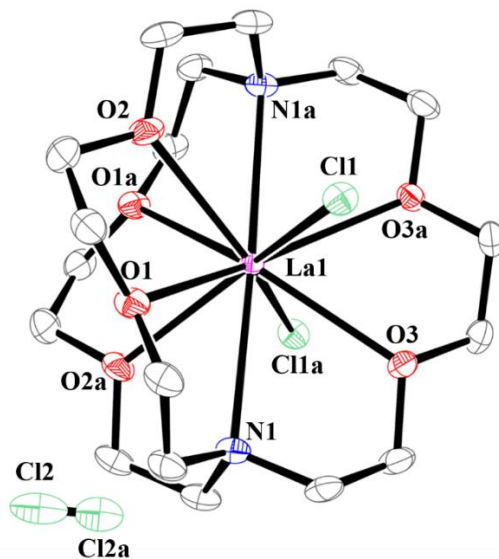


**Figure 5.2.** ORTEP representation of  $[\text{La}(\text{crypt})\text{Cl}_2]\text{Cl}$ , **15-La**, with thermal ellipsoids drawn at the 50% probability level. Outer sphere chloride is disordered over two positions. Hydrogen atoms were omitted for clarity.

In one synthesis of **14-U** in THF, adventitious water was present and an aquated variant of **14-U** was obtained, namely  $[\text{U}(\text{crypt})\text{I}(\text{OH}_2)][\text{I}]_2$ , **16-U**, Figure 3, which was only characterized

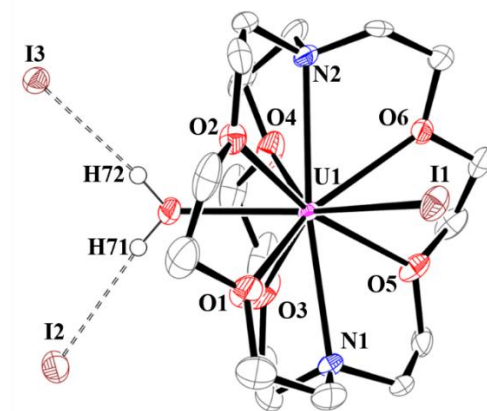


**Figure 5.3.** ORTEP representation of  $[\text{U}(\text{crypt})\text{I}(\text{OH}_2)][\text{I}]_2$ , **16-U**, with thermal ellipsoids drawn at the 50% probability level. Hydrogen atoms except those of  $\text{H}_2\text{O}$  were omitted for clarity.

crystallographically. The structure revealed one water molecule and one iodide ion coordinated to uranium and the complex crystallizes with two outer sphere iodide ions.

Anion exchange of an outer sphere iodide of **14-U** was performed by reaction with NaBPh<sub>4</sub> in acetonitrile (MeCN), eq 5.4. While an iodide was exchanged for (BPh<sub>4</sub>)<sup>1-</sup>, crystallographic characterization revealed that a water adduct again had formed, [U(crypt)I(OH<sub>2</sub>)] [I][BPh<sub>4</sub>], **17-U**, Figure 5.4. As in **16-U**, compound **17-U** was only characterized crystallographically.

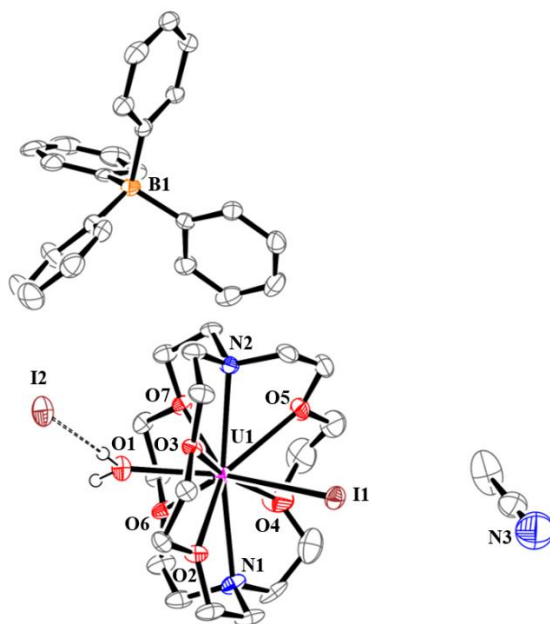
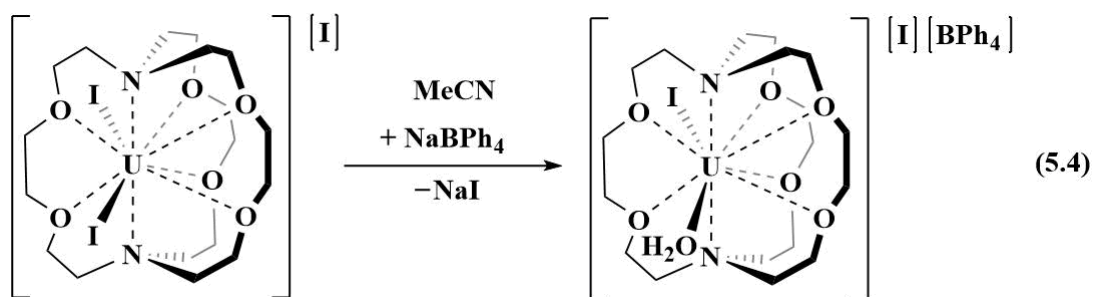


**Figure 5.4.** ORTEP representation of [U(crypt)I(OH<sub>2</sub>)] [I][BPh<sub>4</sub>], **17-U**, with thermal ellipsoids drawn at the 50% probability level. Hydrogens except those of H<sub>2</sub>O were omitted for clarity.

Metrical data on **14-U**, **15-La**, **16-U**, and **17-U** are summarized in Table 5.1 as well as data on the aquated lanthanum complex,  $[\text{La}(\text{crypt})\text{Cl}(\text{OH}_2)][\text{Cl}]_2$ ,<sup>9</sup> for comparison. In each case, the six oxygen donor atoms of the crypt form the shortest distances to the metal. The M–N distances for the two nitrogen donors are 0.1-0.2 Å longer than the M–O distances. The six oxygen atoms of the crypt define a trigonal prismatic geometry, but the range of M–O distances show this has some distortion from a pure  $D_{3h}$  symmetry. The N atoms of the crypt cap the trigonal faces and the additional two ligands in each complex cap two of the three square faces of the  $O_6$  trigonal prism. The U(III)–O(OH<sub>2</sub>) bond distances, 2.549(7) and 2.503(3) Å, in **16-U** and **17-U**, respectively, are distinct from terminally bound U(IV)–O(OH) distances, which range from 2.040(2)-2.137(7) Å.<sup>31, 33, 34, 37, 38</sup> The U(III)-O(OH<sub>2</sub>) distances are in the 2.47(3)-2.595(3) Å range reported for  $\text{UCl}_3(\text{OH}_2)_7$ ,<sup>27</sup>  $\text{UCl}_3(\text{OH}_2)_6$ ,<sup>27</sup>  $[\text{U}(\text{OH}_2)_9][\text{OTf}]_3$ ,<sup>28</sup>  $(\text{NH}_4)[\text{U}(\text{OH}_2)_5(\text{MeCN})_2\text{Br}_2][\text{Br}]_2$ ,<sup>29</sup> and  $(\text{NH}_4)\text{U}(\text{SO}_4)_2(\text{OH}_2)_3 \cdot \text{H}_2\text{O}$ .<sup>30</sup>

**Table 5.1.** Summary of bond distance ranges (Å) of compounds  $[\text{U}(\text{crypt})\text{I}_2]\text{I}$  **14-U**,  $[\text{La}(\text{crypt})\text{Cl}_2]\text{Cl}$  **15-La**,  $[\text{U}(\text{crypt})\text{I}(\text{OH}_2)][\text{I}]_2$  **16-U**,  $[\text{U}(\text{crypt})\text{I}(\text{OH}_2)][\text{I}][\text{BPh}_4]$  **17-U**, and  $[\text{La}(\text{crypt})\text{Cl}(\text{OH}_2)][\text{Cl}]_2$ .<sup>9</sup>

	$[\text{U}(\text{crypt})\text{I}_2]\text{I}$ , <b>14-U</b>	$[\text{U}(\text{crypt})\text{I}(\text{OH}_2)][\text{I}]_2$ , <b>16-U</b>	$[\text{U}(\text{crypt})\text{I}(\text{OH}_2)][\text{I}][\text{BPh}_4]$ , <b>17-U</b>
U–I	3.3106(5)-3.3292(6)	3.2563(7)	3.2845(6)
U–N <sub>crypt</sub>	2.803(3)-2.853(3)	2.80(1)-2.814(8)	2.781(3)-2.822(3)
U–O <sub>crypt</sub>	2.568(2)-2.697(2)	2.602(9)-2.683(7)	2.606(3)-2.659(4)
U–OH <sub>2</sub>		2.549(7)	2.503(3)
	$[\text{La}(\text{crypt})\text{Cl}_2]\text{Cl}$ , <b>15-La</b>	$[\text{La}(\text{crypt})\text{Cl}(\text{OH}_2)][\text{Cl}]_2$ <sup>9</sup>	
La–Cl	2.8161(5)	2.827(2)	
La–N <sub>crypt</sub>	2.893(2)	2.800(7)-2.814(6)	
La–O <sub>crypt</sub>	2.673(1)-2.716(1)	2.651(6)-2.725(6)	
La–OH <sub>2</sub>		2.539(6)	

In complex **14-U**, the outer sphere iodide anion is 3.2 Å from the nearest atom in the  $[\text{U}(\text{crypt})\text{I}_2]^{1+}$  cation. In **16-U** and **17-U**, however, the outer sphere iodide ions are closer to the cation and the hydrogen atoms of the coordinated water are oriented toward the outer sphere

iodides. In **3**, the H...I distances are approximately 2.6 and 2.7 Å and the H...I distance in **17-U** is 2.6 Å. The H...Cl distance in [La(crypt)Cl(OH<sub>2</sub>)]Cl<sub>2</sub><sup>9</sup> is 2.7 Å. The ranges of U–O(crypt) and U–N(crypt) bond distances in **14-U**, **16-U**, and **17-U** all overlap and show a similarity despite the difference in the other ligands on uranium and the extent of hydrogen bonding.

## Conclusion

In summary, simple salts of uranium and lanthanum can readily form crystallographically-characterizable complexes with 2.2.2-cryptand. The crypt coordination environment allows additional ligands to bind to the metals such that productive chemistry is possible with this ligation. The formation of the aquo adducts **16-U** and **17-U** is unusual since U(III) in other coordination environments is known to reduce water to form U(IV)-hydroxo complexes.<sup>31-35</sup> It should also be noted that the solubility of [U(crypt)I<sub>2</sub>]I, **14-U**, differs from the starting reagent UI<sub>3</sub>. Although UI<sub>3</sub> is soluble in THF, **14-U** is not. In contrast, the starting UI<sub>3</sub> is not soluble in CH<sub>2</sub>Cl<sub>2</sub>, but **14-U** is soluble in this solvent. These differences in solubility suggest interesting possibilities for recycling/extraction of radioactive nuclear waste if an appropriately cost-effective chelate were available.

## Experimental

All syntheses and manipulations described below were conducted under Ar with rigorous exclusion of air and water using glovebox, Schlenk-line, and high-vacuum-line techniques. UI<sub>3</sub><sup>39</sup> and LaCl<sub>3</sub><sup>40</sup> materials were prepared according to previously published literature. 2.2.2-Cryptand (4,7,13,16,21,24-hexaoxa-1,10-diazabicyclo[8.8.8]hexacosane, Aldrich) was placed under vacuum (10<sup>-3</sup> Torr) for 12 h before use. THF and Et<sub>2</sub>O were sparged with UHP Ar and dried over columns containing Q-5 and molecular sieves. DMF, MeCN, and CH<sub>2</sub>Cl<sub>2</sub> were dried over 3 Å molecular sieves for 1 week and degassed using three freeze-pump-thaw cycles. IR

samples were prepared as KBr pellets on a Jasco FT/IR-4700 spectrometer. Elemental analyses were performed on a PerkinElmer series II 2400 CHNS analyzer.

**[U(crypt)I<sub>2</sub>]I, 14-U.** In an argon-filled glovebox, a blue solution of UI<sub>3</sub> (100 mg, 0.160 mmol) in THF (2 mL) was added dropwise to a stirred colorless THF (2 mL) solution of 2.2.2-cryptand (60 mg, 0.160 mmol). A green/brown precipitate immediately formed. This mixture was stirred for 30 min. The solvent was removed in vacuo yielding a light green solid (123 mg, 76%). The solid was dissolved in CH<sub>2</sub>Cl<sub>2</sub> (2 mL). The green solution was filtered and then layered with Et<sub>2</sub>O and placed in a -35 °C freezer. After 1 d, X-ray quality green crystals were isolated. IR: 3243w, 3169w, 2943w, 2926w, 2894w, 2860w, 1611w, 1490w, 1479m, 1468m, 1451m, 1437w, 1361w, 1354w, 1335w, 1311w, 1288w, 1262m, 1240w, 1159w, 1103s, 1085s, 1075s, 1050m, 1029m, 960s, 949m, 911w, 873w, 832m, 823m, 803w, 763w, 757w cm<sup>-1</sup>. Anal. Calcd. for [U(crypt)I<sub>2</sub>]I, C<sub>18</sub>H<sub>36</sub>N<sub>2</sub>O<sub>6</sub>I<sub>3</sub>U: C, 21.72; H, 3.65; N, 2.81. Found: C, 21.92; H, 3.49; N, 2.52.

**[La(crypt)Cl<sub>2</sub>]Cl, 15-La.** In an argon-filled box, a suspension of LaCl<sub>3</sub> (100 mg, 0.408 mmol) in DMF (2 mL) was added to a solution of 2.2.2-cryptand (153 mg, 0.408 mmol) in DMF (2 mL). The suspension was stirred for 12 h at room temperature. The colorless solution was layered into Et<sub>2</sub>O at -35 °C. X-ray quality colorless crystals were isolated (220 mg, 85%). IR: 2968m, 2873m, 2821m, 2744w, 1666m, 1641m, 1482m, 1448m, 1427m, 1411w, 1387w, 1373w, 1354m, 1325w, 1304m, 1291m, 1266w, 1256m, 1233w, 1215w, 1162m, 1116s, 1091s, 1068s, 1022m, 957s, 936m, 829m, 805w, 757m cm<sup>-1</sup>. Anal. Calcd. for [La(crypt)Cl<sub>2</sub>]Cl, C<sub>18</sub>H<sub>36</sub>N<sub>2</sub>O<sub>6</sub>Cl<sub>3</sub>La: C, 34.77; H, 5.84; N, 4.51. Found: C, 34.52; H, 5.34; N, 4.93.

**[U(crypt)I(OH<sub>2</sub>)]I<sub>2</sub>, 16-U.** In an argon-filled box, a THF (1 mL) solution of 2.2.2-cryptand (11 mg, 0.030 mmol) was added to a blue solution of UI<sub>3</sub> (19 mg, 0.030 mmol) in THF



(2 mL). The solution immediately became a maroon suspension. The mixture was placed in a –15 °C freezer from which green X-ray quality crystals of  $[\text{U}(\text{crypt})(\text{OH}_2)(\text{I})][\text{I}]_2$  were obtained (15 mg, 50%).

**$[\text{U}(\text{crypt})\text{I}(\text{OH}_2)][\text{I}][\text{BPh}_4]$ , 17-U.** In an argon-filled box, a green MeCN (3 mL) solution of  $[\text{U}(\text{crypt})\text{I}_2]\text{I}$ , **1** (30 mg, 0.03 mmol) was added to a MeCN solution of  $\text{NaBPh}_4$  (10 mg 0.03 mmol). The green mixture was stirred for 2 d and then filtered to remove brown solids. The resulting green solution was filtered and layered with  $\text{Et}_2\text{O}$  and placed in a –35 °C freezer. Brown/green X-ray quality crystals of  $[\text{U}(\text{crypt})\text{I}(\text{OH}_2)][\text{I}][\text{BPh}_4]$  were obtained (10 mg, 28%).

### Spectral Details

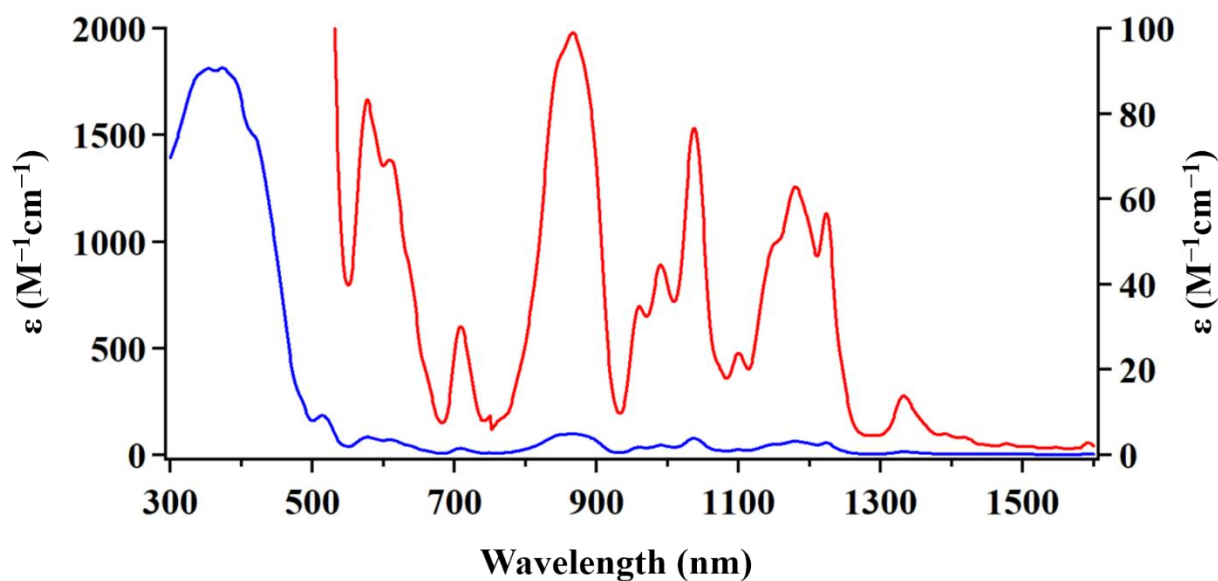


**Figure 5.5.** NIR/UV-Vis of 5mM  $[\text{U}(\text{crypt})\text{I}_2]\text{I}$ , **14-U**, in DMF. Full spectrum (blue, left axis) and 20x zoom of full spectrum (red, right axis).

## Structural Details

### X-ray Data Collection, Structure Solution and Refinement for [U(crypt)I<sub>2</sub>]I, 14-U.

A green crystal of approximate dimensions 0.084 x 0.205 x 0.331 mm was mounted in a cryoloop and transferred to a Bruker SMART APEX II diffractometer. The APEX2<sup>41</sup> program package was used to determine the unit-cell parameters and for data collection (20 sec/frame scan time for a sphere of diffraction data). The raw frame data was processed using SAINT<sup>42</sup> and SADABS<sup>43</sup> to yield the reflection data file. Subsequent calculations were carried out using the SHELXTL<sup>44</sup> program. The diffraction symmetry was  $2/m$  and the systematic absences were consistent with the monoclinic space group  $P2_1/c$  that was later determined to be correct. The structure was solved by dual space methods and refined on  $F^2$  by full-matrix least-squares techniques. The analytical scattering factors<sup>45</sup> for neutral atoms were used throughout the analysis. Hydrogen atoms were included using a riding model. There were three molecules of dichloromethane solvent present. Least-squares analysis yielded  $wR2 = 0.0497$  and  $Goof = 1.059$  for 352 variables refined against 8749 data (0.76 Å),  $R1 = 0.0225$  for those 7986 data with  $I > 2.0\sigma(I)$ .

### X-ray Data Collection, Structure Solution and Refinement for [La(crypt)Cl<sub>2</sub>]Cl, 15-

**La.** A colorless crystal of approximate dimensions 0.089 x 0.117 x 0.283 mm was mounted in a cryoloop and transferred to a Bruker SMART APEX II diffractometer. The APEX2<sup>41</sup> program package was used to determine the unit-cell parameters and for data collection (25 sec/frame scan time for a sphere of diffraction data). The raw frame data was processed using SAINT<sup>42</sup> and SADABS<sup>43</sup> to yield the reflection data file. Subsequent calculations were carried out using the SHELXTL<sup>44</sup> program. The diffraction symmetry was  $2/m$  and the systematic absences were consistent with the monoclinic space groups  $Cc$  and  $C2/c$ . It was later determined that space

group  $C2/c$  was correct. The structure was solved by dual space methods and refined on  $F^2$  by full-matrix least-squares techniques. The analytical scattering factors<sup>45</sup> for neutral atoms were used throughout the analysis. Hydrogen atoms were included using a riding model. The molecule and chloride ion were located on two-fold rotation axes. There was one molecule of diethylether solvent present. The solvent was located on an inversion center. Both the solvent and chloride ion were disordered and included using multiple components with partial site-occupancy-factors. Least-squares analysis yielded  $wR2 = 0.0554$  and  $Goof = 1.069$  for 183 variables refined against 3496 data ( $0.74 \text{ \AA}$ ),  $R1 = 0.0210$  for those 3298 data with  $I > 2.0\sigma(I)$ .

**X-ray Data Collection, Structure Solution and Refinement for [U(crypt)I(OH<sub>2</sub>)](I)<sub>2</sub>, 16-U.** A green crystal of approximate dimensions  $0.154 \times 0.241 \times 0.404$  mm was mounted in a cryoloop and transferred to a Bruker SMART APEX II diffractometer. The APEX2<sup>41</sup> program package was used to determine the unit-cell parameters and for data collection (20 sec/frame scan time for a sphere of diffraction data). The raw frame data was processed using SAINT<sup>42</sup> and SADABS<sup>43</sup> to yield the reflection data file. Subsequent calculations were carried out using the SHELXTL<sup>44</sup> program. The diffraction symmetry was  $2/m$  and the systematic absences were consistent with the monoclinic space group  $P2_1/n$  that was later determined to be correct. The structure was solved by dual space methods and refined on  $F^2$  by full-matrix least-squares techniques. The analytical scattering factors<sup>45</sup> for neutral atoms were used throughout the analysis. Hydrogen atoms H(71) and H(72) were located from a difference-map and refined ( $x,y,z$  and  $U_{iso}$ ). The remaining hydrogen atoms were included using a riding model. At convergence,  $wR2 = 0.1096$  and  $Goof = 1.257$  for 288 variables refined against 6137 data ( $0.78 \text{ \AA}$ ),  $R1 = 0.0474$  for those 5617 data with  $I > 2.0\sigma(I)$ .

**X-ray Data Collection, Structure Solution and Refinement for [U(crypt)I(OH<sub>2</sub>)]I[BPh<sub>4</sub>], 17-U.** A green crystal of approximate dimensions 0.121 x 0.136 x 207 mm was mounted in a cryoloop and transferred to a Bruker SMART APEX II diffractometer. The APEX2<sup>41</sup> program package was used to determine the unit-cell parameters and for data collection (20 sec/frame scan time for a sphere of diffraction data). The raw frame data was processed using SAINT<sup>42</sup> and SADABS<sup>43</sup> to yield the reflection data file. Subsequent calculations were carried out using the SHELXTL<sup>44</sup> program. The diffraction symmetry was  $2/m$  and the systematic absences were consistent with the monoclinic space group  $P2_1/n$  that was later determined to be correct. The structure was solved by dual space methods and refined on  $F^2$  by full-matrix least-squares techniques. The analytical scattering factors<sup>45</sup> for neutral atoms were used throughout the analysis. Hydrogen atoms were included using a riding model. There was one molecule of acetonitrile solvent present. Least-squares analysis yielded  $wR2 = 0.0766$  and  $Goof = 1.019$  for 525 variables refined against 12099 data (0.75 Å),  $R1 = 0.0346$  for those 9551 data with  $I > 2.0\sigma(I)$ . There were several high residuals present in the final difference-Fourier map. It was not possible to determine the nature of the residuals although it was probable that either acetonitrile or diethylether solvent was present. The SQUEEZE<sup>46a</sup> routine in the PLATON<sup>46b</sup> program package was used to account for the electrons in the solvent accessible voids.

## References

- (1) Dietrich, B.; Lehn, J. M.; Sauvage, J. P. *Tetrahedron*, **1973**, *29*, 1647-1658.
- (2) Dietrich, B.; Lehn, J. M.; Sauvage, J. P.; Blanzat, J. *Tetrahedron*, **1973**, *29*, 1629-1645.
- (3) Lehn, J. M. *Pure Appl. Chem.*, **1977**, *49*, 857.
- (4) Lehn, J. M. *Acc. Chem. Res.*, **1978**, *11*, 49-57.

- (5) Yee, E. L.; Gansow, O. A.; Weaver, M. J. *J. Am. Chem. Soc.*, **1980**, *102*, 2278-2285.
- (6) Benetollo, F.; Bombieri, G.; Cassol, A.; De Paoli, G.; Legendziewicz, J. *Inorg. Chim. Acta*, **1985**, *110*, 7-13.
- (7) Yang, G.; Liu, S.; Jin, Z. *Inorg. Chim. Acta*, **1987**, *131*, 125-128.
- (8) Burns, J. H. *Inorg. Chem.*, **1979**, *18*, 3044-3047.
- (9) Mao J.; Jin, Z. *Polyhedron*, **1994**, *13*, 319-323.
- (10) Ciampolini, M.; Dapporto, P.; Nardi, N. *J. Chem. Soc., Dalton Trans.*, **1979**, 974-977.
- (11) Jenks, T. C.; Bailey, M. D.; Hovey, J.; Fernando, S.; Basnayake, G.; Cross, M. E.; Li, W.; Allen, M. J. *Chem. Sci.*, **2018**, *9*, 1273-1278.
- (12) Kuda-Wedagedara, A. N. W.; Wang, C.; Martin, P. D.; Allen, M. J. *J. Am. Chem. Soc.*, **2015**, *137*, 4960-4963.
- (13) Bullock, J. I.; Storey, A. E. *Inorg. Chim. Acta*, **1979**, *36*, L399-L400.
- (14) Brighli, M.; Fux, P.; Lagrange J.; Lagrange, P. *Inorg. Chem.*, **1985**, *24*, 80-84.
- (15) B. Spiess, F. Arnaud-Neu and M. J. Schwing-Weill, *Inorg. Nucl. Chem. Letters*, **1979**, *15*, 13-16.
- (16) Costes, R. M.; Folcher, G.; Plurien P.; Rigny, P. *Inorg. Nucl. Chem. Letters*, **1976**, *12*, 491-499.
- (17) Huh, D. N.; Kotyk, C. M.; Gembicky, M.; Rheingold, A. L.; Ziller, J. W.; Evans, W. J. *Chem. Commun.*, **2017**, *53*, 8664-8666.
- (18) Nipuni-Dhanesha, G. H.; Mei, Y.; Garcia, J.; Allen, M. J. *Angew. Chem., Int. Ed.*, **2010**, *49*, 8923-8925.
- (19) Hitchcock, P. B.; Lappert, M. F.; Maron. L.; Protchenko, A. V. *Angew. Chem., Int. Ed.*, **2008**, *47*, 1488-1491.
- (20) MacDonald, M. R.; Ziller, J. W.; Evans, W. J. *J. Am. Chem. Soc.*, **2011**, *133*, 15914-15917.
- (21) MacDonald, M. R.; Bates, J. E.; Fieser, M. E.; Ziller, J. W.; Furche, F.; Evans, W. J. *J. Am. Chem. Soc.*, **2012**, *134*, 8420-8423.
- (22) MacDonald, M. R.; Bates, J. E.; Ziller, J. W.; Furche, F.; Evans, W. J. *J. Am. Chem. Soc.*, **2013**, *135*, 9857-9868.

- (23) Fieser, M. E.; MacDonald, M. R.; Krull, B. T.; Bates, J. E.; Ziller, J. W.; Furche, F.; Evans, W. J. *J. Am. Chem. Soc.*, **2015**, *137*, 369-382.
- (24) Evans, W. J. *Organometallics*, **2016**, *35*, 3088-3100.
- (25) La Pierre, H. S.; Scheurer, A.; Heinemann, F. W.; Hieringer, W.; Meyer, K. *Angew. Chem., Int. Ed.*, **2014**, *53*, 7158-7162.
- (26) Palumbo, C. T.; Halter, D. P.; Voora, V. K.; Chen, G. P.; Chan, A. K.; Fieser, M. E.; Ziller, J. W.; Hieringer, W.; Furche, F.; Meyer, K.; Evans, W. J. *Inorg. Chem.*, **2018**, *57*, 2823-2833.
- (27) Mech, A.; Karbowiak, M.; Lis, T.; Drożdżyński, J. *Polyhedron*, **2006**, *25*, 2083-2092.
- (28) Apostolidis, C.; Schimmelpfennig, B.; Magnani, N.; Lindqvist-Reis, P.; Walter, O.; Sykora, R.; Morgenstern, A.; Colineau, E.; Caciuffo, R.; Klenze, R.; Haire, R. G.; Rebizant, J.; Bruchertseifer, F.; Fanghänel, T. *Angew. Chem., Int. Ed.*, **2010**, *49*, 6343-6347.
- (29) Zych, E.; Starynowicz, P.; Lis, T.; Drożdżyński, J. *Polyhedron*, **1993**, *12*, 1661-1667.
- (30) Bullock, J. I.; Ladd, M. F. C.; Povey, D. C.; Storey, A. E. *Inorg. Chim. Acta*, **1980**, *43*, 101-108.
- (31) Halter, D. P.; Heinemann, F. W.; Bachmann, J.; Meyer, K. *Nature*, **2016**, *530*, 317.
- (32) Korobkov, I.; Gambarotta, S. *Prog. Inorg. Chem.*, **2005**, *54*, 321-348.
- (33) Karmazin, L.; Mazzanti, M.; Pécaut, J. *Inorg. Chem.*, **2003**, *42*, 5900-5908.
- (34) Natrajan, L.; Mazzanti, M.; Bezombes, J.-P.; Pécaut, J. *Inorg. Chem.*, **2005**, *44*, 6115-6121.
- (35) Lukens, W. W.; Beshouri, S. M.; Bloch, L. L.; Andersen, R. A. *J. Am. Chem. Soc.*, **1996**, *118*, 901-902.
- (36) Windorff, C. J.; Dumas, M. T.; Ziller, J. W.; Gaunt, A. J.; Kozimor, S. A.; Evans, W. J. *Inorg. Chem.*, **2017**, *56*, 11981-11989.
- (37) John, G. H.; May, I.; Sharrad, C. A.; Sutton, A. D.; Collison, D.; Helliwell, M.; Sarsfield, M. J. *Inorg. Chem.*, **2005**, *44*, 7606-7615.
- (38) Ariyaratne, K. A. N. S.; Cramer, R. E.; Jameson, G. B.; Gilje, J. W. *J. Organomet. Chem.*, **2004**, *689*, 2029-2032.

- (39) C. D. Carmichael, N. A. Jones and P. L. Arnold, *Inorg. Chem.*, 2008, **47**, 8577-8579.
- (40) M. D. Taylor, *Chemical Reviews*, 1962, **62**, 503-511.
- (41) APEX2 Version 2014.11-0, Bruker AXS, Inc.; Madison, WI 2014.
- (42) SAINT Version 8.34a, Bruker AXS, Inc.; Madison, WI 2013
- (43) Sheldrick, G. M. SADABS, Version 2014/5, Bruker AXS, Inc.; Madison, WI 2014
- (44) Sheldrick, G. M. SHELXTL, Version 2014/7, Bruker AXS, Inc.; Madison, WI 2014
- (45) International Tables for Crystallography 1992, Vol. C., Dordrecht: Kluwer Academic Publishers.
- (46) (a) Spek, A.L. SQUEEZE, *Acta Cryst.* 2015, C71, 9-19., (b) Spek, A. L. PLATON, *Acta. Cryst.* 2009, D65, 148-155

## CHAPTER 6

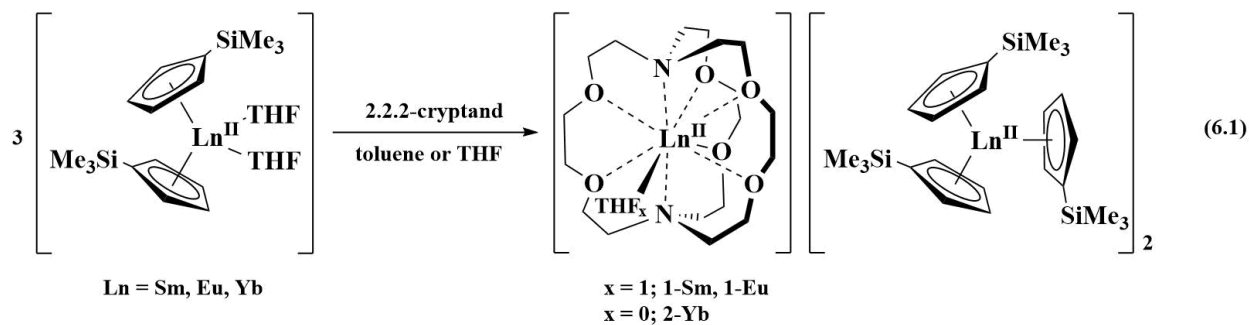
### Facile Encapsulation of Ln(II) Ions into Cryptate Complexes

#### from LnI<sub>2</sub>(THF)<sub>2</sub> Precursors (Ln = Sm, Eu, Yb)

#### Introduction\*

Although the 2.2.2-cryptand (crypt) ligand has been known since 1973<sup>1-2</sup> and lanthanide-encapsulated crypt complexes were reported in 1979,<sup>3</sup> Ln-in-crypt complexes were not heavily studied in subsequent decades. Most of the examples involved lanthanides in the +3 oxidation state.<sup>4-7</sup> However, Allen and co-workers also reported examples of Eu(II)-in-crypt<sup>8-10</sup> complexes as well as related Ln(II)-in-azacrypt<sup>11-12</sup> complexes. Since the crypt ligand has been found to stabilize low oxidation states for rare-earth metals,<sup>6, 8</sup> Ln(II)-in-crypt complexes could be attractive precursors to expand the limits of redox chemistry of rare-earth metals.<sup>13</sup>

Encapsulation of rare-earth ions using crypt first generated interest with the discovery that Sm(II), Eu(II), and Yb(II) can be readily incorporated into crypt from the metallocene precursors, Cp'<sub>2</sub>Ln(THF)<sub>2</sub> (Cp' = C<sub>5</sub>H<sub>4</sub>SiMe<sub>3</sub>)<sup>14</sup> as described in Chapter 4. The trimetallic Ln(II) complexes [Ln(crypt)(THF)][Cp'<sub>3</sub>Ln]<sub>2</sub>, **12-Ln** (Ln = Sm, Eu), and [Yb(crypt)][Cp'<sub>3</sub>Yb]<sub>2</sub>, **13-Yb**, are formed according to eq 6.1.<sup>14</sup> Following this result, it was sought to synthesize Ln(II)-in-



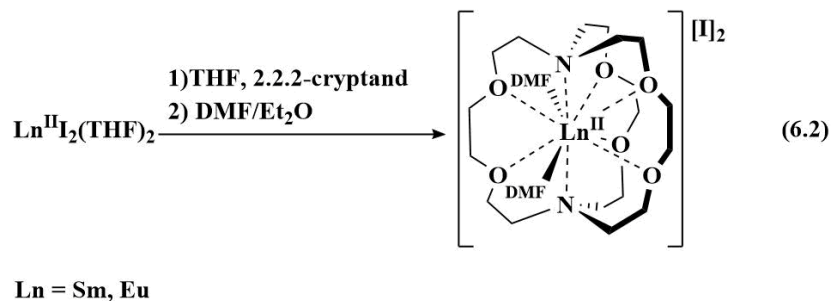
\*Portions of this Chapter have been published: Huh, D. N.; Ziller, J. W.; Evans, W. J. Facile Encapsulation of Ln(II) Ions into Cryptate Complexes from LnI<sub>2</sub>(THF)<sub>2</sub> Precursors (Ln = Sm, Eu, Yb). *Inorg. Chem.*, **2019**, 589, 9613-9617. DOI: 10.1021/acs.inorgchem.9b01049



crypt examples with a single type of Ln(II) coordination environment to better examine the Ln(II)-in-crypt moiety. It was also of interest to synthesize Ln(II)-in-crypt complexes from common Ln(II) starting materials such as the diiodides,  $\text{LnI}_2(\text{THF})_2$ , that are precursors to the metallocenes of eq 6.1. It was found that U(III)-in-crypt and La(III)-in crypt complexes can be synthesized directly from the metal trihalides.<sup>15</sup> Encapsulated Sm(II), Eu(II), and Yb(II) ions can be readily prepared by addition of crypt to  $\text{LnI}_2(\text{THF})_2$  precursors.

## Results and Discussion

**Encapsulation of Sm(II), Eu(II), and Yb(II).** Addition of THF solutions of  $\text{LnI}_2(\text{THF})_2$  (Ln = Sm, Eu) to a THF solution of 2.2.2-cryptand (crypt) generates precipitates that dissolve in DMF. Crystallization of these solutions yields the Ln(II)-in-crypt complexes,  $[\text{Ln}(\text{crypt})(\text{DMF})_2][\text{I}]_2$ , **18-Ln**, identified by X-ray diffraction, eq 6.2, Figure 6.1.



The crystal data show that each metal in **18-Ln** is encapsulated by the crypt ligand and is also coordinated to two molecules of DMF. Both iodides in **18-Ln** are outer-sphere counteranions. The 10-coordinate geometry of the Ln(II) ion can be described as a tetra-capped trigonal prism with crypt nitrogen donor atoms capping the triangular faces and DMF oxygen atoms capping two of the rectangular faces. Similar structures were previously described for the Ln(III) complexes  $[\text{La}(\text{crypt})(\text{OH}_2)\text{Cl}]\text{Cl}_2$ ,<sup>7</sup>  $[\text{La}(\text{crypt})(\text{DMF})(\text{OTf})][\text{OTf}]_2$ ,<sup>7</sup>  $[\text{La}(\text{crypt})\text{Cl}_2]\text{Cl}$ ,<sup>15</sup> and  $[\text{U}(\text{crypt})\text{I}_2]\text{I}$ .<sup>15</sup>

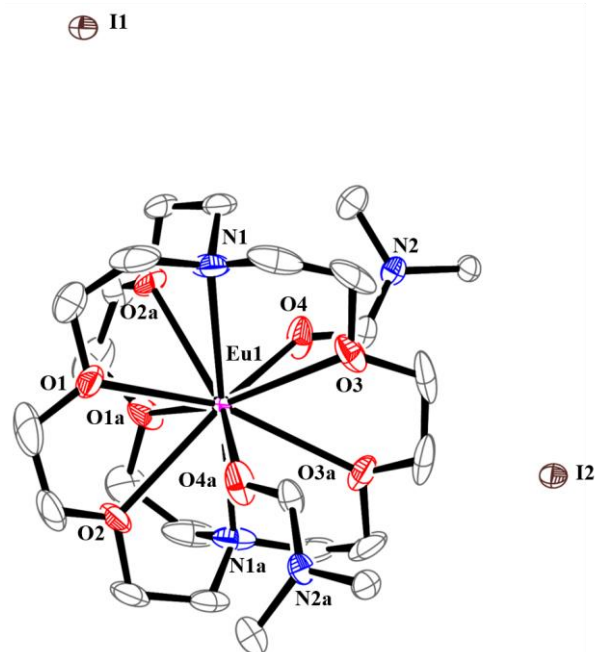


**Figure 6.1.** ORTEP representation of  $[\text{Eu}(\text{crypt})(\text{DMF})_2][\text{I}]_2$ , **18-Eu**, with thermal ellipsoids drawn at the 50% probability level. Hydrogen atoms were omitted for clarity. **18-Sm** is isomorphous with **18-Eu**.

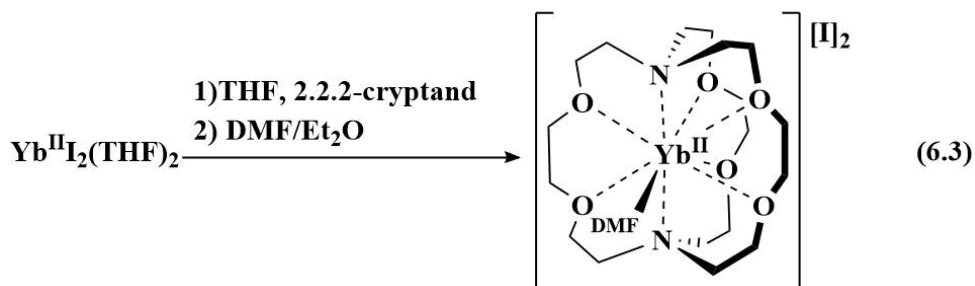
Table 6.1 presents metrical data on all the new Ln(II)-in-crypt complexes in this paper as well as comparisons with  $[\text{Eu}(\text{crypt})(\text{THF})][\text{Cp}'_3\text{Eu}]_2$ , **12-Eu**,  $[\text{Yb}(\text{crypt})][\text{Cp}'_3\text{Yb}]_2$ , **13-Yb**, and  $[\text{Eu}(\text{crypt})\text{Cl}][\text{Cl}]$ . Since the crystal structure of  $[\text{Sm}(\text{crypt})(\text{THF})][\text{Cp}'_3\text{Sm}]_2$ , **12-Sm**, was of insufficient quality to provide metrical data, it is not included. Table 6.1 shows that in the **18-Ln**

**Table 6.1.** Ln(II)–O(crypt) and Ln(II)–N(crypt) bond distance ranges (Å).

	Ln(II)–O(crypt)	Ln(II)–N(crypt)	C.N.	Reference
<b>20-Sm</b>	2.737(1)-2.783(1)	2.934(2)-2.942(2)	10	this study
<b>18-Sm</b>	2.740(1)-2.793(1)	2.876(2)	10	this study
<b>20-Eu</b>	2.731(2)-2.782(2)	2.937(2)-2.945(2)	10	this study
<b>18-Eu</b>	2.731(2)-2.767(3)	2.871(3)	10	this study
<b>12-Eu</b>	2.620(3)-2.681(4)	2.849(5)-2.871(5)	9	ref 14
$[\text{Eu}(\text{crypt})\text{Cl}][\text{Cl}]$	2.659(3)-2.707(4)	2.838(3)-2.859(3)	9	ref 9
<b>19-Yb</b>	2.513(2)-2.717(2)	2.783(3)-2.790(3)	9	this study
<b>13-Yb</b>	2.444(7)-2.539(5)	2.649(6)-2.740(10)	8	ref 14

complexes, the 2.740(1) to 2.793(1) Å Sm(II)–O(crypt) and 2.731(2) to 2.767(3) Å Eu(II)–O(crypt) bond distances are shorter than the 2.876(2) Å Sm(II)–N(crypt) and 2.871(3) Å Eu(II)–N(crypt) distances as is typical in Ln-in-crypt complexes. The Eu(II)–O(crypt) bond distances in 10-coordinate **18-Eu** are longer than the 2.620(3) to 2.681(4) Å distances in the 9-coordinate **12-Eu**,<sup>14</sup> as expected for a higher coordinate complex. However, the Eu(II)–N(crypt) distance in **18-Eu** is in the range of those in **12-Eu**. The 2.546(3) Å Eu(II)–O(DMF) bond distance in **18-Eu** is significantly shorter than the Eu(II)–O(crypt) distances, but it is similar to the 2.558(3) Å Eu(II)–O(THF) distance in **12-Eu**.

An Yb(II)-in-crypt complex, [Yb(crypt)(DMF)][I]<sub>2</sub>, **19-Yb**, was synthesized in a similar manner to eq 6.2. However, in the case of this smaller metal, the product contains only one coordinated DMF, eq 6.3, Figure 6.2. This difference in solvation is similar to the difference



between [Ln(crypt)(THF)][Cp'<sub>3</sub>Ln]<sub>2</sub>, **12-Ln** (Ln = Sm, Eu), and [Yb(crypt)][Cp'<sub>3</sub>Yb]<sub>2</sub>, **13-Yb**, eq 6.1, in that the Yb complex has one less coordinated solvent molecule.<sup>14</sup> The 2.513(2) to 2.717(2) Å Yb(II)–O(crypt) distances in **19-Yb** span a wide range that is not so useful for comparison with the 2.444(7) to 2.539(5) Å distances in **13-Yb**. Although the 2.783(3) and 2.790(3) Å Yb–N(crypt) distances in **19-Yb** are similar, the analogs in **13-Yb** span a wide range, 2.649(6) to 2.740(10) Å. The Yb–N(crypt) distances in **19-Yb** are 0.090 Å and 0.085 Å less than those in **18-Sm** and **18-Eu**, respectively. In contrast, the data available in the Shannon radii

compilation<sup>18</sup> show a 0.18 Å and 0.16 Å difference between the 8-coordinate Yb(II) and 9-coordinate Sm(II) and Eu(II),

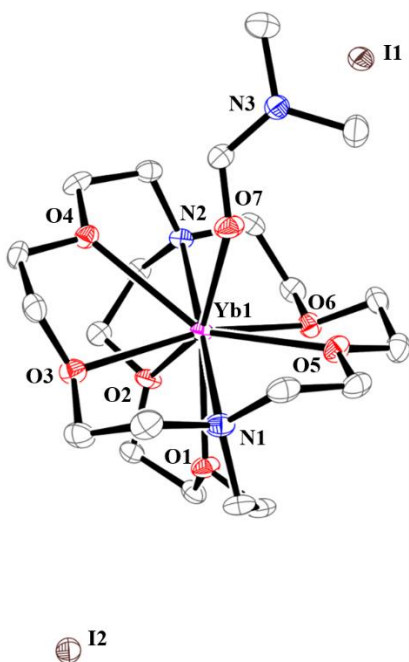


**Figure 6.2.** ORTEP representation of [Yb(crypt)(DMF)](I)<sub>2</sub>, **19-Yb**, with thermal ellipsoids drawn at the 50% probability level. Hydrogen atoms were omitted for clarity.

respectively. On the other hand, the 2.389(2) Å Yb(II)–O(DMF) distance in **19-Yb** is 0.168 Å and 0.157 Å less than the Sm–O(DMF) and Eu–O(DMF) distances in **18-Sm** and **18-Eu**, which is in the range predicted by the Shannon data. Overall, the metrical data suggest that the crypt ligand is quite flexible in its coordination behavior depending on the specific metal and additional ligands present.

**Ionic Metathesis with Sm and Eu.** Addition of two equiv of NaBPh<sub>4</sub> to a DMF solution of [Ln(crypt)(DMF)<sub>2</sub>](I)<sub>2</sub>, **18-Ln** for Ln = Sm, Eu, in DMF generated tetraphenylborate analogs of **18-Ln**, namely the isomorphous Sm and Eu complexes, [Ln(crypt)(DMF)<sub>2</sub>][BPh<sub>4</sub>]<sub>2</sub>, **20-Ln**, eq 6.4, Figure 6.3. The Sm–O(crypt) and Eu–O(crypt) metrical parameters in **20-Ln** are similar to

those in **18-Ln**, but the Sm–N(crypt) is 0.062 Å longer and the Eu–N(crypt) is 0.070 Å longer, Table 6.1. This is another example of the flexibility of the crypt ligand and could be related to the position of the [BPh<sub>4</sub>]<sup>1-</sup> anions as described below.

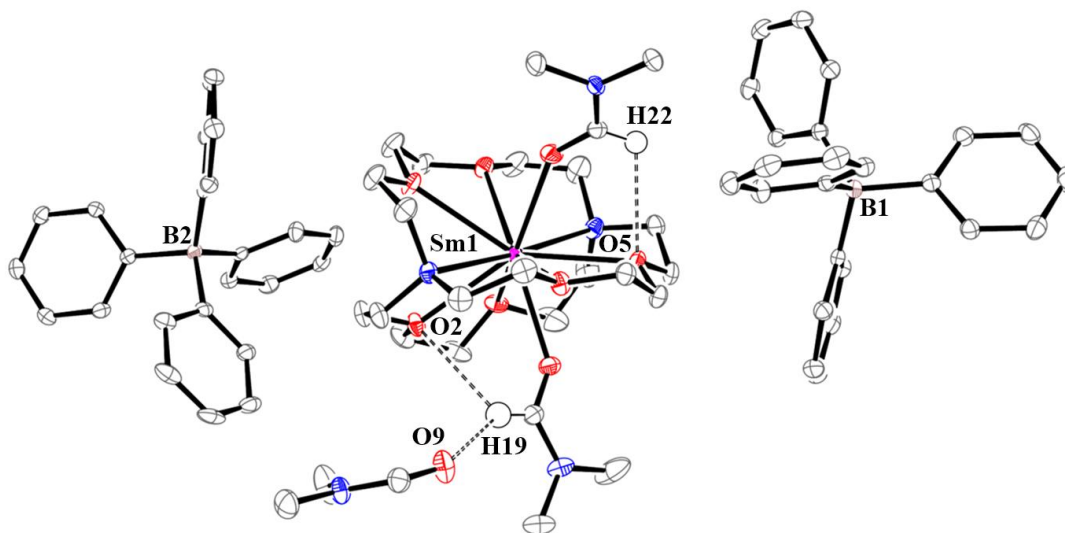
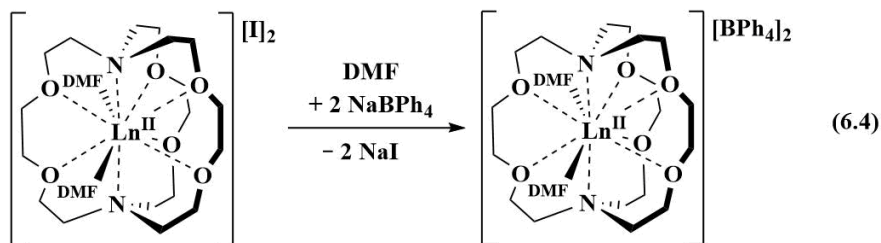
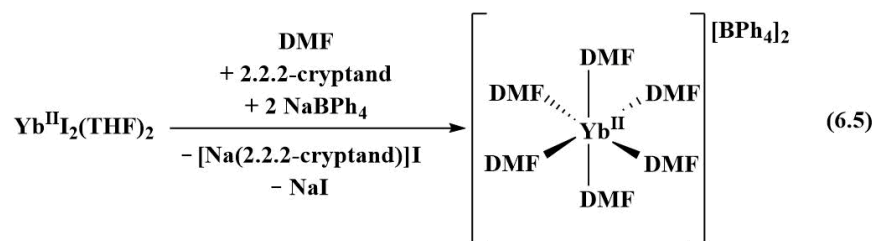


**Figure 6.3.** ORTEP representation of [Sm(crypt)(DMF)<sub>2</sub>][BPh<sub>4</sub>]<sub>2</sub>, **20-Sm**, with thermal ellipsoids drawn at the 50% probability level and dashed lines represent hydrogen bonding. Hydrogen atoms, except for H19 and H22, were omitted for clarity.

In all the new structures above, the formyl hydrogen atoms of the DMF molecules have short distances to the nearest crypt oxygen atoms. In **20-Sm**, these are H22...O5, 2.75(2) Å, and H19...O2, 3.07(2) Å. Hydrogen bonding from an outer sphere DMF oxygen to an inner sphere formyl hydrogen is also observed: H19...O9 is 2.55(2) Å, Figure 6.3. Additionally, hydrogen atoms of the crypt ligand and the methyl group of the DMF molecules have short distances to the

phenyl ring hydrogen atoms in  $[\text{BPh}_4]^{1-}$  ranging from 2.27 to 2.41 Å, which is in the range consistent with dispersion forces.<sup>19-21</sup> It is unknown if these distances and the position of the two  $[\text{BPh}_4]^{1-}$  anions are related to the difference in Sm–N(crypt) distances in **18-Sm** and **20-Sm** (see above). Isomorphous **20-Eu** has similar close contacts.

**Ionic Metathesis with Yb.** Attempts to make **20-Yb** according to eq 6.4 by stepwise addition of  $\text{NaBPh}_4$  to isolated **19-Yb** and by direct reaction of  $\text{NaBPh}_4$  with  $\text{YbI}_2$  and crypt, eq 6.5, were not successful. Instead, encapsulation of Na(I) was confirmed by X-ray crystallography by comparing the unit cell of the product of eq 6.5 with the known  $[\text{Na}(\text{crypt})][\text{I}]$ .<sup>22</sup> The Yb(II) ion in this reaction was isolated as an orange DMF solvate,  $[\text{Yb}(\text{DMF})_6][\text{BPh}_4]_2$ , **21-Yb**, eq 6.5. Solvated Ln(II) complexes have been isolated as  $[\text{BPh}_4]^{1-}$  salts in the past from a variety of reactions, including  $(\text{C}_9\text{H}_7)_2\text{Sm}(\text{THF})_3 + [\text{Et}_3\text{NH}][\text{BPh}_4]$  to form  $[\text{Sm}(\text{THF})_7][\text{BPh}_4]_2$ ,  $(\text{C}_5\text{Me}_5)\text{Sm}[\text{N}(\text{SiMe}_3)_2](\text{THF})_2 + [\text{Et}_3\text{NH}][\text{BPh}_4]$  to form  $[\text{Sm}(\text{THF})_7][\text{BPh}_4]_2$ ,  $[(\text{C}_5\text{Me}_5)\text{Yb}(\text{THF})]_2(\text{C}_8\text{H}_8) + \text{AgBPh}_4$  to form  $[\text{Yb}(\text{THF})_6][\text{BPh}_4]_2$ ,  $[(\text{C}_5\text{Me}_5)\text{Yb}[\text{N}(\text{SiMe}_3)_2](\text{THF})_2 + [\text{Et}_3\text{NH}][\text{BPh}_4]$  to form  $[\text{Yb}(\text{THF})_6][\text{BPh}_4]_2$  and  $[\text{Yb}[\text{N}(\text{SiMe}_3)_2]_2(\text{THF})_2 + [\text{Et}_3\text{NH}][\text{BPh}_4]$  to form  $[\text{Yb}(\text{MeCN})_8][\text{BPh}_4]_2$ .<sup>23</sup>



The Yb–O(DMF) distances range from 2.311(2) to 2.403(2) Å in **21-Yb**, similar to the Yb–O(DMF) distance in **19-Yb**. There are several H...H distances between 2.33 and 2.44 Å in this structure involving DMF/ $(\text{BPh}_4)^{1-}$ , and crypt/ $(\text{BPh}_4)^{1-}$  combinations. The 6-coordinate Shannon radius of Na(I) and Yb(II) are essentially identical with a radius of 1.02 Å.<sup>18</sup> The preferential formation of the  $[\text{Yb}(\text{DMF})_6]^{2+}$  cation over the encapsulated  $[\text{Yb}(\text{crypt})]^{2+}$  cation can

be rationalized by Pauling electroneutrality. Since the DMF molecule can adopt an iminolate resonance structure,  ${}^{-}\text{O}-\text{C}(\text{H})=\text{N}^{+}\text{Me}_2$ , where the oxygen has a partial negative charge and the nitrogen has a partial positive charge, DMF would preferentially coordinate to the higher charged Yb(II) ion, whereas the neutral oxygen donor atoms in crypt would prefer the lower charged Na(I) ion.

## Conclusion

In summary, the complexes  $[\text{Ln}(\text{crypt})(\text{DMF})_2][\text{I}]_2$ , **18-Sm** and **18-Eu**, and  $[\text{Yb}(\text{crypt})(\text{DMF})][\text{I}]_2$ , **19-Yb**, provide new examples of Ln(II)-in-crypt complexes for Sm(II), Eu(II), and Yb(II) and demonstrate that simple starting materials, namely  $\text{LnI}_2(\text{THF})_2$ , can be used to synthesize them directly. The tetraphenylborate salts  $[\text{Ln}(\text{crypt})(\text{DMF})_2][\text{BPh}_4]_2$ , **20-Sm** and **20-Eu**, can be obtained by ionic metathesis. However, attempts to make the tetraphenylborate analog of Yb gave the sodium crypt complex  $[\text{Na}(\text{crypt})]\text{I}$  and  $[\text{Yb}(\text{DMF})_6][\text{BPh}_4]_2$ , **21-Yb**, rather than an Yb crypt product. Previous studies have shown that trivalent  $\text{LaCl}_3$  can also undergo facile encapsulation by crypt in DMF to form  $[\text{La}(\text{crypt})\text{Cl}_2]\text{Cl}$ ,<sup>15</sup> but in that case, two of the halide ligands are retained on the metal. In **18-Ln**, **19-Yb**, and **20-Ln**, the Ln(II) ions are free of any anionic coordinating ligands. This may facilitate further reduction of the metal.

## Experimental

All syntheses and manipulations described below were conducted under argon with rigorous exclusion of air and water using glovebox, Schlenk-line, and high-vacuum-line techniques. All  $\text{LnI}_2(\text{THF})_2$  (Ln = Sm, Eu, Yb)<sup>16-17</sup> materials were prepared according to previously published literature. 2.2.2-Cryptand (4,7,13,16,21,24-hexaoxa-1,10-diazabicyclo[8.8.8]hexacosane, Aldrich) was placed under vacuum ( $10^{-3}$  Torr) for 12 h before

use. NaBPh<sub>4</sub> was purchased from Aldrich and recrystallized from acetone/hexanes. Solvents were sparged with UHP Ar and dried over columns containing Q-5 and molecular sieves. DMF-*d*<sub>7</sub> was dried with 3 Å molecular sieves and degassed by three freeze-pump-thaw cycles. <sup>1</sup>H NMR spectra were recorded on Bruker CRYO500 MHz or GN500 MHz spectrometer and referenced internally to residual protio-solvent resonances. IR samples were prepared as KBr pellets on a Varian 1000 FT-IR or a Jasco FT/IR-4700 spectrometer. Elemental analyses were performed on a PerkinElmer series II 2400 CHNS analyzer.

**[Sm(2.2.2-cryptand)(DMF)<sub>2</sub>][I]<sub>2</sub>, 18-Sm.** In an argon-filled glovebox, a blue THF (3 mL) solution of SmI<sub>2</sub>(THF)<sub>2</sub> (100 mg, 0.18 mmol) was added to a colorless THF (1 mL) solution of 2.2.2-cryptand (69 mg, 0.18 mmol) dropwise while stirring. A green precipitate immediately formed. After 1 h of stirring, THF was removed *in vacuo* and 1 mL of DMF was added to dissolve the green solid to form a purple solution. This solution was layered into Et<sub>2</sub>O and placed in a -35 °C freezer. After 1 d, purple crystals suitable for X-ray crystallography (133 mg, 79%). <sup>1</sup>H NMR (DMF-*d*<sub>7</sub>): δ 4.03 [12H, OCH<sub>2</sub>CH<sub>2</sub>O], 3.94 [12H, NCH<sub>2</sub>CH<sub>2</sub>O], 2.42 [s, 12H, NCH<sub>2</sub>]. IR: 2913m, 2877m, 2849w, 2827w, 2797w, 1653w, 1484m, 1462m, 1380w, 1354s, 1320m, 1281m, 1271m, 1246m, 1174w, 1128m, 1116m, 1094s, 1074s, 1064s, 1025m, 954s, 936s, 902m, 872w, 842m, 826m, 814m, 754m, 677w. Calcd for desolvated [Sm(crypt)]I<sub>2</sub>, C<sub>18</sub>H<sub>36</sub>N<sub>2</sub>O<sub>6</sub>I<sub>2</sub>Sm: C, 27.69; H, 4.65; N, 3.59. Found: C, 27.85; H, 4.59; N, 3.69.

**[Eu(2.2.2-cryptand)(DMF)<sub>2</sub>][I]<sub>2</sub>, 18-Eu.** As described for **18-Sm**, a light green THF solution of EuI<sub>2</sub>(THF)<sub>2</sub> (100 mg, 0.18 mmol) was added to a solution of 2.2.2-cryptand (68 mg, 0.18 mmol) dropwise while stirring. A colorless precipitate immediately formed. DMF was added to dissolve the colorless solid to form a colorless solution. This solution was layered into Et<sub>2</sub>O and placed in a -35 °C freezer. After 1 d, colorless crystals suitable for X-ray



crystallography (148 mg, 88%). IR: 2913m, 2876m, 2857w, 2825w, 2799w, 1653w, 1481m, 1460m, 1422w, 1372m, 1353s, 1320m, 1280m, 1273m, 1246m, 1174w, 1128m, 1117s, 1094s, 1073s, 1062s, 1025m, 953, 937s, 902m, 873w, 843m, 826m, 816m, 754m. Calcd for desolvated [Eu(crypt)]I<sub>2</sub>, C<sub>18</sub>H<sub>36</sub>N<sub>2</sub>O<sub>6</sub>I<sub>2</sub>Eu: C, 27.64; H, 4.64; N, 3.58. Found: C, 27.98; H, 4.39; N, 3.56.

**[Yb(2.2.2-cryptand)(DMF)]<sub>2</sub>[I]<sub>2</sub>, 19-Yb.** As described for **18-Sm**, a yellow THF solution of YbI<sub>2</sub>(THF)<sub>2</sub> (100 mg, 0.18 mmol) was added to a THF solution of 2.2.2-cryptand (66 mg, 0.18 mmol) forming a colorless precipitate. After removal of THF, addition of DMF to the colorless solid formed a light yellow solution. This was layered in Et<sub>2</sub>O and placed in a -35 °C and after 1 d, pale yellow crystals suitable for X-ray crystallography were isolated (113 mg, 74%). <sup>1</sup>H NMR (DMF-*d*<sub>7</sub>): δ 3.93 [12H, OCH<sub>2</sub>CH<sub>2</sub>O], 3.90 [12H, NCH<sub>2</sub>CH<sub>2</sub>O], 2.83 [12H, NCH<sub>2</sub>]. IR: 2912m, 2876m, 2840m, 2803w, 1641s, 1492w, 1470w, 1462m, 1456m, 1435m, 1417m, 1379m, 1352s, 1291m, 1273m, 1257w, 1248w, 1240m, 1170w, 1112m, 1079s, 1066s, 1059m, 1046m, 1026w, 948m, 935m, 899w, 835w, 819m, 752m, 681m, 664m. Calcd for [Yb(crypt)(DMF)]<sub>2</sub>, C<sub>21</sub>H<sub>43</sub>N<sub>3</sub>O<sub>7</sub>I<sub>2</sub>Yb: C, 28.78; H, 4.95; N, 4.79. Found: C, 27.94; H, 4.75; N, 4.69.

**[Sm(2.2.2-cryptand)(DMF)<sub>2</sub>][BPh<sub>4</sub>]<sub>2</sub>, 20-Sm.** In an argon-filled glovebox, a colorless DMF (1 mL) solution of NaBPh<sub>4</sub> (37 mg, 0.11 mmol) was added dropwise to a stirring purple DMF (3 mL) solution of [Sm(crypt)(DMF)<sub>2</sub>][I]<sub>2</sub>, **18-Sm**, (50 mg, 0.054 mmol). After stirring overnight, a white precipitate formed, presumably NaI, and was removed via filtration. The purple DMF solution was layered into Et<sub>2</sub>O and placed in a -35 °C freezer. After 1 d, purple crystals suitable for X-ray crystallography were isolated (51 mg, 71%).

**[Yb(DMF)<sub>6</sub>][BPh<sub>4</sub>]<sub>2</sub>, 21-Yb.** In an argon-filled glovebox, YbI<sub>2</sub>(THF)<sub>2</sub> (100 mg, 0.18 mmol), 2.2.2-cryptand (66 mg, 0.18 mmol), and NaBPh<sub>4</sub> (120 mg, 0.35 mmol) were stirred in

DMF overnight. The solution became orange without sign of precipitate. The solution was layered into Et<sub>2</sub>O overnight and orange crystals suitable for X-ray crystallography were isolated.

### Spectral Details

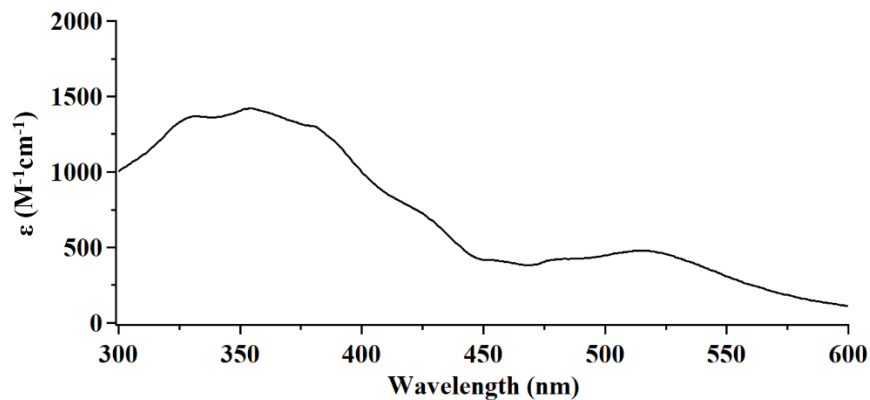


**Figure 6.4.** UV-visible spectrum of [Sm(crypt)(DMF)][I]<sub>2</sub>, **18-Sm**, in DMF (5 mM).

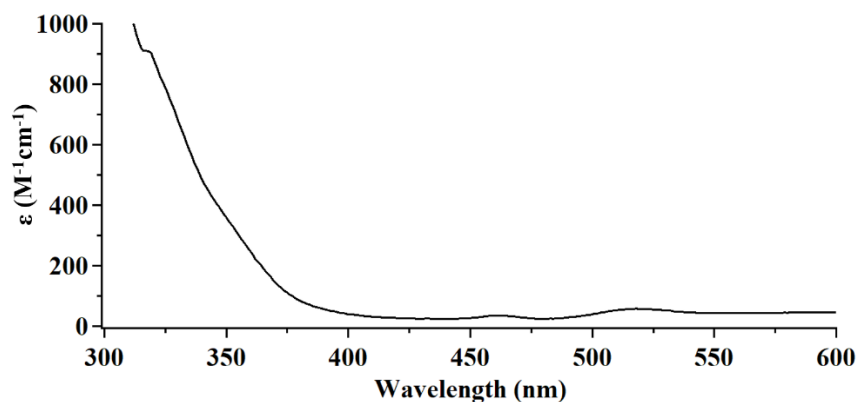


**Figure 6.5.** UV-visible spectrum of [Eu(crypt)(DMF)][I]<sub>2</sub>, **18-Eu**, in DMF (5 mM).

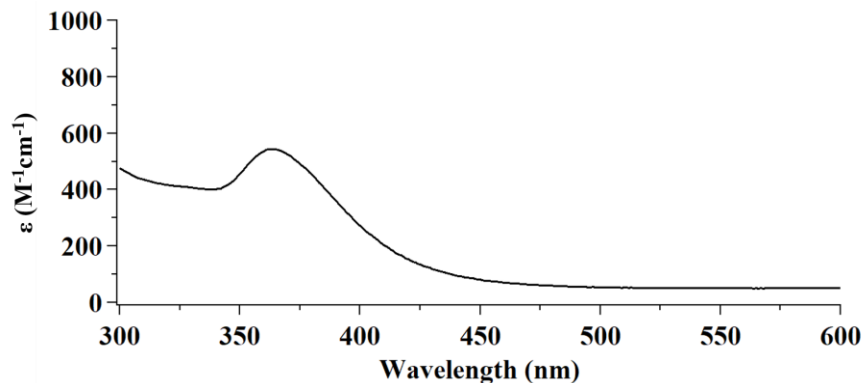


**Figure 6.6.** UV-visible spectrum of [Yb(crypt)(DMF)][I]<sub>2</sub>, **19-Yb**, in DMF (10 mM).

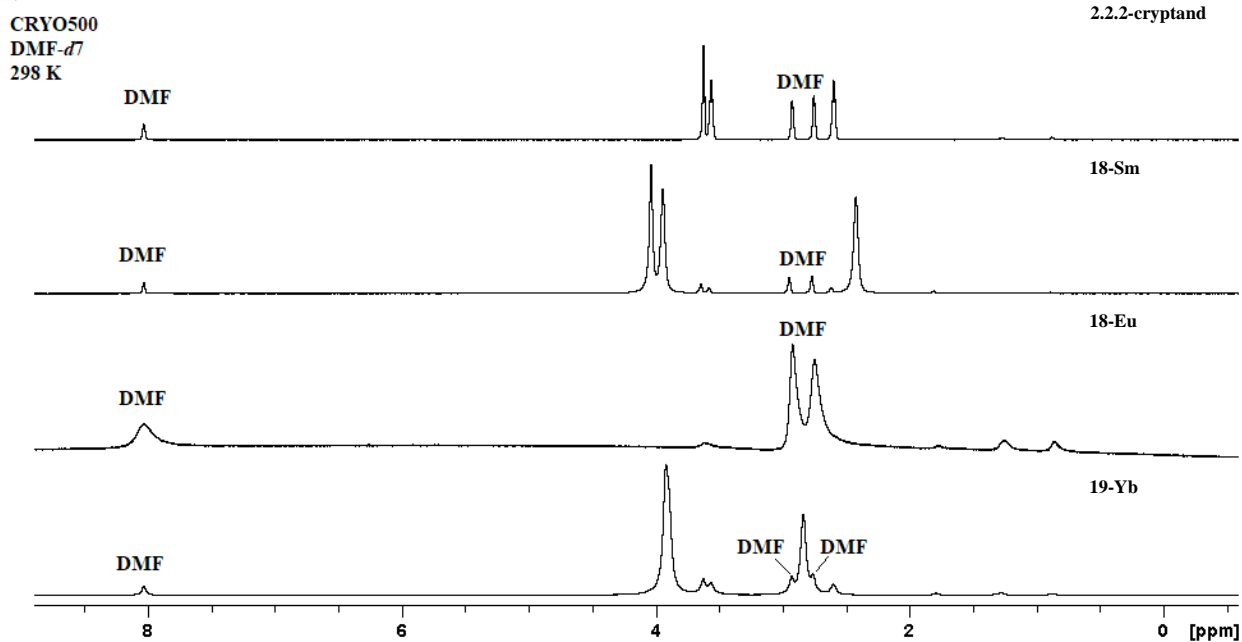


**Figure 6.7.** NMR (500 MHz, DMF-*d*<sub>7</sub>) spectra of 2.2.2-cryptand, [Sm(crypt)(DMF)<sub>2</sub>][I]<sub>2</sub>, **18-Sm**, [Eu(crypt)(DMF)][I]<sub>2</sub>, **18-Eu**, and [Yb(crypt)(DMF)][I]<sub>2</sub>, **19-Yb**.

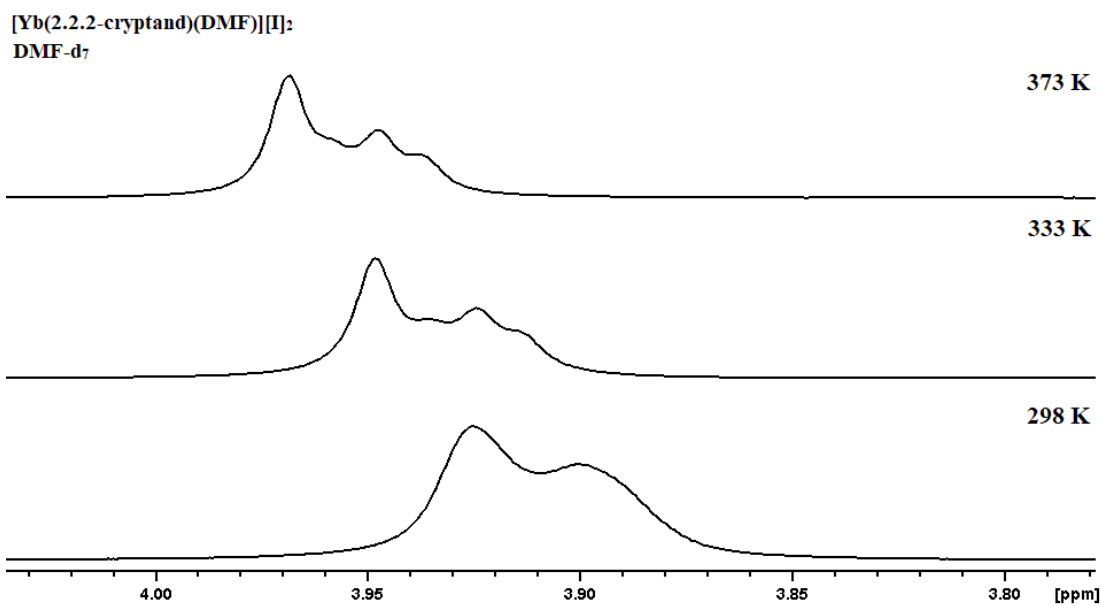


**Figure 6.8.** Variable temperature NMR (500 MHz, DMF-*d*<sub>7</sub>) of [Yb(crypt)(DMF)][I]<sub>2</sub>, **19-Yb**, at temperatures of 298 K (bottom), 333 K (middle), and 373K (top) zoomed at OCH<sub>2</sub>CH<sub>2</sub>O and NCH<sub>2</sub>CH<sub>2</sub>O 2.2.2-cryptand resonances.

## Structural Details

**X-ray Data Collection, Structure Solution and Refinement for [Sm(crypt)(DMF)<sub>2</sub>][I]<sub>2</sub>, 18-Sm.** A purple crystal of approximate dimensions 0.394 x 0.207 x 0.128 mm was mounted in a cryoloop and transferred to a Bruker SMART APEX II diffractometer. The APEX2<sup>24</sup> program package was used to determine the unit-cell parameters and for data collection (45 sec/frame scan time for a sphere of diffraction data). The raw frame data was processed using SAINT<sup>25</sup> and SADABS<sup>26</sup> to yield the reflection data file. Subsequent calculations were carried out using the SHELXTL<sup>27</sup> program. The diffraction symmetry was *2/m* and the systematic absences were consistent with the monoclinic space groups *Cc* and *C2/c*. It was later determined that space group *C2/c* was correct. The structure was solved by direct methods and refined on  $F^2$  by full-matrix least-squares techniques. The analytical scattering factors<sup>28</sup> for neutral atoms were used throughout the analysis. Hydrogen atoms were located from a difference-Fourier map and refined (*x,y,z* and  $U_{iso}$ ). Least-squares analysis yielded  $wR2 = 0.0358$  and  $Goof = 1.053$  for 180 variables refined against 4130 data (0.74 Å),  $R1 = 0.0155$  for those 3900 data with  $I > 2.0\sigma(I)$ .

**X-ray Data Collection, Structure Solution and Refinement for [Eu(crypt)(DMF)<sub>2</sub>][I]<sub>2</sub>, 18-Eu.** A colorless crystal of approximate dimensions 0.117 x 0.152 x 0.219 mm was mounted in a cryoloop and transferred to a Bruker SMART APEX II diffractometer. The APEX2<sup>24</sup> program package was used to determine the unit-cell parameters and for data collection (60 sec/frame scan time for a sphere of diffraction data). The raw frame data was processed using SAINT<sup>25</sup> and SADABS<sup>26</sup> to yield the reflection data file. Subsequent calculations were carried out using the SHELXTL<sup>27</sup> program. The diffraction symmetry was *2/m* and the systematic absences were consistent with the monoclinic space groups *Cc* and *C2/c*. It

was later determined that space group  $C2/c$  was correct. The structure was solved by dual space methods and refined on  $F^2$  by full-matrix least-squares techniques. The analytical scattering factors<sup>28</sup> for neutral atoms were used throughout the analysis. Hydrogen atoms were included using a riding model. The molecule was located on a two-fold rotation axis. Least-squares analysis yielded  $wR2 = 0.0542$  and  $Goof = 1.041$  for 180 variables refined against 3697 data ( $0.78 \text{ \AA}$ ),  $R1 = 0.0250$  for those 3276 data with  $I > 2.0\sigma(I)$ .

**X-ray Data Collection, Structure Solution and Refinement for [Yb(crypt)(DMF)][I]<sub>2</sub>, 19-Yb.** A pale yellow crystal of approximate dimensions  $0.217 \times 0.164 \times 0.116$  mm was mounted in a cryoloop and transferred to a Bruker SMART APEX II diffractometer. The APEX2<sup>24</sup> program package was used to determine the unit-cell parameters and for data collection (30 sec/frame scan time for a sphere of diffraction data). The raw frame data was processed using SAINT<sup>25</sup> and SADABS<sup>26</sup> to yield the reflection data file. Subsequent calculations were carried out using the SHELXTL<sup>27</sup> program. The diffraction symmetry was  $2/m$  and the systematic absences were consistent with the monoclinic space group  $P2_1/c$  that was later determined to be correct. The structure was solved by direct methods and refined on  $F^2$  by full-matrix least-squares techniques. The analytical scattering factors<sup>28</sup> for neutral atoms were used throughout the analysis. Hydrogen atoms were located from a difference-Fourier map and refined ( $x, y, z$  and  $U_{iso}$ ). Least-squares analysis yielded  $wR2 = 0.0574$  and  $Goof = 1.034$  for 479 variables refined against 7197 data ( $0.74 \text{ \AA}$ ),  $R1 = 0.0269$  for those 6053 data with  $I > 2.0\sigma(I)$ .

**X-ray Data Collection, Structure Solution and Refinement for [Sm(crypt)(DMF)<sub>2</sub>][BPh<sub>4</sub>]<sub>2</sub>, 20-Sm.** A purple crystal of approximate dimensions  $0.132 \times 0.191 \times 0.249$  mm was mounted in a cryoloop and transferred to a Bruker SMART APEX II diffractometer. The APEX2<sup>24</sup> program package was used to determine the unit-cell parameters

and for data collection (90 sec/frame scan time for a sphere of diffraction data). The raw frame data was processed using SAINT<sup>25</sup> and SADABS<sup>26</sup> to yield the reflection data file. Subsequent calculations were carried out using the SHELXTL<sup>27</sup> program. There were no systematic absences nor any diffraction symmetry other than the Friedel condition. The centrosymmetric triclinic space group  $P\bar{1}$  was assigned and later determined to be correct. The structure was solved by direct methods and refined on  $F^2$  by full-matrix least-squares techniques. The analytical scattering factors<sup>28</sup> for neutral atoms were used throughout the analysis. Hydrogen atoms were located from a difference-Fourier map and refined ( $x,y,z$  and  $U_{iso}$ ). Least-squares analysis yielded  $wR2 = 0.0637$  and  $Goof = 1.048$  for 932 variables refined against 16298 data (0.74 Å),  $R1 = 0.0264$  for those 15044 data with  $I > 2.0\sigma(I)$ .

**X-ray Data Collection, Structure Solution and Refinement for [Eu(crypt)(DMF)<sub>2</sub>][BPh<sub>4</sub>]<sub>2</sub>, 20-Eu.** A colorless crystal of approximate dimensions 0.068 x 0.082 x 0.203 mm was mounted in a cryoloop and transferred to a Bruker SMART APEX II diffractometer. The APEX2<sup>24</sup> program package was used to determine the unit-cell parameters and for data collection (60 sec/frame scan time for a sphere of diffraction data). The raw frame data was processed using SAINT<sup>25</sup> and SADABS<sup>26</sup> to yield the reflection data file. Subsequent calculations were carried out using the SHELXTL<sup>27</sup> program. There were no systematic absences nor any diffraction symmetry other than the Friedel condition. The centrosymmetric triclinic space group  $P\bar{1}$  was assigned and later determined to be correct. The structure was solved by dual space methods and refined on  $F^2$  by full-matrix least-squares techniques. The analytical scattering factors<sup>28</sup> for neutral atoms were used throughout the analysis. Hydrogen atoms were included using a riding model. Least-squares analysis yielded  $wR2 = 0.0672$  and

Goof = 1.043 for 835 variables refined against 13766 data (0.80 Å), R1 = 0.0310 for those 11998 data with  $I > 2.0\sigma(I)$ .

**X-ray Data Collection, Structure Solution and Refinement for [Yb(DMF)<sub>6</sub>][BPh<sub>4</sub>]<sub>2</sub>, 21-Yb.** An orange crystal of approximate dimensions 0.382 x 0.268 x 0.196 mm was mounted in a cryoloop and transferred to a Bruker SMART APEX II diffractometer. The APEX2<sup>24</sup> program package was used to determine the unit-cell parameters and for data collection (30 sec/frame scan time for a sphere of diffraction data). The raw frame data was processed using SAINT<sup>25</sup> and SADABS<sup>26</sup> to yield the reflection data file. Subsequent calculations were carried out using the SHELXTL<sup>27</sup> program. The diffraction symmetry was  $2/m$  and the systematic absences were consistent with the monoclinic space group  $P2_1/c$  that was later determined to be correct. The structure was solved by direct methods and refined on  $F^2$  by full-matrix least-squares techniques. The analytical scattering factors<sup>28</sup> for neutral atoms were used throughout the analysis. Disorder of one coordinated DMF molecule was modeled in two parts with 67% and 33% occupancy. Hydrogen atoms were located from a difference-Fourier map and refined ( $x, y, z$  and  $U_{iso}$ ) with the exception of the hydrogen atoms located on the disordered DMF which were included using a riding model. Least-squares analysis yielded  $wR2 = 0.0733$  and Goof = 1.035 for 1104 variables refined against 16576 data (0.74 Å), R1 = 0.0301 for those 13983 data with  $I > 2.0\sigma(I)$ .

## References

- (1) Dietrich, B.; Lehn, J. M.; Sauvage, J. P., Cryptates—XI: Complexes macrobicycliques, formation, structure, proprietes. *Tetrahedron* **1973**, *29*, 1647-1658.
- (2) Dietrich, B.; Lehn, J. M.; Sauvage, J. P.; Blanzat, J., Cryptates—X: Syntheses et proprietes physiques de systemes diaza-polyoxa-macrobicycliques. *Tetrahedron* **1973**, *29*, 1629-1645.
- (3) Burns, J. H., Crystal and molecular structure of a cryptate complex of samarium:  $C_{18}H_{36}O_6N_2Sm_2(NO_3)_6 \cdot H_2O$ . *Inorg. Chem.* **1979**, *18*, 3044-3047.

- (4) Benetollo, F.; Bombieri, G.; Cassol, A.; De Paoli, G.; Legendziewicz, J., Coordination chemistry of lanthanides with cryptands. An X-ray and spectroscopic study of the complex  $\text{Nd}_2(\text{NO}_3)_6 [\text{C}_{18}\text{H}_{36}\text{O}_6\text{N}_2] \cdot \text{H}_2\text{O}$ . *Inorg. Chim. Acta* **1985**, *110*, 7-13.
- (5) Yang, G.; Liu, S.; Jin, Z., Coordination chemistry and structure characterization of  $\text{C}_{18}\text{H}_{36}\text{O}_6\text{N}_2\text{Eu}_2(\text{NO}_3)_6 \cdot \text{H}_2\text{O}$ . *Inorg. Chim. Acta* **1987**, *131*, 125-128.
- (6) Yee, E. L.; Gansow, O. A.; Weaver, M. J., Electrochemical studies of europium and ytterbium cryptate formation in aqueous solution. Effects of varying the metal oxidation state upon cryptate thermodynamics and kinetics. *J. Am. Chem. Soc.* **1980**, *102*, 2278-2285.
- (7) Mao, J.; Jin, Z., Synthesis and structure characterization of lanthanum [2,2,2]cryptates,  $[\text{LaCl}[2,2,2](\text{H}_2\text{O})]\text{Cl}_2 \cdot \text{H}_2\text{O}$  and  $[\text{La}(\text{CF}_3\text{SO}_3)[2,2,2](\text{DMF})](\text{CF}_3\text{SO}_3)_2$ . *Polyhedron* **1994**, *13*, 319-323.
- (8) Gamage, N.-D. H.; Mei, Y.; Garcia, J.; Allen, M. J., Oxidatively Stable, Aqueous Europium(II) Complexes through Steric and Electronic Manipulation of Cryptand Coordination Chemistry. *Angew. Chem. Int. Ed.* **2010**, *49*, 8923-8925.
- (9) Lenora, C. U.; Carniato, F.; Shen, Y.; Latif, Z.; Haacke, E. M.; Martin, P. D.; Botta, M.; Allen, M. J., Structural Features of Europium(II)-Containing Cryptates That Influence Relaxivity. *Chem. Eur. J.* **2017**, *23*, 15404-15414.
- (10) Ekanger, L. A.; Polin, L. A.; Shen, Y.; Haacke, E. M.; Martin, P. D.; Allen, M. J., A EuII-Containing Cryptate as a Redox Sensor in Magnetic Resonance Imaging of Living Tissue. *Angew. Chem. Int. Ed.* **2015**, *54*, 14398-14401.
- (11) Jenks, T. C.; Bailey, M. D.; Hovey, Jessica L.; Fernando, S.; Basnayake, G.; Cross, M. E.; Li, W.; Allen, M. J., First use of a divalent lanthanide for visible-light-promoted photoredox catalysis. *Chem. Sci.* **2018**, *9*, 1273-1278.
- (12) Jenks, T. C.; Bailey, M. D.; Corbin, B. A.; Kuda-Wedagedara, A. N. W.; Martin, P. D.; Schlegel, H. B.; Rabuffetti, F. A.; Allen, M. J., Photophysical characterization of a highly luminescent divalent-europium-containing azacryptate. *Chem. Commun.* **2018**, *54*, 4545-4548.
- (13) Evans, W. J., Tutorial on the Role of Cyclopentadienyl Ligands in the Discovery of Molecular Complexes of the Rare-Earth and Actinide Metals in New Oxidation States. *Organometallics* **2016**, *35*, 3088-3100.
- (14) Huh, D. N.; Kotyk, C. M.; Gembicky, M.; Rheingold, A. L.; Ziller, J. W.; Evans, W. J., Synthesis of rare-earth-metal-in-cryptand dication,  $[\text{Ln}(2.2.2\text{-cryptand})]^{2+}$ , from  $\text{Sm}^{2+}$ ,  $\text{Eu}^{2+}$ , and  $\text{Yb}^{2+}$  silyl metallocenes  $(\text{C}_5\text{H}_4\text{SiMe}_3)_2\text{Ln}(\text{THF})_2$ . *Chem. Commun.* **2017**, *53*, 8664-8666.
- (15) Huh, D. N.; Windorff, C. J.; Ziller, J. W.; Evans, W. J., Synthesis of uranium-in-cryptand complexes. *Chem. Commun.* **2018**, *54*, 10272-10275.



- (16) Heckmann, G.; Niemeyer, M., Synthesis and First Structural Characterization of Lanthanide(II) Aryls: Observation of a Schlenk Equilibrium in Europium(II) and Ytterbium(II) Chemistry. *J. Am. Chem. Soc.* **2000**, *122*, 4227-4228.
- (17) Girard, P.; Namy, J. L.; Kagan, H. B., Divalent lanthanide derivatives in organic synthesis. 1. Mild preparation of samarium iodide and ytterbium iodide and their use as reducing or coupling agents. *J. Am. Chem. Soc.* **1980**, *102*, 2693-2698.
- (18) Shannon, R., Revised effective ionic radii and systematic studies of interatomic distances in halides and chalcogenides. *Acta Crystallographica Section A* **1976**, *32*, 751-767.
- (19) Lin, C.-Y.; Guo, J.-D.; Fettingner, J. C.; Nagase, S.; Grandjean, F.; Long, G. J.; Chilton, N. F.; Power, P. P., Dispersion Force Stabilized Two-Coordinate Transition Metal–Amido Complexes of the  $-N(\text{SiMe}_3)\text{Dipp}$  (Dipp =  $\text{C}_6\text{H}_3\text{-2,6-Pri}_2$ ) Ligand: Structural, Spectroscopic, Magnetic, and Computational Studies. *Inorg. Chem.* **2013**, *52*, 13584-13593.
- (20) Liptrot, D. J.; Guo, J.-D.; Nagase, S.; Power, P. P., Dispersion Forces, Disproportionation, and Stable High-Valent Late Transition Metal Alkyls. *Angew. Chem. Int. Ed.* **2016**, *55*, 14766-14769.
- (21) Liptrot, D. J.; Power, P. P., London dispersion forces in sterically crowded inorganic and organometallic molecules. *Nat. Chem. Rev.* **2017**, *1*, 0004.
- (22) Moras, D.; Weiss, R., Etude structurale des cryptates. III. Structure cristalline et moleculaire du cryptate de sodium  $\text{C}_{18}\text{H}_{36}\text{N}_2\text{O}_6\cdot\text{NaI}$ . *Acta Cryst. B* **1973**, *29*, 396-399.
- (23) Evans, W. J.; Johnston, M. A.; Greci, M. A.; Gummersheimer, T. S.; Ziller, J. W., Divalent lanthanide complexes free of coordinating anions: facile synthesis of fully solvated dicationic  $[\text{LnL}_x]^{2+}$  compounds. *Polyhedron* **2003**, *22*, 119-126.
- (24) APEX2 Version 2014.11-0, Bruker AXS, Inc.; Madison, WI 2014.
- (25) SAINT Version 8.34a, Bruker AXS, Inc.; Madison, WI 2013.
- (26) Sheldrick, G. M. SADABS, Version 2014/5, Bruker AXS, Inc.; Madison, WI 2014.
- (27) Sheldrick, G. M. SHELXTL, Version 2014/7, Bruker AXS, Inc.; Madison, WI 2014.
- (28) International Tables for Crystallography 1992, Vol. C., Dordrecht: Kluwer Academic Publishers.

## CHAPTER 7

### Isolation of Lanthanide Cryptate Complexes Containing Triflates

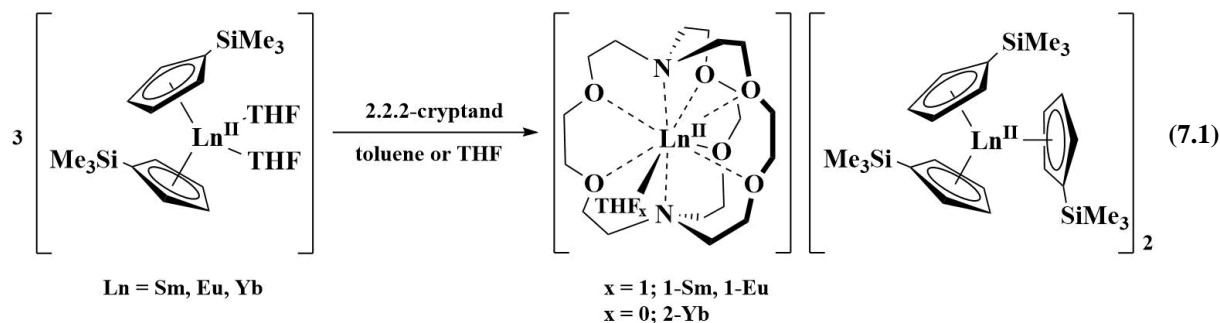
#### Introduction

As described in Chapter 6, complexes containing lanthanide ions encapsulated by the 2.2.2-cryptand ligand (crypt) were first reported in 1979.<sup>1</sup> However, in the ensuing four decades, only sixteen crystallographically-characterized Ln-in-crypt complexes were reported in the literature.<sup>1-10</sup> The majority of these complexes involved lanthanides in the common +3 oxidation state.<sup>1-4, 10</sup> Ln(II)-in-crypt complexes were only identified in the 2010's.<sup>5-9</sup> These crystallographically-characterized Ln(II)-in-crypt complexes were accessible only from Ln(II) precursors.

Ln-in-crypt complexes are of interest because it appears that this ligand may favor lower oxidation states as suggested by Gansow<sup>11</sup> and Allen.<sup>5</sup> Hence, the crypt coordination environment could allow the isolation of additional classes of the new Ln(II) ions.<sup>12</sup> On the other hand, electrochemical studies of Ln-in-crypt complexes of Eu, Sm and Yb by Albrecht-Schmitt and co-workers found Ln(III)/Ln(II) redox couples comparable to those in the literature for non-crypt complexes and some of which were only quasi-reversible.<sup>13</sup>

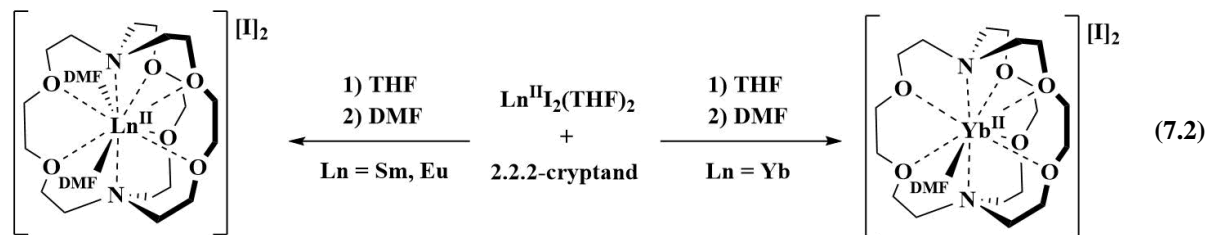
Ln-in-crypt complexes are of interest in light of the discovery that isolable molecular complexes of Ln(II) ions are not limited to the traditional +2 ions of Eu, Yb, Sm, Tm, Dy, and Nd.<sup>12, 14-16</sup> The new Ln(II) ions for La, Ce, Pr, Gd, Tb, Ho, Er, Lu, and Y were made by alkali metal reduction in the presence of 2.2.2-cryptand to stabilize the alkali metal. However, since the lanthanides can be sequestered by crypt, it is important to know the relevant Ln(II)-in-crypt chemistry.

Chapter 6 described examples of Ln(II)-in-crypt complexes formed from Ln(II) metallocene precursors as shown in eq 7.1.



Chapter 6 also describes how simple  $\text{LnI}_2(\text{THF})_2$  precursors can also form Ln(II)-in-crypt complexes such as  $[\text{Ln}(\text{crypt})(\text{DMF})_2][\text{I}]_2$  (Ln = Sm, Eu) and  $[\text{Yb}(\text{crypt})(\text{DMF})][\text{I}]_2$ , eq 7.2.

Since these complexes were insoluble in



etheral solvents, DMF was necessary to dissolve these complexes and the crystal structures of the compounds revealed that DMF was coordinated to the lanthanide center.<sup>8</sup>

To obtain more information about Ln-in-crypt complexes, reactions of lanthanide triflates with crypt were investigated. This Chapter describes attempt to make Ln(III)-in-crypt from lanthanide triflates,  $\text{Ln}^{\text{III}}(\text{OTf})_3$ . In a collaboration with Sierra R. Ciccone, a variety of Ln(III)-in-crypt complexes were identified whose solubility depends on the size of the metal and the presence or absence of coordinating solvents. This Chapter also describes the reduction chemistry of these complexes and demonstrates that reductions of Ln(III)-in-crypt complexes to Ln(II)-in-crypt compounds (Ln = Sm, Nd) are possible with crystallographically-characterized

precursors and products. These are the first Ln(II)-in-crypt compounds synthesized from Ln(III) precursors.

## Results and Discussions

Dy(OTf)<sub>3</sub> is insoluble in THF and addition of crypt does not solubilize the complex. The Dy(III)-in-crypt complex, [Dy(crypt)(OTf)](OTf)<sub>2</sub>, **22-Dy**, was isolated by reacting Dy(OTf)<sub>3</sub> and crypt in MeCN, eq 7.3, Figure 7.1. No other smaller lanthanide encapsulated by crypt has

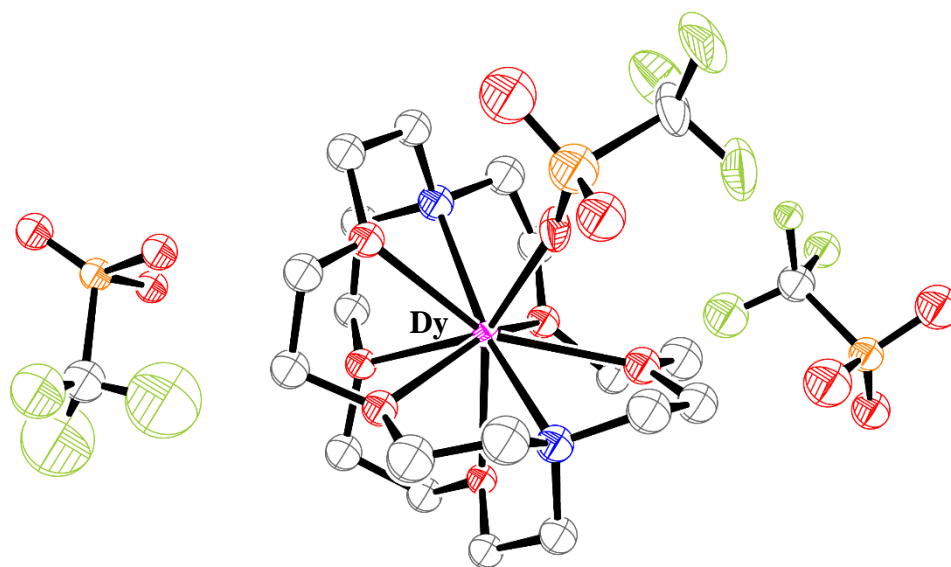
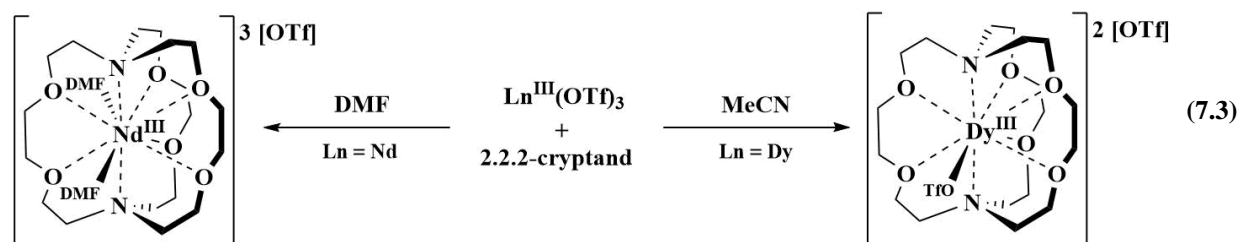


**Figure 7.1.** ORTEP representation of [Dy(crypt)(OTf)](OTf)<sub>2</sub>, **22-Dy**, with thermal ellipsoids drawn at the 50% probability level. Hydrogen atoms and disorder were omitted for clarity.

has been previously reported. The smallest crystallographically-characterized lanthanide in crypt reported in the literature is a Eu(III)-in-crypt, [Eu(crypt)(NO<sub>3</sub>)](Eu(NO<sub>3</sub>)<sub>5</sub>(OH<sub>2</sub>)).<sup>3</sup> Additionally,

only one example of a Ln(III)-in-crypt complex containing a coordinated triflate has been previously reported in the literature, [La(crypt)(OTf)(DMF)][OTf]<sub>2</sub>.<sup>4</sup>

Reaction of Nd(OTf)<sub>3</sub> with crypt in DMF also produced a crystallographically-characterized product, [Nd(crypt)(DMF)<sub>2</sub>][OTf]<sub>3</sub>, **23-Nd**, and it was found that the Nd(III) metal center was solvated with two molecules of DMF with three outer-sphere triflates, (OTf)<sup>1-</sup>, eq 7.3, Figure 7.2. Unlike the encapsulation reactions using THF, the DMF solvent preferentially

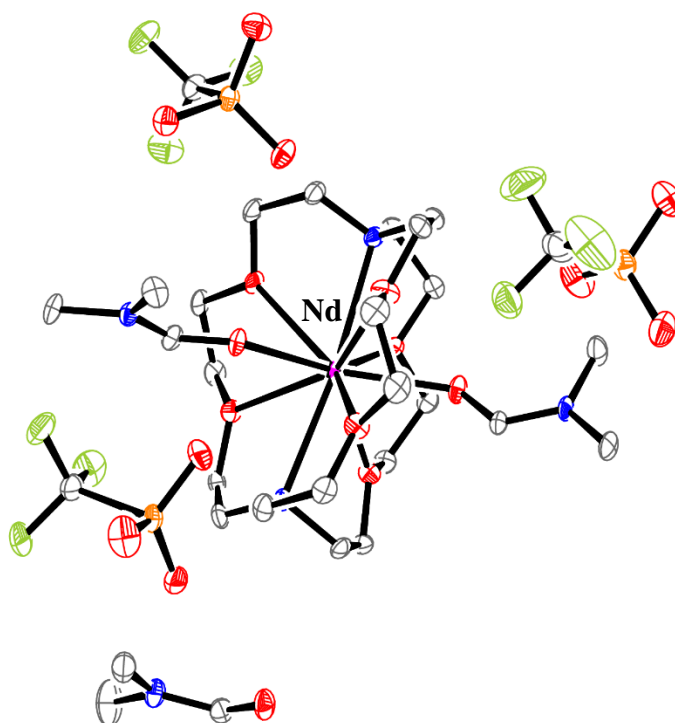
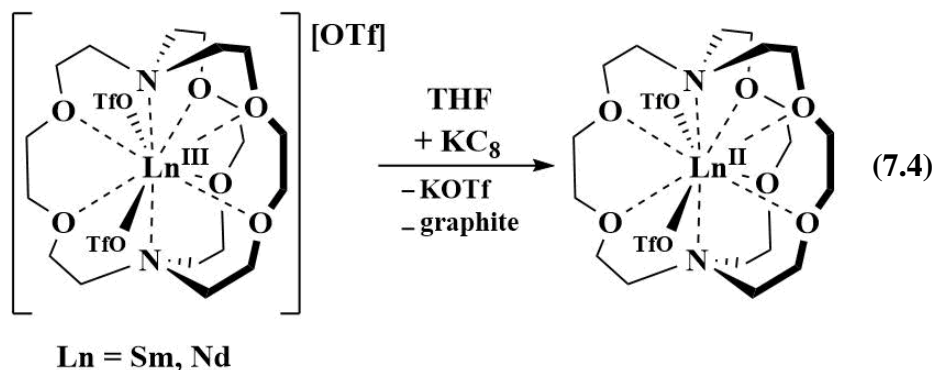


**Figure 7.2.** ORTEP representation of [Nd(crypt)(DMF)<sub>2</sub>][OTf]<sub>3</sub>, **23-Nd**, with thermal ellipsoids drawn at the 50% probability level. Hydrogen atoms were omitted for clarity.

coordinates to the Nd(III) metal center. This type of coordination mode has been previously observed with [Ln(crypt)(DMF)<sub>2</sub>][X]<sub>2</sub> (Ln = Sm, Eu; X = I, BPh<sub>4</sub>).<sup>8</sup> The geometry of these

Ln(III)-in-crypt complexes is 10-coordinate tetra-capped trigonal prism with the nitrogen donors capping both trigonal faces and the DMF oxygens capping two of the rectangular faces. This geometry has been previously reported for other Ln-in-crypt complexes,  $[\text{Ln}(\text{crypt})(\text{DMF})_2][\text{I}]_2$  (Ln = Sm, Eu),<sup>8</sup>  $[\text{Ln}(\text{crypt})(\text{DMF})_2][\text{BPh}_4]_2$  (Ln = Sm, Eu),<sup>8</sup>  $[\text{La}(\text{crypt})(\text{OH}_2)\text{Cl}]\text{Cl}_2$ ,<sup>4</sup>  $[\text{La}(\text{crypt})(\text{DMF})(\text{OTf})][\text{OTf}]_2$ ,<sup>4</sup>  $[\text{La}(\text{crypt})\text{Cl}_2]\text{Cl}$ .<sup>10</sup>

**Isolation of the  $[\text{Ln}^{\text{II}}(\text{crypt})(\text{OTf})_2]$ .** Inspired by the results obtained by Sierra R. Ciccone, the Ln(III)-in-crypt complexes,  $[\text{Ln}(\text{crypt})(\text{OTf})_2][\text{OTf}]$  (Ln = Sm, Nd), **24-Ln**, were chemically reduced to form the neutral complex  $[\text{Ln}(\text{crypt})(\text{OTf})_2]$ , **25-Ln**, eq 7.4. A THF solution



of **24-Ln** was added to  $\text{KC}_8$  to form dark solutions. The reduction product,  $[\text{Nd}(\text{crypt})(\text{OTf})_2]$ , **25-Nd**, were crystallographically-characterized and the Nd metal center retained both inner-sphere triflate ligands, Figure 7.3.

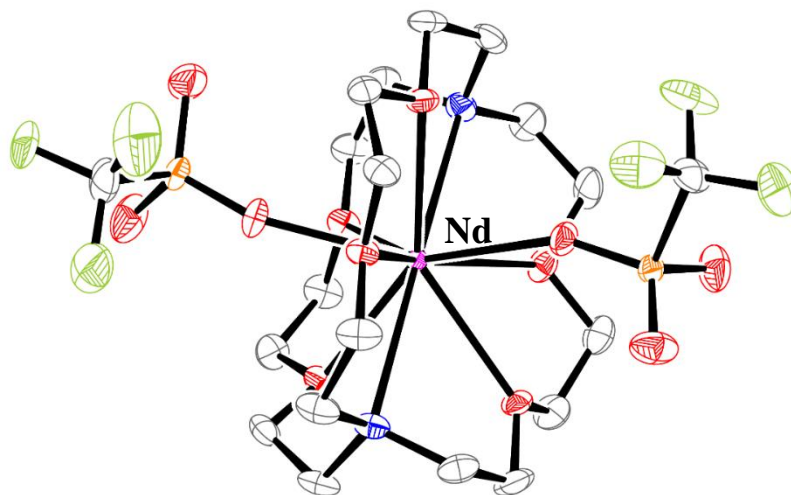


**Figure 7.3.** ORTEP representation of  $[\text{Nd}(\text{crypt})(\text{OTf})_2]$ , **25-Nd**, with thermal ellipsoids drawn at the 50% probability level. Hydrogen atoms were omitted for clarity.

**Electronic Structure Calculations.** Density functional theory (DFT) calculations were performed by Saswata Roy in the group of Prof. Filipp Furche using (TPSSh) functional. Calculations on  $[\text{Nd}(\text{crypt})(\text{OTf})_2]$ , **25-Nd**, suggest a  $4f^4$  quintet ground state, Figure 7.4. This electronic assignment is similar to the previously reported  $[\text{K}(\text{crypt})][((^{\text{Ad,Me}}\text{ArO})_3\text{mes})\text{Nd}^{\text{II}}]$ , however, two electrons were assigned to f orbitals and two electrons in  $f/\pi^*$  orbitals.<sup>17</sup> This also differs from the  $[\text{Cp}'_3\text{Nd}]^{1-}$  and  $[\text{Cp}''_3\text{Nd}]^{1-}$  electronic assignment of  $4f^35d^1$ .<sup>16, 18</sup>

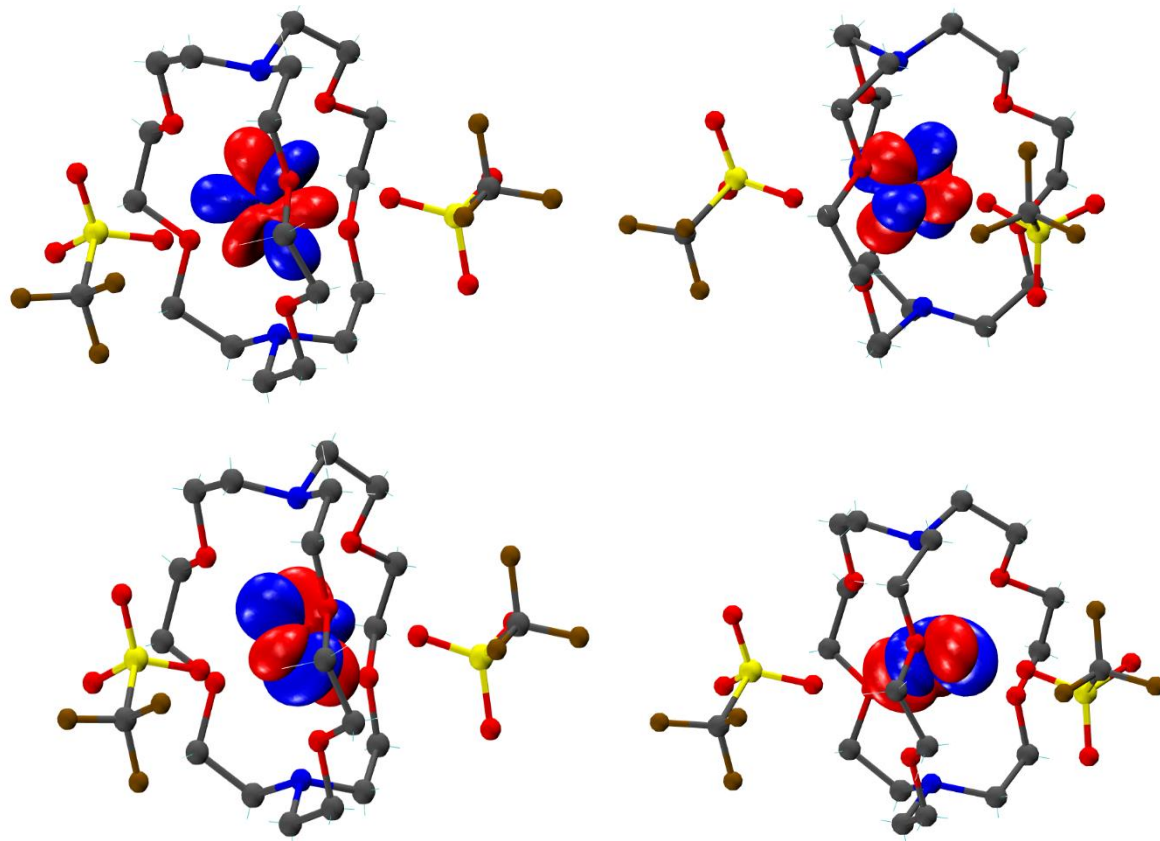


**Figure 7.4.** HOMO of  $[\text{Nd}(\text{crypt})(\text{OTf})_2]$ , **25-Nd**, with  $4f^4$  electron configuration. DFT calculations were performed by Saswata Roy in the laboratory of Prof. Filipp Furche.

The simulated UV-vis spectrum using TD-DFT calculations show two broad peaks around 430 nm and 500 nm, Figure 7.5. Analyzing the orbitals in these excitations reveals them to be of metal to ligand charge transfer (MLCT). The transition around 370 nm is assigned as a f to d transition.



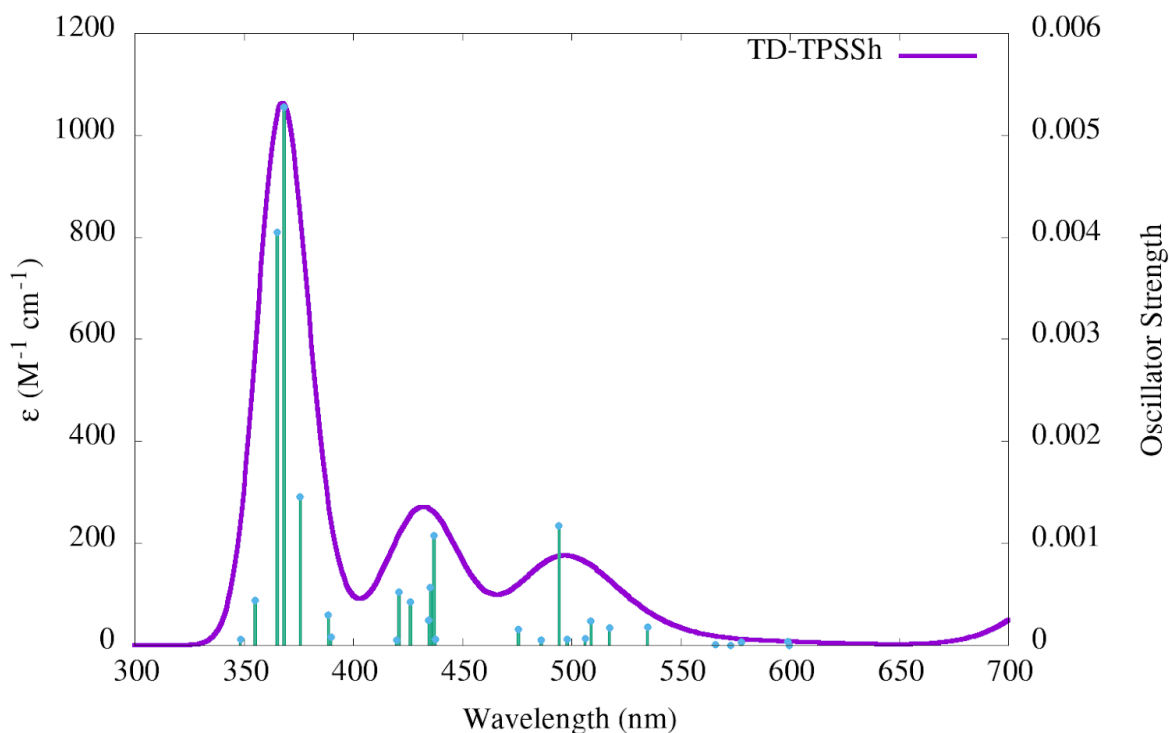


**Figure 7.5.** Simulated UV-Vis spectrum using TD-DFT and TPSSh functional. DFT calculations were performed by Saswata Roy in the laboratory of Prof. Filipp Furche.

## Conclusion

Additional examples of Ln(III) and Ln(II) cryptate complexes are isolable using Ln(OTf)<sub>3</sub> starting materials. The smallest lanthanide cryptate has been isolated by reacting Dy(OTf)<sub>3</sub> and crypt in MeCN to yield [Dy(crypt)(OTf)][OTf]<sub>2</sub>, **22-Dy**. The solubility of these smaller lanthanide triflates are limited to polar solvents such as MeCN which restricts the ability to explore their reductive chemistry. Coordinating triflates can be substituted by solvents such as DMF. When Nd(OTf)<sub>3</sub> is reacted with crypt in DMF, two solvent molecules of DMF coordinate to the metal center and three triflate anions are outer-sphere, [Nd(crypt)(DMF)<sub>2</sub>][OTf]<sub>3</sub>, **23-Nd**. This coordination mode has been previously seen with [Ln(crypt)(DMF)<sub>2</sub>][X]<sub>2</sub> (Ln = Sm, Eu; X = I, BPh<sub>4</sub>).<sup>8</sup> Reactions of larger lanthanide triflates with crypt yield THF soluble products which were later characterized by Sierra R. Ciccone as [Ln(crypt)(OTf)<sub>2</sub>][OTf] (Ln = La, Ce, Pr, Nd,

Sm). The solubility of these Ln(III)-in-crypt complexes in THF allows for reductions using  $\text{KC}_8$  to yield the first Nd(II)-in-crypt which was determined by DFT, in collaboration with Saswata Roy, have a  $4f^4$  electron configuration.

### Experimental Details

All manipulations and syntheses described below were conducted with the rigorous exclusion of air and water using standard glovebox and high-vacuum line techniques under an argon atmosphere. Solvents were sparged with UHP argon and dried by passage through columns containing Q-5 and molecular sieves prior to use. Deuterated tetrahydrofuran ( $\text{THF-}d_8$ ) was dried over NaK alloy, degassed by three freeze-pump-thaw cycles, and vacuum transferred before use.  $^1\text{H}$  NMR spectra were recorded on GN500, or CRYO500 MHz spectrometers at 298 K unless otherwise stated and referenced internally to residual protio-solvent resonances.  $\text{Nd}(\text{OTf})_3$  and  $\text{Sm}(\text{OTf})_3$  (Fischer Scientific) were dried under high vacuum ( $10^{-5}$  Torr) for 48 h at 220 °C before use. 2.2.2-cryptand (4,7,13,16,21,24-hexaoxa-1,10-diazabicyclo[8.8.8]hexacosane, Aldrich) was placed under vacuum ( $1 \times 10^{-3}$  Torr) for 12 h before use.

**[Dy(crypt)(OTf)][OTf]<sub>2</sub>, 22-Dy.** In an argon filled glovebox, a solution of crypt in MeCN (2 mL) was added to a stirring suspension of  $\text{Dy}(\text{OTf})_3$  in MeCN (2 mL). The suspension was left to stir and became clear after 30 min. After 1d of stirring, the solution was layered into  $\text{Et}_2\text{O}$  and placed in the freezer at  $-35$  °C. After 1d, colorless crystals suitable for X-ray crystallography were obtained.

**[Nd(crypt)(DMF)<sub>2</sub>][OTf]<sub>3</sub>, 23-Nd.** In an argon filled glovebox, a solution of crypt in DMF (2 mL) was added to a stirring suspension of  $\text{Nd}(\text{OTf})_3$  in DMF (2 mL). The suspension was left to stir and became clear after 30 min. After 1d of stirring, the solution was layered into

Et<sub>2</sub>O and placed in the freezer at -35 °C. After 1d, colorless crystals suitable for X-ray crystallography were obtained.

**[Nd(crypt)(OTf)<sub>2</sub>][OTf], 24-Nd.** In an argon filled glovebox, a solution of crypt in THF (5 mL) was added to a stirring suspension of Nd(OTf)<sub>3</sub> in THF (10 mL). The suspension was left to stir and became clear after 30 min. After 24 h of stirring, the solution was concentrated to 1 mL and placed in the freezer at -25 °C. After 1d, colorless crystals suitable for X-ray crystallography were obtained.

**[Nd(crypt)(OTf)<sub>2</sub>], 25-Nd.** A pale purple THF solution of **1-Nd** was added to a vial of KC<sub>8</sub> forming a black mixture. The black mixture was filtered to remove graphite and afforded a black solution which was layered into Et<sub>2</sub>O and placed into a -35 °C freezer. After 1 d, black crystals of 2-Nd suitable for X-ray crystallography were obtained.

**Computational details.** Density functional theory (DFT) calculations were performed by Saswata Roy on the structure obtained from the solutions of X-Ray crystallography of **26-Nd** in *C<sub>1</sub>* symmetry. The split valence basis functions (def2-SVP<sup>19</sup>) was used for all the atoms, and the small-core scalar relativistic effective core potential (ECP<sup>20</sup>) was used for neodymium atom. The resolution-of-identity (*RI-J*) approximation was invoked for the direct Coulomb integrals.<sup>21</sup> The energy and the density was converged to thresholds of 10<sup>-6</sup> a.u. A gauge-invariant implementation of the meta generalized gradient approximation (meta-GGA) functional, TPSSh was used for the exchange-correlation energy.<sup>22</sup> The conductor like solvation model (COSMO<sup>23</sup>) with a dielectric constant of 7.520<sup>24</sup> was used to model the solvation effects of THF along with Grimme's dispersion correction. Linear response time dependent density functional theory (TD-DFT) calculations were used for the UV-vis absorption spectrum. The lowest 45 excitations were evaluated using the same TPSSh functional. The spectrum was plotted by overlaying Gaussian

function of RMS line width of 0.1 eV at each excitation and was blue-shifted by 0.15 eV. All calculations were performed using Turbomole 7.2.<sup>25</sup>

## Structural Details

**X-ray Data Collection, Structure Solution and Refinement for [Nd(crypt)(OTf)<sub>2</sub>], 26-Nd.** A black crystal of approximate dimensions 0.281 x 0.185 x 0.169 mm was mounted in a cryoloop and transferred to a Bruker SMART APEX II diffractometer. The APEX2<sup>1</sup> program package was used to determine the unit-cell parameters and for data collection (10 sec/frame scan time for a sphere of diffraction data). The raw frame data was processed using SAINT<sup>2</sup> and SADABS<sup>3</sup> to yield the reflection data file. Subsequent calculations were carried out using the SHELXTL<sup>4</sup> program. The diffraction symmetry was  $2/m$  and the systematic absences were consistent with the monoclinic space group  $P2_1/c$  that was later determined to be correct. The structure was solved using the coordinates of the isomorphous samarium complex and refined on  $F^2$  by full-matrix least-squares techniques. The analytical scattering factors<sup>5</sup> for neutral atoms were used throughout the analysis. Hydrogen atoms were included using a riding model. A coordinated triflate (CF<sub>3</sub>SO<sub>3</sub>) was found to be disordered and modeled as a two part disorder (9:1). Least-squares analysis yielded  $wR2 = 0.0942$  and  $Goof = 1.045$  for 9046 variables refined against 385 data (0.70 Å),  $R1 = 0.0403$  for those 7284 data with  $I > 2.0\sigma(I)$ .

**X-ray Data Collection, Structure Solution and Refinement for [Nd(crypt)(DMF)<sub>2</sub>][OTf]<sub>3</sub>, 25-Nd.** A colorless crystal of approximate dimensions 0.127 x 0.151 x 0.285 mm was mounted in a cryoloop and transferred to a Bruker SMART APEX II diffractometer. The APEX2<sup>1</sup> program package was used to determine the unit-cell parameters and for data collection (30 sec/frame scan time for a sphere of diffraction data). The raw frame data was processed using SAINT<sup>2</sup> and SADABS<sup>3</sup> to yield the reflection data file. Subsequent

calculations were carried out using the SHELXTL<sup>4</sup> program. There were no systematic absences nor any diffraction symmetry other than the Friedel condition. The centrosymmetric triclinic space group  $P\bar{1}$  was assigned and later determined to be correct. The structure was solved by dual space methods and refined on  $F^2$  by full-matrix least-squares techniques. The analytical scattering factors<sup>5</sup> for neutral atoms were used throughout the analysis. Hydrogen atoms were included using a riding model. Least-squares analysis yielded  $wR2 = 0.1219$  and  $Goof = 1.000$  for 601 variables refined against 10765 data ( $0.75 \text{ \AA}$ ),  $R1 = 0.0475$  for those 9360 data with  $I > 2.0\sigma(I)$ .

## References

- (1) Burns, J. H. Crystal and molecular structure of a cryptate complex of samarium:  $C_{18}H_{36}O_6N_2Sm_2(NO_3)_6 \cdot H_2O$ . *Inorg. Chem.* **1979**, *18*, 3044-3047.
- (2) Benetollo, F.; Bombieri, G.; Cassol, A.; De Paoli, G.; Legendziewicz, J. Coordination chemistry of lanthanides with cryptands. An X-ray and spectroscopic study of the complex  $Nd_2(NO_3)_6 [C_{18}H_{36}O_6N_2] \cdot H_2O$ . *Inorg. Chim. Acta* **1985**, *110*, 7-13.
- (3) Yang, G.; Liu, S.; Jin, Z. Coordination chemistry and structure characterization of  $C_{18}H_{36}O_6N_2Eu_2(NO_3)_6 \cdot H_2O$ . *Inorg. Chim. Acta* **1987**, *131*, 125-128.
- (4) Mao, J.; Jin, Z. Synthesis and structure characterization of lanthanum [2,2,2]cryptates,  $[LaCl[2,2,2](H_2O)]Cl_2 \cdot H_2O$  and  $[La(CF_3SO_3)[2,2,2](DMF)](CF_3SO_3)_2$ . *Polyhedron* **1994**, *13*, 319-323.
- (5) Gamage, N.-D. H.; Mei, Y.; Garcia, J.; Allen, M. J. Oxidatively Stable, Aqueous Europium(II) Complexes through Steric and Electronic Manipulation of Cryptand Coordination Chemistry. *Angew. Chem. Int. Ed.* **2010**, *49*, 8923-8925.
- (6) Lenora, C. U.; Carniato, F.; Shen, Y.; Latif, Z.; Haacke, E. M.; Martin, P. D.; Botta, M.; Allen, M. J. Structural Features of Europium(II)-Containing Cryptates That Influence Relaxivity. *Chem. Eur. J.* **2017**, *23*, 15404-15414.
- (7) Ekanger, L. A.; Polin, L. A.; Shen, Y.; Haacke, E. M.; Martin, P. D.; Allen, M. J. A EuII-Containing Cryptate as a Redox Sensor in Magnetic Resonance Imaging of Living Tissue. *Angew. Chem. Int. Ed.* **2015**, *54*, 14398-14401.

- (8) Huh, D. N.; Ziller, J. W.; Evans, W. J. Facile Encapsulation of Ln(II) Ions into Cryptate Complexes from  $\text{LnI}_2(\text{THF})_2$  Precursors (Ln = Sm, Eu, Yb). *Inorg. Chem.* **2019**, *58*, 9613-9617.
- (9) Huh, D. N.; Kotyk, C. M.; Gembicky, M.; Rheingold, A. L.; Ziller, J. W.; Evans, W. J. Synthesis of rare-earth-metal-in-cryptand dications,  $[\text{Ln}(2.2.2\text{-cryptand})]^{2+}$ , from  $\text{Sm}^{2+}$ ,  $\text{Eu}^{2+}$ , and  $\text{Yb}^{2+}$  silyl metallocenes  $(\text{C}_5\text{H}_4\text{SiMe}_3)_2\text{Ln}(\text{THF})_2$ . *Chem. Commun.* **2017**, *53*, 8664-8666.
- (10) Huh, D. N.; Windorff, C. J.; Ziller, J. W.; Evans, W. J. Synthesis of uranium-in-cryptand complexes. *Chem. Commun.* **2018**, *54*, 10272-10275.
- (11) Yee, E. L.; Gansow, O. A.; Weaver, M. J. Electrochemical studies of europium and ytterbium cryptate formation in aqueous solution. Effects of varying the metal oxidation state upon cryptate thermodynamics and kinetics. *J. Am. Chem. Soc.* **1980**, *102*, 2278-2285.
- (12) Evans, W. J. Tutorial on the Role of Cyclopentadienyl Ligands in the Discovery of Molecular Complexes of the Rare-Earth and Actinide Metals in New Oxidation States. *Organometallics* **2016**, *35*, 3088-3100.
- (13) Marsh, M. L.; White, F. D.; Meeker, D. S.; McKinley, C. D.; Dan, D.; Van Alstine, C.; Poe, T. N.; Gray, D. L.; Hobart, D. E.; Albrecht-Schmitt, T. E. Electrochemical Studies of Selected Lanthanide and Californium Cryptates. *Inorg. Chem.* **2019**, *58*, 9602-9612.
- (14) MacDonald, M. R.; Bates, J. E.; Ziller, J. W.; Furche, F.; Evans, W. J. Completing the Series of +2 Ions for the Lanthanide Elements: Synthesis of Molecular Complexes of  $\text{Pr}^{2+}$ ,  $\text{Gd}^{2+}$ ,  $\text{Tb}^{2+}$ , and  $\text{Lu}^{2+}$ . *J. Am. Chem. Soc.* **2013**, *135*, 9857-9868.
- (15) MacDonald, M. R.; Bates, J. E.; Fieser, M. E.; Ziller, J. W.; Furche, F.; Evans, W. J. Expanding Rare-Earth Oxidation State Chemistry to Molecular Complexes of Holmium(II) and Erbium(II). *J. Am. Chem. Soc.* **2012**, *134*, 8420-8423.
- (16) Fieser, M. E.; MacDonald, M. R.; Krull, B. T.; Bates, J. E.; Ziller, J. W.; Furche, F.; Evans, W. J. Structural, Spectroscopic, and Theoretical Comparison of Traditional vs Recently Discovered  $\text{Ln}^{2+}$  Ions in the  $[\text{K}(2.2.2\text{-cryptand})][(\text{C}_5\text{H}_4\text{SiMe}_3)_3\text{Ln}]$  Complexes: The Variable Nature of  $\text{Dy}^{2+}$  and  $\text{Nd}^{2+}$ . *J. Am. Chem. Soc.* **2015**, *137*, 369-382.
- (17) Fieser, M. E.; Palumbo, C. T.; La Pierre, H. S.; Halter, D. P.; Voora, V. K.; Ziller, J. W.; Furche, F.; Meyer, K.; Evans, W. J. Comparisons of lanthanide/actinide +2 ions in a tris(aryloxy)arene coordination environment. *Chem. Sci.* **2017**, *8*, 7424-7433.
- (18) Palumbo, C. T.; Darago, L. E.; Windorff, C. J.; Ziller, J. W.; Evans, W. J. Trimethylsilyl versus Bis(trimethylsilyl) Substitution in Tris(cyclopentadienyl) Complexes of La, Ce, and Pr: Comparison of Structure, Magnetic Properties, and Reactivity. *Organometallics* **2018**, *37*, 900-905.
- (19) Schäfer, A.; Horn, H.; Ahlrichs, R. Fully optimized contracted Gaussian basis sets for atoms Li to Kr. *J. Chem. Phys.* **1992**, *97*, 2571-2577.

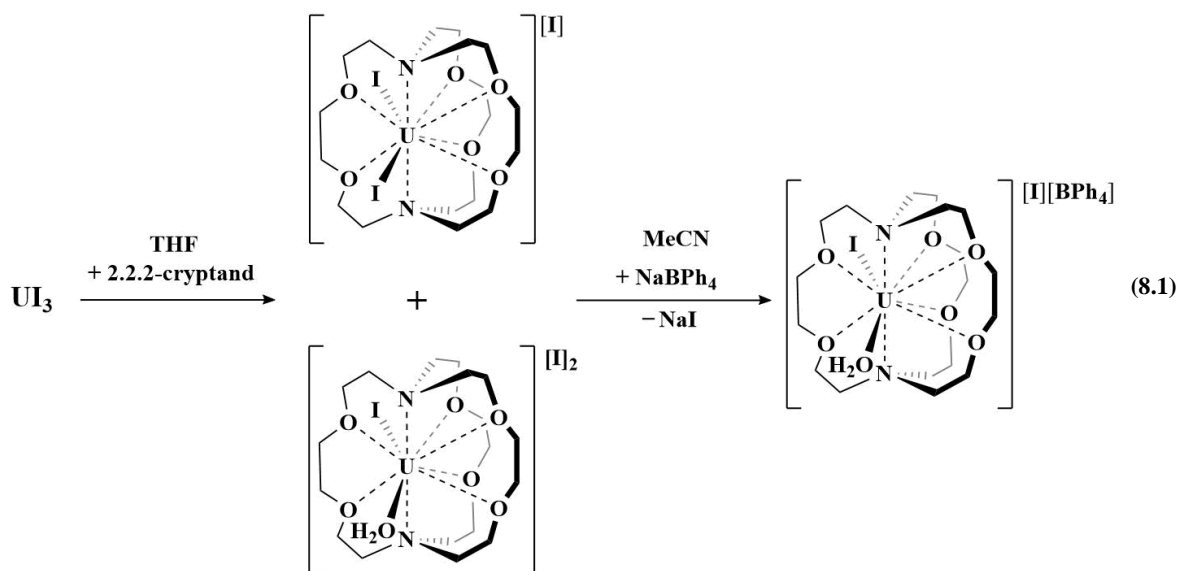
- (20) Dolg, M.; Stoll, H.; Savin, A.; Preuss, H. Energy-adjusted pseudopotentials for the rare earth elements. *Theor. Chim. Acta* **1989**, *75*, 173-194.
- (21) Weigend, F. Accurate Coulomb-fitting basis sets for H to Rn. *Phys. Chem. Chem. Phys.*, **2006**, *9*, 1057-1065.
- (22) Tao, J.; Perdew, J. P.; Staroverov, V. N.; Scuseria, G. E. Climbing the Density Functional Ladder: Nonempirical Meta--Generalized Gradient Approximation Designed for Molecules and Solids. *Phys. Rev. Lett.* **2003**, *91*, 146401.
- (23) Schäfer, A.; Klamt, A.; Sattel, D.; Lohrenz, J. C. W.; Eckert, F. COSMO Implementation in TURBOMOLE: Extension of an efficient quantum chemical code towards liquid systems. *Phys. Chem. Chem. Phys.*, **2000**, *2*, 2187-2193.
- (24) CRC Handbook of Chemistry and Physics, 81st ed. Lide, D. R., Ed.; CRC Press: Boca Raton, FL, 2008; Chapter 8, p 136.
- (25) Furche, F.; Ahlrichs, R.; Hättig, C.; Klopper, W.; Sierka, M.; Weigend, F. Turbomole. *WIREs Comput. Mol. Sci.* **2014**, *4* (2), 91– 100

## CHAPTER 8

### Synthesis and Electrochemical Analysis of Complexes of U(III) Encapsulated in 2.2.2-Cryptand in Acetonitrile and Dimethylformamide

#### Introduction

The 2.2.2-cryptand ligand (crypt) was studied extensively with alkali and alkaline earth metals<sup>1, 2</sup> and the number of examples with lanthanides in the literature was increasing.<sup>3, 4 5-13</sup> However, only a single report of crystalline actinide-in-crypt complexes was in the literature as described in Chapter 5.<sup>13</sup> This was particularly surprising since solution studies of actinides and crypt have been in the literature for many years.<sup>14-17</sup> As described in Chapter 5, the crystalline examples  $[\text{U}(\text{crypt})\text{I}_2]\text{I}$ ,  $[\text{U}(\text{crypt})\text{I}(\text{OH}_2)]\text{I}_2$ , and  $[\text{U}(\text{crypt})\text{I}(\text{OH}_2)]\text{I}[\text{BPh}_4]$ ,<sup>13</sup> eq 8.1, all involve



uranium in the +3 oxidation state. In two of these examples, a water molecule is coordinated to the U(III) center which suggests some the stability of U(III) in this coordination environment toward water. Although six previous examples of U(III) water adducts have been reported in the

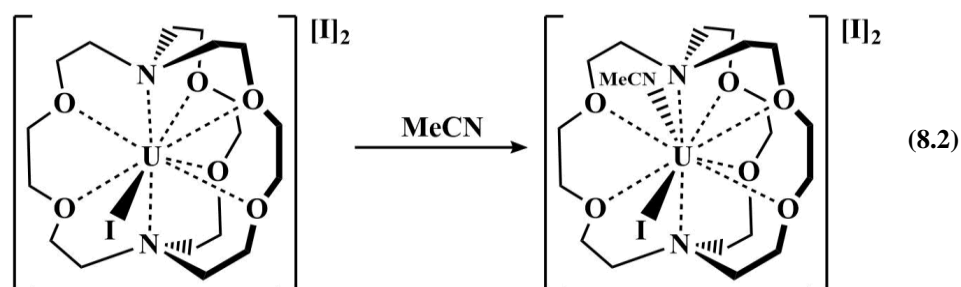


literature,<sup>18-21</sup> in all cases the metal complexes were found to undergo decomposition from hours to 2 days even as solids. In contrast, the crystalline water-solvated U(III)-in-crypt complexes  $[\text{U}(\text{crypt})\text{I}(\text{OH}_2)][\text{I}]_2$ , and  $[\text{U}(\text{crypt})\text{I}(\text{OH}_2)][\text{I}][\text{BPh}_4]$ , appear to be stable indefinitely under an inert atmosphere.

Efforts were made to probe this stabilization of U(III) by crypt through electrochemical analysis of the U(IV)/U(III) couple in the absence and presence of water through a collaboration with Jeffery M. Barlow in the laboratory of Prof. Jenny Yang. These results reinforce the early observations and show how actinides in lower oxidation states can be stabilized in the presence of water. As part of this study, additional examples of a crystalline water-solvated U(III) complex were identified.

## Results and Discussion

**Isolation of U(III)-in-Crypt.** Dissolving  $[\text{U}(\text{crypt})\text{I}_2]\text{I}$  in MeCN generates green-yellow solutions. Crystallographic-characterization of the reaction product revealed the presence of  $[\text{U}(\text{crypt})(\text{MeCN})\text{I}][\text{I}]_2$ , **26-U**, eq 8.4, Figure 8.2. In this U(III)-in-crypt complex, one MeCN and one iodide are coordinated to the metal center. The U–I bond distance is consistent with other previously reported ten-coordinate U(III)-in-crypt complexes, Table 8.1. The U(III)–N(MeCN)



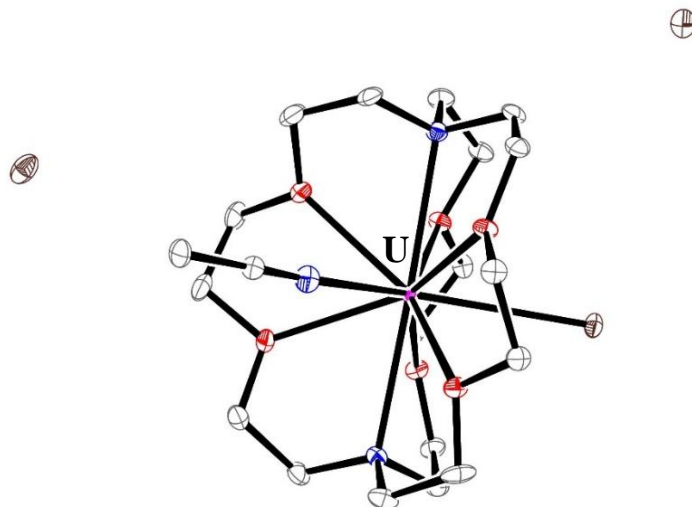


**Figure 8.1.** ORTEP representation of  $[\text{U}(\text{crypt})(\text{MeCN})\text{I}][\text{I}]_2$ , **26-U**, with thermal ellipsoids drawn at the 50% probability level. Hydrogen atoms were omitted for clarity.

**Table 8.1.** U(III)-in-crypt metrical parameters of **26-U**, **27-U**, **28-U**,  $[\text{U}(\text{crypt})\text{I}_2]\text{I}$  **14-U**,  $[\text{U}(\text{crypt})\text{I}(\text{OH}_2)][\text{I}]_2$  **16-U**, and  $[\text{U}(\text{crypt})(\text{OH}_2)\text{I}][\text{I}][\text{BPh}_4]$  **17-U**.

	<b>26-U</b>	<b>27-U</b>	<b>28-U</b>	<b>14-U</b> <sup>13</sup> [U(crypt)I <sub>2</sub> ][I]	<b>16-U</b> <sup>13</sup> [U(crypt)I(OH <sub>2</sub> )] <sub>2</sub>	<b>17-U</b> <sup>13</sup> [U(crypt)(OH <sub>2</sub> )I][I][BPh <sub>4</sub> ]
U–I	3.2594(7)			3.3106(5)- 3.3292(6)	3.2563(7)	3.2845(6)
U–N(crypt)	2.797(3)- 2.840(3)	2.746(3)- 2.817(2)	2.757(6)- 2.768(5)	2.803(3)- 2.853(3)	2.80(1)- 2.814(8)	2.781(3)- 2.822(3)
U–O(crypt)	2.597(2)- 2.679(2)	2.595(2)- 2.677(2)	2.593(5)- 2.778(6)	2.568(2)- 2.697(2)	2.602(9)- 2.683(7)	2.606(3)- 2.659(4)
U–O(OH <sub>2</sub> )		2.517(3)	2.518(6)		2.549(7)	2.503(3)

distance in **26-U** is 2.647(3) Å which is similar to other previously reported U(III)–N(MeCN) reported distances:  $[\text{U}(\text{9S3})\text{I}_3(\text{MeCN})_2]$  (9S3 = 1,4,7-trithiacyclononane),<sup>22</sup>  $[\text{U}(\text{MeCN})_9][\text{I}]_3$ ,<sup>23</sup>  $[\text{U}(\text{tpza})\text{I}_3(\text{MeCN})]$  (tpza = tris[(2-pyrazinyl)methyl]amine),<sup>24</sup> and  $[\text{U}(\text{ArO}_3)\text{tacn}]\text{U}(\text{MeCN})]$  (tacn = 1,4,7-triazacyclononane).<sup>25</sup>

Other attempts to crystallize  $[\text{U}(\text{crypt})\text{I}_2]\text{I}$  from MeCN yielded  $[\text{U}(\text{crypt})(\text{OH}_2)\text{I}][\text{I}]_2$ , **14-U**, a previously reported structure,<sup>13</sup> and  $[\text{U}(\text{crypt})(\text{OH}_2)_2][\text{I}]_3$ , **27-U**, Figure 8.2, where the U(III)-in-crypt complex is formally a trication. The U–O(OH<sub>2</sub>) distances in **28-U** are similar to other

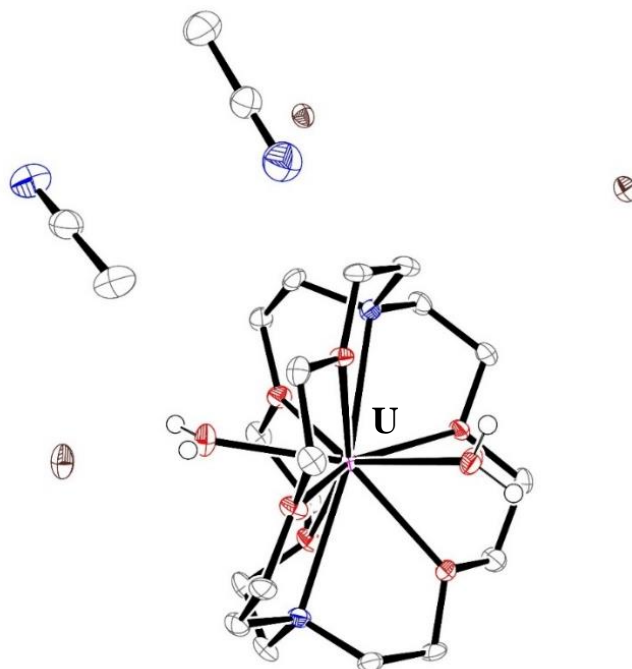


**Figure 8.2.** ORTEP representation of  $[U(\text{crypt})(\text{OH}_2)_2][\text{I}]_3$ , **27-U**, with thermal ellipsoids drawn at the 50% probability level. Hydrogen atoms were omitted for clarity except for water.

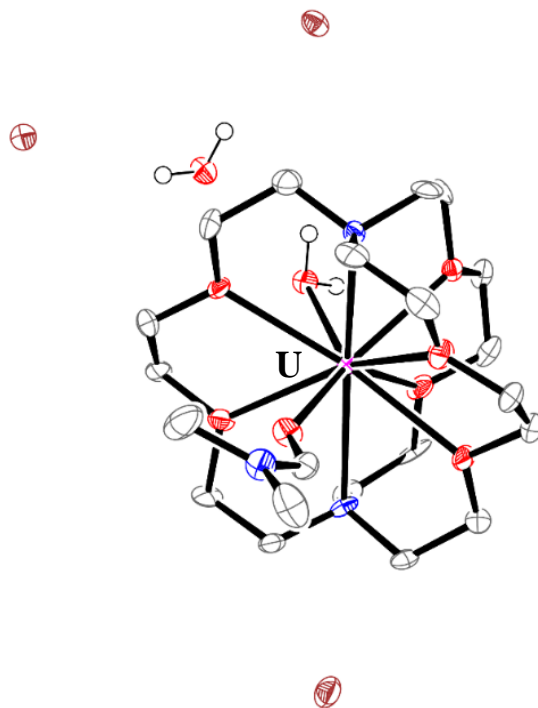


**Figure 8.3.** ORTEP representation of  $[U(\text{crypt})(\text{DMF})(\text{OH}_2)][\text{I}]_3$ , **28-U**, and thermal ellipsoids drawn at the 50% probability level. Hydrogen atoms were omitted for clarity except for water.

previously reported U(III)–O(OH<sub>2</sub>) bond distances as previously described in Chapter 5.

Dissolving [U(crypt)I<sub>2</sub>]I in DMF yields crystals of [U(crypt)(DMF)(OH<sub>2</sub>)]I<sub>3</sub>, **28-U**, Figure 8.3. The U–O(OH<sub>2</sub>) distances in are consistent with a U(III) and similar to previously reported U(III)–O(OH<sub>2</sub>) distances, Table 8.1.<sup>18-21</sup> Other f element cryptate complexes containing coordinated DMF have also been reported: [La(crypt)(OTf)(DMF)]I<sub>2</sub>,<sup>7</sup> [Ln(crypt)(DMF)<sub>2</sub>]I<sub>2</sub> (Ln = Sm, Eu),<sup>11</sup> [Ln(crypt)(DMF)<sub>2</sub>][BPh<sub>4</sub>]<sub>2</sub> (Ln = Sm, Eu),<sup>11</sup> and [Yb(crypt)(DMF)]I<sub>2</sub>.<sup>11</sup>

**Electrochemistry.** Electrochemical analysis of [U(crypt)I<sub>2</sub>]I, was performed by Jeffery M. Barlow in the laboratory of Prof. Jenny Y. Yang. The cyclic voltammograms of [U(crypt)I<sub>2</sub>]I in DMF supported with tetrabutylammonium hexafluorophosphate [<sup>n</sup>Bu<sub>4</sub>N][PF<sub>6</sub>] electrolyte are shown in Figure 8.4. Two iodide oxidation events are present in both DMF solutions of

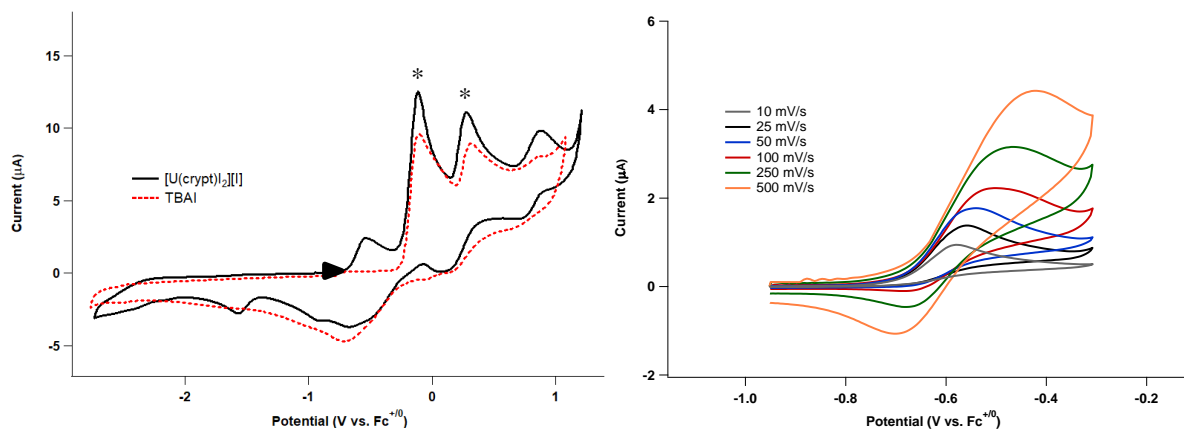


**Figure 8.4.** Comparison of [U(crypt)I<sub>2</sub>]I in DMF and tetrabutylammonium iodide (TBAI) showing that the two oxidations (\*) arise from free iodide in solution (left). Variable scan rates of [U(crypt)I<sub>2</sub>]I in DMF (500 mM TBAI) of the first oxidation event U(III) to U(IV) (E<sub>pa1</sub>) from 10 to 500 mV/s scan rates (right).

[U(crypt)I<sub>2</sub>]I and tetrabutylammonium iodide DMF solutions. These oxidation states, denoted with an asterisk (\*), are the iodide (I<sup>-</sup>) oxidation to iodine (I<sub>2</sub>) and the triiodide (I<sub>3</sub><sup>-</sup>) oxidation to I<sub>2</sub>.<sup>26</sup> A U(IV)/U(III) irreversible oxidation is observed at -0.60 V vs Fc<sup>+</sup>/Fc at slow scan rates, however a return peak is observed as the scan rate is increased. The lack of reversibility indicates that the complex may be undergoing a change in geometry or ligand dissociation/substitution upon oxidation. After the basic electrochemistry was established for [U(crypt)I<sub>2</sub>]I in DMF, the solution was titrated with 1 to 500 equivalents of water with scans taken at 100 mV/sec, Figure 8.5.

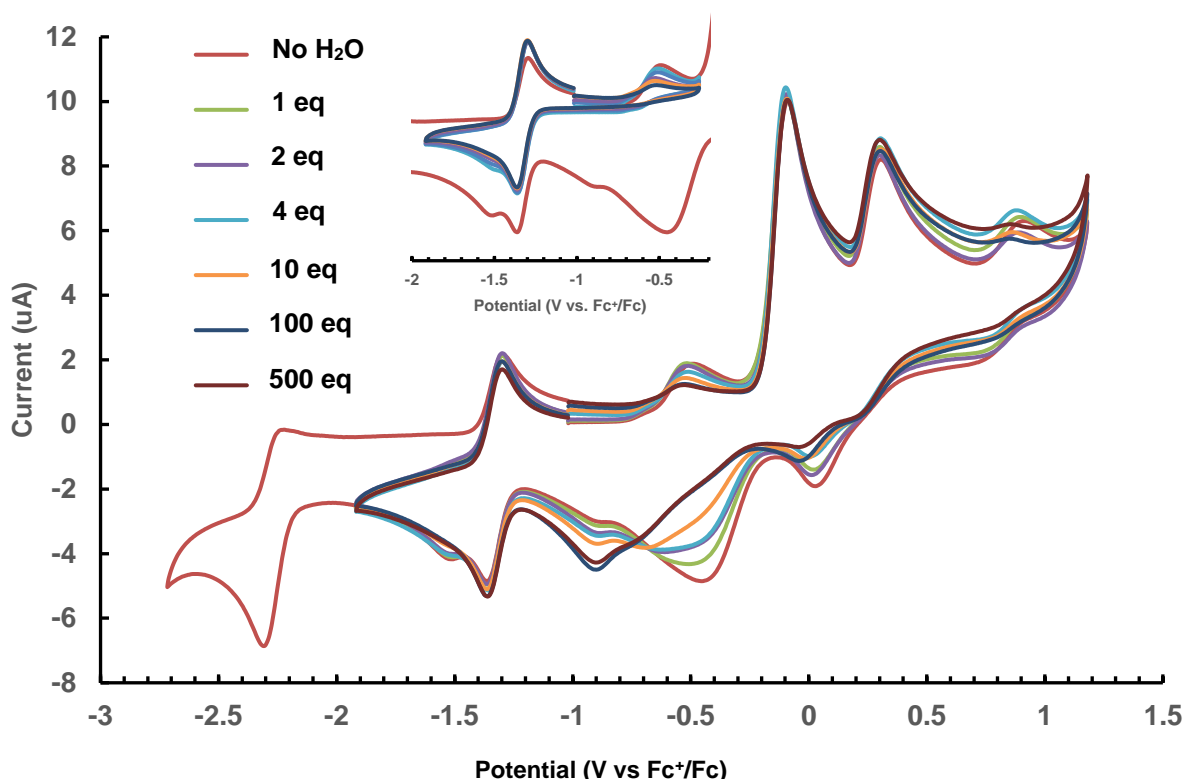


**Figure 8.5.** DMF solution of [U(crypt)I<sub>2</sub>]I titrated with water (full spectrum, top; zoom, inset) scanning anodically. The oxidations centered at  $E_{pa1} = -0.510$  V and  $E_{pa2} = 0.880$  V vs. Fc<sup>+0</sup> both disappear as more equivalents are added, indicating a reaction with water (either binding or reduction).

Cyclic voltammograms of  $[\text{U}(\text{crypt})\text{I}_2]\text{I}$  in MeCN were also conducted. Both DMF and MeCN cyclic voltammograms displayed similar features, *i.e.* iodide oxidation events denoted by asterisks (\*) and U(IV)/U(III) oxidation. However, unlike in DMF, in the MeCN cyclic voltammogram an irreversible U(III)/U(II) reduction wave at  $-1.80\text{ V}$  (vs  $\text{Fc}^+/\text{Fc}$ ) is found, Figure 8.6. Unlike the cyclic voltammograms in DMF, the oxidation event at  $E_{\text{pa}3} = 0.880\text{ V}$  vs.  $\text{Fc}^{+/0}$

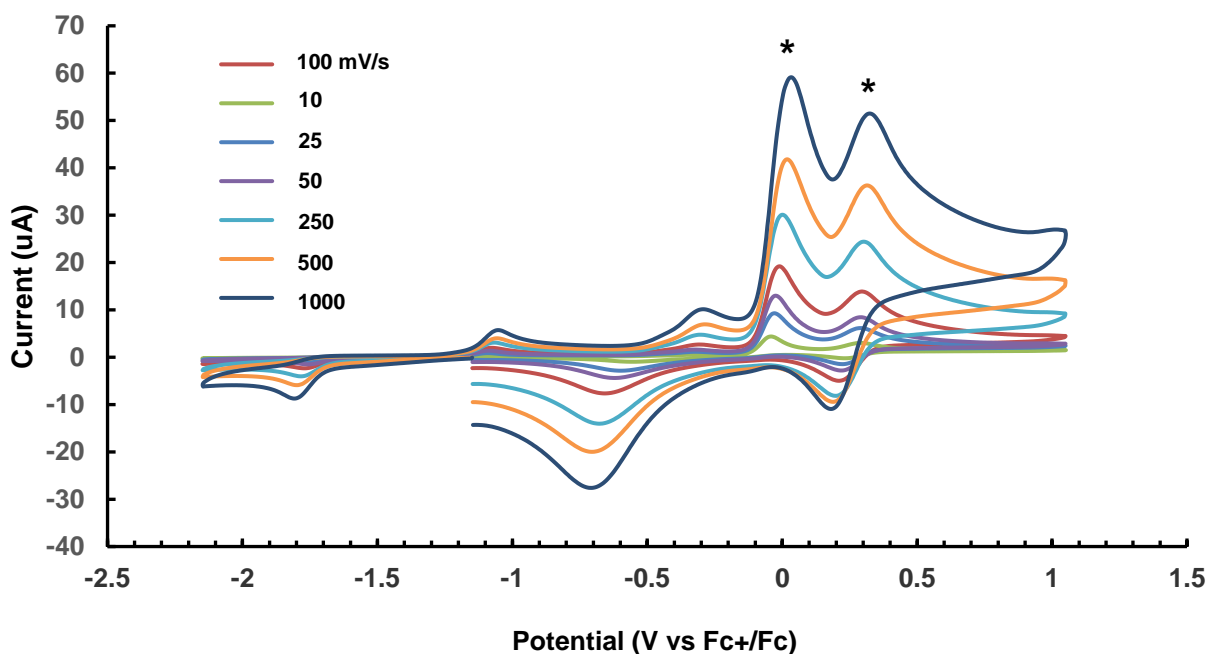


**Figure 8.6.** Variable scan rates of  $[\text{U}(\text{crypt})\text{I}_2]\text{I}$  in MeCN scanning cathodically. Reduction and oxidation are observed at  $E_{\text{pc}1} = -1.78\text{ V}$  and  $E_{\text{pa}1} = -1.12\text{ V}$  (vs.  $\text{Fc}^+/\text{Fc}$ ). Asterisks are denote iodide oxidation.

is no longer present. These events may correspond to U(III/II) reduction and corresponding U(II/III) oxidations. The two events move apart by  $\sim 65\text{ mV}/10$  fold increase in scan rate.

When one equivalent of  $[\text{CoCp}_2][\text{PF}_6]$  is added to the MeCN solution of **1**, the reduction becomes more prominent and becomes reversible, Figure 8.7. Additionally, the U(IV)/U(III)

oxidation is shifted to more negative values (from  $-0.29$  V to  $-0.42$  V vs.  $\text{Fc}^{+/0}$ ). The first iodide

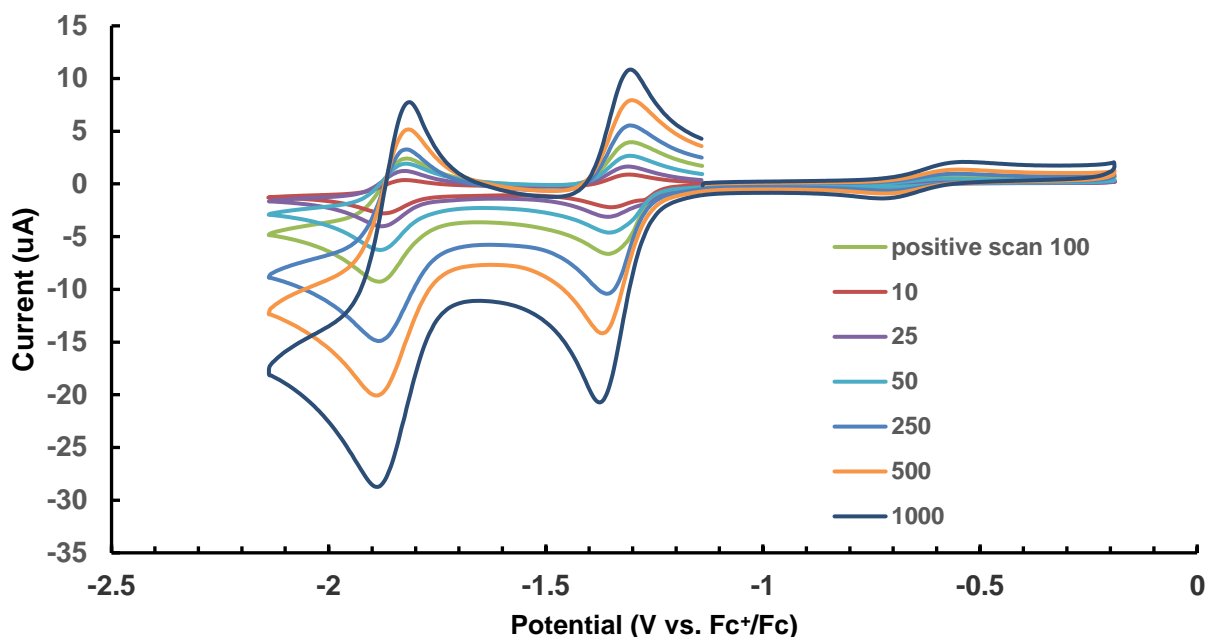


**Figure 8.7.** Variable scan rates of  $[\text{U}(\text{crypt})\text{I}_2]\text{I}$  and  $[\text{CoCp}_2][\text{PF}_6]$  in MeCN scanning cathodically.  $\text{U}(\text{III})/\text{U}(\text{II})$   $E_{1/2} = -1.85$  V vs  $\text{Fc}^+/\text{Fc}$  and  $\text{Co}(\text{III})/\text{Co}(\text{II})$   $E_{1/2} = -1.33$  V vs  $\text{Fc}^+/\text{Fc}$ .

reduction also shifts to more negative potentials, while the reduction at  $E_{\text{pc}2} = -0.64$  V vs.  $\text{Fc}^{+/0}$  is shifted  $\sim 40$  mV positive. Variable scan rates were performed scanning anodically. The  $\text{U}(\text{IV}/\text{III})$  oxidation is much smaller in size and becomes more reversible than when scanning cathodically first. The  $\text{U}(\text{III}/\text{II})$  couple ( $E_{1/2} = -1.85$  V vs  $\text{Fc}^+/\text{Fc}$ ) appears to be fully reversible at all scan rates investigated. It is possible that  $[\text{CoCp}_2]^+$  acts as a redox mediator, allowing oxidation/reduction to occur more easily with the electrode. Additionally, the  $E_{1/2}$  of the  $\text{U}(\text{III})/\text{U}(\text{II})$  redox event is significantly lower than the  $E_{1/2}$  of  $-2.50$  V vs  $\text{Fc}^+/\text{Fc}$  reported for  $[\{(\text{Ad},\text{MeArO})_3\text{-mes}\}\text{U}] \text{U}(\text{III})/\text{U}(\text{II})$  by Meyer and co-workers.<sup>27</sup>

## Conclusion

Additional examples of U(III)-in-crypt complexes have been crystallographically-characterized, two of which are new U(III)-aquo complexes and one of which is a water free [U(crypt)(MeCN)I][I]<sub>2</sub>. These examples of U(III)-in-crypt complexes demonstrate the stability offered by the crypt ligand toward coordinating solvents such as DMF, MeCN, and even water. Formation of these stable U(III) base-adducts expands the scope of solvents that are typically unavailable for highly reducing metal complexes containing low valent f element ions. Electrochemical analyses of these U(III)-in-crypt complexes suggests the U(II) ion could be accessible in DMF and MeCN at more positive potentials than previously reported. In the presence of MeCN and [CoCp<sub>2</sub>][PF<sub>6</sub>], the U(III)/U(II) couple becomes reversible. This could be attributed to [CoCp<sub>2</sub>] acting as an electron-transfer mediator.

## Experimental

All syntheses and manipulations described below were conducted under nitrogen or argon with rigorous exclusion of air and water using glovebox, Schlenk-line, and high-vacuum techniques. [U(crypt)I][I]<sub>2</sub> was prepared using previously published procedures.<sup>13</sup> 2.2.2-Cryptand (4,7,13,16,21,24-hexaoxa-1,10-diazabicyclo[8.8.8]hexacosane, Aldrich) THF and Et<sub>2</sub>O were sparged with UHP argon and dried over columns containing Q-5 and molecular sieves. MeCN and DMF were sparged with UPH argon and dried over molecular sieves for 1 week.

**[U(crypt)(MeCN)I][I]<sub>2</sub>, 26-U.** Addition of MeCN (3 mL) to green [U(crypt)I][I]<sub>2</sub> (100 mg, 0.10 mmol) formed a green-yellow solution. The solution was stirred for 1 h and layered with Et<sub>2</sub>O and placed in a -35 °C freezer. After 1 d, X-ray quality green crystals were isolated.

**[U(crypt)(OH<sub>2</sub>)I][I]<sub>2</sub>, 16-U.** As described for **26-U**, MeCN was added to green [U(crypt)I][I]<sub>2</sub> (100 mg, 0.10 mmol) formed a green-yellow solution. After 1 d, X-ray quality



green crystals were isolated and it was found to have the same unit cell as the previously reported compound.<sup>13</sup>

**[U(crypt)(OH<sub>2</sub>)<sub>2</sub>][I]<sub>3</sub>, 27-U.** As described for **26-U**, MeCN was added to green [U(crypt)I][I]<sub>2</sub> (100 mg, 0.10 mmol) formed a green-yellow solution. After 1 d, X-ray quality green crystals were isolated.

**[U(crypt)(DMF)(OH<sub>2</sub>)][I]<sub>3</sub>, 28-U.** As described for **26-U**, DMF was added to green [U(crypt)I][I]<sub>2</sub> (100 mg, 0.10 mmol) formed a green-yellow solution. After 1 d, X-ray quality green crystals were isolated.

### **Structural Details**

**X-ray Data Collection, Structure Solution and Refinement for [U(crypt)(DMF)(OH<sub>2</sub>)][I]<sub>3</sub>, 28-U.** A green crystal of approximate dimensions 0.044 x 0.063 x 0.069 mm was mounted in a cryoloop and transferred to a Bruker SMART APEX II diffractometer. The APEX2<sup>28</sup> program package was used to determine the unit-cell parameters and for data collection (240 sec/frame scan time for a sphere of diffraction data). The raw frame data was processed using SAINT<sup>29</sup> and SADABS<sup>30</sup> to yield the reflection data file. Subsequent calculations were carried out using the SHELXTL<sup>31</sup> program. The diffraction symmetry was *2/m* and the systematic absences were consistent with the monoclinic space group *P2<sub>1</sub>/n* that was later determined to be correct. The structure was solved by direct methods and refined on F<sup>2</sup> by full-matrix least-squares techniques. The analytical scattering factors<sup>32</sup> for neutral atoms were used throughout the analysis. Hydrogen atoms were included using a riding model. Carbon atom C(14) was disordered and modeled using multiple components and with partial site-occupancy-factors (3:1). There was one molecule of free water present which was hydrogen bonded to both the bound water O(8) and iodine atoms I(1) and I(2). Least-squares analysis yielded wR2 =

0.0736 and Goof = 0.992 for 339 variables refined against 6825 data (0.80 Å), R1 = 0.0432 for those 4915 data with  $I > 2.0\sigma(I)$ .

**X-ray Data Collection, Structure Solution and Refinement for [U(crypt)(OH<sub>2</sub>)<sub>2</sub>][I]<sub>3</sub>, 27-U.** A green crystal of approximate dimensions 0.169 x 0.238 x 0.289 mm was mounted in a cryoloop and transferred to a Bruker SMART APEX II diffractometer. The APEX2<sup>28</sup> program package was used to determine the unit-cell parameters and for data collection (10 sec/frame scan time for a sphere of diffraction data). The raw frame data was processed using SAINT<sup>29</sup> and SADABS<sup>30</sup> to yield the reflection data file. Subsequent calculations were carried out using the SHELXTL<sup>31</sup> program. The diffraction symmetry was  $2/m$  and the systematic absences were consistent with the monoclinic space group  $P2_1/n$  that was later determined to be correct. The structure was solved by dual space methods and refined on  $F^2$  by full-matrix least-squares techniques. The analytical scattering factors<sup>32</sup> for neutral atoms were used throughout the analysis. A disordered solvent molecule (MeCN) was model in 2 parts (85:15). Hydrogen atoms were included using a riding model. Least-squares analysis yielded  $wR2 = 0.494$  and Goof = 1.106 for 347 variables refined against 8499 data (0.74 Å), R1 = 0.0231 for those 8040 data with  $I > 2.0\sigma(I)$ .

**X-ray Data Collection, Structure Solution and Refinement for [U(crypt)(MeCN)I][I]<sub>2</sub>, 26-U.** A brown crystal of approximate dimensions 0.106 x 0.188 x 0.291 mm was mounted in a cryoloop and transferred to a Bruker SMART APEX II diffractometer. The APEX2<sup>28</sup> program package was used to determine the unit-cell parameters and for data collection (30 sec/frame scan time for a sphere of diffraction data). The raw frame data was processed using SAINT<sup>29</sup> and SADABS<sup>30</sup> to yield the reflection data file. Subsequent calculations were carried out using the SHELXTL<sup>31</sup> program. The diffraction symmetry was

*mmm* and the systematic absences were consistent with the orthorhombic space group *Pccn* that was later determined to be correct. The structure was solved by dual space methods and refined on  $F^2$  by full-matrix least-squares techniques. The analytical scattering factors<sup>32</sup> for neutral atoms were used throughout the analysis. Hydrogen atoms were included using a riding model. One non-coordinated iodide was disordered and was modeled as a two-part (1:1) disorder. Least-squares analysis yielded  $wR2 = 0.0522$  and  $Goof = 1.021$  for 300 variables refined against 8990 data (0.70 Å),  $R1 = 0.0265$  for those 7708 data with  $I > 2.0\sigma(I)$ .

## References

- (1) Dietrich, B.; Lehn, J. M.; Sauvage, J. P.; Blanzat, J. Cryptates—X: Syntheses et propriétés physiques de systèmes diaza-polyoxa-macrobicycliques. *Tetrahedron* **1973**, *29*, 1629-1645.
- (2) Dietrich, B.; Lehn, J. M.; Sauvage, J. P. Cryptates—XI: Complexes macrobicycliques, formation, structure, propriétés. *Tetrahedron* **1973**, *29*, 1647-1658.
- (3) Burns, J. H. Crystal and molecular structure of a cryptate complex of samarium:  $C_{18}H_{36}O_6N_2Sm_2(NO_3)_6 \cdot H_2O$ . *Inorg. Chem.* **1979**, *18*, 3044-3047.
- (4) Benetollo, F.; Bombieri, G.; Cassol, A.; De Paoli, G.; Legendziewicz, J. Coordination chemistry of lanthanides with cryptands. An X-ray and spectroscopic study of the complex  $Nd_2(NO_3)_6[C_{18}H_{36}O_6N_2] \cdot H_2O$ . *Inorg. Chim. Acta* **1985**, *110*, 7-13.
- (5) Yang, G.; Liu, S.; Jin, Z. Coordination chemistry and structure characterization of  $C_{18}H_{36}O_6N_2Eu_2(NO_3)_6 \cdot H_2O$ . *Inorg. Chim. Acta* **1987**, *131*, 125-128.
- (6) Yee, E. L.; Gansow, O. A.; Weaver, M. J. Electrochemical studies of europium and ytterbium cryptate formation in aqueous solution. Effects of varying the metal oxidation state upon cryptate thermodynamics and kinetics. *J. Am. Chem. Soc.* **1980**, *102*, 2278-2285.
- (7) Mao, J.; Jin, Z. Synthesis and structure characterization of lanthanum [2,2,2]cryptates,  $[LaCl[2,2,2](H_2O)]Cl_2 \cdot H_2O$  and  $[La(CF_3SO_3)[2,2,2](DMF)](CF_3SO_3)_2$ . *Polyhedron* **1994**, *13*, 319-323.
- (8) Gamage, N.-D. H.; Mei, Y.; Garcia, J.; Allen, M. J. Oxidatively Stable, Aqueous Europium(II) Complexes through Steric and Electronic Manipulation of Cryptand Coordination Chemistry. *Angew. Chem. Int. Ed.* **2010**, *49*, 8923-8925.
- (9) Lenora, C. U.; Carniato, F.; Shen, Y.; Latif, Z.; Haacke, E. M.; Martin, P. D.; Botta, M.; Allen, M. J. Structural Features of Europium(II)-Containing Cryptates That Influence Relaxivity. *Chem. Eur. J.* **2017**, *23*, 15404-15414.

- (10) Ekanger, L. A.; Polin, L. A.; Shen, Y.; Haacke, E. M.; Martin, P. D.; Allen, M. J. A Eu<sup>II</sup>-Containing Cryptate as a Redox Sensor in Magnetic Resonance Imaging of Living Tissue. *Angew. Chem. Int. Ed.* **2015**, *54*, 14398-14401.
- (11) Huh, D. N.; Ziller, J. W.; Evans, W. J. Facile Encapsulation of Ln(II) Ions into Cryptate Complexes from LnI<sub>2</sub>(THF)<sub>2</sub> Precursors (Ln = Sm, Eu, Yb). *Inorg. Chem.* **2019**, *58*, 9613-9617.
- (12) Huh, D. N.; Kotyk, C. M.; Gembicky, M.; Rheingold, A. L.; Ziller, J. W.; Evans, W. J. Synthesis of rare-earth-metal-in-cryptand dications, [Ln(2.2.2-cryptand)]<sup>2+</sup>, from Sm<sup>2+</sup>, Eu<sup>2+</sup>, and Yb<sup>2+</sup> silyl metallocenes (C<sub>5</sub>H<sub>4</sub>SiMe<sub>3</sub>)<sub>2</sub>Ln(THF)<sub>2</sub>. *Chem. Commun.* **2017**, *53*, 8664-8666.
- (13) Huh, D. N.; Windorff, C. J.; Ziller, J. W.; Evans, W. J. Synthesis of uranium-in-cryptand complexes. *Chem. Commun.* **2018**, *54*, 10272-10275.
- (14) Bullock, J. I.; Storey, A. E. Chemistry of the trivalent actinoids. Part 6 [1]. Uranium(III) complexes with a variety of neutral, oxygen-donor ligands and hexacyanoferrate(II). *Inorg. Chim. Acta* **1979**, *36*, L399-L400.
- (15) Brighli, M.; Fux, P.; Lagrange, J.; Lagrange, P. Discussion on the complexing ability of the uranyl ion with several crown ethers and cryptands in water and in propylene carbonate. *Inorg. Chem.* **1985**, *24*, 80-84.
- (16) Spiess, B.; Arnaud-Neu, F.; Schwing-Weill, M. J. Behaviour of uranium(VI) with some cryptands in aqueous solution. *Inorg. Nucl. Chem. Lett.* **1979**, *15*, 13-16.
- (17) Costes, R. M.; Folcher, G.; Plurien, P.; Rigny, P. New uranium and thorium cryptates. *Inorg. Nul. Chem. Lett.* **1976**, *12*, 491-499.
- (18) Mech, A.; Karbowski, M.; Lis, T.; Drożdżyński, J. Monomeric, dimeric and polymeric structure of the uranium trichloride hydrates. *Polyhedron* **2006**, *25*, 2083-2092.
- (19) Apostolidis, C.; Schimmelpfennig, B.; Magnani, N.; Lindqvist-Reis, P.; Walter, O.; Sykora, R.; Morgenstern, A.; Colineau, E.; Caciuffo, R.; Klenze, R.; Haire, R. G.; Rebizant, J.; Bruchertseifer, F.; Fanghänel, T. [An(H<sub>2</sub>O)<sub>9</sub>](CF<sub>3</sub>S<sub>3</sub>O<sub>3</sub>)<sub>3</sub> (An=U-Cm, Cf): Exploring Their Stability, Structural Chemistry, and Magnetic Behavior by Experiment and Theory. *Angew. Chem. Int. Ed.* **2010**, *49*, 6343-6347.
- (20) Zych, E.; Starynowicz, P.; Lis, T.; Drożdżyński, J. Crystal structure and spectroscopic properties of (NH<sub>4</sub>[UBr<sub>2</sub>(CH<sub>3</sub>CN)<sub>2</sub>(H<sub>2</sub>O)<sub>5</sub>]Br<sub>2</sub>). *Polyhedron* **1993**, *12*, 1661-1667.
- (21) Bullock, J. I.; Ladd, M. F. C.; Povey, D. C.; Storey, A. E. The Chemistry of the trivalent actinoids. Part 7 [1]. Crystal structure analysis of [NH<sub>4</sub>]U[SO<sub>4</sub>]<sub>2</sub>·4H<sub>2</sub>O and comments on the structure of U<sub>2</sub>[SO<sub>4</sub>]<sub>3</sub>·9H<sub>2</sub>O. *Inorg. Chim. Acta* **1980**, *43*, 101-108.

- (22) Karmazin, L.; Mazzanti, M.; Pécaut, J. Unique crown thioether complexes of f elements: the crystal structure of U(III) and La(III) complexes of 1,4,7-trithiacyclononane. *Chem. Commun.* **2002**, 654-655.
- (23) Enriquez, A. E.; Matonic, J. H.; Scott, B. L.; Neu, M. P. Preparation and structures of homoleptic Pu(III) and U(III) acetonitrile salts. *Chem. Commun.* **2003**, 1892-1893.
- (24) Mazzanti, M.; Wietzke, R.; Pécaut, J.; Latour, J.-M.; Maldivi, P.; Remy, M. Structural and Density Functional Studies of Uranium(III) and Lanthanum(III) Complexes with a Neutral Tripodal N-Donor Ligand Suggesting the Presence of a U–N Back-Bonding Interaction. *Inorg. Chem.* **2002**, *41*, 2389-2399.
- (25) Castro-Rodriguez, I.; Olsen, K.; Gantzel, P.; Meyer, K. Uranium Tris-aryloxide Derivatives Supported by Triazacyclononane: Engendering a Reactive Uranium(III) Center with a Single Pocket for Reactivity. *J. Am. Chem. Soc.* **2003**, *125*, 4565-4571.
- (26) Bentley, C. L.; Bond, A. M.; Hollenkamp, A. F.; Mahon, P. J.; Zhang, J. Voltammetric Determination of the Iodide/Iodine Formal Potential and Triiodide Stability Constant in Conventional and Ionic Liquid Media. *J. Phys. Chem. C* **2015**, *119*, 22392-22403.
- (27) La Pierre, H. S.; Kameo, H.; Halter, D. P.; Heinemann, F. W.; Meyer, K. Coordination and Redox Isomerization in the Reduction of a Uranium(III) Monoarene Complex. *Angew. Chem. Int. Ed.* **2014**, *53*, 7154-7157.
- (28) APEX2 Version 2014.11-0, Bruker AXS, Inc.; Madison, WI 2014.
- (29) SAINT Version 8.34a, Bruker AXS, Inc.; Madison, WI 2013.
- (30) Sheldrick, G. M. SADABS, Version 2014/5, Bruker AXS, Inc.; Madison, WI 2014.
- (31) Sheldrick, G. M. SHELXTL, Version 2014/7, Bruker AXS, Inc.; Madison, WI 2014.
- (32) International Tables for Crystallography 1992, Vol. C., Dordrecht: Kluwer Academic Publishers.

## CHAPTER 9

### Isolation of a Square Planar Th(III) Complex:

#### Synthesis and Structure of $[\text{Th}(\text{OC}_6\text{H}_2^t\text{Bu}_2\text{-2,6-Me-4})_4]^{1-}$

#### Introduction\*

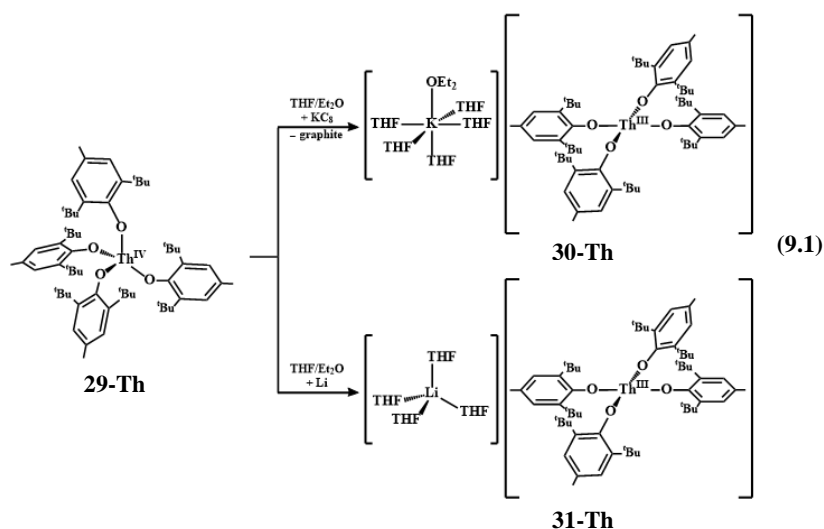
Although Th(IV) *alkoxide* complexes were synthesized in the 1950s by Bradley and coworkers,<sup>1-4</sup> it was not until the 1980s that Th(IV) *aryloxide* complexes were reported by Lappert.<sup>5, 6</sup> In 1992, Clark and Sattelberger isolated the first homoleptic aryloxide Th(IV) complex,  $\text{Th}(\text{OC}_6\text{H}_3^t\text{Bu}_2\text{-2,6})_4$ , which had the expected tetrahedral geometry.<sup>7</sup>

In contrast, neither alkoxides nor aryloxides of *Th(III)* had been reported before the research in this Chapter was done. Crystallographically-characterizable Th(III) complexes are rare in general and most contain cyclopentadienyl ancillary ligands. There were only ten structurally-characterized examples at the time of this research:  $[\text{K}(\text{DME})_2]\{\text{Th}[\eta^8\text{-C}_8\text{H}_6(\text{SiMe}_2^t\text{Bu})_2]_2\}$ ,<sup>8</sup>  $[\text{C}_5\text{H}_3(\text{SiMe}_2^t\text{Bu})_2]_3\text{Th}$ ,<sup>9</sup>  $[\text{C}_5\text{H}_3(\text{SiMe}_3)_2]_3\text{Th}$ ,<sup>9</sup>  $(\text{C}_5\text{Me}_5)_2\text{Th}[\text{iPrNC}(\text{Me})\text{N}^i\text{Pr}]$ ,<sup>10</sup>  $(\text{C}_5\text{Me}_4\text{H})_3\text{Th}$ ,<sup>11</sup>  $[\text{K}(\text{18-crown-6})(\text{Et}_2\text{O})][\{\text{C}_5\text{H}_3(\text{SiMe}_3)_2\}_2\text{ThH}_2]_2$ ,<sup>12</sup>  $[\text{K}(\text{18-crown-6})(\text{THF})][(\text{C}_5\text{Me}_5)_2\text{ThH}_2]_2$ ,<sup>12</sup>  $(\text{C}_5\text{Me}_5)_3\text{Th}$ ,<sup>13</sup>  $(\text{C}_5\text{H}_3^t\text{Bu}_2)_3\text{Th}$ ,<sup>14</sup> and  $(\text{C}_5\text{H}_3^t\text{Bu}_2)_2\text{Th}(\mu\text{-H})_3\text{AlC}(\text{SiMe}_3)_3$ .<sup>15</sup> Gambarotta attempted to reduce  $\text{Th}[\text{OC}_6\text{H}_3(\text{Ph})_2\text{-2,6}]_4$  with potassium, but isolated only the Th(IV) hydroxide compound  $[\text{K}(\text{18-crown-6})(\text{THF})_2][\text{Th}(\text{OC}_6\text{H}_3(\text{Ph})_2\text{-2,6})_4(\text{OH})(\text{THF})]$ .<sup>16</sup> The first examples of Th(III) aryloxides and their unusual structure are described in this Chapter.

Treatment of a colorless THF solution of  $\text{Th}^{\text{IV}}(\text{OAr}')_4$  ( $\text{OAr}' = \text{OC}_6\text{H}_2^t\text{Bu}_2\text{-2,6-Me-4}$ ),

\*Portions of this chapter have been published: Huh, D. N.; Roy, S.; Ziller, J. W.; Furche, F.; Evans, W. J. Isolation of a Square Planar Th(III) Complex: Synthesis and Structure of  $[\text{Th}(\text{OC}_6\text{H}_2^t\text{Bu}_2\text{-2,6-Me-4})_4]^{1-}$ . *J. Am. Chem. Soc.*, **2019**, *141*, 12458-12463. DOI: 10.1021/jacs.9b04399

**29-Th**, with  $\text{KC}_8$  at room temperature forms a dark purple solution similar to that of  $(\text{C}_5\text{Me}_4\text{H})_3\text{Th}$ ,<sup>11</sup>  $(\text{C}_5\text{Me}_5)_3\text{Th}$ ,<sup>13</sup> and  $(\text{C}_5\text{Me}_5)_2[\text{iPrNC}(\text{Me})\text{N}^{\text{iPr}}]\text{Th}$ .<sup>10</sup> The product crystallizes from a THF/ $\text{Et}_2\text{O}$  solution forming dark purple crystals that were structurally characterized as  $[\text{K}(\text{THF})_5(\text{Et}_2\text{O})][\text{Th}^{\text{III}}(\text{OAr}')_4]$ , **30-Th**, eq 9.1, Figure 9.1. Treatment of **29-Th** with Li metal did not immediately form a dark solution, but after storage at  $-35\text{ }^\circ\text{C}$  overnight, a purple solution was present. Crystallization from THF/ $\text{Et}_2\text{O}$  yielded  $[\text{Li}(\text{THF})_4][\text{Th}^{\text{III}}(\text{OAr}')_4]$ , **31-Th**, eq 9.1, Figure 9.2, as large, dark purple blocks that had to be cut for X-ray diffraction. Reactions with



cesium also formed a dark purple solution, but attempts to crystallize the reduction product yielded intractable colorless solids.

The  $[\text{Th}^{\text{III}}(\text{OAr}')_4]^{1-}$  anions are the first examples of square planar geometry in f element chemistry. The closest example to this anion is the  $\text{U}^{\text{IV}}[\text{N}(\text{C}_6\text{F}_5)_2]_4$  complex of Schelter.<sup>17</sup> This U(IV) complex has a square planar array of nitrogen donor atoms enforced by additional fluorine-uranium interactions that make it formally 8-coordinate. The U(III) complex,  $\{\text{K}[\text{U}^{\text{III}}(\text{OC}_6\text{H}_2^{\text{tBu}})_4]\}_n$ , synthesized by Arnold, has a tetrahedral array of oxygen donor atoms.<sup>18</sup>

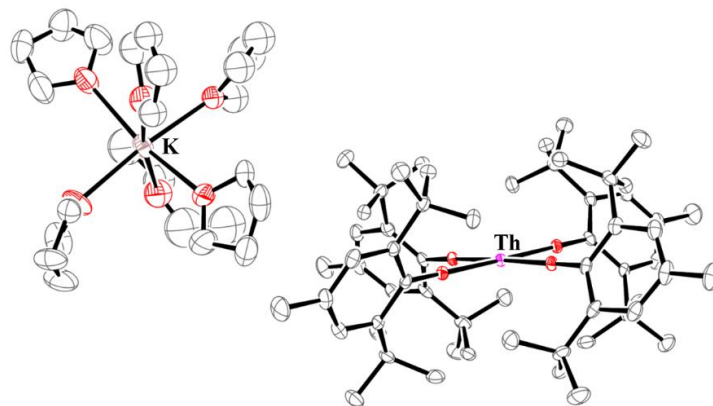


**Figure 9.1.** ORTEP representation of  $[\text{K}(\text{THF})_5(\text{Et}_2\text{O})][\text{Th}(\text{OAr}')_4]$ , **30-Th**, with side-on view and thermal ellipsoids drawn at the 50% probability level. Hydrogen atoms were omitted for clarity.

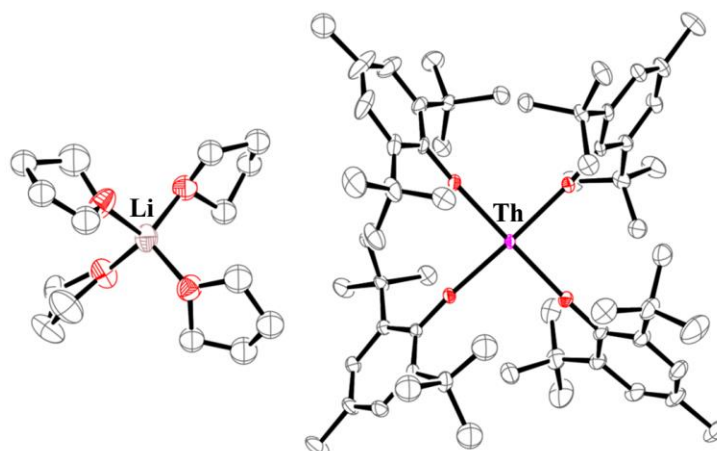


**Figure 9.2.** ORTEP representation of  $[\text{Li}(\text{THF})_4][\text{Th}(\text{OAr}')_4]$ , **31-Th**, with top view and thermal ellipsoids drawn at the 50% probability level. Hydrogen atoms were omitted for clarity.

Table 9.1 summarizes the metrical parameters of **30-Th** and **31-Th**. The  $[\text{K}(\text{THF})_5(\text{Et}_2\text{O})]^{1+}$  and  $[\text{Li}(\text{THF})_4]^{1+}$  counteranions are well separated from the square planar anion. The Th(III) ion and four oxygen donor atoms are coplanar to within  $< 0.05 \text{ \AA}$ . The O–Th–O angles range from  $88.9(1)$  to  $90.5(2)^\circ$  for the cis ligands and from  $175.45(1)$  to  $179.6(2)^\circ$  for the trans ligands. Interestingly, the Th–O–C(ipso) angles in **30-Th** and **31-Th**



range from 173.9(2) to 178.6(4)°. In contrast, the tetrakis(aryloxy) complexes of Th(IV), [Th<sup>IV</sup>(OC<sub>6</sub>H<sub>3</sub><sup>t</sup>Bu<sub>2-2,6</sub>)<sub>4</sub>],<sup>7</sup> **32-Th**, and [Th<sup>IV</sup>(OC<sub>6</sub>H<sub>3</sub>Ph<sub>2-2,6</sub>)<sub>4</sub>],<sup>16</sup> **33-Th**, have bent Th–O–C angles of 153.5(10)° and 152.8(7) to 170.7(7)°, respectively, Table 9.1. The 2.235(3)-2.260(3) Å Th(III)–O distances are larger than the 2.177(7)-2.211(9) Å Th(IV)–O distances in **4** and **5**. It is well established that M–O distances do not necessarily correlate with M–O–C(ipso) angles,<sup>19-21</sup> but this comparison is complicated by the difference in oxidation state.

**Table 9.1.** Selected bond distances (Å) and angles (°) of [K(THF)<sub>5</sub>(Et<sub>2</sub>O)][Th<sup>III</sup>(OAr')<sub>4</sub>], **30-Th**, [Li(THF)<sub>4</sub>][Th<sup>III</sup>(OAr')<sub>4</sub>], **31-Th**, [Th<sup>IV</sup>(OC<sub>6</sub>H<sub>3</sub><sup>t</sup>Bu<sub>2-2,6</sub>)<sub>4</sub>],<sup>7</sup> **32-Th**, and [Th<sup>IV</sup>(OC<sub>6</sub>H<sub>3</sub>Ph<sub>2-2,6</sub>)<sub>4</sub>],<sup>16</sup> **33-Th**.

	<b>30-Th</b>	<b>31-Th</b>	<b>32-Th</b>	<b>33-Th</b>
Th–O	2.235(3)	2.238(2)	2.189(6)	2.177(7)
	2.239(3)	2.244(2)		2.187(10)
	2.257(3)	2.244(2)		2.189(8)
	2.260(3)	2.247(2)		2.211(9)
O–C(ipso)	1.349(6)	1.355(4)	1.341(19)	1.34(1)
	1.355(6)	1.355(4)		1.35(1)
	1.356(6)	1.358(4)		1.354(8)
	1.371(6)	1.358(4)		1.36(1)
Th–O–C(ipso)	174.2(3)	173.9(2)	153.5(10)	152.8(7)
	176.1(3)	174.7(2)		152.8(7)
	178.5(3)	174.7(2)		155.6(7)
	178.6(4)	176.5(2)		170.7(7)
Th–O <sub>4</sub> (plane) <sup>a</sup>	0.004	0.031		
C <sub>6</sub> torsion angle <sup>b</sup>	63.21-65.10	58.46-61.81		

<sup>a</sup>Distance of Th from the plane defined by the four O atoms of the (OAr')<sup>1-</sup> ligands. <sup>b</sup>Range of dihedral angles between the C<sub>6</sub> aryl rings of the (OAr')<sup>1-</sup> ligands and the O<sub>4</sub> atom plane.

Complex **30-Th** exhibits an isotropic EPR signal at room temperature, Figure 9.3, with a  $g_{\text{iso}} = 1.84$ . This value is the lowest  $g_{\text{iso}}$  value for a Th(III) complex reported so far Table 9.2.<sup>8-11, 13, 13</sup> The 77 K EPR spectrum of **30-Th** produced an axial signal with  $g_{\parallel} = 1.99$  and  $g_{\perp} = 1.79$ . This is consistent with data on  $[\text{C}_5\text{H}_3(\text{SiMe}_3)_2]_3\text{Th}^9$  ( $g_{\parallel} = 1.97$  and  $g_{\perp} = 1.88$ ),  $(\text{C}_5\text{Me}_5)_3\text{Th}^{13}$  ( $g_{\parallel} = 1.97$  and  $g_{\perp} = 1.85$ ) and  $(\text{C}_5\text{H}_3^t\text{Bu}_2)_3\text{Th}^{14}$  ( $g_{\parallel} = 1.974$  and  $g_{\perp} = 1.880$ ). In all previous cases, the Th(III) ions were assigned a  $6d^1$  ground state. The 298 K and 77 K EPR spectra of **31-Th** and  $[\text{K}(\text{crypt})][\text{Th}(\text{OAr}')_4]$  are indistinguishable from those of **30-Th**, Figure 9.12 and 9.13 (Chapter 9, Spectroscopic Details).

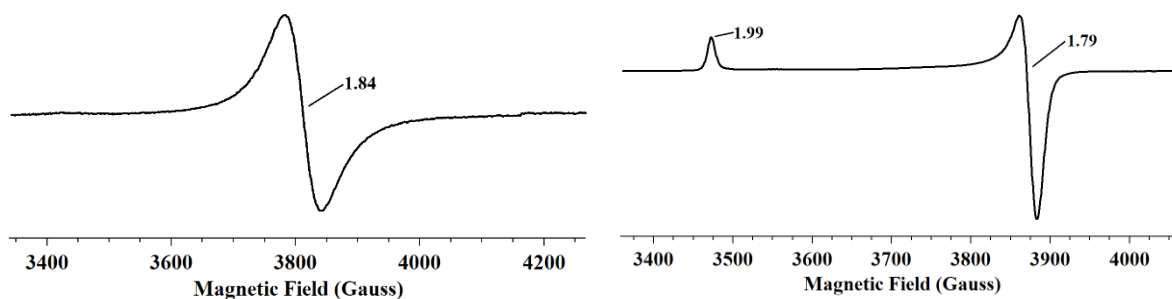


**Figure 9.3.** Experimental X-band EPR spectra of  $[\text{Th}(\text{OAr}')_4]^{1-}$  dissolved in THF (10 mM) collected at 298 K (left; mode: perpendicular;  $g_{\text{iso}} = 1.84$ ;  $\nu = 9.817$  GHz;  $P = 0.0202$ ; modulation amplitude = 0.902 mT) and 77 K (right; mode: perpendicular;  $g_{\parallel} = 1.99$ ,  $g_{\perp} = 1.79$ ;  $\nu = 9.672$  GHz;  $P = 0.0203$ ; modulation amplitude = 0.902 mT) and analyzed using EasySpin.<sup>22</sup>

**Table 9.2.** Room temperature EPR  $g_{\text{iso}}$  values and 77 K  $g_{\parallel}$  and  $g_{\perp}$  values of Th(III) complexes.

Th(III) Complex	$g_{\text{iso}}$	$g_{\parallel}$	$g_{\perp}$
$[\text{K}(\text{DME})_2][\text{C}_8\text{H}_6(\text{Si}^t\text{BuMe}_2)_2]_2\text{Th}^8$	1.916	-	-
$[\text{C}_5\text{H}_3(\text{SiMe}_2^t\text{Bu})_2]_3\text{Th}^9$	1.910	-	-
$[\text{C}_5\text{H}_3(\text{SiMe}_3)_2]_3\text{Th}^9$	1.910	1.97	1.88
$(\text{C}_5\text{Me}_5)_2\text{Th}[\text{PrNC}(\text{Me})\text{N}^i\text{Pr}]^{10}$	1.871	-	-
$(\text{C}_5\text{Me}_4\text{H})_3\text{Th}^{11}$	1.92	-	-
$(\text{C}_5\text{Me}_5)_3\text{Th}^{13}$	1.88	1.97	1.85
$(\text{C}_5\text{H}_3^t\text{Bu}_2)_3\text{Th}^{14}$	-	1.974 <sup>a</sup>	1.880 <sup>a</sup>
$[\text{Th}(\text{OAr}')_4]^{1-}$	1.84	1.99	1.79

<sup>a</sup> 100 K EPR  $g_{\parallel}$  and  $g_{\perp}$  values

The neutral **29-Th** as well as the anion in **30-Th** and **31-Th** were examined by Saswata Roy in the laboratory of Filipp Furche using density functional theory (DFT). For the neutral compound, two qualitatively different minimum energy structures were identified: an  $S_4$ -symmetric structure with a tetrahedral Th coordination environment and a  $C_4$ -symmetric structure with a square planar coordination of Th. The square planar geometry for  $\text{Th}(\text{OAr}')_4$  is less stable than the tetrahedral structure by 11 kcal/mol, Table 9.3. This is the expectation based on steric factors and it matches the structures of **32-Th** and **33-Th**.

**Table 9.3.** Computed relative energies (kcal/mol) of the  $S_4$ -symmetric minimum of **29-Th**,  $C_4$ -symmetric minimum of the neutral species from **31-Th** and the  $C_4$ - and  $S_4$ -symmetric minima of anion of **31-Th**.

	Square planar ( $C_4$ )	Tetrahedral ( $S_4$ )
$[\text{Th}(\text{OAr}')_4]^{1-}$	0	33
$\text{Th}(\text{OAr}')_4$	44	29

For  $[\text{Th}(\text{OAr}')_4]^{1-}$ , the calculations show that the square planar structure is lower in energy than the tetrahedral structure by 33 kcal/mol. Addition of an electron to tetrahedral  $\text{Th}(\text{OAr}')_4$  is

endothermic and yields a positive HOMO energy, indicating that tetrahedral  $\text{Th}(\text{OAr}')_4$  cannot be reduced. The calculated square-planar  $C_4$ -symmetric structure of the anion agrees with the X-ray diffraction data within error margins typical of the current methodology, approximately 0.01 Å in covalent bond distance and a few degrees in bond angles. The O–Th–O bond angles are calculated to be 90° and 180° for cis and trans ligands, respectively, and the Th–O<sub>4</sub>(plane) distance is calculated to be zero within the accuracy of the present approach. The 2.245 Å calculated Th–O bond length and the 1.376 Å O–C distance are similar to those in Table 9.1. The nearly linear Th–O–C(ipso) angles are predicted to be 178°. The calculated 57° C<sub>6</sub> torsion angle matches the angular arrangement of the ligands found in the structures.

Mulliken population analysis of the HOMO from the DFT calculations of  $[\text{Th}(\text{OAr}')_4]^{1-}$  suggests it is predominantly  $6d_z^2$  in character, Figure 9.4, with some 7s-type Rydberg admixture which is allowed in  $C_4$  symmetry, Figure 9.5.<sup>23</sup> Although  $d_z^2$  is usually not the energetically lowest d orbital in square planar geometry, there are examples such as  $[\text{PtCl}_4]^{2-}$ ,<sup>24, 25</sup> where metal orbitals with  $d_z^2$  character are energetically most stable particularly for ligands with  $\pi$ -donating lone pairs. To update the calculations from 1958<sup>24</sup> and 1983,<sup>25</sup>  $[\text{PtCl}_4]^{2-}$  was examined by modern methods to confirm the conclusion of a low-lying  $d_z^2$  orbital.

In  $[\text{Th}(\text{OAr}')_4]^{1-}$ , the doubly occupied  $\pi$  lone pairs repulsively interact with the  $d_{xy}$  orbital as well as the degenerate  $d_{xz}$  and the  $d_{yz}$  orbitals. Schrock *et al.*<sup>26</sup> have synthesized a square planar  $d^2$  W(IV) complex,  $\text{W}(\text{OC}_6\text{H}_3^i\text{Pr}_{2-2,6})_4$  which Hoffman *et al.*<sup>27</sup> described as having the doubly occupied  $\pi$  lone pairs repulsively interacting with the  $d_{xy}$ ,  $d_{xz}$ , and  $d_{yz}$  orbitals. Hayton *et al.*<sup>28</sup> have described similar behavior in a pseudo-square planar  $d^4$  Fe(IV) ketimide,  $[\text{Fe}(\text{N}=\text{C}^t\text{Bu}_2)_4]$ , where the  $\pi$  lone pairs of the ketimide repulsively interact with the degenerate  $d_{xz}$  and  $d_{yz}$  orbitals. Figure 9.5 shows the orbitals responsible for this effect in  $[\text{Th}(\text{OAr}')_4]^{1-}$ . A

qualitative molecular orbital diagram of the  $[\text{Th}(\text{OAr}')_4]^{1-}$  anion displaying important frontier molecular orbital energies is shown in Figure 9.6. This is the first  $6d^1$  square planar complex.<sup>29</sup>

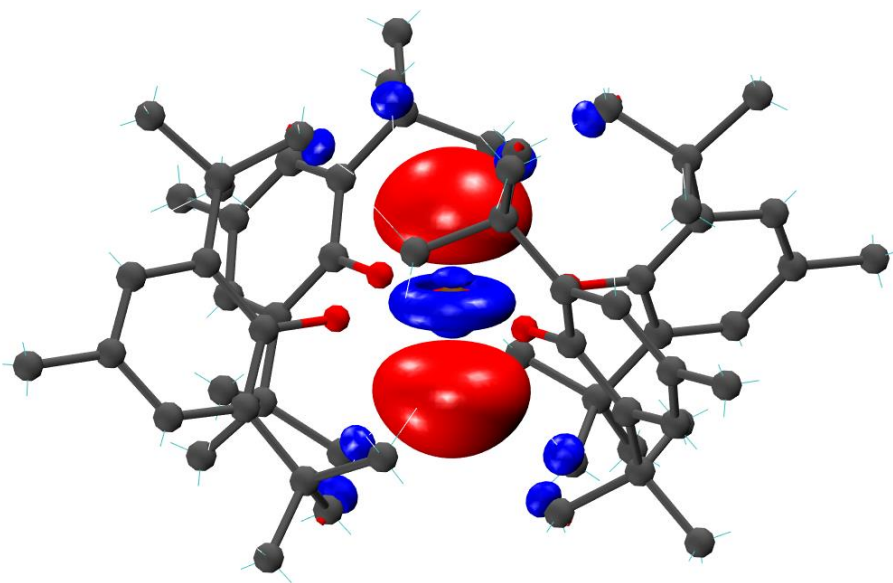


**Figure 9.4.** HOMO of  $[\text{Th}(\text{OAr}')_4]^{1-}$  plotted with an isovalue =  $\pm 0.05$ .

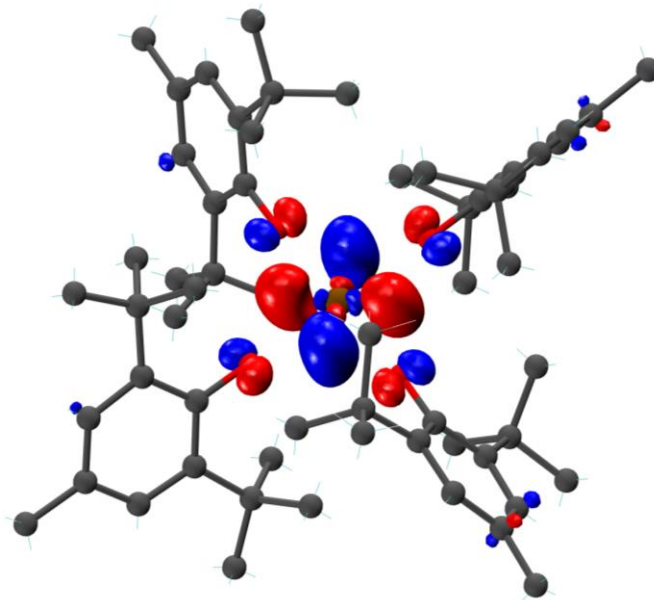


**Figure 9.5.** Example of antibonding orbitals of  $[\text{Th}(\text{OAr}')_4]^{1-}$  (isovalue =  $\pm 0.05$ ) involving the  $\pi$  orbitals on oxygen and the  $d_{xy}$  orbital on thorium.

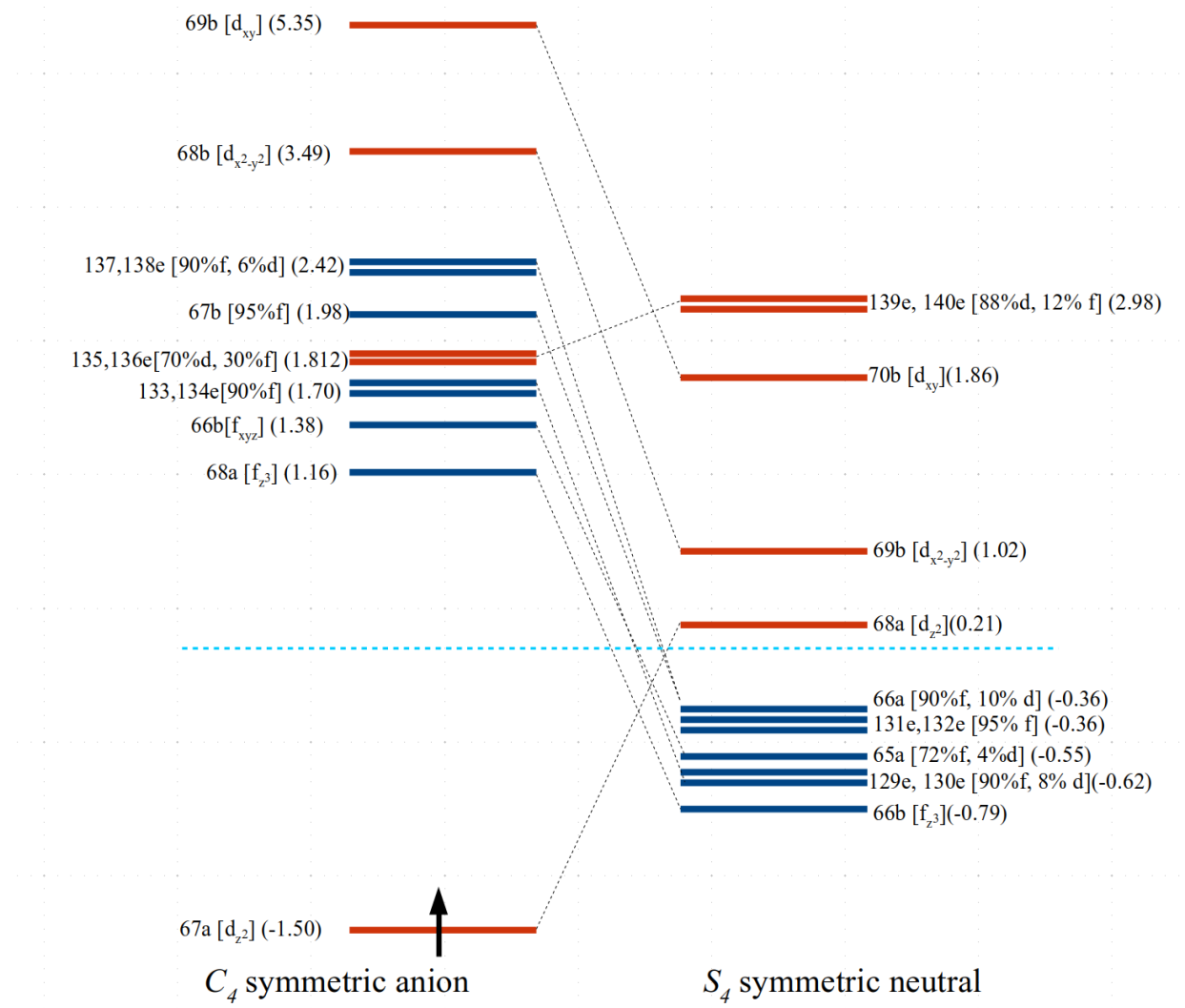


**Figure 9.6.** Simplified frontier molecular orbital diagram of  $[\text{Th}(\text{OAr}')_4]^{1-}$  showing  $\alpha$  spin orbitals with strong Th character. Red and blue levels represent computed energies of predominantly d and f orbitals, respectively; numerical values in eV are given in parentheses. The dashed blue line is the Fermi energy. Atomic orbital designations are reported in brackets whenever possible.

The UV-visible spectrum of **30-Th**, Figure 9.7, shows two absorption bands at 483 and 581 nm with high extinction coefficients ( $\epsilon = 4000$  and  $5000 \text{ M}^{-1} \text{ cm}^{-1}$ , respectively) and a more intense peak at 320 nm ( $\epsilon = 9000 \text{ M}^{-1} \text{ cm}^{-1}$ ). The simulated spectrum calculated using time dependent DFT (TD-DFT) calculations, Figure 9.7, suggests that the two broad peaks in the visible spectrum arise from several transitions originating from the  $6d_z^2$  orbital. The 581 nm peak corresponds to symmetry-allowed metal-centered transitions into orbitals of significant 5f character, whereas the 483 nm band has additional metal to ligand charge transfer character Table 9.4, 9.5, and 9.6. The intense absorption near 320 nm is attributed to a transition from the  $6d_z^2$  to a diffuse p-type Rydberg orbital, Figure 9.8.

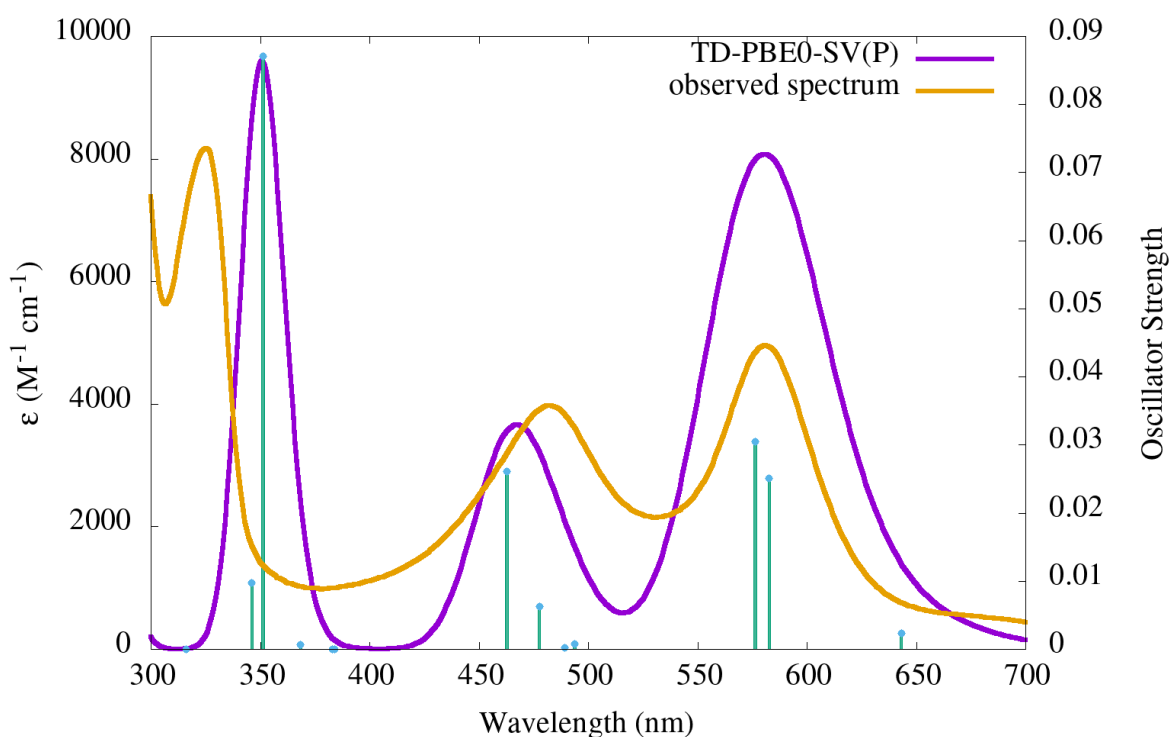


**Figure 9.7.** Observed UV-visible spectrum of  $[\text{K}(\text{THF})_5(\text{Et}_2\text{O})][\text{Th}(\text{OAr}')_4]$ , **30-Th**, in THF (700  $\mu\text{M}$ ) (yellow) and simulated UV-visible spectra of  $[\text{Th}(\text{OAr}')_4]^{1-}$  (purple) with the excitations shown as vertical lines. Calculated extinction coefficients are scaled down by a factor of 1.5.

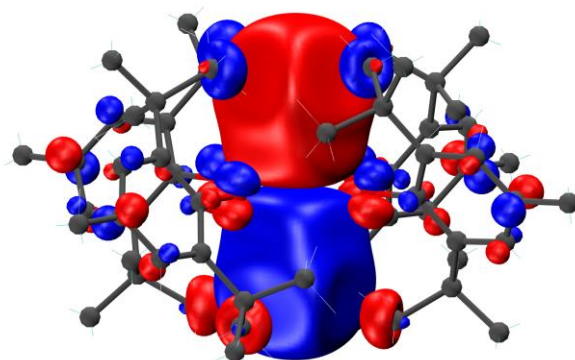


**Figure 9.8.** Rydberg orbital 71 a (2.73 eV) plotted with isovalue =  $\pm 0.02$ . The band located at 321 nm in the UV-visible spectrum results predominately from a transition out of the  $d_{z^2}$  HOMO into 71 a.

**Table 9.4.** Selected electronic excitations of  $[\text{Th}(\text{OAr}')_4]^{1-}$  using PBE0 functional in the  $C_2$  symmetry. Oscillator strength are in length representation.

Wavelength (nm)	Oscillator Strength ( $10^{-2}$ )	IRREP	occupied	unoccupied	% contribution	Assignment
612	1.37	E	67 a	130 e	70	$6d_{z^2} \rightarrow \pi^*$
			67 a	134 e	30	$6d_{z^2} \rightarrow 5f$
581	2.36	A	67 a	68 a	95	$6d_{z^2} \rightarrow 5f_z^3$
568	0.94	E	67 a	130 e	56	$6d_{z^2} \rightarrow \pi^*$
			67 a	134 e	24	$6d_{z^2} \rightarrow 5f$
431	3.61	A	67 a	70 a	99	$6d_{z^2} \rightarrow \pi^*$



**Table 9.5.** Select electronic excitations (with oscillator strengths larger than 0.01) of  $[\text{Th}(\text{OAr}')_4]^{1-}$  using PBE0 functional in the  $C_4$  symmetry using single- $\zeta$  basis sets on the ligands. Oscillator strength are in length representation.

Wavelength (nm)	Oscillator Strength ( $10^{-2}$ )	IRREP	occupied	unoccupied	% contribution	Assignment
602	1.44	E	67 a	130 e	50	$6d_z^2 \rightarrow \pi^*$
			67 a	134 e	34	$6d_z^2 \rightarrow 5f$
576	3.57	A	67 a	68 a	83	$6d_z^2 \rightarrow 5f_z^3$
574	1.16	E	67 a	134 e	55	$6d_z^2 \rightarrow \pi^*$
				130 e	31	$6d_z^2 \rightarrow 5f$
389	5.07	A	67a	70 a	88	$6d_z^2 \rightarrow \pi^*$
322	13.15	A	67a	71 a	82	$6d_z^2 \rightarrow 7p_z$

**Table 9.6.** Select electronic excitations (with oscillator strengths larger than 0.01) of  $[\text{Th}(\text{OAr}')_4]^{1-}$  using PBE0 functional in the  $C_4$  symmetry using def2-SV(P) basis sets on the ligands. Oscillator strength are in length representation.

Wavelength (nm)	Oscillator Strength ( $10^{-2}$ )	IRREP	occupied	unoccupied	% contribution	Assignment
582	2.51	E	67 a	134 e	79	$6d_z^2 \rightarrow 5f$
			67 a	136 e	13	$6d_z^2 \rightarrow 5f$
576	3.04	A	67 a	70 a	79	$6d_z^2 \rightarrow 5f_z^3$
462	2.61	A	67a	69 a	94	$6d_z^2 \rightarrow \pi^*$
351	8.71	A	67a	72 a	60	$6d_z^2 \rightarrow 7p_z$

The square planar coordination geometry in  $[\text{Th}(\text{OAr}')_4]^{1-}$  was surprising given that tetrahedral geometry is sterically favored and the electron configuration of the new complex is not one of the  $d^7$ - $d^9$  electron configurations that electronically favor square planar geometries.<sup>30-</sup><sup>32</sup> It is possible that the arrangement of the eight *tert*-butyl groups is optimized with the OAr' ligands in a square planar array, although most eight coordinate structures are similar in energy.<sup>33, 34</sup> The eight *tert*-butyl tertiary carbon atoms define a square anti-prism which is one of the several common geometries for  $\text{ML}_8$  compounds and  $\text{M}_8\text{L}_x$  clusters.

Dispersion forces between the tert-butyl groups may also lead to the square planar geometry. The importance of dispersion forces in inorganic chemistry has been thoroughly summarized.<sup>35</sup> It has also been previously shown that *tert*-butyl-substituted trityl compound  $[\text{C}(\text{C}_6\text{H}_3\text{-}3,5\text{-}^t\text{Bu}_2)_3]_2$  has significant dispersion forces, which give it a simple dimeric structure and a melting point of 214 °C!<sup>36-38</sup> The C(Me)...C(Me) distances between the tert-butyl groups in  $[\text{Th}(\text{OAr}')_4]^{1-}$  are as low as 3.30(1) to 3.55(1) Å which are well below the 3.95(2)-4.15(2) Å range of distances in  $[\text{C}(\text{C}_6\text{H}_3\text{-}3,5\text{-}^t\text{Bu}_2)_3]_2$ .<sup>36-39</sup> Consistent with this, the closest H(CMe<sub>3</sub>)...H(CMe<sub>3</sub>) distances in **30-Th** and **31-Th** are 2.21-2.35 Å which is less than twice the sum of the 1.2 Å Van der Waals radius of hydrogen (SI). However, calculated structures optimized without dispersion correction showed little difference from calculated structures optimized with dispersion correction.

The main difference in the electronic structure of the square planar and tetrahedral coordination geometries is the accessibility of a low-lying Th orbital with 6d/7s character in square planar. This suggests that the main driving force for the reorganization of the structure upon reduction from Th(IV) to Th(III) is a gain in ligand field stabilization energy for a 6d<sup>1</sup> configuration in the square planar relative to the tetrahedral coordination geometry. The calculations also revealed different orientations of the tert-butyl groups for tetrahedral and square planar. In the tetrahedral geometry, one C–Me bond of the tert-butyl groups is aligned nearly parallel to the O–Th bonds, whereas it is nearly antiparallel in the square planar geometry Figure 9.9 and 9.10. The latter orientation with more methyl groups near the metal facilitates stronger dispersive interactions and is better accommodated in the anion since the Th–O distances are longer for Th(III) than for Th(IV).

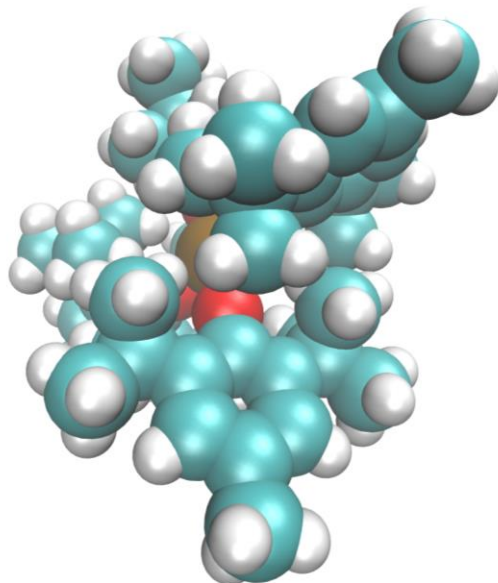


**Figure 9.9.** Space filling model for the  $C_4$  structure demonstrating the eclipsed conformation of the tert-butyl groups on the aryl rings. None of the methyls are parallel to the C(ipso)–O bond.

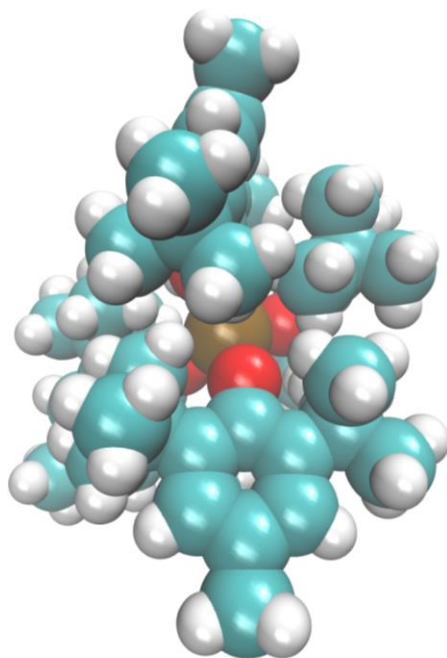


**Figure 9.10.** Space filling model for the  $S_4$  structure demonstrating the staggered conformation of the tert-butyl groups on the aryl rings. One of the methyls is parallel the C(ipso)–O bond.

In summary, a square planar geometry is accessible to thorium in the +3 oxidation state with the suitable ligands. The aryloxy ligands, which are  $\pi$ -donors, favor the formation of a square planar  $d^1$  complex with a low energy  $d_{z^2}$  orbital. This geometry, which is unusual for an f element and for  $d^1$  complexes, is likely also favored by the positioning of the eight *tert*-butyl substituents on the four aryloxy ligands.

### Experimental Details

All manipulations and syntheses described below were conducted with the rigorous exclusion of air and water using standard Schlenk line and glovebox techniques under an argon atmosphere.  $\text{HO}C_6H_2^t\text{Bu}_{2,6}\text{-Me-4}$ ,  $\text{HOAr}'$  (Acros), was sublimed before use.  $\text{KOC}_6H_2^t\text{Bu}_{2,6}\text{-Me-4}$ ,  $\text{KOAr}'$ , was synthesized by a literature procedure.<sup>40</sup>  $\text{KC}_8$  was synthesized according to literature methods<sup>41</sup> and Li metal (99+%) was purchased as granules from Strem and used as received. In an adaptation of a literature procedure,  $\text{Th}(\text{OAr}')_4$  was synthesized by stirring  $\text{ThBr}_4(\text{THF})_4$  (1 equiv) and  $\text{KOAr}'$  or  $\text{LiOAr}' \cdot \text{Et}_2\text{O}$  (4 equiv) overnight in THF under argon.<sup>7</sup> Solvents were sparged with UHP argon and dried by passage through columns containing Q-5 and molecular sieves prior to use.  $\text{THF-}d_8$  was stirred in NaK alloy for 1 week and degassed by three freeze-pump-thaw cycles, then vacuum transferred.  $^1\text{H}$  NMR spectra were recorded on Bruker GN500 spectrometer and referenced internally to residual protio-solvent resonances at 298 K. Elemental analyses were conducted on a Perkin-Elmer 2400 Series II CHNS elemental analyzer. UV-visible spectra were collected in THF using a Varian Cary 60 Scan UV-visible spectrophotometer. EPR spectra were collected using X-band frequency (9.3–9.8 GHz) on a Bruker EMX spectrometer equipped with an ER041XG microwave bridge, and the magnetic field was calibrated with DPPH ( $g = 2.0036$ ). Infrared (IR) transmittance measurements were

taken as compressed solids on an Agilent Cary 630 spectrophotometer with a diamond ATR attachment.

**[K(THF)<sub>5</sub>(Et<sub>2</sub>O)][Th(OAr')<sub>4</sub>], 30-Th.** In an argon-filled glovebox, a colorless solution of Th(OAr')<sub>4</sub> (50 mg, 0.05 mmol) in THF (2 mL) and a vial containing KC<sub>8</sub> (10 mg, 0.07 mmol) were chilled to (−35 °C). The THF solution was transferred to the vial of KC<sub>8</sub> and vigorously swirled forming a dark maroon mixture. The mixture was immediately filtered and layered into cold Et<sub>2</sub>O (−35 °C). After 2 d, X-ray quality dark maroon crystals were isolated (49 mg, 69%). IR: 2909s, 2875s, 2834m, 1643m, 1459s, 1417m, 1375w, 1352s, 1318w, 1301w, 1271m, 1241m, 1213w, 1176w, 1118m, 1097m, 1080s, 1051s, 960w, 947s, 931s, 899m, 874w, 843w, 816m, 802m, 779w, 751m, 667w cm<sup>−1</sup>. Anal. Calcd for desolvated [K][Th(OAr')<sub>4</sub>], C<sub>60</sub>H<sub>92</sub>KO<sub>4</sub>Th: C, 62.74; H, 8.07; Found: C, 55.63; H, 7.03. Elemental analysis was complicated by incomplete combustion which has been observed before for f element complexes.<sup>42-49</sup> However, the CH ratio of C<sub>60</sub>H<sub>90.3</sub> vs calcd C<sub>60</sub>H<sub>92</sub> was found. It was determined that the elemental analytical data did not fit with partially desolvated complexes. However, the observed CH ratios fit reasonably well and may be due to complications of incomplete combustion.

**[Li(THF)<sub>4</sub>][Th(OAr')<sub>4</sub>], 31-Th.** In an argon-filled glovebox, a colorless solution of Th(OAr')<sub>4</sub> (50 mg, 0.05 mmol) in THF (2 mL) and a vial containing excess Li smear (5 mg) were chilled to (−35 °C). The THF solution was transferred to the vial of Li forming a light maroon solution. The solution with Li metal was placed in a (−35 °C) freezer overnight. After 2 d, X-ray quality dark maroon crystals were isolated (55 mg, 87%). IR: 2911s, 2879s, 2837m, 1645m, 1459s, 1411s, 1384w, 1373w, 1354s, 1319w, 1303w, 1280m, 1271m, 1245m, 1229m, 1212m, 1198w, 1176w, 1118m, 1083s, 1057s, 1040s, 1026s, 948s, 935s, 901m, 886w, 875w, 858w, 841w, 817s, 802s, 779w, 680w, 668w cm<sup>−1</sup>. Anal. for desolvated [Li][Th(OAr')<sub>4</sub>],

$C_{60}H_{92}LiO_4Th$ : C, 64.55; H, 8.31;. Found: C, 54.44; H, 7.25. Elemental analysis was complicated by incomplete combustion which has been observed before for f element complexes.<sup>42-49</sup> However, the CH ratio of  $C_{60}H_{95.2}$  vs calcd  $C_{60}H_{92}$  was found. It was determined that the elemental analytical data did not fit with partially desolvated complexes. However, the observed CH ratios fit reasonably well and may be due to complications of incomplete combustion

**[K(2.2.2-cryptand)][Th(OAr')<sub>4</sub>]**. In an argon-filled glovebox, a colorless solution of Th(OAr')<sub>4</sub> (50 mg, 0.05 mmol) and 2.2.2-cryptand (17 mg, 0.05 mmol) in THF (2 mL) and a vial containing KC<sub>8</sub> (10 mg, 0.07 mmol) were chilled to (−35 °C). The THF solution was transferred to the vial of KC<sub>8</sub> and vigorously swirled forming a dark maroon mixture. The mixture was immediately filtered and layered into cold Et<sub>2</sub>O (−35 °C). Dark maroon crystalline solids were isolated (60 mg, 91%). IR: 2950s, 2883s, 2865s, 2813m, 1737w, 1599w, 1476w, 1456w, 1443w, 1407s, 1384m, 1354s, 1319w, 1295m, 1257s, 1227s, 1212s, 1196m, 1131m, 1101s, 1077s, 1029w, 949s, 930m, 886w, 959m, 816s, 800s, 778m, 752w cm<sup>−1</sup>. Anal. for [K(2.2.2-cryptand)][Th(OAr')<sub>4</sub>], C<sub>78</sub>H<sub>128</sub>KN<sub>2</sub>O<sub>10</sub>Th: C, 61.43; H, 8.46; N, 1.84. Found: C, 61.27; H, 8.85; N, 1.78.

## Spectroscopic Details

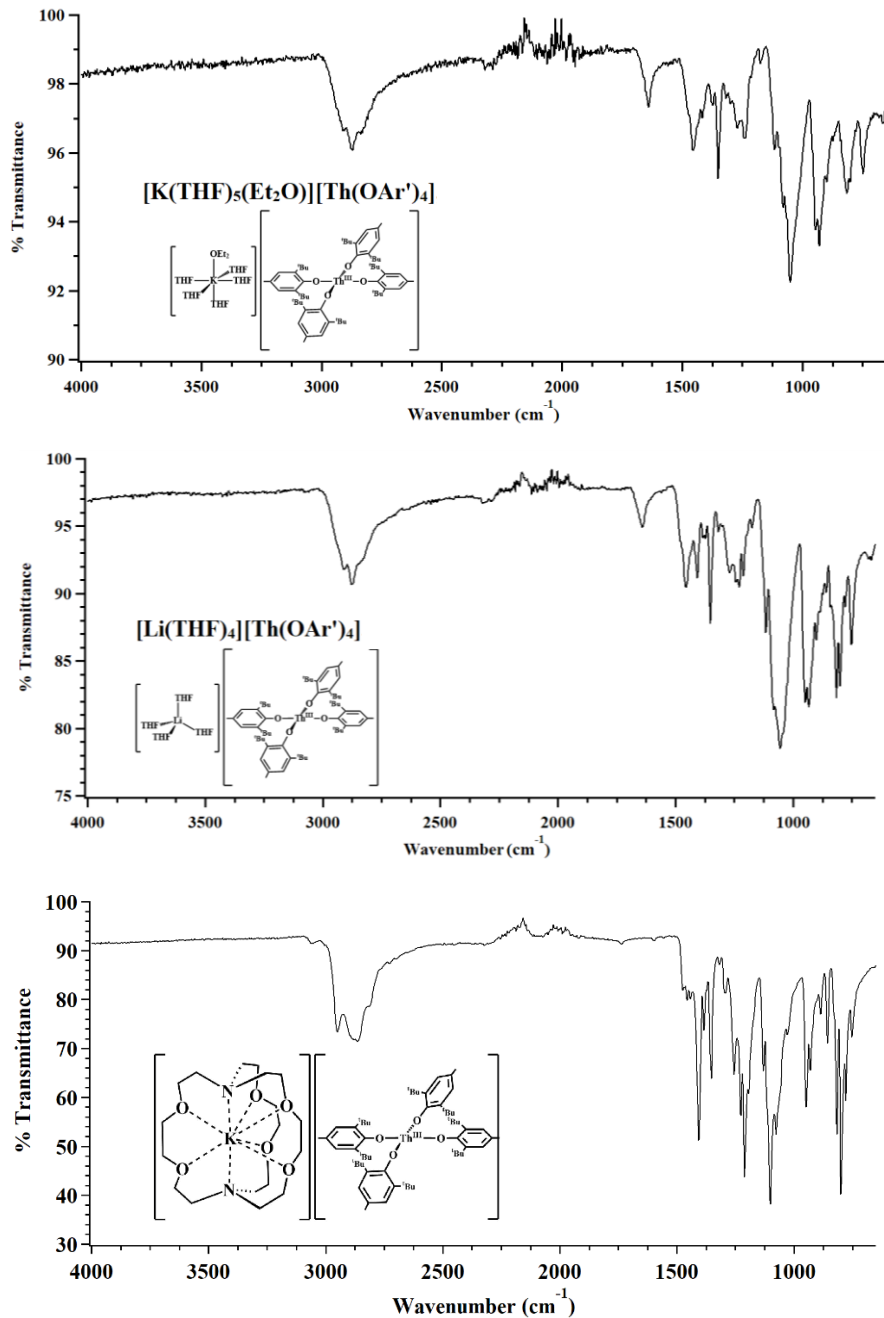


**Figure 9.11.** IR spectra of  $[\text{K}(\text{THF})_5(\text{Et}_2\text{O})][\text{Th}(\text{OAr}')_4]$ , **30-Th** (top),  $[\text{Li}(\text{THF})_4][\text{Th}(\text{OAr}')_4]$ , **31-Th** (middle), and  $[\text{K}(\text{crypt})][\text{Th}(\text{OAr}')_4]$  (bottom).

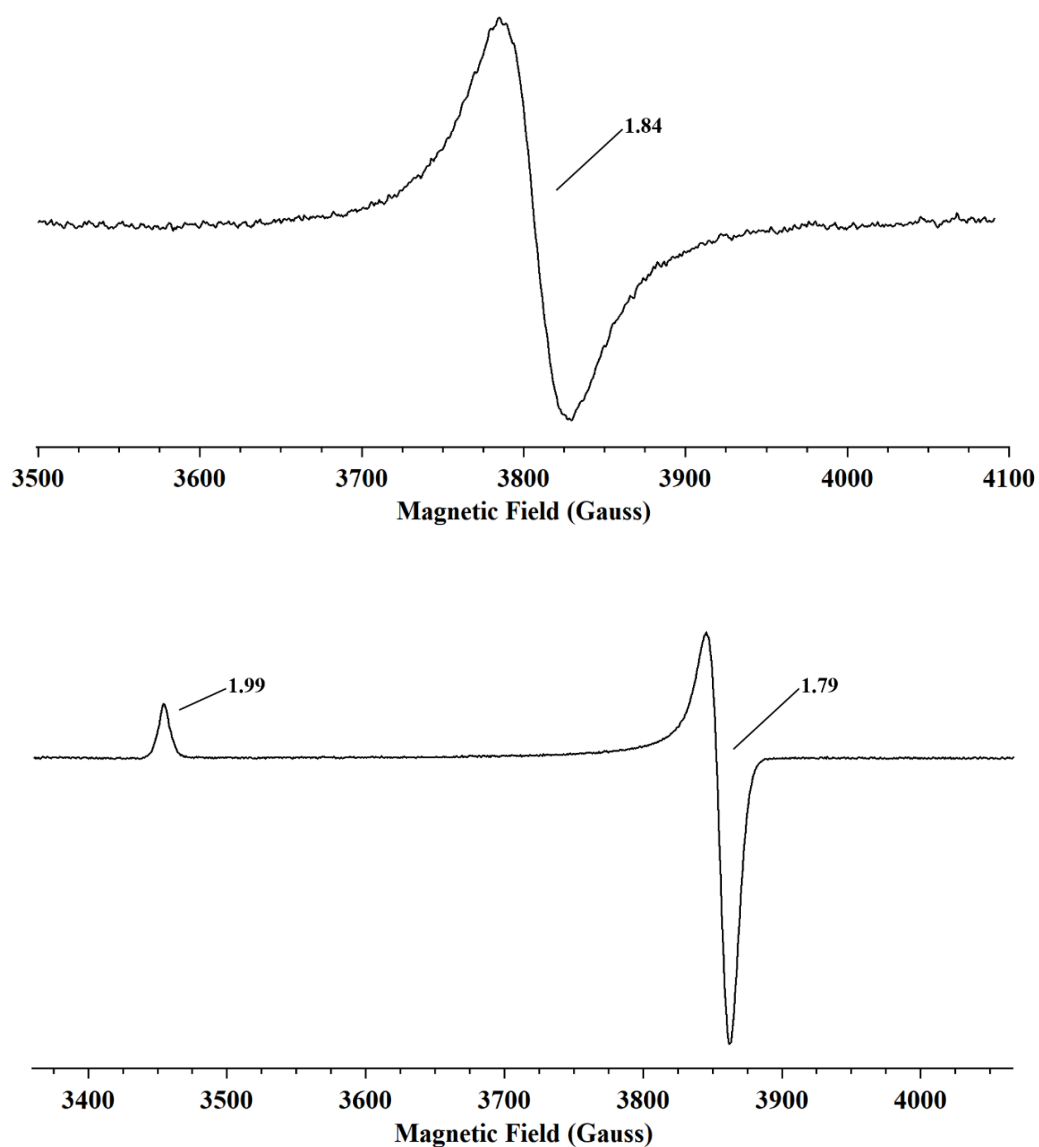


**Figure 9.12.** Experimental X-band EPR spectra of  $[\text{Li}(\text{THF})_4][\text{Th}(\text{OAr}')_4]$ , **31-Th**, dissolved in THF (5 mM) collected at 298 K (top; mode: perpendicular;  $g_{\text{iso}} = 1.84$ ;  $\nu = 9.819$  GHz;  $P = 0.0604$ ; modulation amplitude = 0.902 mT) and 77 K (bottom; mode: perpendicular;  $g_{\parallel} = 1.99$ ,  $g_{\perp} = 1.79$ ;  $\nu = 9.622$  GHz;  $P = 0.0202$ ; modulation amplitude = 0.902 mT) and analysed using EasySpin.<sup>22</sup>



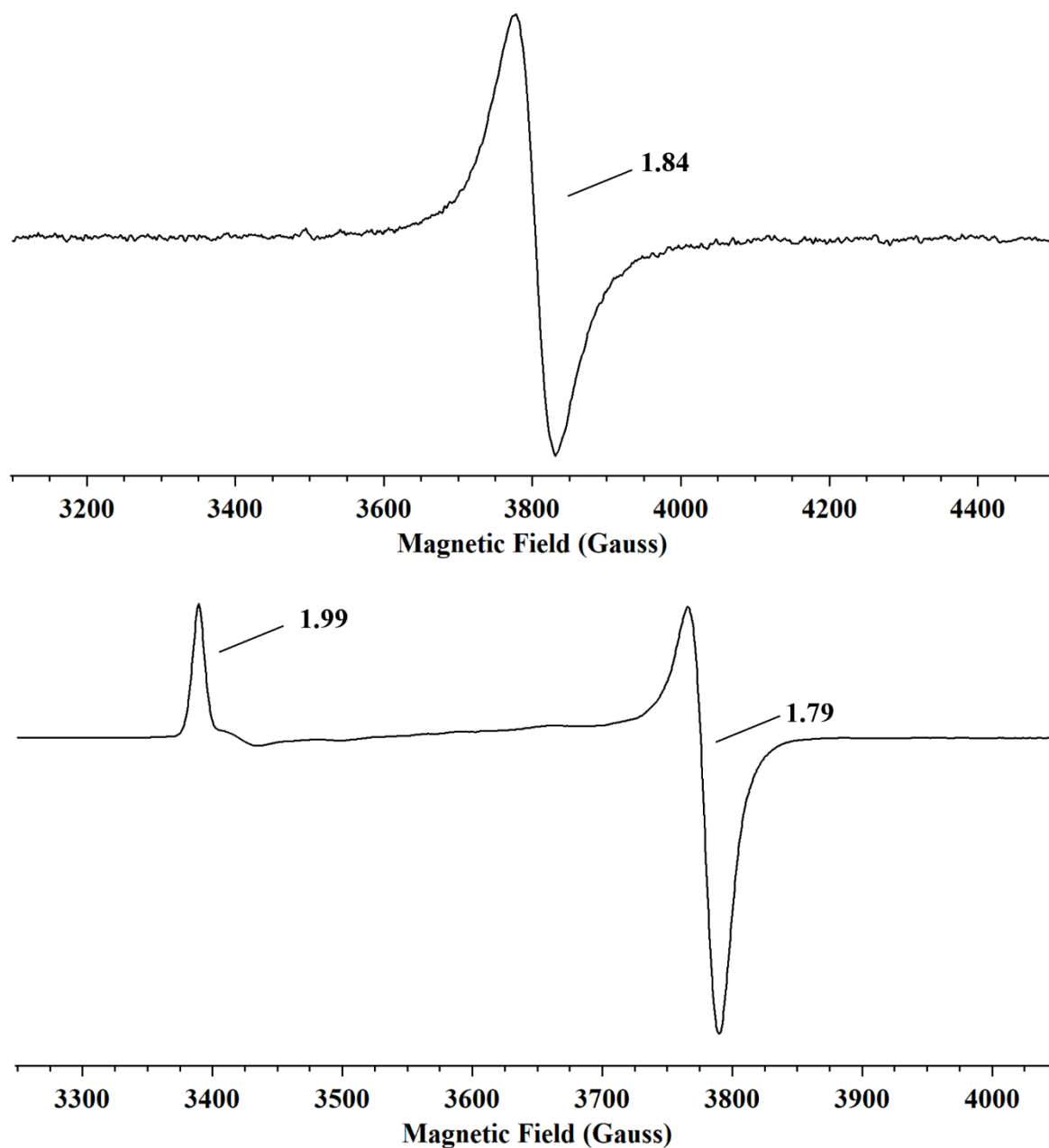


**Figure 9.13.** Experimental X-band EPR spectra of  $[\text{K}(\text{crypt})][\text{Th}(\text{OAr}')_4]$  dissolved in THF (5 mM) collected at 298 K (top; mode: perpendicular;  $g_{\text{iso}} = 1.84$ ;  $\nu = 9.796$  GHz;  $P = 2.15$  mW; modulation amplitude = 0.902 mT) and 77 K (bottom; mode: perpendicular;  $g_{\parallel} = 1.99$ ,  $g_{\perp} = 1.79$ ;  $\nu = 9.434$  GHz;  $P = 2.155$  mW; modulation amplitude = 0.902 mT) and analysed using EasySpin.<sup>22</sup>

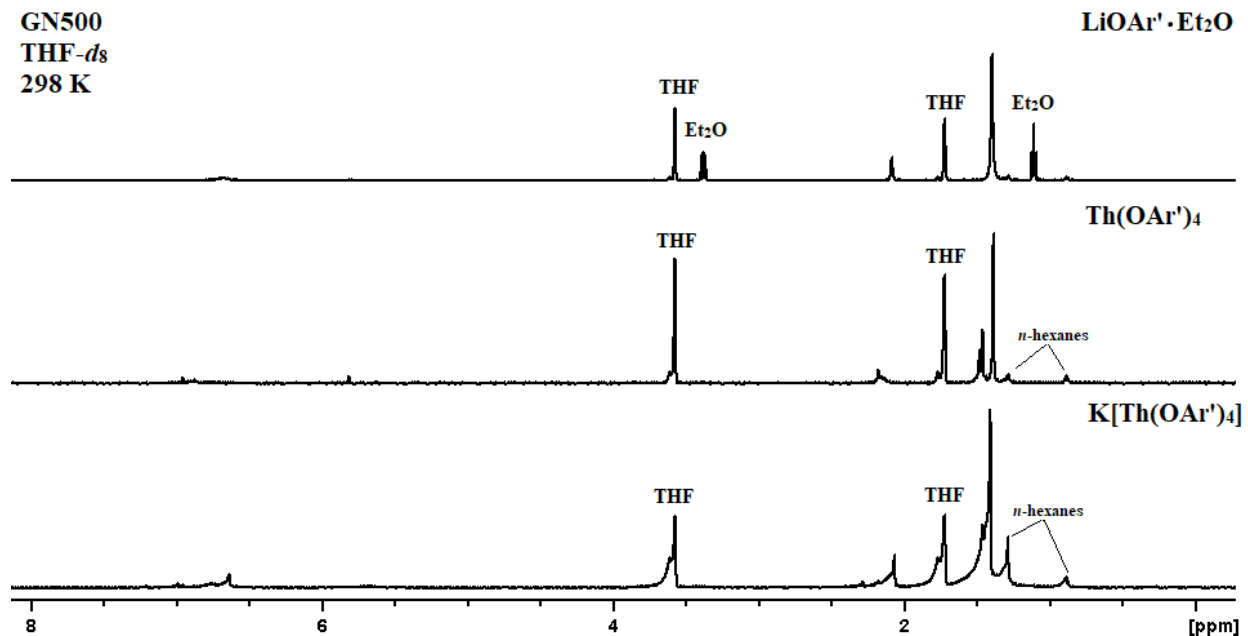


**Figure 9.14.** NMR (500 MHz, THF- $d_8$ ) spectra of  $K[Th(OAr')_4]$  (bottom),  $Th(OAr')_4$  (middle) and  $LiOAr' \cdot Et_2O$  (top) at 298 K.

### Computational Details

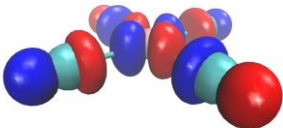
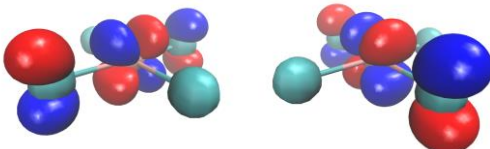
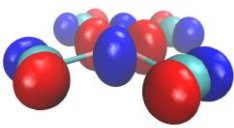
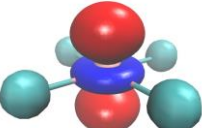
**Density functional calculations.** DFT calculations were performed by Saswata Roy in the laboratory of Prof. Filipp Furche. The molecular structure of the anion of **2** was optimized starting from the X-ray structure using the TPSS meta-generalized gradient approximation (meta-GGA) functional<sup>50</sup> along with Grimme's D3 dispersion correction.<sup>51</sup> Small-core scalar-relativistic effective core Stuttgart-Cologne potentials (ECPs)<sup>52</sup> were used for Th along with the corresponding valence basis sets.<sup>53</sup> Polarized split valence basis sets def2-SVP<sup>54</sup> were used for oxygen, and group optimized single- $\zeta$  bases<sup>54</sup> were used for all other atoms. Fine (size m4<sup>55</sup>) quadrature grids along with the resolution-of-the-identity approximation<sup>30</sup> were used throughout. The conductor like solvation model (COSMO)<sup>56</sup> was used to model THF solution ( $\epsilon = 7.520$ ).<sup>57</sup> Ground state energies were converged to  $10^{-7}$  Hartrees. For structural optimization, the DFT gradients were calculated including the derivatives of the quadrature weights for the density grid and converged to a maximum gradient norm of  $<10^{-4}$  au. Unconstrained optimization of the

anionic Th(III) species resulted in a  $C_2$  symmetric structure. Two structures were optimized for the neutral Th(IV) species. Starting from a  $S_4$  symmetric structure the neutral Th(IV) species optimized to a tetrahedral structure. Optimizing the Th(IV) species starting from the  $C_2$  structure resulted in a square planar structure. Attempts to converge structures with tetrahedral Th(III) coordination were unsuccessful. Mulliken population analysis is used to analyse the frontier molecular orbitals. As expected, the 6d orbitals show a single radial node (since the ECP accounts for the 3d and the 4d orbitals).

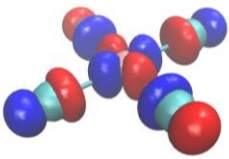
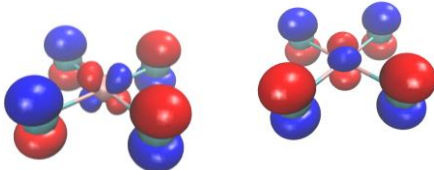
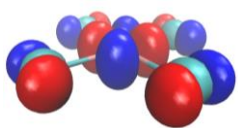
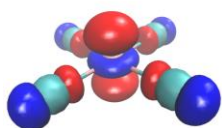
Numerical second derivative calculations were carried out to confirm that the optimized  $C_2$  and  $S_4$  structures are minima. Electronic excitation spectrum for the anionic  $C_4$  structure was computed using time-dependent density functional theory (TD-DFT) with the Perdew-Burke-Ernzerhof hybrid. PBE0<sup>58</sup> and the hybrid TPSSh functional.<sup>50, 59</sup> TD-DFT calculations were carried within  $C_4$  symmetry and 8 excitations of  $A$  and 7 excitations of  $E$  IRREPS were evaluated using both the group optimized single- $\zeta$  bases and the def2-SV(P)<sup>54</sup> bases for all the ligand atoms. The UV/Vis line spectrum was broadened by superimposing Gaussian functions of RMS line width of 0.1 eV. The TPSSh spectrum was blue shifted by 0.15 eV and the PBE0 spectrum with the def2-SV(P) bases were blue shifted by 0.075 eV. The excitation corresponding to the peak near 483 nm is a charge transfer excitation and hence is sensitive to the extent of exact-exchange in the hybrid functional as well as the incompleteness error arising from the basis sets.

Structures of  $[\text{PtCl}_4]^{2-}$  and  $[\text{PdCl}_4]^{2-}$  complexes were optimized using TPSS functional and triple- $\zeta$  def2-TZVP basis sets along with small-core ECPs.<sup>52</sup> COSMO was used to model water as solvent ( $\epsilon = 80.1$ ).<sup>57</sup> The optimized structures assumed  $D_{4h}$  symmetry. The relative d-orbital energies are reported in Tables 9.7 and 9.8. All calculations were performed using Turbomole V7-3.<sup>59</sup>

**Table 9.7.** d-Orbital splitting in square planar structure for  $[\text{PtCl}_4]^{2-}$  using TPSS density functional and triple- $\zeta$  bases.<sup>24, 25</sup>

Orbital	orbital energy (eV)	molecular orbital plot (isovalue=0.05)
6 b <sub>1g</sub>	-2.1	
3 e <sub>g</sub>	-4.64	
3 b <sub>2g</sub>	-4.89	
7 a <sub>1g</sub>	-5.11	

**Table 9.8.** d-Orbital splitting in square planar structure for  $[\text{PdCl}_4]^{2-}$  using TPSS density functional and triple- $\zeta$  bases.<sup>25</sup>

Orbital	orbital energy (eV)	molecular orbital plot (isovalue=0.05)
6 b <sub>2g</sub>	-2.09	
3 e <sub>g</sub>	-4.99	
3 b <sub>1g</sub>	-5.24	
7 a <sub>1g</sub>	-5.29	

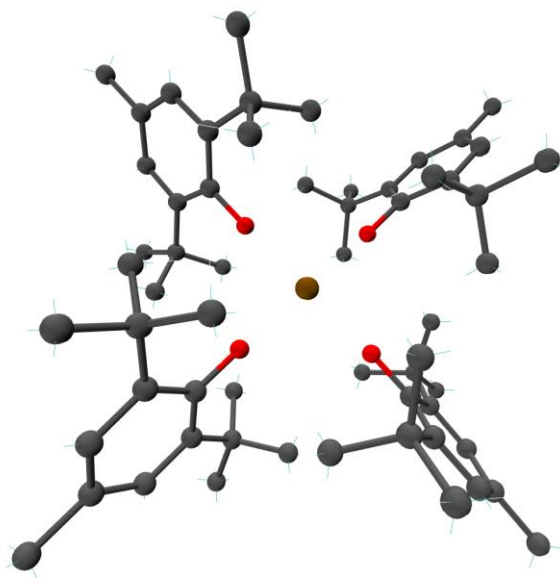


**Figure 9.15.** Structure of optimized anion of **31-Th** in  $C_4$  symmetry.

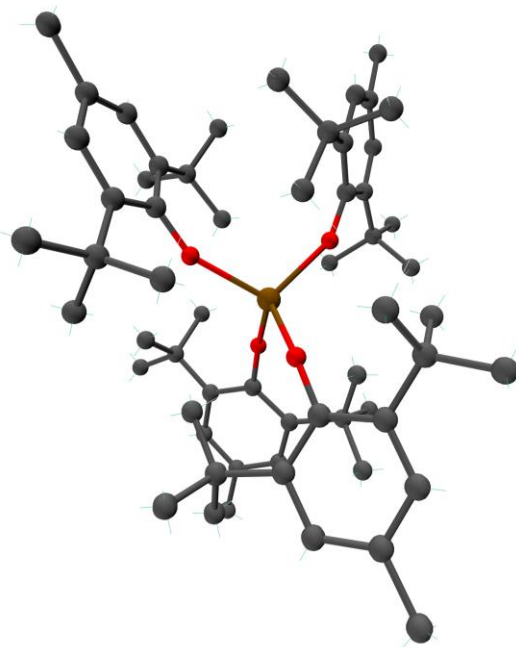


**Figure 9.16.** Structure of optimized neutral Th(OAr)<sub>4</sub> in  $S_4$  symmetry.

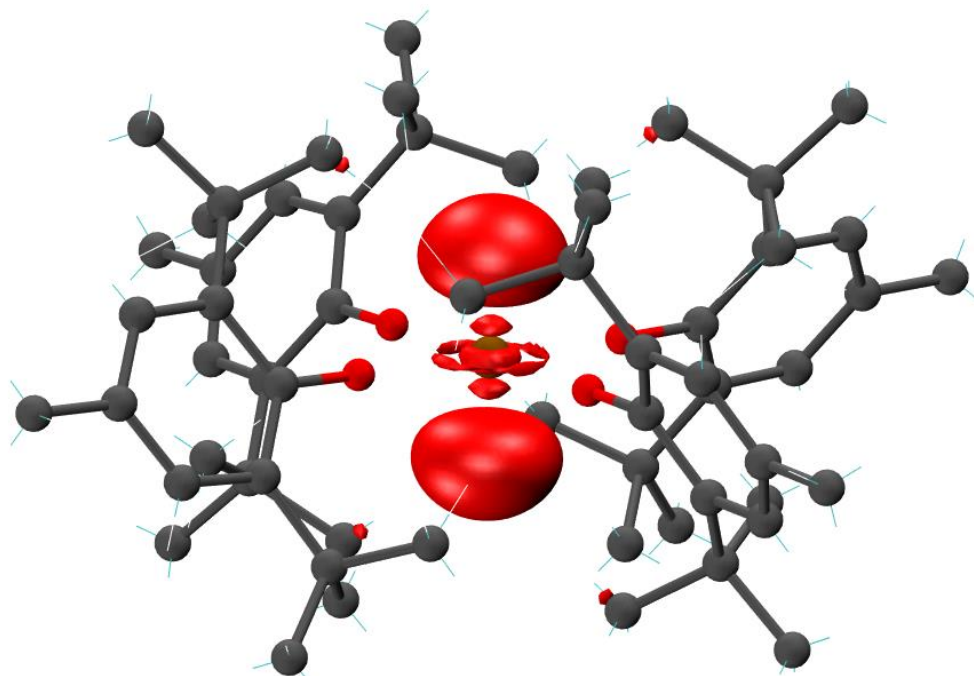


**Figure 9.17.** Spin density of  $[\text{Th}(\text{OAr}')_4]^{1-}$  plotted with an isovalue  $=\pm 0.005$

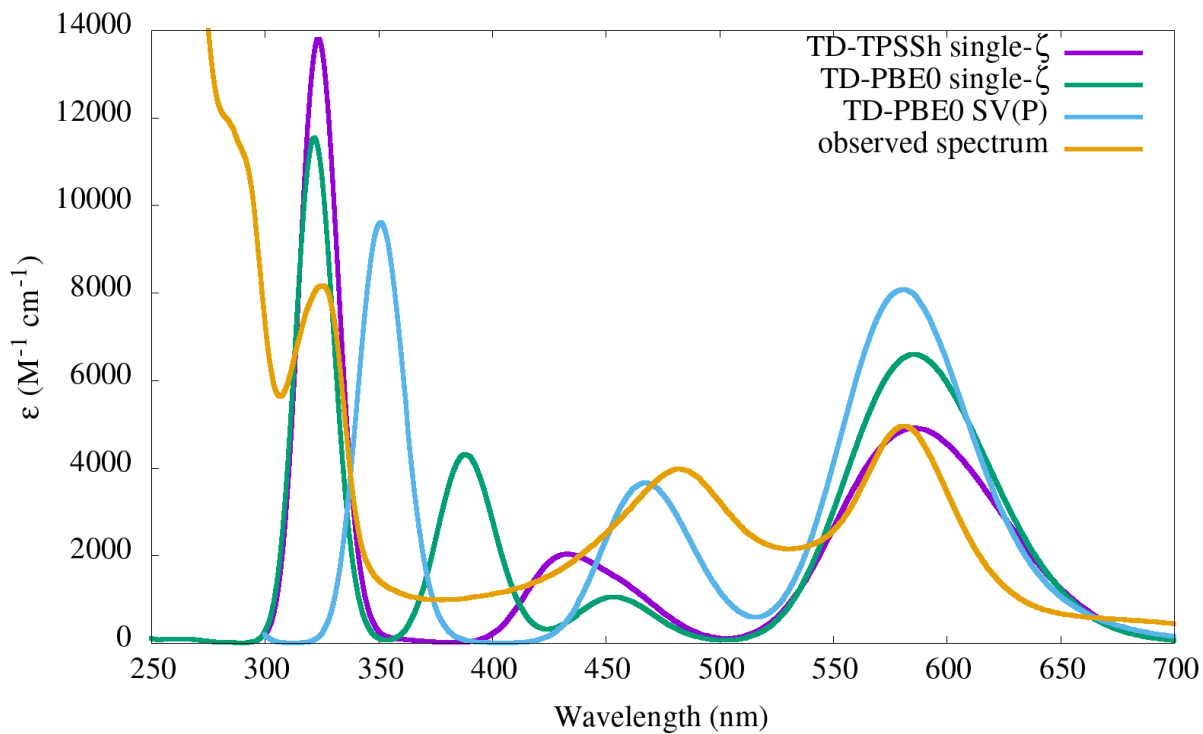


**Figure 9.18.** The simulated absorption spectrum using TD-TPSSh single- $\zeta$  (purple), TD-PBE0 single- $\zeta$  (green), and TD-PBE0 SV(P) (blue) functionals compared to the experimentally observed spectrum (orange).

## Structural Details

**Table 9.9.** Table of bond distances and angles for [K(THF)<sub>5</sub>(Et<sub>2</sub>O)][Th(OAr')<sub>4</sub>], **30-Th**, and [Li(THF)<sub>4</sub>][Th(OAr')<sub>4</sub>], **31-Th**.

### [K(THF)<sub>5</sub>(Et<sub>2</sub>O)][Th(OAr')<sub>4</sub>], **30-Th**

Th1–O1	Th1–O2	Th2–O3	Th2–O4		
2.260(3)	2.239(3)	2.235(3)	2.257(3)		
O1–C1	O2–C16	O3–C31	O4–C46		
1.349(6)	1.355(6)	1.371(6)	1.356(6)		
Th1–O1–C1	Th1–O2–C16	Th2–O3–C31	Th2–O4–C46		
178.6(4)	176.1(3)	174.2(3)	178.5(3)		
O1–Th1–O1a	O1–Th1–O2	O1–Th1–O2a	O1a–Th1–O2	O1a–Th1–O2a	O2–Th1–O2a
178.94(15)	89.50(15)	90.51(15)	90.52(15)	89.50(15)	178.49(16)
O3–Th2–O3a	O3–Th2–O4	O3–Th2–O4a	O3a–Th2–O4	O3a–Th2–O4a	O4–Th2–O4a
178.13(16)	89.75(12)	90.26(12)	90.26(12)	89.75(12)	179.58(16)

### [Li(THF)<sub>4</sub>][Th(OAr')<sub>4</sub>], **31-Th**

Th1–O1	Th1–O2	Th1–O3	Th1–O4
2.244(2)	2.244(2)	2.238(2)	2.247(2)
O1–C1	O2–C16	O3–C31	O4–C46
1.355(4)	1.355(4)	1.358(4)	1.358(4)
Th1–O1–C1	Th1–O2–C16	Th1–O3–C31	Th1–O4–C46
173.9(2)	174.7(2)	176.5(2)	174.7(2)
O1–Th1–O3	O1–Th1–O2	O1–Th1–O4	O2–Th1–O3
178.54(9)	89.27(8)	88.92(8)	89.87(8)



**Table 9.10.** Selected C...C (CMe<sub>3</sub>) distances of [K(THF)<sub>5</sub>(Et<sub>2</sub>O)][Th(OAr')<sub>4</sub>], **30-Th**, and [Li(THF)<sub>4</sub>][Th(OAr')<sub>4</sub>], **31-Th**.

<b>30-Th</b>			<b>31-Th</b>		
		Distance (Å)			Distance (Å)
C7	C12	5.234(7)	C22	C27	5.233(5)
C7	C12	5.234(7)	C7	C12	5.235(6)
C22	C27	5.249(8)	C42	C37	5.236(6)
C22	C27	5.249(8)	C57	C52	5.247(5)
C12	C27	5.442(7)	C22	C12	5.344(5)
C12	C27	5.442(7)	C7	C57	5.403(5)
C7	C22	5.456(8)	C52	C42	5.429(5)
C7	C22	5.456(8)	C42	C27	5.438(5)
C27	C12	5.494(8)	C27	C12	5.445(5)
C27	C12	5.494(8)	C22	C7	5.446(5)
C22	C7	5.527(7)	C57	C42	5.461(6)
C22	C7	5.527(7)	C12	C52	5.476(5)
C22	C12	5.553(8)	C37	C22	5.565(5)
C22	C12	5.553(8)	C37	C27	5.582(6)
C7	C27	5.716(7)	C7	C52	5.705(6)
C7	C27	5.716(7)	C57	C37	5.856(5)

**Table 9.11.** Selected H...H distances of [K(THF)<sub>5</sub>(Et<sub>2</sub>O)][Th(OAr')<sub>4</sub>], **30-Th**, and [Li(THF)<sub>4</sub>][Th(OAr')<sub>4</sub>], **31-Th**.

<b>30-Th</b>			<b>31-Th</b>		
		Distance (Å)			Distance (Å)
H28C	H9C	2.293	H45C	H59C	2.211
H9B	H24C	2.351	H55C	H9C	2.287
H25B	H10C	2.396	H15C	H55B	2.312
H25C	H15C	2.409	H39B	H23C	2.338
H15B	H29C	2.444	H59A	H45A	2.339
H25C	H10A	2.500	H29C	H39C	2.350
H28B	H13C	2.502	H24C	H14C	2.384
H15A	H25A	2.624	H24A	H14A	2.444
H9C	H24A	2.649	H29B	H44C	2.485
H13A	H28C	2.665	H8C	H24B	2.505
H28A	H9A	2.673	H23A	H39C	2.551
H15C	H29A	2.727	H55C	H15A	2.581

**X-ray Data Collection, Structure Solution and Refinement for [K(THF)<sub>5</sub>(Et<sub>2</sub>O)][Th(OAr')<sub>4</sub>], 30-Th.** A dark purple crystal of approximate dimensions 0.239 x 0.206 x 0.102 mm was mounted in a cryoloop and transferred to a Bruker SMART APEX II diffractometer. The APEX2<sup>60</sup> program package was used to determine the unit-cell parameters and for data collection (90 sec/frame scan time for a sphere of diffraction data). The raw frame data was processed using SAINT<sup>61</sup> and SADABS<sup>62</sup> to yield the reflection data file. Subsequent calculations were carried out using the SHELXTL<sup>63</sup> program. The diffraction symmetry was *mmm* and the systematic absences were consistent with the orthorhombic space group *P2<sub>1</sub>2<sub>1</sub>2* that was later determined to be correct. The structure was solved by direct methods and refined on F<sup>2</sup> by full-matrix least-squares techniques. The analytical scattering factors<sup>64</sup> for neutral atoms were used throughout the analysis. Hydrogen atoms were included using a riding model. Least-squares analysis yielded wR<sub>2</sub> = 0.0734 and Goof = 1.058 for 846 variables refined against 20184 data (0.75 Å), R<sub>1</sub> = 0.0346 for those 17359 data with I > 2.0σ(I). Refinement of the Flack parameter was inconclusive (BASF<sup>17</sup> = 0.49515). The structure was refined as a two-component inversion twin.

**X-ray Data Collection, Structure Solution and Refinement for [Li(THF)<sub>4</sub>][Th(OAr')<sub>4</sub>], 31-Th.** A purple crystal of approximate dimensions 0.130 x 0.210 x 0.281 mm was mounted in a cryoloop and transferred to a Bruker SMART APEX II diffractometer. The APEX2<sup>60</sup> program package was used to determine the unit-cell parameters and for data collection (60 sec/frame scan time for a sphere of diffraction data). The raw frame data was processed using SAINT<sup>61</sup> and SADABS<sup>62</sup> to yield the reflection data file. Subsequent calculations were carried out using the SHELXTL<sup>63</sup> program. The diffraction symmetry was *2/m* and the systematic absences were consistent with the monoclinic space groups *Cc* and *C2/c*. It

was later determined that space group  $C2/c$  was correct. The structure was solved by direct methods and refined on  $F^2$  by full-matrix least-squares techniques. The analytical scattering factors<sup>64</sup> for neutral atoms were used throughout the analysis. Hydrogen atoms were included using a riding model. Least-squares analysis yielded  $wR2 = 0.0967$  and  $Goof = 1.035$  for 786 variables refined against 19934 data ( $0.74 \text{ \AA}$ ),  $R1 = 0.0385$  for those 16597 data with  $I > 2.0\sigma(I)$ . There were several high residuals present in the final difference-Fourier map. It was not possible to determine the nature of the residuals although it was probable that THF solvent was present. The SQUEEZE<sup>65</sup> routine in the PLATON<sup>65</sup> program package was used to account for the electrons in the solvent accessible voids.

## References

- (1) Bradley, D. C.; Saad, M. A.; Wardlaw, W. The preparation of thorium alkoxides. *J. Chem. Soc.* **1954**, 1091-1094.
- (2) Bradley, D. C.; Saad, M. A.; Wardlaw, W. Tertiary alkoxides of thorium. *J. Chem. Soc.* **1954**, 3488-3490.
- (3) Bradley, D. C.; Chatterjee, A. K.; Wardlaw, W. 439. Structural chemistry of the alkoxides. Part VI. Primary alkoxides of quadrivalent cerium and thorium. *J. Chem. Soc.* **1956**, 2260-2264.
- (4) Bradley, D. C.; Chatterjee, A. K.; Wardlaw, W. 671. Structural chemistry of the alkoxides. Part VII. Secondary alkoxides of quadrivalent cerium and thorium. *J. Chem. Soc.* **1956**, 3469-3472.
- (5) Blake, P. C.; Lappert, M. F.; Taylor, R. G.; Atwood, J. L.; Zhang, H. Some aspects of the coordination and organometallic chemistry of thorium and uranium ( $M^{III}$ ,  $M^{IV}$ ,  $U^V$ ) in +3 and +4 oxidation states. *Inorg. Chim. Acta* **1987**, 139, 13-20.
- (6) Hitchcock, P. B.; Lappert, M. F.; Singh, A.; Taylor, R. G.; Brown, D. Hydrocarbon-soluble, crystalline, four-co-ordinate chloro(aryl oxide)s, dialkylamido(aryl oxide)s and di[bis(trimethylsilyl)cyclopentadienyl]s of  $Th^{IV}$  and  $U^{IV}$ ; X-ray crystal structure of diethylamidotris(2,6-di-*t*-butylphenoxo)uranium(IV). *J. Chem. Soc., Chem. Commun.* **1983**, 561-563.
- (7) Berg, J. M.; Clark, D. L.; Huffman, J. C.; Morris, D. E.; Sattelberger, A. P.; Streib, W. E.; Van der Sluys, W. G.; Watkin, J. G. Early actinide alkoxide chemistry. Synthesis,

characterization, and molecular structures of thorium(IV) and uranium(IV) aryloxide complexes. *J. Am. Chem. Soc.* **1992**, *114*, 10811-10821.

(8) Parry, J. S.; Cloke, G. N.; Coles, S. J.; Hursthouse, M. B. Synthesis and Characterization of the First Sandwich Complex of Trivalent Thorium: A Structural Comparison with the Uranium Analogue. *J. Am. Chem. Soc.* **1999**, *121*, 6867-6871.

(9) Blake, P. C.; Edelstein, N. M.; Hitchcock, P. B.; Kot, W. K.; Lappert, M. F.; Shalimoff, G. V.; Tian, S. Synthesis, properties and structures of the tris(cyclopentadienyl)thorium(III) complexes  $[\text{Th}\{\eta^5\text{-C}_5\text{H}_3(\text{SiMe}_2\text{R})_{2-1,3}\}_3]$  (R=Me or <sup>t</sup>Bu). *J. Organomet. Chem.* **2001**, *636*, 124-129.

(10) Walensky, J. R.; Martin, R. L.; Ziller, J. W.; Evans, W. J. Importance of Energy Level Matching for Bonding in  $\text{Th}^{3+}\text{-Am}^{3+}$  Actinide Metallocene Amidinates,  $(\text{C}_5\text{Me}_5)_2[\text{PrNC}(\text{Me})\text{NPr}]\text{An}$ . *Inorg. Chem.* **2010**, *49*, 10007-10012.

(11) Siladke, N. A.; Webster, C. L.; Walensky, J. R.; Takase, M. K.; Ziller, J. W.; Grant, D. J.; Gagliardi, L.; Evans, W. J. Actinide Metallocene Hydride Chemistry: C–H Activation in Tetramethylcyclopentadienyl Ligands to Form  $[\mu\text{-}\eta^5\text{-C}_5\text{Me}_3\text{H}(\text{CH}_2)\text{-}\kappa\text{C}]^{2-}$  Tuck-over Ligands in a Tetrathorium Octahydride Complex. *Organometallics* **2013**, *32*, 6522-6531.

(12) Langeslay, R. R.; Fieser, M. E.; Ziller, J. W.; Furche, F.; Evans, W. J. Expanding Thorium Hydride Chemistry Through  $\text{Th}^{2+}$ , Including the Synthesis of a Mixed-Valent  $\text{Th}^{4+}/\text{Th}^{3+}$  Hydride Complex. *J. Am. Chem. Soc.* **2016**, *138*, 4036-4045.

(13) Langeslay, R. R.; Chen, G. P.; Windorff, C. J.; Chan, A. K.; Ziller, J. W.; Furche, F.; Evans, W. J. Synthesis, Structure, and Reactivity of the Sterically Crowded  $\text{Th}^{3+}$  Complex  $(\text{C}_5\text{Me}_5)_3\text{Th}$  Including Formation of the Thorium Carbonyl,  $[(\text{C}_5\text{Me}_5)_3\text{Th}(\text{CO})][\text{BPh}_4]$ . *J. Am. Chem. Soc.* **2017**, *139*, 3387-3398.

(14) Formanuk, A.; Ariciu, A.-M.; Ortu, F.; Beekmeyer, R.; Kerridge, A.; Tuna, F.; McInnes, E. J. L.; Mills, D. P. Actinide covalency measured by pulsed electron paramagnetic resonance spectroscopy. *Nat. Chem.* **2016**, *9*, 578.

(15) Altman, A. B.; Brown, A. C.; Rao, G.; Lohrey, T. D.; Britt, R. D.; Maron, L.; Minasian, S. G.; Shuh, D. K.; Arnold, J. Chemical structure and bonding in a thorium(III)–aluminum heterobimetallic complex. *Chem. Sci.* **2018**, *9*, 4317-4324.

(16) Korobkov, I.; Arunachalampillai, A.; Gambarotta, S. Cyclometalation and Solvent Deoxygenation during Reduction of a Homoleptic  $\text{Th}(\text{OAr})_4$  Complex: Serendipitous Formation of a Terminally Bonded Th–OH Function. *Organometallics* **2004**, *23*, 6248-6252.

(17) Yin, H.; Lewis, A. J.; Williams, U. J.; Carroll, P. J.; Schelter, E. J. Fluorinated diarylamide complexes of uranium(III, IV) incorporating ancillary fluorine-to-uranium dative interactions. *Chem. Sci.* **2013**, *4*, 798-805.

- (18) Mansell, S. M.; Kaltsoyannis, N.; Arnold, P. L. Small Molecule Activation by Uranium Tris(aryloxides): Experimental and Computational Studies of Binding of N<sub>2</sub>, Coupling of CO, and Deoxygenation Insertion of CO<sub>2</sub> under Ambient Conditions. *J. Am. Chem. Soc.* **2011**, *133*, 9036-9051.
- (19) Kerschner, J. L.; Fanwick, P. E.; Rothwell, I. P.; Huffman, J. C. Synthesis, structure, and spectroscopic properties of octahedral complexes of tungsten(VI), -(V), and -(IV) containing 2,6-diphenylphenoxide ligation. *Inorg. Chem.* **1989**, *28*, 780-786.
- (20) Coffindaffer, T. W.; Steffy, B. D.; Rothwell, I. P.; Folting, K.; Huffman, J. C.; Streib, W. E. Synthesis, structure, and bonding of mononuclear aryloxide derivatives of niobium in oxidation states +5, +3, +2, and +1. *J. Am. Chem. Soc.* **1989**, *111*, 4742-4749.
- (21) Steffey, B. D.; Fanwick, P. E.; Rothwell, I. P. Solid state structure of the tantalum bis-aryl compounds Ta(OAr-2,6R<sub>2</sub>)<sub>3</sub>(C<sub>6</sub>H<sub>5</sub>)<sub>2</sub> (R = CH<sub>3</sub>, Pr<sup>i</sup>; OAr-2,6R<sub>2</sub> = 2,6-dialkylphenoxide): Observation of a lack of correlation of M–OAr distances and M–O–Ar angles for aryloxide derivatives of niobium(V) and tantalum(V). *Polyhedron* **1990**, *9*, 963-968.
- (22) Stoll, S.; Schweiger, A. EasySpin, a comprehensive software package for spectral simulation and analysis in EPR. *J. Magn. Reson.* **2006**, *178*, 42-55.
- (23) Thomsen, M. K.; Nyvang, A.; Walsh, J. P. S.; Bunting, P. C.; Long, J. R.; Neese, F.; Atanasov, M.; Genoni, A.; Overgaard, J. Insights into Single-Molecule-Magnet Behavior from the Experimental Electron Density of Linear Two-Coordinate Iron Complexes. *Inorg. Chem.* **2019**, *58*, 3211-3218.
- (24) Chatt, J.; Gamlen, G. A.; Orgel, L. E. 86. The visible and ultraviolet spectra of some platinous amines. *J. Chem. Soc.* **1958**, 486-496.
- (25) Larsson, S.; Olsson, L.-F.; Rosén, A. Electronic structure of the PdCl<sub>4</sub><sup>2-</sup> and PtCl<sub>4</sub><sup>2-</sup> ions. *Int. J. Quantum Chem.* **1984**, *25*, 201-209.
- (26) Listemann, M. L.; Dewan, J. C.; Schrock, R. R. Monomeric tungsten(IV) phenoxide and thiolate complexes. *J. Am. Chem. Soc.* **1985**, *107*, 7207-7208.
- (27) Soriaga, R. A. D.; Nguyen, J. M.; Albright, T. A.; Hoffman, D. M. Diamagnetic Group 6 Tetrakis(di-tert-butylketimido)metal(IV) Complexes. *J. Am. Chem. Soc.* **2010**, *132*, 18014-18016.
- (28) Lewis, R. A.; Wu, G.; Hayton, T. W. Synthesis and Characterization of an Iron(IV) Ketimide Complex. *J. Am. Chem. Soc.* **2010**, *132*, 12814-12816.
- (29) Cirera, J.; Alemany, P.; Alvarez, S. Mapping the Stereochemistry and Symmetry of Tetracoordinate Transition-Metal Complexes. *Chem. Eur. J.* **2004**, *10*, 190-207.
- (30) Holleman, A. F.; Wiberg, E. *Inorganic Chemistry*. 1st ed.; Academic Press: Berlin, 2001.

- (31) Crabtree, R. H. *The Organometallic Chemistry of the Transition Metals*. 5th ed.; John Wiley & Sons, Inc.: Hoboken, NJ, 2009.
- (32) Hartwig, J. F. *Organotransition Metal Chemistry*. University of Science Books: Mill Valley, CA, 2010.
- (33) Kepert, D. L.; (2007). Aspects of the Stereochemistry of Eight-Coordination. In Progress in Inorganic Chemistry; Lippard, S. J.; (Ed.).
- (34) Lippard, S. J.; (2007). Eight-Coordination Chemistry. In Progress in Inorganic Chemistry; Cotton, F. A.; (Ed.).
- (35) Liptrot, D. J.; Power, P. P. London dispersion forces in sterically crowded inorganic and organometallic molecules. *Nat. Rev. Chem.* **2017**, *1*, 0004.
- (36) Osawa, E.; Onuki, Y.; Mislow, K. The central bond length in hexaphenylethane and hexakis(2,6-di-tert-butyl-4-biphenyl)ethane. *J. Am. Chem. Soc.* **1981**, *103*, 7475-7479.
- (37) Hounshell, W. D.; Dougherty, D. A.; Hummel, J. P.; Mislow, K. Structure of hexaphenylethane and congeners as determined by empirical force field calculations. *J. Am. Chem. Soc.* **1977**, *99*, 1916-1924.
- (38) Grimme, S.; Schreiner, P. R. Steric Crowding Can Stabilize a Labile Molecule: Solving the Hexaphenylethane Riddle. *Angew. Chem. Int. Ed.* **2011**, *50*, 12639-12642.
- (39) Kahr, B.; Van Engen, D.; Mislow, K. Length of the ethane bond in hexaphenylethane and its derivatives. *J. Am. Chem. Soc.* **1986**, *108*, 8305-8307.
- (40) Evans, W. J.; Traina, C. A.; Ziller, J. W. Synthesis of Heteroleptic Uranium ( $\mu$ - $\eta^6$ : $\eta^6$ -C<sub>6</sub>H<sub>6</sub>)<sub>2</sub>- Sandwich Complexes via Facile Displacement of ( $\eta^5$ -C<sub>5</sub>Me<sub>5</sub>)<sub>1</sub>- by Ligands of Lower Hapticity and Their Conversion to Heteroleptic Bis(imido) Compounds. *J. Am. Chem. Soc.* **2009**, *131*, 17473-17481.
- (41) Bergbreiter, D. E.; Killough, J. M. Reactions of potassium-graphite. *J. Am. Chem. Soc.* **1978**, *100*, 2126-2134.
- (42) Moehring, S. A.; Beltrán-Leiva, M. J.; Páez-Hernández, D.; Arratia-Pérez, R.; Ziller, J. W.; Evans, W. J. Rare-Earth Metal(II) Aryloxides: Structure, Synthesis, and EPR Spectroscopy of [K(2.2.2-cryptand)][Sc(OC<sub>6</sub>H<sub>2</sub>tBu<sub>2</sub>-2,6-Me-4)<sub>3</sub>]. *Chem. Eur. J.* **2018**, *24*, 18059-18067.
- (43) Chilton, N. F.; Goodwin, C. A. P.; Mills, D. P.; Winpenny, R. E. P. The first near-linear bis(amide) f-block complex: a blueprint for a high temperature single molecule magnet. *Chem. Commun.* **2015**, *51*, 101-103.
- (44) Goodwin, C. A. P.; Joslin, K. C.; Lockyer, S. J.; Formanuk, A.; Morris, G. A.; Ortu, F.; Vitorica-Yrezabal, I. J.; Mills, D. P. Homoleptic Trigonal Planar Lanthanide Complexes Stabilized by Superbulky Silylamide Ligands. *Organometallics* **2015**, *34*, 2314-2325.

- (45) Goodwin, C. A. P.; Chilton, N. F.; Vettese, G. F.; Moreno Pineda, E.; Crowe, I. F.; Ziller, J. W.; Winpenny, R. E. P.; Evans, W. J.; Mills, D. P. Physicochemical Properties of Near-Linear Lanthanide(II) Bis(silylamide) Complexes (Ln = Sm, Eu, Tm, Yb). *Inorg. Chem.* **2016**, *55*, 10057-10067.
- (46) Hitchcock, P. B.; Lappert, M. F.; Maron, L.; Protchenko, A. V. Lanthanum Does Form Stable Molecular Compounds in the +2 Oxidation State. *Angew. Chem. Int. Ed.* **2008**, *47*, 1488-1491.
- (47) Gabbaï, F. P.; Chirik, P. J.; Fogg, D. E.; Meyer, K.; Mindiola, D. J.; Schafer, L. L.; You, S.-L. An Editorial About Elemental Analysis. *Organometallics* **2016**, *35*, 3255-3256.
- (48) Rabe, G. W.; Ziller, J. W. Phosphido Complexes of the Lanthanides. Synthesis and x-ray Crystal Structure Determination of a Tris(phosphido) Species of Neodymium: Nd[P(SiMe<sub>3</sub>)<sub>2</sub>]<sub>3</sub>(thf)<sub>2</sub>. *Inorg. Chem.* **1995**, *34*, 5378-5379.
- (49) Palumbo, C. T.; Halter, D. P.; Voora, V. K.; Chen, G. P.; Chan, A. K.; Fieser, M. E.; Ziller, J. W.; Hieringer, W.; Furche, F.; Meyer, K.; Evans, W. J. Metal versus Ligand Reduction in Ln<sup>3+</sup> Complexes of a Mesitylene-Anchored Tris(Aryloxy) Ligand. *Inorg. Chem.* **2018**, *57*, 2823-2833.
- (50) Tao, J.; Perdew, J. P.; Staroverov, V. N.; Scuseria, G. E. Climbing the Density Functional Ladder: Nonempirical Meta--Generalized Gradient Approximation Designed for Molecules and Solids. *Phys. Rev. Lett.* **2003**, *91*, 146401.
- (51) Grimme, S. Semiempirical GGA-type density functional constructed with a long-range dispersion correction. *J. Comput. Chem.* **2006**, *27*, 1787-1799.
- (52) Küchle, W.; Dolg, M.; Stoll, H.; Preuss, H. Energy-adjusted pseudopotentials for the actinides. Parameter sets and test calculations for thorium and thorium monoxide. *J. Chem. Phys.* **1994**, *100*, 7535-7542.
- (53) Cao, X.; Dolg, M. Segmented contraction scheme for small-core actinide pseudopotential basis sets. *Comput. Theor. Chem.* **2004**, *673*, 203-209.
- (54) Schäfer, A.; Horn, H.; Ahlrichs, R. Fully optimized contracted Gaussian basis sets for atoms Li to Kr. *J. Chem. Phys.* **1992**, *97*, 2571-2577.
- (55) Treutler, O.; Ahlrichs, R. Efficient molecular numerical integration schemes. *J. Chem. Phys.* **1995**, *102*, 346-354.
- (56) Schäfer, A.; Klamt, A.; Sattel, D.; Lohrenz, J. C. W.; Eckert, F. COSMO Implementation in TURBOMOLE: Extension of an efficient quantum chemical code towards liquid systems. *Phys. Chem. Chem. Phys.* **2000**, *2*, 2187-2193.

- (57) CRC Handbook of Chemistry and Physics, 81st ed. Lide, D. R., Ed.; CRC Press: Boca Raton, FL, 2008; Chapter 8, p 136.
- (58) Adamo, C.; Barone, V. Toward reliable density functional methods without adjustable parameters: The PBE0 model. *J. Chem. Phys.* **1999**, *110*, 6158-6170.
- (59) Furche, F. A., R.; Haettig, C.; Klopper, W.; Sierka, M.; Weigend, F. Turbomole. *Comp. Mol. Sci.* **2014**, *4*, 91-100.
- (60) APEX2 Version 2014.11-0, B. A., Inc.; Madison, WI 2014, In.
- (61) SAINT Version 8.34a, B. A., Inc.; Madison, WI 2013.
- (62) SADABS; Sheldrick, G. M., Version 2014/5, Bruker AXS, Inc.; Madison, WI 2014.
- (63) SHELXTL; Sheldrick, G. M., Version 2014/7, Bruker AXS, Inc.; Madison, WI 2014.
- (64) International Tables for Crystallography 1992, V. C., Dordrecht: Kluwer Academic; Publishers.
- (65) Spek, A. L., PLATON, Acta. Cryst. 2009, D65, 148-155.



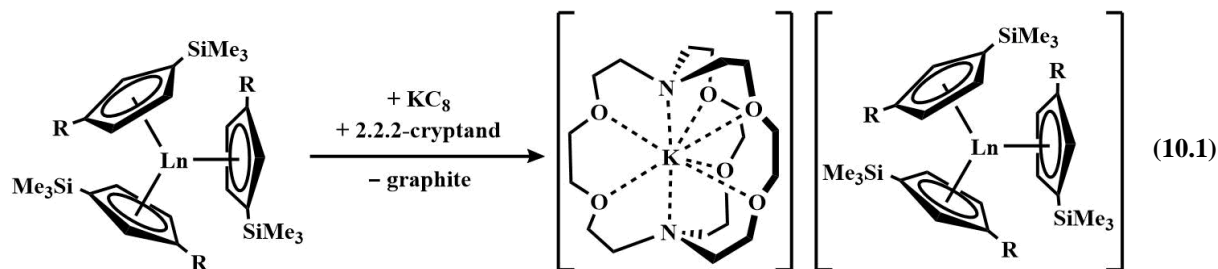
## CHAPTER 10

### Exploring $4f^{n+1}$ vs $4f^n 5d^1$ Electron Configurations for Complexes of Lanthanide(II) Ions Using X-ray Photoelectron Spectroscopy

#### Introduction

As described in Chapter 1, in the lanthanide series the +2 oxidation state has been extended from six examples, Eu, Yb, Sm, Tm, Dy, and Nd, to all the metals in the series except Pm which was not studied due to its radioactivity.<sup>1-2</sup> This was surprising since the reduction potentials calculated to convert a  $4f^n$  Ln(III) ion to a  $4f^{n+1}$  Ln(II) ion were predicted to be too large for the metals other than, Eu, Yb, Sm, Tm, Dy, and Nd, to form isolable complexes that would not react with solvents.<sup>3</sup> Solid state data were also consistent with this picture in that Ln + I<sub>2</sub> reactions under forcing conditions gave  $4f^{n+1}$  Ln(II) products, Ln<sup>II</sup>I<sub>2</sub>, only for the six metals listed above. For all the other metals, the LnI<sub>2</sub> products were identified as Ln<sup>III</sup>(I)<sub>2</sub>(e), *i.e.* Ln(III) salts with a delocalized electron in the lattice.<sup>4-6</sup>

The new molecular examples of lanthanides in the +2 oxidation state were synthesized by reducing the  $4f^n$  Ln(III) precursors, Cp'<sub>3</sub>Ln (Ln = La, Ce, Pr, Nd)<sup>7-8</sup> and Cp'<sub>3</sub>Ln (Cp' = C<sub>5</sub>H<sub>4</sub>SiMe<sub>3</sub>; Ln = La, Ce, Pr, Gd, Tb, Dy, Ho, Er, Lu),<sup>1-2</sup> using potassium graphite (KC<sub>8</sub>) in the presence of a chelating agent 2.2.2-cryptand (crypt) to form [K(crypt)][Cp'<sub>3</sub>Ln], eq 10.1.



R = H, Ln = Y, La, Ce, Pr, Nd, Gd, Tb, Dy, Ho, Er, and Lu  
R = SiMe<sub>3</sub>, Ln = La, Ce, Pr, Nd

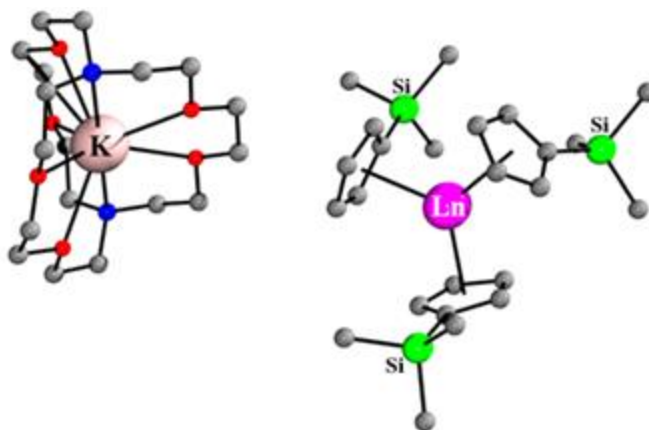


**Figure 10.1.** Ball-and-stick model of single-crystal X-ray structure of  $[\text{K}(\text{crypt})][(\text{C}_5\text{H}_4\text{SiMe}_3)_3\text{Ln}]$ .

Additional examples of Ln(II) complexes were subsequently isolated using various cyclopentadienyl analogs such as  $(\text{C}_5\text{Me}_4\text{H})^{1-}$ ,<sup>9</sup>  $[\text{C}_5\text{H}_2(\text{CMe}_3)_3]^{1-}$ ,<sup>10</sup>  $[\text{C}_5\text{H}_4(\text{CMe}_3)]^{1-}$ ,<sup>11</sup> and  $(\text{C}_5\text{H}_4\text{Me})^{1-}$ <sup>12</sup> as well as  $[\text{N}(\text{SiMe}_3)_2]^{1-}$ ,<sup>13</sup>  $[\text{OC}_6\text{H}_2(\text{CMe}_3)_{2-2,6-\text{Me}-4}]^{1-}$ ,<sup>14</sup> and the tris(aryloxy)mesitylene,  $[(^{\text{Ad,Me}}\text{ArO})_3\text{mes}]^{1-}$ .<sup>15-16</sup> For all the new examples of complexes of Ln(II) ions, structural, spectroscopic, and magnetic data as well as analysis by density functional theory (DFT), indicated that the product of reducing a  $4f^n$  Ln(III) ion was not the expected  $4f^{n+1}$  Ln(II) but instead a  $4f^n 5d^1$  Ln(II) ion.<sup>1-2, 17</sup> This meant that the previously calculated reduction potentials did not apply. This result also matched with the solid-state data since the delocalized electron in the  $\text{Ln}^{\text{III}}\text{I}_2(\text{e})$  compounds was assigned to a 5d band.

The unusual nature of the  $4f^n 5d^1$  mixed principal quantum number configuration made it an ideal topic for detailed spectroscopic studies. For example, the electronic structure of the  $[\text{K}(\text{crypt})][\text{Cp}'_3\text{Ln}]$  complexes of Ln = Pr, Nd, Sm, Gd, Tb, Dy, Y, Ho, Er, Tm, Yb and Lu was examined by X-ray absorption near-edge spectroscopy (XANES).<sup>18</sup> Surprisingly, the XANES shifts of the new ions are only slightly different than those of the Ln(III)  $\text{Cp}'_3\text{Ln}$

precursors. Initially, there was concern that the samples decomposed on the way to the synchrotron or in the beam. However, calculations showed why the spectra were similar for the  $4f^n5d^1$  ions.<sup>18</sup>

X-ray photoelectron spectroscopy (XPS) provides a complementary approach to defining electronic structure of molecules by evaluation of the core and valence orbitals. Since excellent XPS facilities are available at UC Irvine that have a sample entry system inside a glovebox, it was of interest to examine the highly reactive Ln(II) complexes by this method. Samples could be crystallized the night before analysis and loaded into the instrument with little risk of decomposition.

Molecular organometallic lanthanide complexes of this type have yet to be characterized by XPS. Prior studies of XPS of lanthanides have focused on the metals, metal oxides, metal chalcogenides, phosphates, and alloys.<sup>19-25</sup> These are also known to have complicated surface chemistry that involves adsorbed water or other contaminants that further complicate the interpretation of the data. Preliminary data are presented here on a pristine set of crystalline molecular species which serve to interrogate the electronic structure of the new ions by a new method and to demonstrate the value of XPS in molecular lanthanide chemistry. The complexes  $[\text{Cp}'_3\text{Ln}]^{1-}$  (Ln = Sm, Eu, Gd, Tb) were chosen because Sm(II) and Eu(II) are traditional Ln(II) ion with a  $4f^6$  and  $4f^7$  configurations, respectively, electron configuration and because Gd(II) and Tb(II) have been assigned  $4f^75d^1$  and  $4f^85d^1$  configurations. These four were also selected because they are adjacent in the periodic table which means that their ionic radii are similar and any charge/radius effects should be similar. The neutral Ln(III) precursors,  $\text{Cp}'_3\text{Ln}$ , were also examined for comparison.

## Results and Discussion

**Sample Preparation and Data Collection.** With the assistance of Sierra R. Ciccone, crystalline samples of  $\text{Cp}'_3\text{Ln}$  and  $[\text{K}(\text{crypt})][\text{Cp}'_3\text{Ln}]$  ( $\text{Cp}' = [\text{C}_5\text{H}_4\text{SiMe}_3]^{1-}$ ; Ln = Sm, Eu, Gd, Tb) were prepared according to previously published procedures.<sup>17</sup> The prepared samples were transferred to a Schlenk tube with a Teflon screw cap and then placed on a high-vacuum line ( $10^{-5}$  torr) overnight to remove residual solvent from sample preparation. The Schlenk tube was then transferred to a  $\text{N}_2$  glovebox which is directly attached to the XPS instrument, AXIS Supra by Kratos Analytical. In the glovebox, the lanthanide samples were then mounted on a stainless-steel stub with double-sided copper tape. The stub was then transferred from the glovebox into the XPS instrument for measurement and samples were measured with the assistance of Dr. Jared P. Bruce from the laboratory of Prof. John C. Hemminger. Control samples of  $\text{KCp}'$  and 2.2.2-cryptand were also measured and analyzed by XPS. All data are summarized in Table 10.1.

**Table 10.1.** Summary of binding energies (eV) of measured samples  $\text{Cp}'_3\text{Ln}$  and  $[\text{K}(\text{crypt})][\text{Cp}'_3\text{Ln}]$  (Ln = Sm, Eu, Gd, Tb).

	Ln 4d <sub>3/2</sub>	Ln 4d <sub>5/2</sub>	Si 2s	C 1s <sub>ring</sub>	C 1s <sub>methyl</sub>	C 1s <sub>crypt</sub>
$\text{Cp}'_3\text{Sm}$	134.5	130.8	149.2	281.3	282.2	
$[\text{Cp}'_3\text{Sm}]^{1-}$			148.9	280.9	281.8	283.3
$\text{Cp}'_3\text{Eu}$	139.2	133.8	149.1	281.3	282.3	
$[\text{Cp}'_3\text{Eu}]^{1-}$	138.3	132.5	148.5	280.6	281.7	283.3
$\text{Cp}'_3\text{Gd}$	145.9	139.9	148.7			
$[\text{Cp}'_3\text{Gd}]^{1-}$	144.9	138.7	148.3	280.5	281.7	283.3
$\text{Cp}'_3\text{Tb}$			148.7	281.1	282.4	
$[\text{Cp}'_3\text{Tb}]^{1-}$			148.2	280.5	282.0	283.3

**Samarium.** The 4d regions of both  $\text{Cp}'_3\text{Sm}^{\text{III}}$  and  $[\text{K}(\text{crypt})][\text{Cp}'_3\text{Sm}^{\text{II}}]$  were measured, Figure 10.2. The Sm(III) and Sm(II)  $4d_{3/2}$  and  $4d_{5/2}$  peaks are not well resolved. However, a

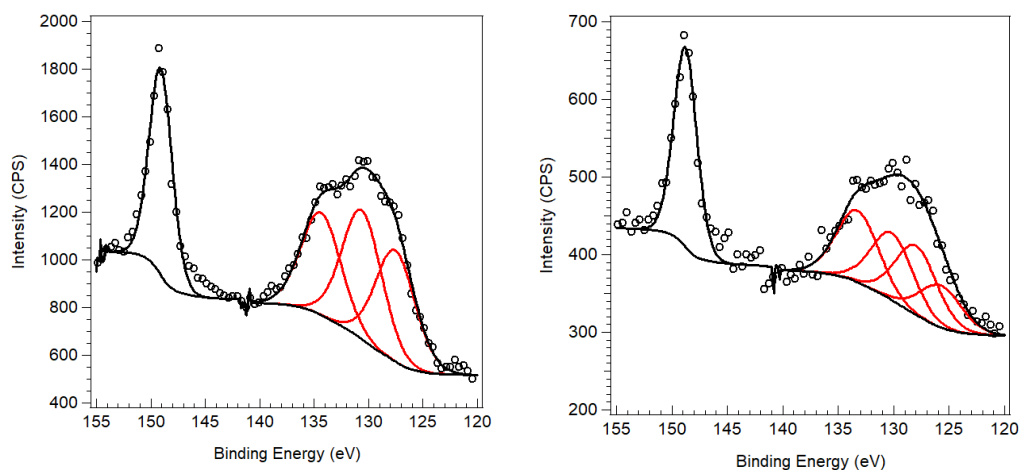


**Figure 10.2.** Sm 4d XPS region of  $\text{Cp}'_3\text{Sm}^{\text{III}}$  (left) and  $[\text{K}(\text{crypt})][\text{Cp}'_3\text{Sm}^{\text{II}}]$  (right).

70% Gaussian and 30% Lorentzian model of the Sm(III) spectrum reveals three unique traces, shown in red, which could be attributed to  $4d_{3/2}$  (134.5 eV),  $4d_{5/2}$  (130.8 eV), and a satellite peak (127.7 eV). The satellite peak could be a result of a shake-down process which will be discussed in the Eu 4d section below. In the Sm(II) spectrum, similar features are observed, however, higher resolution is necessary to confidently assign the  $4d_{3/2}$  and  $4d_{5/2}$  peaks. The Si 2s peak is also present in both Sm(III) (Si 2s: 149.2 eV) and Sm(II) (148.9 eV) spectra.

The C 1s regions of the Sm(III) and Sm(II) complexes were also examined, Figure 10.3. In the Sm(III) spectrum, three features can be modeled. The peak located at 281.3 eV is assigned as the cyclopentadienide ring (C 1<sub>sring</sub>) and the peak at 282.2 eV is attributed to the methyl carbon (C 1<sub>smethyl</sub>). However, the smaller peak at 283.4 eV is unknown. In the Sm(II) spectrum, similar features are observed for the C 1<sub>sring</sub> (280.9 eV) and C 1<sub>smethyl</sub> (281.8 eV). Unlike the

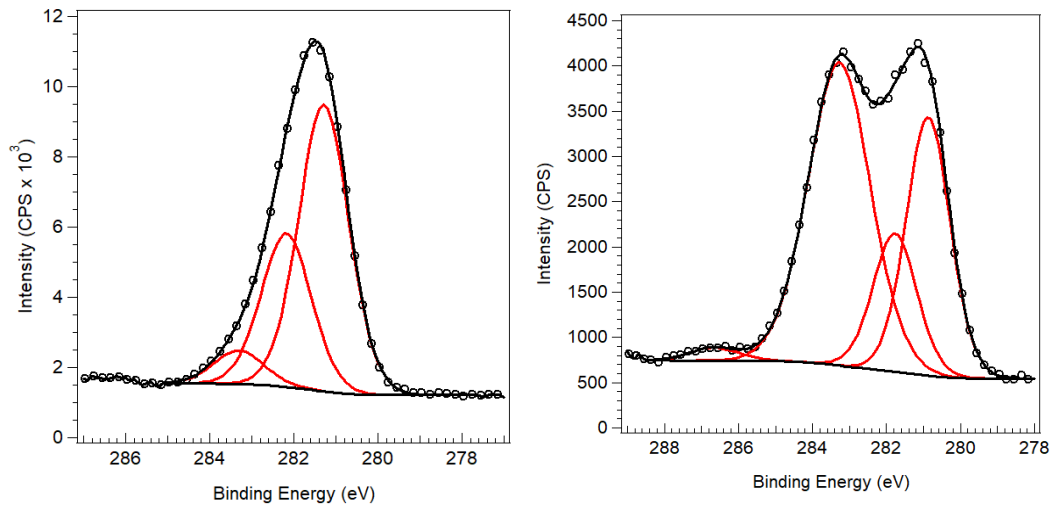


**Figure 10.3.** C 1s XPS region of Cp'3Sm<sup>III</sup> (left) and [K(crypt)][Cp'3Sm<sup>II</sup>] (right).

Sm(III) C 1s spectrum, an additional intense feature is present at 283.3 eV which is assigned as the carbon atoms in the [K(crypt)]<sup>1+</sup> cation (C 1<sub>crypt</sub>). At higher binding energies, a weak shake-up peak at 286.7 eV is present.

**Europium.** The 4d regions of both Cp'3Eu<sup>III</sup> and [K(crypt)][Cp'3Eu<sup>II</sup>] were measured, Figure 10.4. Binding energies of the well-separated Eu 4d<sub>3/2</sub> and Eu 4d<sub>5/2</sub> peaks, unlike the

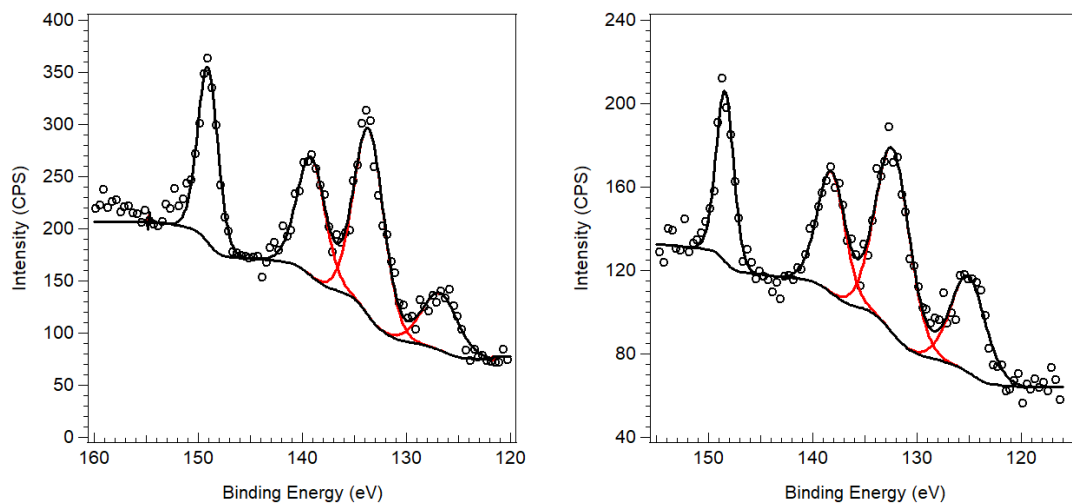


**Figure 10.4.** Eu 4d XPS region of Cp'3Eu<sup>III</sup> (left) and [K(crypt)][Cp'3Eu<sup>II</sup>] (right).

above-mentioned Sm spectra, were determined for both the Eu(III) ( $4d_{3/2}$ : 139.2 eV,  $4d_{5/2}$ : 133.8 eV) and Eu(II) ( $4d_{3/2}$ : 138.3 eV,  $4d_{5/2}$ : 132.5 eV) complexes and are summarized in Table 10.1. A satellite peak is present in both the Eu(III) (127.0 eV) and Eu(II) (125.3 eV) spectra at binding energies lower than the  $4d_{5/2}$  peak. These features have been previously reported as a shake-down satellite peak due to a reorganization of the 4f sub-shell.<sup>22</sup> This shake-down peak is likely also present in the Sm 4d spectra described above. However, this satellite peak overlaps with the Sm  $4d_{3/2}$  and  $4d_{5/2}$  peaks. Additionally, the Si 2s peak from the Cp' ligand is observed in both the Eu(III) (Si 2s: 149.1 eV) and Eu(II) (Si 2s: 148.5 eV) spectra as presented in Figure 10.2. These are nearly identical to the Si 2s peaks in the Sm spectra as well. The Eu 4d and Si 2s peaks are overall shifted to more negative binding energies from the Eu(III) to Eu(II) sample which is suggestive of a reductive change in oxidation state.

The C 1s regions of the Eu(III) and Eu(II) samples were also analyzed, Figure 10.3. Several features are nearly identical to the peaks described in the Sm C 1s spectra. These are identified as the Cp' ring carbon atoms for both Eu(III) and Eu(II) compounds and the carbon atoms in the [K(crypt)]<sup>1+</sup> cation for the Eu(II) compound. In the Eu(III) C 1s spectrum (Figure 10.3; left), the most intense feature in the fitted red trace ( $C\ 1s_{ring}$ : 281.3 eV) could be best attributed to the ring carbon atoms. The negative charge in the cyclopentadienide ring shifts the carbon binding energies more negative in comparison to the methyl carbon atoms ( $C\ 1s_{methyl}$ : 282.3 eV) in the trimethylsilyl group. In the Eu(II) C 1s spectrum (Figure 10.3; right), similar

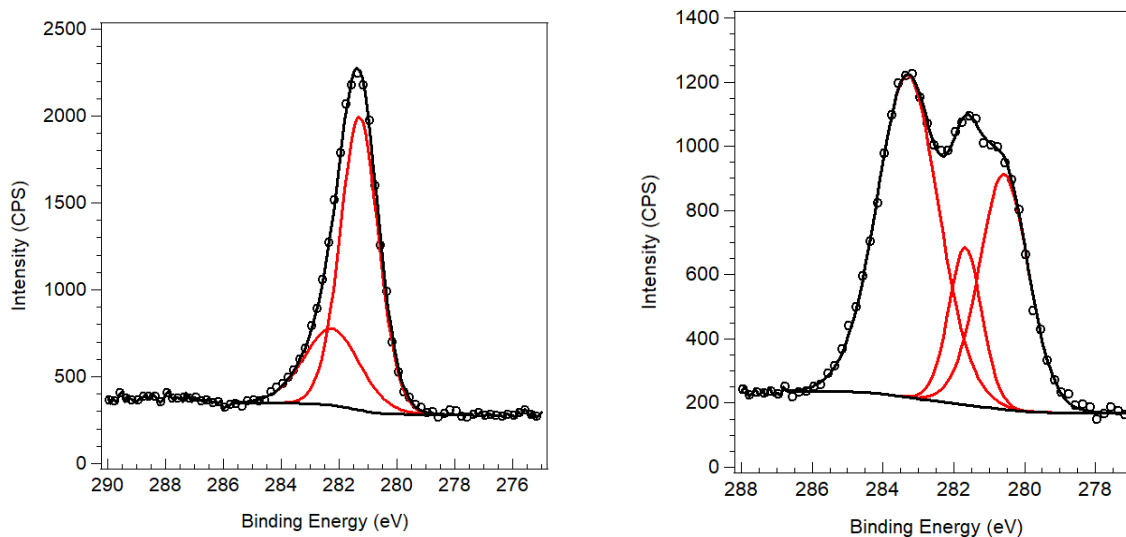


**Figure 10.5.** C 1s XPS region of Cp'<sub>3</sub>Eu<sup>III</sup> (left) and [K(crypt)][Cp'<sub>3</sub>Eu<sup>II</sup>] (right).

Cp' features with more negative shifts are observed (C 1s<sub>ring</sub>: 280.6 eV; C 1s<sub>methyl</sub>: 281.7 eV). An additional intense feature is present which could be assigned C 1s crypt intensities from the [K(crypt)]<sup>1+</sup> cation (C 1s<sub>crypt</sub>: 283.3 eV).

**Gadolinium.** The Gd(III) and Gd(II) spectra measured for the 4d region and the Gd 4d<sub>3/2</sub> and Gd 4d<sub>5/2</sub> peaks are well-resolved, Figure 10.6. The Gd(III) 4d<sub>3/2</sub> is located at 145.9 eV and Gd(III) 4d<sub>5/2</sub> is located at 139.9 eV. For the Gd(II), the 4d<sub>3/2</sub> is located at 144.9 eV and 4d<sub>5/2</sub> is located at 138.7 eV. The peak shifts between the two spectra is approximately 1 eV which is suggestive of a change in oxidation state from Gd(III) and Gd(II). Additionally, unlike the Sm and Eu 4d regions, shake-down features are not evident in these Gd 4d spectra. The Si 2s peak in the Gd(III) spectrum is located at 148.7 eV and 148.3 eV in the Gd(II) spectrum. These Si 2s shifts are nearly identical to the previously described Sm and Eu Si 2s spectra.



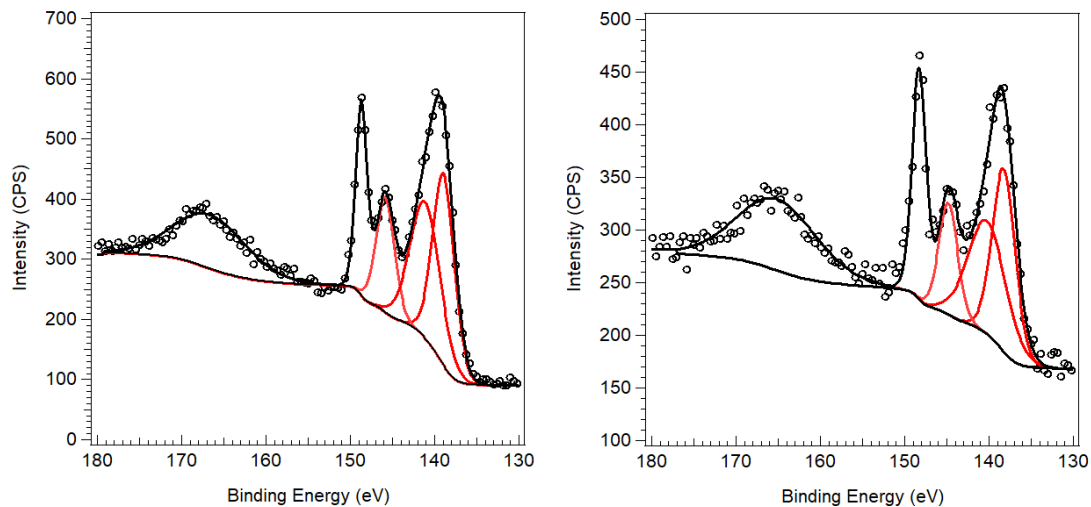


**Figure 10.6.** Gd 4d XPS region of  $\text{Cp}'_3\text{Gd}^{\text{III}}$  (left) and  $[\text{K}(\text{crypt})][\text{Cp}'_3\text{Gd}^{\text{II}}]$  (right).

The C 1s region of the Gd(III) complex possesses features similar to the previously described Sm(III) and Eu(III) complexes. However, unlike the Sm(III) and Eu(III) C 1s spectra, the weaker intensity peaks are not observed, Figure 10.7. The features in the Gd(II) C 1s

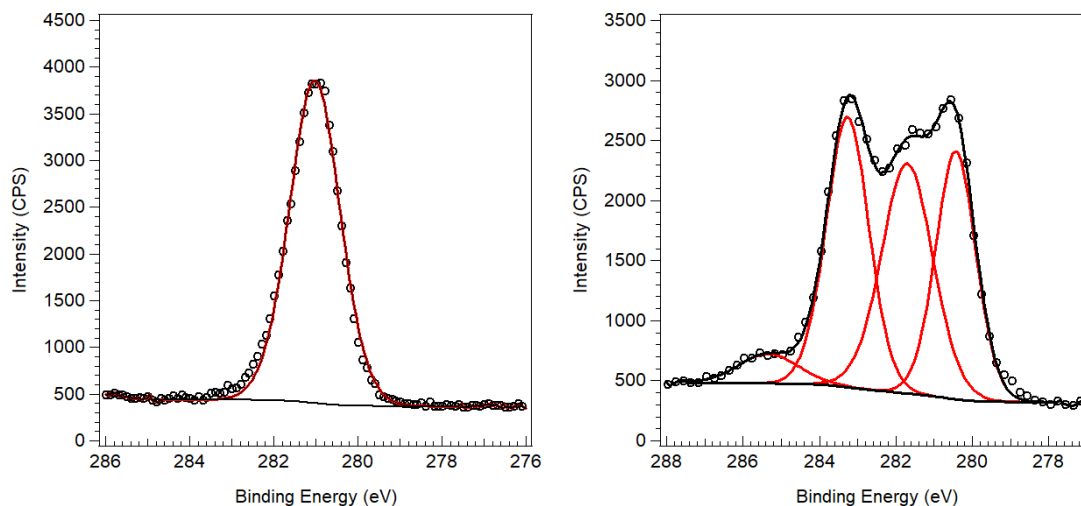


**Figure 10.7.** C 1s XPS region of  $\text{Cp}'_3\text{Gd}^{\text{III}}$  (left) and  $[\text{K}(\text{crypt})][\text{Cp}'_3\text{Gd}^{\text{II}}]$  (right).

spectrum are similar to the features previously described for the Sm(II) C 1s spectrum including a weak shake-up peak located at 285.4 eV.

The valence spectrum was measured and analyzed for Gd(III) and Gd(II) because this region is less complicated in comparison to Sm, Eu, and Tb, Figure 10.8. The most intense

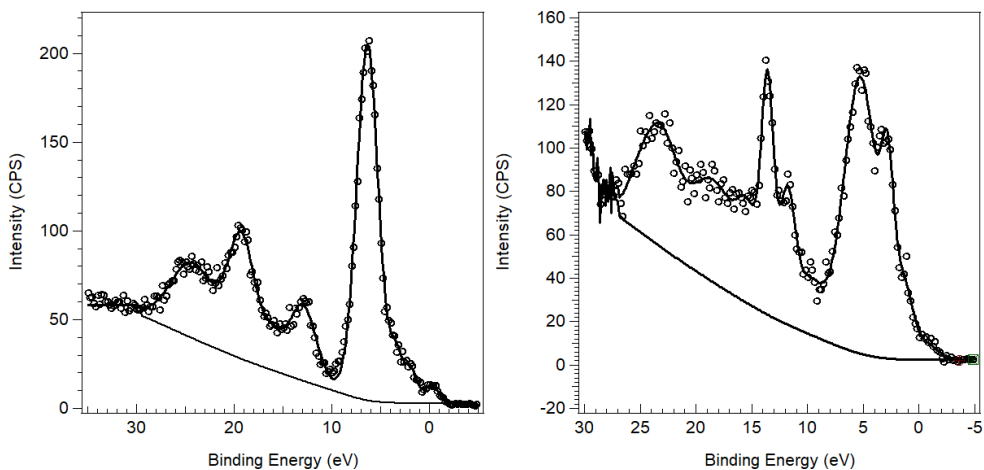


**Figure 10.8.** Valence XPS region of Cp'3Gd<sup>III</sup> (left) and [K(crypt)][Cp'3Gd<sup>II</sup>] (right).

peaks in both spectra are the Gd 4f peaks: Gd(III) 4f: 6.4 eV and Gd(II) 4f: 5.4 eV. The Gd 5p peaks are also observable in both spectra: Gd(III) 5p<sub>1/2</sub>: 24.5 eV, Gd(III) 5p<sub>3/2</sub>: 19.4 eV, Gd(II) 5p<sub>1/2</sub>: 23.6 eV, Gd(II) 5p<sub>3/2</sub>: 18.8 eV. Peaks associated with Cp' are also identifiable in the valence region. Measurements from the KCp' control sample, Figure 10.9, revealed a K 3p (13.7 eV) peak

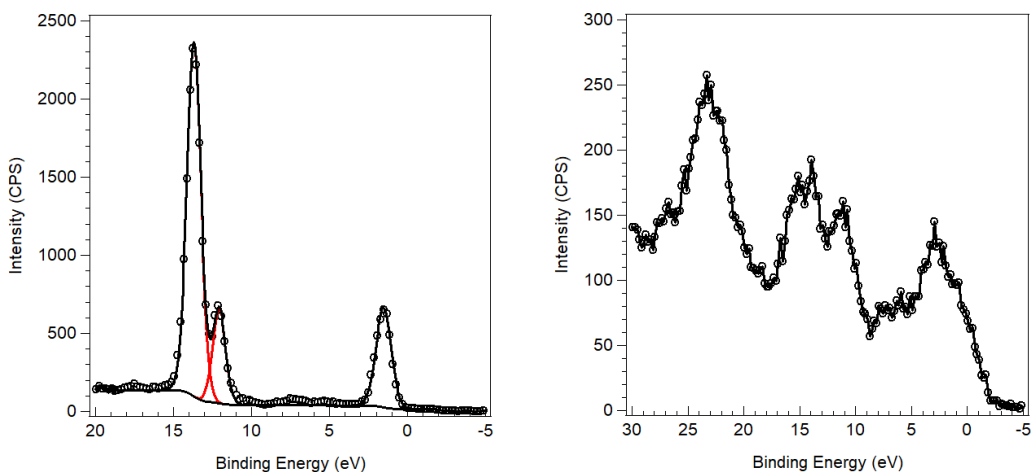


**Figure 10.9.** Valence XPS region of KCp' (left) and 2.2.2-cryptand (right).

and two ligand based peaks at 12.1 and 1.6 eV. Therefore, the valence peaks in the Gd(III) spectrum located at 13.1 eV and the shoulder at 3.4 eV arise from the Cp' ligand and these are 11.8 and 3.0 eV in the Gd(II) valence spectrum, Table 10.1. The K 3p peak in the Gd(II) valence spectrum is located at 13.6 eV. The shoulder in the Gd(II) spectrum (Figure 10.8, left) located at 1.3 eV could be assigned as the 5d orbital, but theoretical calculations that will be discussed later in this Chapter were necessary to confirm its identity.

**Terbium.** The Tb(III) and Tb(II) 4d regions contain three peaks attributed to 4d. However the 4d<sub>3/2</sub> and 4d<sub>5/2</sub> peaks cannot be specified. However, the Si 2s peak is identifiable by its most intense peak: Tb(III) Si 2s (148.7 eV) and Tb(II) Si 2s (148.2 eV).

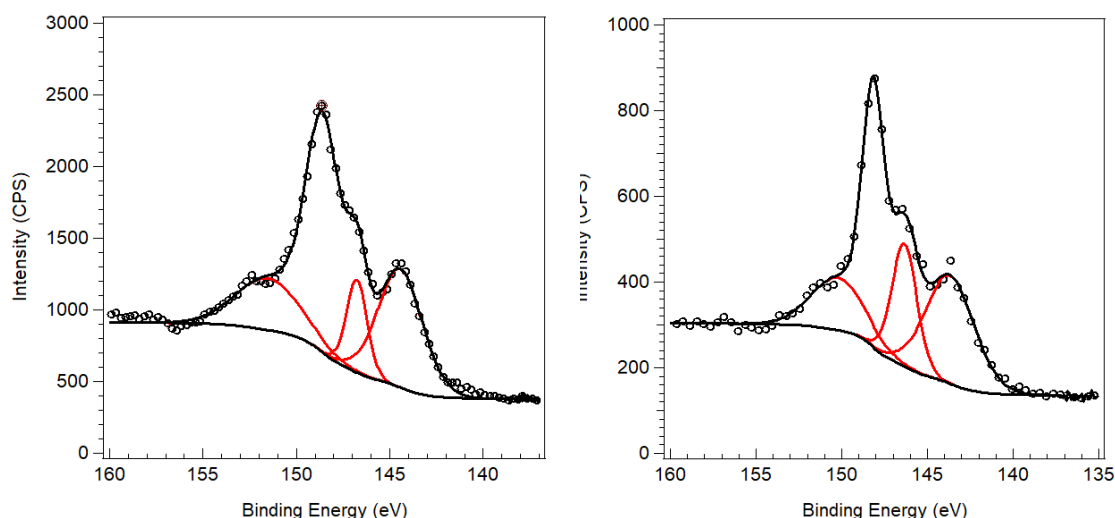


**Figure 10.10.** Tb 4d XPS region of Cp'3Tb<sup>III</sup> (left) and [K(crypt)][Cp'3Tb<sup>II</sup>] (right).

The Tb(III) C 1s spectrum contain peaks, the C 1s<sub>ring</sub> (281.1 eV) and C 1s<sub>methyl</sub> (282.4 eV) with similar in binding energies to the Sm(III), Eu(III), and Gd(III) C 1s peaks. Additionally, the Tb(II) C 1s peaks are nearly identical to the Sm(II), Eu(II), and Gd(II) spectra with shake-up (285.8 eV) and shake-down (279.4 eV) peaks.

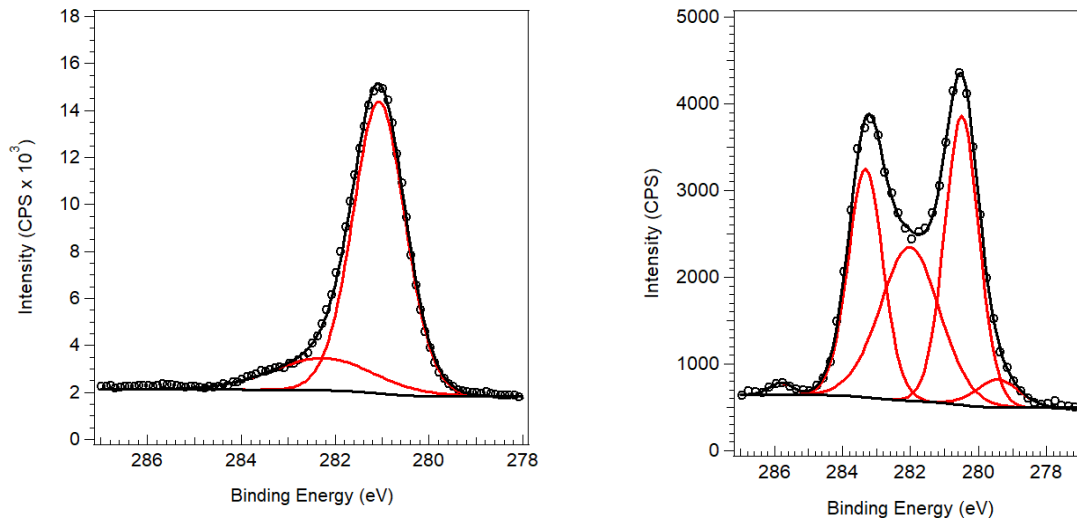


**Figure 10.11.** C 1s XPS region of Cp'3Tb<sup>III</sup> (left) and [K(crypt)][Cp'3Tb<sup>II</sup>] (right).

**Theoretical Calculations.** Calculations were performed by Sree Ganesh Balasubramani in the laboratory of Prof. Filipp Furche. The calculations use the random phase approximation (RPA) which is a post-Kohn-Sham density functional approximation that incorporates van der Waals interactions. The RPA occupation number derivatives approach is used for the calculation of the valence and core ionization potentials of these lanthanide complexes.

The geometries of the [Cp'3Ln]<sup>1-</sup> (Ln = Eu, Gd) complexes were optimized within DFT using the hybrid Tao-Perdew-Scuseria-Staroverov (TPSSH) functional including the D3 dispersion correction of Grimme. Gridsize 4 with weight derivatives were used for the DFT numerical integration. The conductor like solvation model (COSMO) was used to model the effects of the THF solvent (dielectric constant of 7.52). The def2-SVP basis set was used for all the atoms except for H atoms for which the def2-SV(P) basis set was used.

For the calculation of ionization potentials (IPs), RPA occupation number derivatives were used with the TPSS input orbitals and orbital energies. The basis sets that were used for the geometry optimizations were the same ones used for the IP calculations also except for the metal

atom for which the def2-TZVPP basis set was used to better describe the valence ionization spectrum.

**Table 10.2.** Calculated binding energies (eV) of Cp<sub>3</sub>Gd and [Cp<sub>3</sub>Gd]<sup>1-</sup>.

Orbital	Gd(III)	Gd(II)	Shift
<b>4f</b>	-10.16	-8.64	1.52
	-9.95	-8.35	1.60
	-9.83	-8.36	1.46
	-9.69	-8.40	1.29
	-10.13	-7.98	2.15
	-10.13	-8.20	1.93
	-9.67	-8.61	1.07
<b>5d</b>		-1.76	

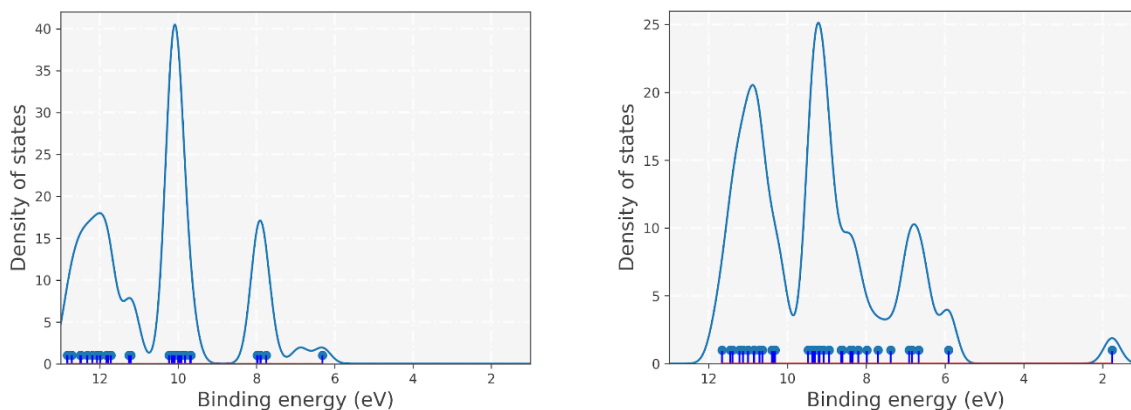


**Figure 10.12.** The density of states in the valence region for the Gd(III) (left) and the Gd(II) (right) complexes broadened using gaussian functions with a half width at half maximum of 0.5 eV.

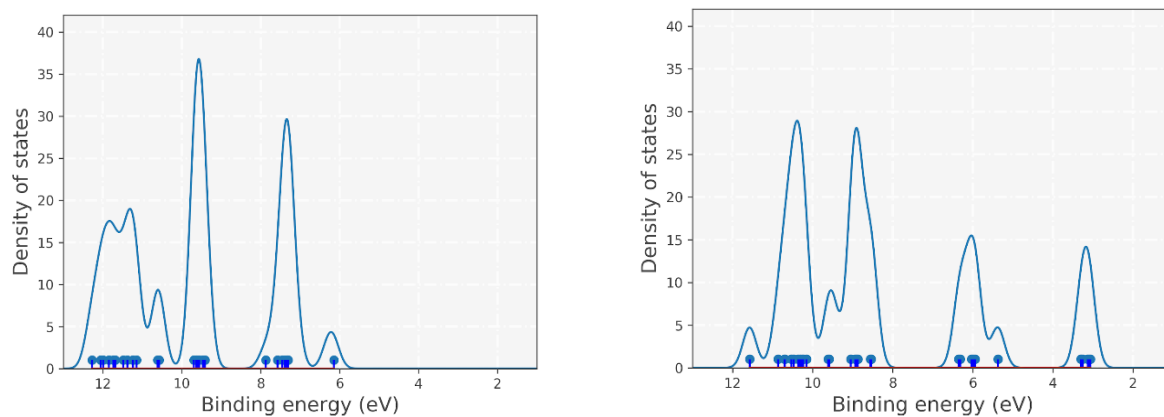


**Figure 10.13.** The density of states in the valence region for the Eu(III) (left) and the Eu(II) (right) complexes broadened using gaussian functions with a half width at half maximum of 0.5 eV.

## Conclusions

XPS measurements of  $\text{Cp}'_3\text{Ln}$  and  $[\text{K}(\text{crypt})][\text{Cp}'_3\text{Ln}]$  ( $\text{Ln} = \text{Sm}, \text{Eu}, \text{Gd}, \text{Tb}$ ) were analyzed for the Ln 4d, Si 2s, and C 1s regions. Experimentally, the oxidation state shifts from Ln(III) to Ln(II) range from 0.3 to 1.0 eV based on the Ln 4d and Si 2s peaks. Diagnostically, the Si 2s peak has been simple to identify despite its overlap in the Gd and Tb 4d region for all analyzed complexes. Shake-up and shake-down features are observed in the Ln 4d and C 1s regions. However, more analysis is required to understand the final state effects associated for each satellite feature. The valence regions of the Gd(III) and Gd(II) complex were analyzed and all Gd, K, and ligand peaks were confirmed by binding energy comparisons with  $\text{KCp}'$ . A shoulder peak in the valence Gd(II) region at approximately 1.3 eV was identified as a 5d peak which was then corroborated by DFT calculations. The simplified Gd valence region allows for easier experimental identification of the 5d orbital and simplified DFT calculations due to its spin-only  $4f^7$  and  $4f^75d^1$  electron configuration. Both the data and the calculations are consistent

with a change in formal metal oxidation state of +3 to +2 upon reduction of Cp<sub>3</sub>Ln to [K(crypt)][Cp<sub>3</sub>Ln].

## Experimental

XPS was performed on a Kratos Axis Supra DLD spectrometer (Kratos Analytical Ltd.) with monochromated Al K $\alpha$  radiation (1486.6 eV) at 10-mA emission current and 15-kV anode voltage with a base pressure of  $1 \times 10^{-9}$  Torr. One set of experiments was performed with the charge neutralizer with a filament current of 1.8 A and a bias of 3.0 V while the remaining spectra were collected without charge neutralization. Spectra were collected with a fixed-analyzer transmission mode, survey scans were collected with a pass energy of 160 eV while high-resolution scans of individual elements were collected with a pass energy of 20 eV. All samples were mounted on a stainless steel stub with double-sided copper tape in a nitrogen - filled glovebox attached to the XPS. Samples were fabricated in a different argon-filled glovebox and transported under vacuum in a sealed vial to the glovebox attached to the XPS. Peak fitting was performed with CasaXPS software (Casa Software Ltd.) using a Shirley baseline and 70% Gaussian – 30% Lorentzian function for the peaks unless otherwise indicated.

## References

- (1) MacDonald, M. R.; Bates, J. E.; Ziller, J. W.; Furche, F.; Evans, W. J., Completing the Series of +2 Ions for the Lanthanide Elements: Synthesis of Molecular Complexes of Pr<sup>2+</sup>, Gd<sup>2+</sup>, Tb<sup>2+</sup>, and Lu<sup>2+</sup>. *J. Am. Chem. Soc.* **2013**, *135* (26), 9857-9868.
- (2) MacDonald, M. R.; Bates, J. E.; Fieser, M. E.; Ziller, J. W.; Furche, F.; Evans, W. J., Expanding Rare-Earth Oxidation State Chemistry to Molecular Complexes of Holmium(II) and Erbium(II). *J. Am. Chem. Soc.* **2012**, *134* (20), 8420-8423.
- (3) Morss, L. R., Thermochemical properties of yttrium, lanthanum, and the lanthanide elements and ions. *Chem. Rev.* **1976**, *76* (6), 827-841.
- (4) Nief, F., Non-classical divalent lanthanide complexes. *Dalton Trans.* **2010**, *39* (29), 6589-6598.

- (5) Bochkarev, M. N., Molecular compounds of “new” divalent lanthanides. *Coordination Chem. Rev.* **2004**, *248* (9), 835-851.
- (6) Meyer, G.; Wickleder, M., Handbook on the Physics and Chemistry of Rare Earths. *Elsevier Sciences Publishers, New York* **2000**, *28* (177), 53.
- (7) Palumbo, C. T.; Darago, L. E.; Windorff, C. J.; Ziller, J. W.; Evans, W. J., Trimethylsilyl versus Bis(trimethylsilyl) Substitution in Tris(cyclopentadienyl) Complexes of La, Ce, and Pr: Comparison of Structure, Magnetic Properties, and Reactivity. *Organometallics* **2018**, *37* (6), 900-905.
- (8) Hitchcock, P. B.; Lappert, M. F.; Maron, L.; Protchenko, A. V., Lanthanum Does Form Stable Molecular Compounds in the +2 Oxidation State. *Angew. Chem. Int. Ed.* **2008**, *47* (8), 1488-1491.
- (9) Jenkins, T. F.; Woen, D. H.; Mohanam, L. N.; Ziller, J. W.; Furche, F.; Evans, W. J., Tetramethylcyclopentadienyl Ligands Allow Isolation of Ln(II) Ions across the Lanthanide Series in [K(2.2.2-cryptand)][(C<sub>5</sub>Me<sub>4</sub>H)<sub>3</sub>Ln] Complexes. *Organometallics* **2018**, *37* (21), 3863-3873.
- (10) Jaroschik, F.; Momin, A.; Nief, F.; Le Goff, X.-F.; Deacon, G. B.; Junk, P. C., Dinitrogen Reduction and C-H Activation by the Divalent Organoneodymium Complex [(C<sub>5</sub>H<sub>2</sub><sup>1</sup>Bu<sub>3</sub>)<sub>2</sub>Nd(μ-D)K([18]crown-6)]. *Angew. Chem. Int. Ed.* **2009**, *48* (6), 1117-1121.
- (11) Angadol, M. A.; Woen, D. H.; Windorff, C. J.; Ziller, J. W.; Evans, W. J., tert-Butyl(cyclopentadienyl) Ligands Will Stabilize Nontraditional +2 Rare-Earth Metal Ions. *Organometallics* **2019**, *38* (5), 1151-1158.
- (12) Huh, D. N.; Ziller, J. W.; Evans, W. J., Isolation of reactive Ln(II) complexes with C<sub>5</sub>H<sub>4</sub>Me ligands (Cp<sup>Me</sup>) using inverse sandwich counteranions: synthesis and structure of [(18-crown-6)K(μ-Cp<sup>Me</sup>)K(18-crown-6)][Cp<sup>Me</sup><sub>3</sub>Ln<sup>II</sup>] (Ln = Tb, Ho). *Dalton Trans.* **2018**, *47* (48), 17285-17290.
- (13) Ryan, A. J.; Darago, L. E.; Balasubramani, S. G.; Chen, G. P.; Ziller, J. W.; Furche, F.; Long, J. R.; Evans, W. J., Synthesis, Structure, and Magnetism of Tris(amide) [Ln{N(SiMe<sub>3</sub>)<sub>2</sub>}<sub>3</sub>]<sup>1-</sup> Complexes of the Non-traditional +2 Lanthanide Ions. *Chem. Eur. J.* **2018**, *24* (30), 7702-7709.
- (14) Moehring, S. A.; Beltrán-Leiva, M. J.; Páez-Hernández, D.; Arratia-Pérez, R.; Ziller, J. W.; Evans, W. J., Rare-Earth Metal(II) Aryloxides: Structure, Synthesis, and EPR Spectroscopy of [K(2.2.2-cryptand)][Sc(OC<sub>6</sub>H<sub>2</sub><sup>4</sup>Bu<sub>2</sub>-2,6-Me-4)<sub>3</sub>]. *Chem. Eur. J.* **2018**, *24* (68), 18059-18067.
- (15) Fieser, M. E.; Palumbo, C. T.; La Pierre, H. S.; Halter, D. P.; Voora, V. K.; Ziller, J. W.; Furche, F.; Meyer, K.; Evans, W. J., Comparisons of lanthanide/actinide +2 ions in a tris(aryloxide)arene coordination environment. *Chem. Sci.* **2017**, *8* (11), 7424-7433.



- (16) Palumbo, C. T.; Halter, D. P.; Voora, V. K.; Chen, G. P.; Chan, A. K.; Fieser, M. E.; Ziller, J. W.; Hieringer, W.; Furche, F.; Meyer, K.; Evans, W. J., Metal versus Ligand Reduction in  $\text{Ln}^{3+}$  Complexes of a Mesitylene-Anchored Tris(Aryloxy) Ligand. *Inorg. Chem.* **2018**, *57* (5), 2823-2833.
- (17) Fieser, M. E.; MacDonald, M. R.; Krull, B. T.; Bates, J. E.; Ziller, J. W.; Furche, F.; Evans, W. J., Structural, Spectroscopic, and Theoretical Comparison of Traditional vs Recently Discovered  $\text{Ln}^{2+}$  Ions in the  $[\text{K}(2.2.2\text{-cryptand})][(\text{C}_5\text{H}_4\text{SiMe}_3)_3\text{Ln}]$  Complexes: The Variable Nature of  $\text{Dy}^{2+}$  and  $\text{Nd}^{2+}$ . *J. Am. Chem. Soc.* **2015**, *137* (1), 369-382.
- (18) Fieser, M. E.; Ferrier, M. G.; Su, J.; Batista, E.; Cary, S. K.; Engle, J. W.; Evans, W. J.; Lezama Pacheco, J. S.; Kozimor, S. A.; Olson, A. C.; Ryan, A. J.; Stein, B. W.; Wagner, G. L.; Woen, D. H.; Vitova, T.; Yang, P., Evaluating the electronic structure of formal  $\text{Ln}^{\text{II}}$  ions in  $\text{Ln}^{\text{II}}(\text{C}_5\text{H}_4\text{SiMe}_3)_3^{1-}$  using XANES spectroscopy and DFT calculations. *Chem. Sci.* **2017**, *8* (9), 6076-6091.
- (19) Raiser, D.; Deville, J. P., Study of XPS photoemission of some gadolinium compounds. *Journal of Electron Spectroscopy and Related Phenomena* **1991**, *57* (1), 91-97.
- (20) Callahan, W. R., Spectrum of Doubly Ionized Gadolinium\*. *J. Opt. Soc. Am.* **1963**, *53* (6), 695-700.
- (21) Glorieux, B.; Berjoan, R.; Matecki, M.; Kammouni, A.; Perarnau, D., XPS analyses of lanthanides phosphates. *Appl. Surf. Sci.* **2007**, *253* (6), 3349-3359.
- (22) Mercier, F.; Alliot, C.; Bion, L.; Thromat, N.; Toulhoat, P., XPS study of Eu(III) coordination compounds: Core levels binding energies in solid mixed-oxo-compounds  $\text{Eu}_m\text{X}_x\text{O}_y$ . *Journal of Electron Spectroscopy and Related Phenomena* **2006**, *150* (1), 21-26.
- (23) Lademan, W. J.; See, A. K.; Klebanoff, L. E.; van der Laan, G., Multiplet structure in high-resolution and spin-resolved x-ray photoemission from gadolinium. *Phys. Rev. B* **1996**, *54* (23), 17191-17198.
- (24) Campagna, M.; Wertheim, G.; Baer, Y., Unfilled inner shells: Rare earths and their compounds. In *Photoemission in Solids II*, Springer: 1979; pp 217-260.
- (25) Wachter, P.; Kamba, S.; Grioni, M., Empty 4f states in TmS. *Physica B: Condensed Matter* **1998**, *252* (3), 178-185.

## APPENDIX A

### Synthesis and Structural Characterization of $\{(C_5H_4SiMe_3)_2Ba(THF)\}_n$ and Barium-in-2.2.2-Cryptand Complexes

This Appendix describes the synthesis of Ba(II) coordination complexes using Cp' (Cp' = C<sub>5</sub>H<sub>4</sub>SiMe<sub>3</sub>) and 2.2.2-cryptand as ligands. BaI<sub>2</sub> reacts with two equivalents of KCp' in THF to form a product that crystallizes out of Et<sub>2</sub>O as the crystallographically-characterizable colorless complex  $\{Cp'_2Ba(THF)\}_n$  oligomer, Figure A.1. Although there are 38 examples of Ba(II) complexes with at least one coordinated cyclopentadienyl ligand in the literature, there are only two reported examples of oligomeric barium metallocenes.<sup>1-2</sup>

Coordination complexes of Ba(II)-in-2.2.2-cryptand were also synthesized by reacting BaX<sub>2</sub> (X = I, OTf) starting materials with crypt (2.2.2-cryptand). Both crystallized out of Et<sub>2</sub>O. The colorless complex [Ba(crypt)(DMF)<sub>2</sub>][I]<sub>2</sub> was formed by reacting BaI<sub>2</sub> with crypt in DMF and crystallographically-characterized, Figure A.2. The colorless complex [Ba(crypt)(OTf)<sub>2</sub>] was formed by reacting Ba(OTf)<sub>2</sub> with crypt in THF and crystallographically-characterized, Figure A.3. This structure was found to be isomorphous with [Ln(crypt)(OTf)<sub>2</sub>] (Ln = Nd, Sm) as described in Chapter 7. There are only 11 other examples of Ba(II)-in-crypt complexes reported in literature.<sup>3-11</sup>

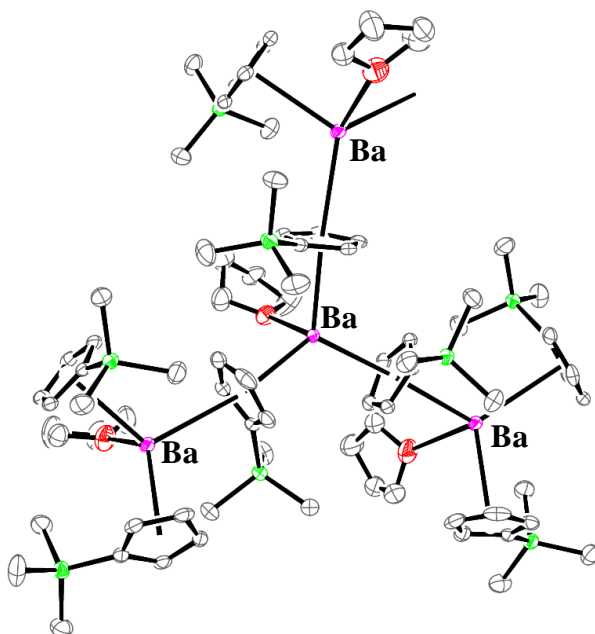


**Figure A.1.** ORTEP representation of extended structure of  $\{\text{Cp}'_2\text{Ba}(\text{THF})\}_n$ , with thermal ellipsoids drawn at the 50% probability level. Hydrogen atoms were omitted for clarity.

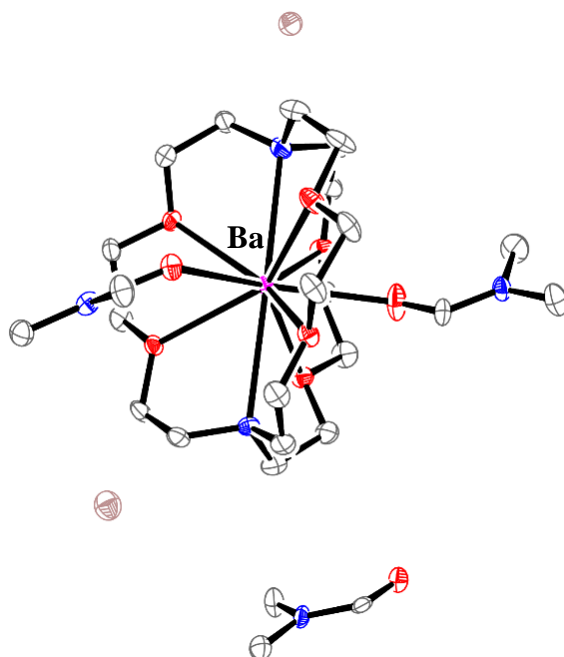


**Figure A.2.** ORTEP representation of  $[\text{Ba}(\text{crypt})(\text{DMF})_2][\text{I}]_2$ , with thermal ellipsoids drawn at the 50% probability level. Hydrogen atoms were omitted for clarity.

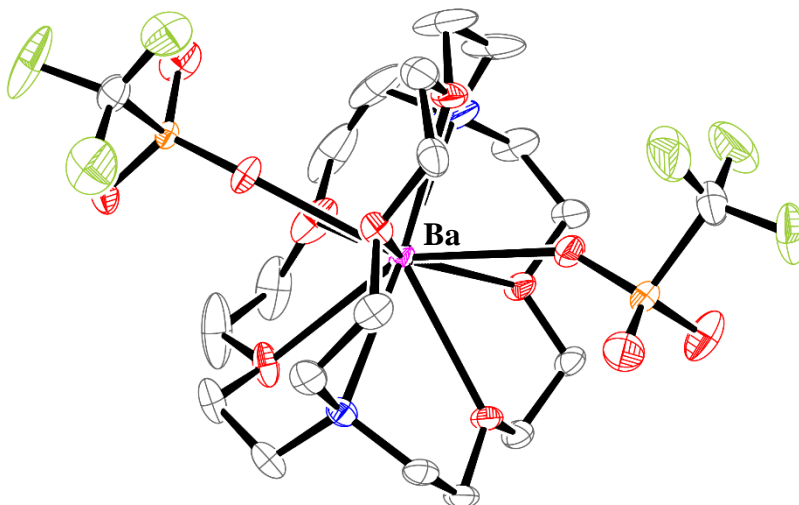


**Figure A.3.** ORTEP representation of [Ba(crypt)(OTf)<sub>2</sub>], with thermal ellipsoids drawn at the 50% probability level. Hydrogen atoms were omitted for clarity.

### Structural Details

**X-ray Data Collection, Structure Solution and Refinement for {Cp'<sub>2</sub>Ba(THF)}<sub>n</sub>.** A colorless crystal of approximate dimensions 0.102 x 0.104 x 0.199 mm was mounted in a cryoloop and transferred to a Bruker SMART APEX II diffractometer. The APEX2<sup>1</sup> program package was used to determine the unit-cell parameters and for data collection (120 sec/frame scan time for a sphere of diffraction data). The raw frame data was processed using SAINT<sup>2</sup> and SADABS<sup>3</sup> to yield the reflection data file. Subsequent calculations were carried out using the SHELXTL<sup>4</sup> program. The diffraction symmetry was *mmm* and the systematic absences were consistent with the orthorhombic space group *Pbca* that was later determined to be correct. The structure was solved by dual space methods and refined on F<sup>2</sup> by full-matrix least-squares techniques. The analytical scattering factors<sup>5</sup> for neutral atoms were used throughout the analysis. A THF molecule was modeled as a two-part disorder (1:1). Hydrogen atoms were included using a riding model. Least-squares analysis yielded wR2 = 0.0930 and Goof = 1.034

for 9424 variables refined against 359 data (0.75 Å),  $R1 = 0.0352$  for those 7293 data with  $I > 2.0\sigma(I)$ .

**X-ray Data Collection, Structure Solution and Refinement for [Ba(crypt)(DMF)<sub>2</sub>][I]<sub>2</sub>.** A colorless crystal of approximate dimensions 0.064 x 0.103 x 0.394 mm was mounted in a cryoloop transferred to a Bruker SMART APEX II diffractometer. The APEX2<sup>1</sup> program package was used to determine the unit-cell parameters and for data collection (120 sec/frame scan time for a sphere of diffraction data). The raw frame data was processed using SAINT<sup>2</sup> and SADABS<sup>3</sup> to yield the reflection data file. Subsequent calculations were carried out using the SHELXTL<sup>4</sup> program. The diffraction symmetry was  $2/m$  and the systematic absences were consistent with the monoclinic space groups  $Cc$  and  $C2/c$ . It was later determined that space group  $C2/c$  was correct. The structure was solved by dual space methods and refined on  $F^2$  by full-matrix least-squares techniques. The analytical scattering factors<sup>5</sup> for neutral atoms were used throughout the analysis.

Hydrogen atoms were included using a riding model. Least-squares analysis yielded  $wR2 = 0.1162$  and  $Goof = 1.013$  for 10501 variables refined against 581 data (0.82 Å),  $R1 = 0.0442$  for those 7396 data with  $I > 2.0\sigma(I)$ .

**X-ray Data Collection, Structure Solution and Refinement for [Ba(crypt)(OTf)<sub>2</sub>].** A colorless crystal of approximate dimensions 0.320 x 0.231 x 0.084 mm was mounted in a cryoloop and transferred to a Bruker SMART APEX II diffractometer. The APEX2<sup>1</sup> program package was used to determine the unit-cell parameters and for data collection (25 sec/frame scan time for a sphere of diffraction data). The raw frame data was processed using SAINT<sup>2</sup> and SADABS<sup>3</sup> to yield the reflection data file. Subsequent calculations were carried out using the SHELXTL<sup>4</sup> program. The diffraction symmetry was  $2/m$  and the systematic absences were

consistent with the monoclinic space group  $P2_1/c$  that was later determined to be correct. The structure was solved using the coordinates of the isomorphous samarium/neodymium complex and refined on  $F^2$  by full-matrix least-squares techniques. The analytical scattering factors<sup>5</sup> for neutral atoms were used throughout the analysis. Hydrogen atoms were located from a difference-Fourier map and refined ( $x,y,z$  and  $U_{iso}$ ) and included using a riding model. A coordinated triflate ( $CF_3SO_3$ ) was found to be disordered and modeled as a two-part disorder (1:1). Least-squares analysis yielded  $wR2 = 0.0611$  and  $Goof = 1.027$  for 7515 variables refined against 560 data ( $0.74 \text{ \AA}$ ),  $R1 = 0.0261$  for those 6726 data with  $I > 2.0\sigma(I)$ .

## References

- (1) Fichtel, K.; Hofmann, K.; Behrens, U., Polymeric and Monomeric Barocene: Synthesis and Structure of  $Ba(C_5H_5)_2 \cdot DMSO$  and  $Ba(C_5H_5)_2(18\text{-crown-6})$  (DMSO = dimethylsulfoxide). *Organometallics* **2004**, *23* (17), 4166-4168.
- (2) Harder, S.,  $[Cp_3Ba]^-$ : The First Structurally Characterized Barate Complex. *Angew. Chem. Int. Ed.* **1998**, *37* (9), 1239-1241.
- (3) Biella, S.; Gattuso, G.; Notti, A.; Metrangolo, P.; Pappalardo, S.; Parisi, M. F.; Pilati, T.; Resnati, G.; Terraneo, G., Halogen bonding-based anion coordination in calixarene/inorganic halide/diiodoperfluorocarbon assemblies. *Supramolecular Chemistry* **2009**, *21* (1-2), 149-156.
- (4) Chekhlov, A. N., *Russ. J. Inorg. Chem.* **2003**, *48*, 1808.
- (5) Chekhlov, A. N., *Russ. J. Inorg. Chem.* **2004**, *49*, 463.
- (6) Fox, D. B.; Liantonio, R.; Metrangolo, P.; Pilati, T.; Resnati, G., Perfluorocarbon-hydrocarbons self-assembly: halogen bonding mediated intermolecular recognition. *J. Fluorine Chem.* **2004**, *125* (2), 271-281.
- (7) König, T.; Eisenmann, B.; Schäfer, H., Zur Reaktion von  $BaBiSe_3$  mit dem Cryptanden [2.2.2] in Ethylendiamin Darstellung und Kristallstruktur von  $[Ba-222Crypt]Se_4 \cdot en$ . *Z. Anorg. Allg. Chem.* **1983**, *498* (3), 99-104.
- (8) Masci, B.; Thuéry, P., Complex-within-complex assemblages from  $\{M([2.2.2]cryptand)(H_2O)_2\}^{2+}$  ( $M = Sr, Ba$ ) and  $\{UO_2(p\text{-tert-butyl}[3.1.3.1]homooxalixarene - 4H)\}^{2-}$ . *Cryst. Eng. Comm.* **2006**, *8* (10), 764-772.

- (9) Metz, B.; Moras, D.; Weiss, R., Coordination des cations alcalino-terreux dans leurs complexes avec des molécules macrobicycliques. II. Structure cristalline et moléculaire du cryptate de baryum  $C_{18}H_{36}N_2O_6 \cdot Ba(SCN)_2 \cdot H_2O$ . *Acta Crystallographica Section B* **1973**, 29 (7), 1382-1387.
- (10) Wojtczak, W. A.; Hampden-Smith, M. J.; Duesler, E. N., Synthesis, Characterization, and Thermal Behavior of Polydentate Ligand Adducts of Barium Trifluoroacetate. *Inorg. Chem.* **1998**, 37 (8), 1781-1790.
- (11) Zagler, R. E., B., *Z.Naturforsch., B: Chem. Sci.* **1991**, 46, 593.

## APPENDIX B

### Synthesis of $\{\text{Cs}(\text{THF})(\text{C}_5\text{H}_4\text{SiMe}_3)_3\text{Yb}\}_n$

This Appendix describes the synthesis of the complex  $\{\text{Cs}(\text{THF})\text{Cp}'_3\text{Yb}\}_n$  ( $\text{Cp}' = \text{C}_5\text{H}_4\text{SiMe}_3$ ). A THF solution of  $\text{Cp}'_3\text{Yb}$  was reduced with a smear of Cs metal generating a green solution. The green solution was layered into  $\text{Et}_2\text{O}$  and green crystals of  $\{\text{Cs}(\text{THF})\text{Cp}'_3\text{Yb}\}_n$  were isolated after 1 d. This chelate free Yb(II) oligomer is similar to the complexes  $[\text{Cp}''\text{M}(\mu\text{-Cp}'')_2\text{Cs}(\text{THF})_2]$  ( $\text{M} = \text{La}, \text{U}$ ) where Cs coordinates to the backside of two cyclopentadienyl ligands to form a bent metallocene cesium unit,  $[\text{Cp}'_2\text{Cs}(\text{THF})]^{1-}$ , as described in Chapter 2. In this case, only one THF is coordinated to Cs. Attempts to isolate a  $\{\text{Cs}(\text{THF})\text{Cp}'_3\text{La}\}_n$  analog were unsuccessful as the dark purple solution from the reaction of  $\text{Cp}'_3\text{La}$  and Cs metal decomposed overnight at  $-35\text{ }^\circ\text{C}$ .

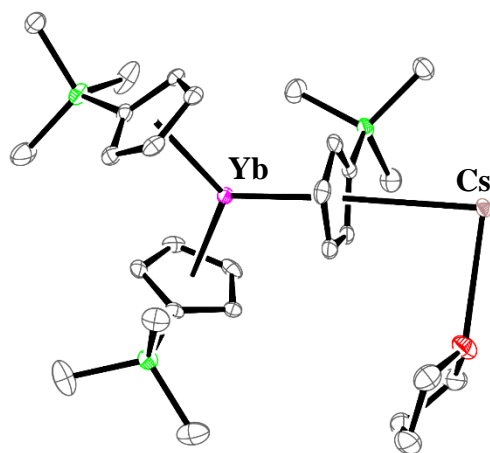


**Figure B.1.** ORTEP representation of  $\{\text{Cs}(\text{THF})\text{Cp}'_3\text{Yb}\}_n$ , with thermal ellipsoids drawn at the 50% probability level. Hydrogen atoms were omitted for clarity.



## Structural Details

### X-ray Data Collection, Structure Solution and Refinement for $\{\text{Cs}(\text{THF})\text{Cp}'_3\text{Yb}\}_n$ .

A green crystal of approximate dimensions 0.079 x 0.086 x 0.148 mm was mounted on in a cryoloop and transferred to a Bruker SMART APEX II diffractometer. The APEX2<sup>1</sup> program package was used to determine the unit-cell parameters and for data collection (90 sec/frame scan time for a sphere of diffraction data). The raw frame data was processed using SAINT<sup>2</sup> and SADABS<sup>3</sup> to yield the reflection data file. Subsequent calculations were carried out using the SHELXTL<sup>4</sup> program. The diffraction symmetry was  $2/m$  and the systematic absences were consistent with the monoclinic space group  $P2_1/n$  that was later determined to be correct. The structure was solved by dual space methods and refined on  $F^2$  by full-matrix least-squares techniques. The analytical scattering factors<sup>5</sup> for neutral atoms were used throughout the analysis. Hydrogen atoms were included using a riding model. Least-squares analysis yielded  $wR2 = 0.0562$  and  $Goof = 1.018$  for 316 variables refined against 8223 data (0.75 Å),  $R1 = 0.0315$  for those 6580 data with  $I > 2.0\sigma(I)$ .

## APPENDIX C

### Synthesis of $(C_5Me_5)_2Yb(2.2.2\text{-cryptand})$ and $[Sm_2(2.2.2\text{-cryptand})_2(\mu\text{-I})][(C_5H_4SiMe_3)_3Sm]_3$

Reaction of  $Cp^*Yb(BPh_4)$  ( $Cp^* = C_5Me_5$ ) with crypt (2.2.2-cryptand) in toluene generated a light green solution with white precipitate. The green solution was decanted from the white precipitate and layered with hexane. After 1 d, green crystals of  $Cp^*_2Yb(crypt)$  were isolated. The crystal data collected was sufficient for connectivity only, Figure C.1.

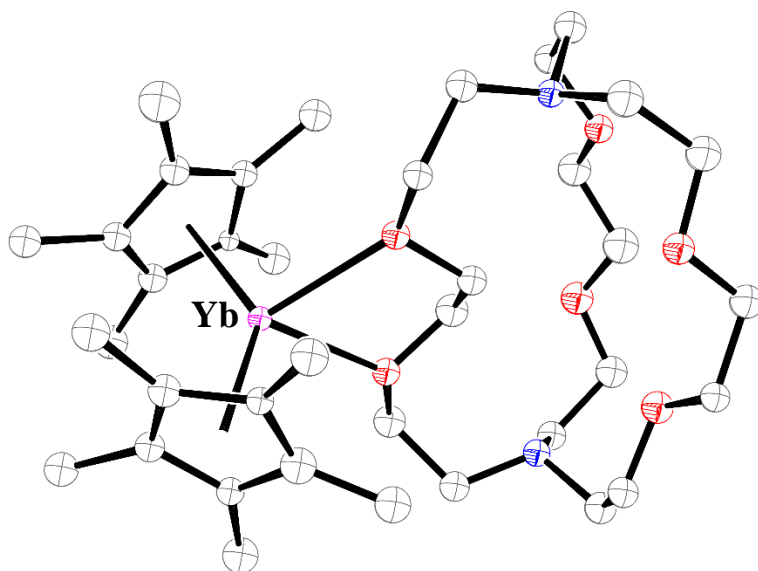


**Figure C.1.** Connectivity structure of  $Cp^*_2Yb(crypt)$  drawn at the 50% probability level. Hydrogens have been omitted for clarity.

From an attempted reaction to isolate  $[\text{Sm}(\text{crypt})(\text{THF})][\text{Cp}'_3\text{Sm}]_2$  ( $\text{Cp}' = \text{C}_5\text{H}_4\text{SiMe}$ ), previously described in Chapter 4, a crystal of  $[\text{Sm}_2(\text{crypt})_2(\mu\text{-I})][\text{Cp}'_3\text{Sm}]_3$  and structurally characterized, Figure C.2. Although the crystal data collected was sufficient for connectivity only, the structure depicts two  $[\text{Sm}(\text{crypt})]^{2+}$  bridged by an iodide with three  $[\text{Cp}'_3\text{Sm}]^{1-}$  anions. This structure shows that Ln-in-crypt complexes can bridge to each other, despite the steric bulk offered by the chelating crypt.

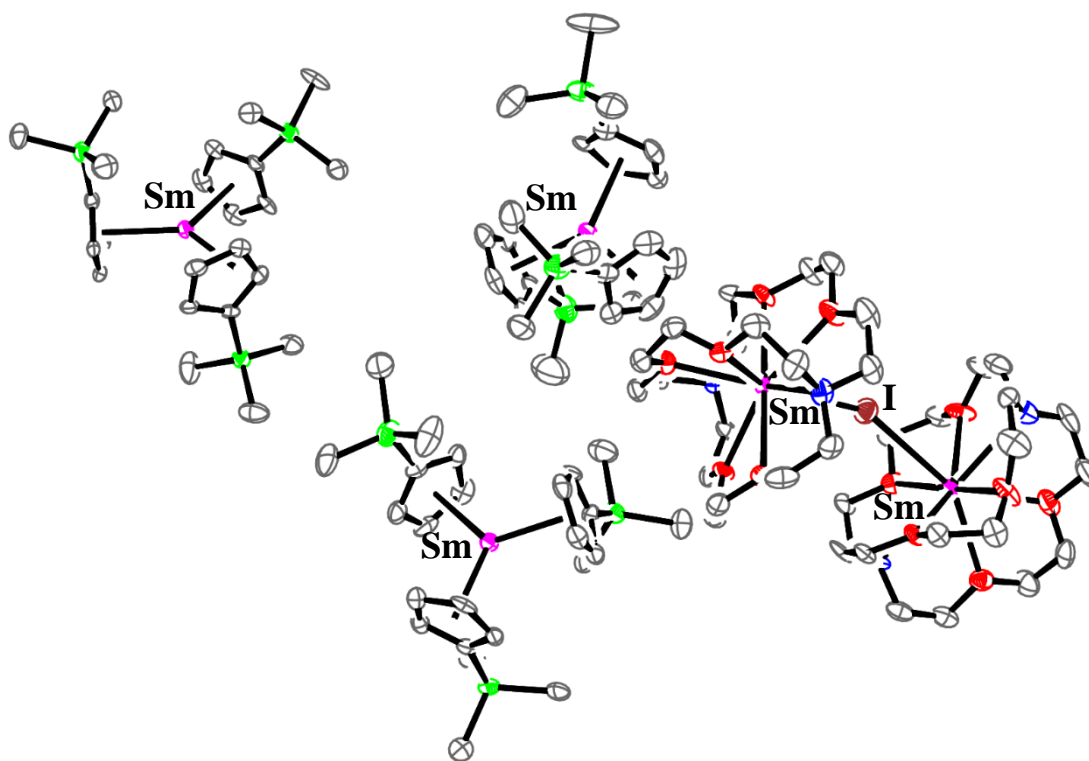


**Figure C.2.** Connectivity structure of  $[\text{Sm}_2(\text{crypt})_2(\mu\text{-I})][\text{Cp}'_3\text{Sm}]_3$  drawn at the 50% probability level. Hydrogens have been omitted for clarity.

## APPENDIX D

### Synthesis of $[\text{Cp}'_2\text{Y}(\mu\text{-OH})]_2$ and $[\text{Li}(\text{Me}_6\text{TREN})][\{\text{N}(\text{SiMe}_3)_2\}_2\text{Y}\{\text{N}(\text{SiMe}_3)_2\text{SiMe}_2\text{CH}_2\}]$

Reduction of  $\text{Cp}'_3\text{Y}$  ( $\text{Cp}' = \text{C}_5\text{H}_4\text{SiMe}_3$ ) using Li metal without the presence of a chelating agent yielded a bridging hydroxide species  $[\text{Cp}'_2\text{Y}(\mu\text{-OH})]_2$ , Figure D.1.

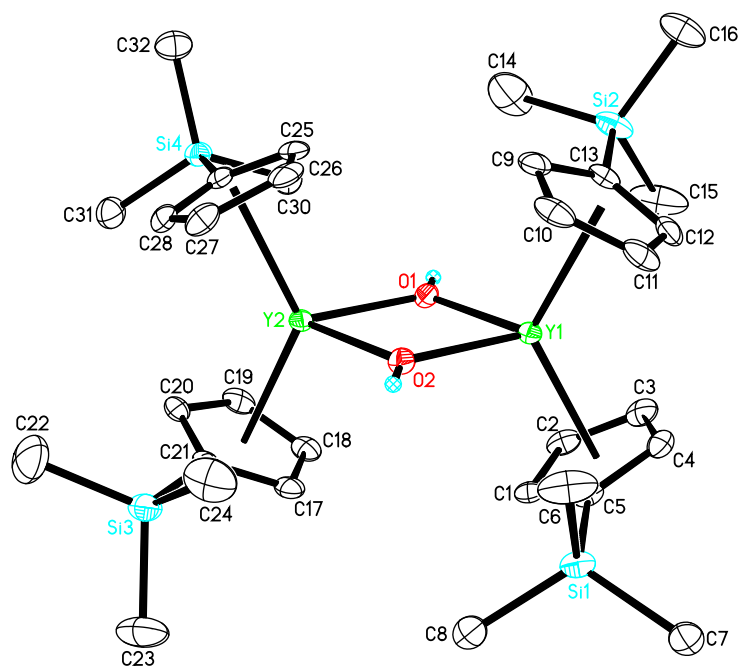


**Figure D.1.** ORTEP representation of  $[\text{Cp}'_2\text{Y}(\mu\text{-OH})]_2$ , thermal ellipsoids drawn at the 50% probability level. Hydrogen atoms, except for O–H hydrogens, were omitted for clarity.

Reduction of  $\text{YN}^*_3$  [ $\text{N}^* = \text{N}(\text{SiMe}_3)_2$ ] using Li metal in the presence of  $\text{Me}_6\text{TREN}$  chelating agent yielded the cyclometalated product  $[\text{Li}(\text{Me}_6\text{TREN})][\{\text{N}(\text{SiMe}_3)_2\}_2\text{Y}\{\text{N}(\text{SiMe}_3)_2\text{SiMe}_2\text{CH}_2\}]$ , Figure D.2.

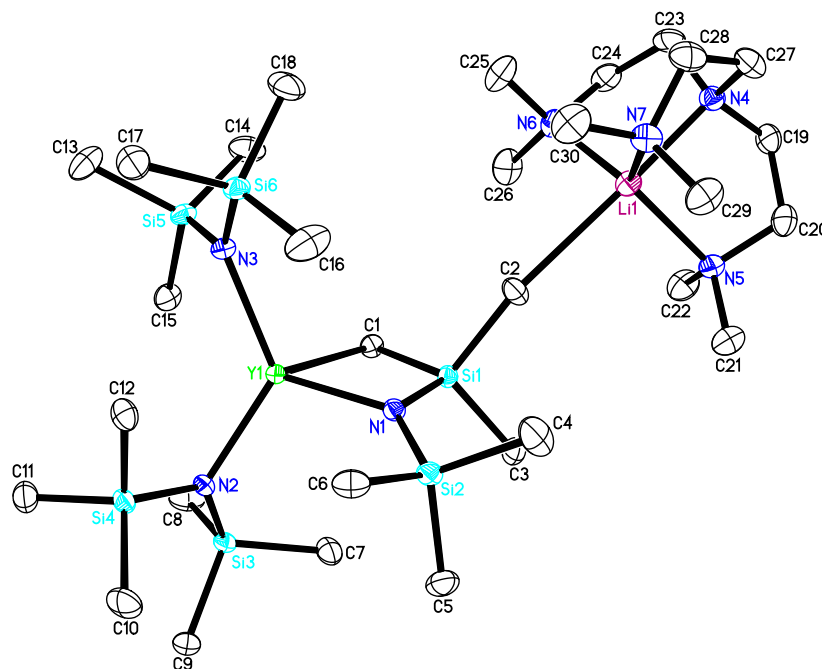


**Figure D.2.** ORTEP representation of  $[\text{Li}(\text{Me}_6\text{TREN})][\{\text{N}(\text{SiMe}_3)_2\}_2\text{Y}\{\text{N}(\text{SiMe}_3)_2\text{SiMe}_2\text{CH}_2\}]$ , thermal ellipsoids drawn at the 50% probability level. Hydrogen atoms, except for O-H hydrogens, were omitted for clarity.

## Experimental

$[\text{Cp}'_2\text{Y}(\mu\text{-OH})]_2$ . In an argon-filled glovebox, a cold ( $-35\text{ }^\circ\text{C}$ ) yellow solution of  $\text{Cp}'_3\text{Y}$  (200 mg, 0.400 mmol) in THF (3 mL) was added to a flask containing a smear of lithium metal and a dark maroon solution immediately formed. The dark purple solution became orange after 2 h. The solution was crystallized over 2 d by vapor diffusion with  $\text{Et}_2\text{O}$  produced X-ray quality colorless crystals of  $[\text{Cp}'_2\text{Y}(\mu\text{-OH})]_2$ .

## Structural Details

**X-ray Data Collection, Structure Solution and Refinement for [Cp'<sub>2</sub>Y( $\mu$ -OH)]<sub>2</sub>.** A colorless crystal of approximate dimensions 0.138 x 0.321 x 0.413 mm was mounted in a cryoloop and transferred to a Bruker SMART APEX II diffractometer. The APEX2<sup>1</sup> program package was used to determine the unit-cell parameters and for data collection (30 sec/frame scan time for a sphere of diffraction data). The raw frame data was processed using SAINT<sup>2</sup> and SADABS<sup>3</sup> to yield the reflection data file. Subsequent calculations were carried out using the SHELXTL<sup>4</sup> program. The diffraction symmetry was  $2/m$  and the systematic absences were consistent with the monoclinic space group  $P2_1/c$  that was later determined to be correct. The structure was solved by dual space methods and refined on  $F^2$  by full-matrix least-squares techniques. The analytical scattering factors<sup>5</sup> for neutral atoms were used throughout the analysis. Hydrogen atoms were included using a riding model. There were two molecules of the formula-unit present ( $Z = 8$ ). At convergence,  $wR2 = 0.0881$  and  $Goof = 1.017$  for 745 variables refined against 16921 data (0.78 Å),  $R1 = 0.0378$  for those 12992 data with  $I > 2.0\sigma(I)$ .

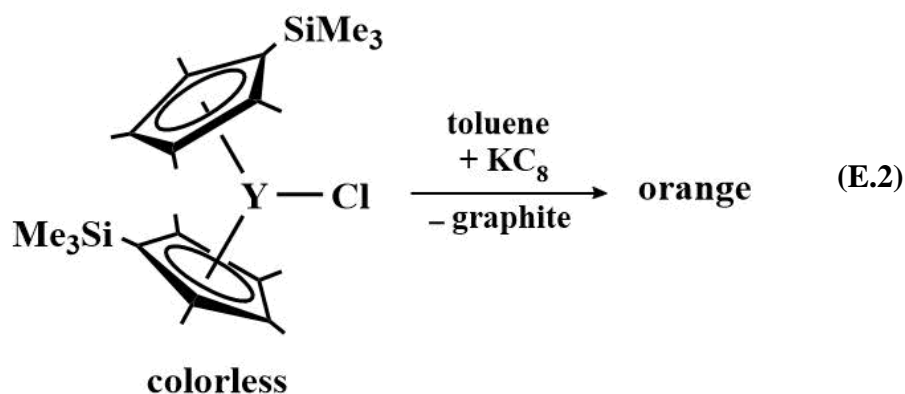
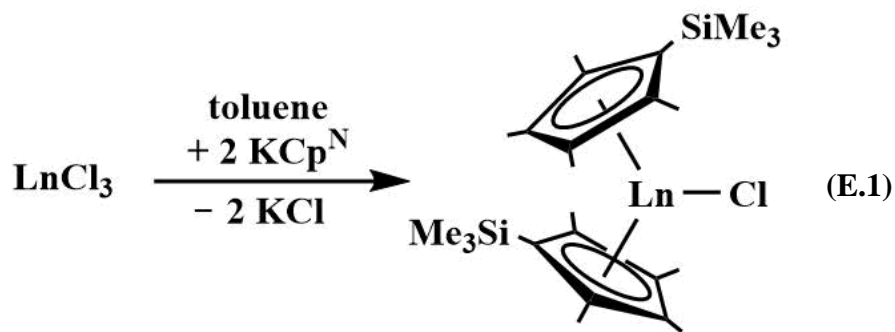
**X-ray Data Collection, Structure Solution and Refinement for [Li(Me<sub>6</sub>TREN)][{N(SiMe<sub>3</sub>)<sub>2</sub>Y{N(SiMe<sub>3</sub>)<sub>2</sub>SiMe<sub>2</sub>CH<sub>2</sub>}}].** A blue crystal of approximate dimensions 0.216 x 0.227 x 0.584 mm was mounted in a cryoloop and transferred to a Bruker SMART APEX II diffractometer. The APEX2<sup>1</sup> program package was used to determine the unit-cell parameters and for data collection (15 sec/frame scan time for a sphere of diffraction data). The raw frame data was processed using SAINT<sup>2</sup> and SADABS<sup>3</sup> to yield the reflection data file. Subsequent calculations were carried out using the SHELXTL<sup>4</sup> program. The diffraction symmetry was  $2/m$  and the systematic absences were consistent with the monoclinic space group  $P2_1/c$  that was later determined to be correct. The structure was solved by direct

methods and refined on  $F^2$  by full-matrix least-squares techniques. The analytical scattering factors<sup>5</sup> for neutral atoms were used throughout the analysis. Hydrogen atoms associated with C(1) and C(2) were located from a difference-Fourier map and refined ( $x,y,z$  and  $U_{iso}$ ). The remaining hydrogen atoms were included using a riding model. At convergence,  $wR2 = 0.0770$  and  $Goof = 1.019$  for 448 variables refined against 11841 data ( $0.75\text{\AA}$ ),  $R1 = 0.0344$  for those 9728 data with  $I > 2.0\sigma(I)$ .

## APPENDIX E

### EPR Spectroscopy of the $(C_5Me_4SiMe_3)_2YCl + KC_8$ Reduction Product

This Appendix describes the preliminary results of the reduction of  $Cp^N_2YCl$  ( $Cp^N = C_5Me_4SiMe_3$ ) using  $KC_8$  in toluene. The complex  $Cp^N_2YCl$  can be synthesized by reacting  $YCl_3$  with 2 equivalents of  $KCp^N$ , eq E.1. When a toluene solution of  $Cp^N_2YCl$  is reduced with  $KC_8$  at  $-35\text{ }^\circ\text{C}$ , an orange solution forms, eq E.2. The orange reduction product was analyzed using



EPR spectroscopy and a rhombic pattern was observed in the spectrum, Figure E.1. Generally, the spectrum has a two-line hyper fine with some rhombic features at room temperature which would be suggestive of a Y(II) in an low symmetry geometry. There are also five assignable features in the spectrum.



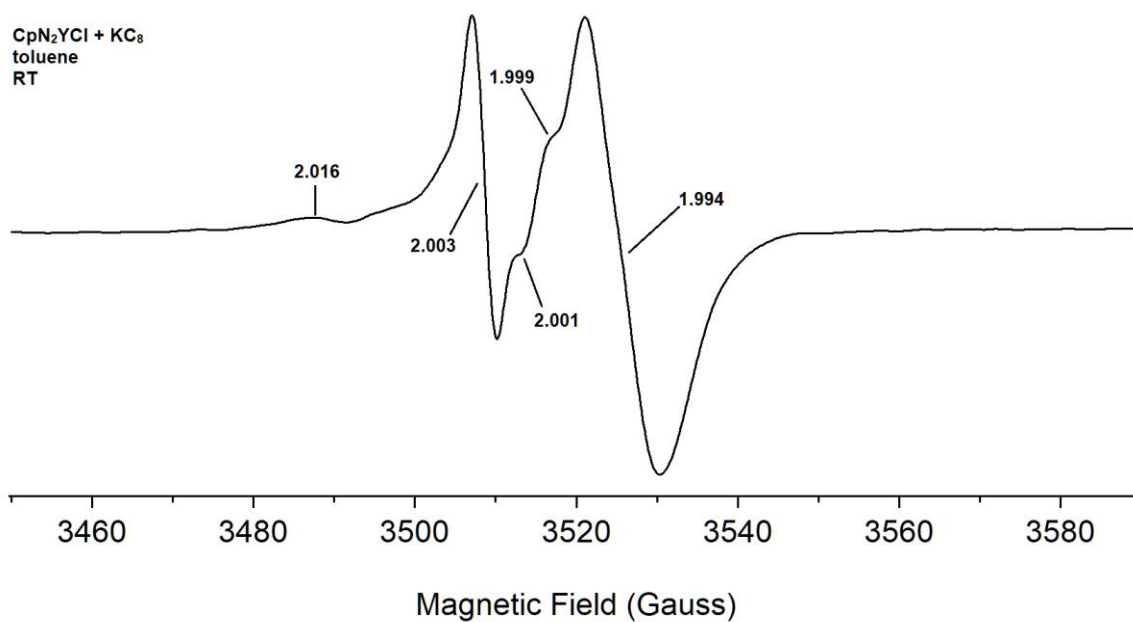


**Figure E.1.** Room temperature EPR spectrum of CpN<sub>2</sub>YCl + KC<sub>8</sub> reduction product in toluene.

## APPENDIX F

### List of Crystal Structures, Cell Parameters, and UCI X-ray Codes

DNH	Formula	<i>a</i>	<i>b</i>	<i>c</i>	$\alpha$	$\beta$	$\gamma$	Volume
1	[(Cp' <sub>2</sub> Y( <i>u</i> -OH)) <sub>2</sub> ]	13.09	23.6	25.36	90	102.14	90	7834.31
2	Li(Cp')(12-c-4)	10.45	22.93	11.81	90	101.43	90	2829.89
3	[Li(THF) <sub>4</sub> ] <sub>2</sub> [(N* <sub>3</sub> Y) <sub>2</sub> ( <i>u</i> -O)]	28.11	15.3	26.56	90	105.95	90	11423
4	[Li(Me <sub>6</sub> TREN)][N* <sub>2</sub> Y{N(TMS)SiMe <sub>2</sub> CH <sub>2</sub> }]	14.51	14.85	22.53	90	95.97	90	4854.62
5	[Li(Me <sub>6</sub> TREN)][N* <sub>2</sub> Y{N(TMS)SiMe <sub>2</sub> CH <sub>2</sub> }]	14.51	14.85	22.53	90	95.97	90	4854.62
6	YCp' <sub>3</sub> (THF)	13.07	13.35	17.16	90	90	90	2994.15
7	S <sub>8</sub>	10.87	12.86	24.49	90	90	90	3423.41
8	[Li(crypt)][TbCp' <sub>3</sub> ]	12.85	14.81	15.8	85.25	86.25	66.53	3006.87
9	[Li(crypt)][HoCp' <sub>3</sub> ]	12.81	14.62	15.72	85.34	86.68	66.63	2944.08
10	[Li(crypt)][DyCp' <sub>3</sub> ]	12.98	14.9	15.97	85.26	86.48	66.48	3088.63
11	[Li(crypt)][YCp' <sub>3</sub> ]	12.86	14.68	15.81	85.09	86.45	66.6	2984.69
12	[Li(crypt)][TbCp' <sub>4</sub> ]	13.16	14.2	16.79	101.1 8	92.06	111.89	3137.58
13	[Li(crypt)][(HoCp' <sub>3</sub> ) <sub>2</sub> ( <i>u</i> -H)]	21.34	21.34	21.34	90	90	90	9718.14
14	[YN* <sub>2</sub> (THF) <sub>2</sub> ( <i>u</i> -N <sub>2</sub> H <sub>2</sub> )	13.73	14.21	15.93	81.43	84.71	88.64	3108
15	(anthracene) <sub>2</sub>	18.6	12.1	8.5	90	102.5	90	1913.01
16	[Sm(crypt)THF][SmCp' <sub>3</sub> ] <sub>2</sub>	15.6	25.8	26.7	68.4	82.9	82.2	10746.2
evans3	[Eu(crypt)THF][EuCp' <sub>3</sub> ] <sub>2</sub>	16.6	24.18	27.71	112	94.1	104.4	11122.5
17	Sm(OH) <sub>many</sub>	12.95	13.12	15.92	77.49	71.74	88.15	2704.87
18	SmI <sub>2</sub> (THF) <sub>5</sub>	8.69	8.69	35.93	90	90	90	2713.29
20	[Sm <sub>2</sub> (crypt) <sub>2</sub> ( <i>u</i> -I)][Cp' <sub>3</sub> Sm] <sub>3</sub>	16.07	31.72	27.64	90	94.76	90	14089.2
22	[Eu(crypt)OTMS][Eu <sub>6</sub> (OH) <sub>8</sub> (O)Cp'' <sub>6</sub> ]	16.34	16.48	16.95	72.52	74.74	83.41	4564.35
23	[K(crypt)][Cp]	11.01	23.9	9.78	90	94.7	90	2564
24	[Eu(crypt)THF][EuCp' <sub>3</sub> ] <sub>2</sub>	15.64	16.64	21.9	86.4	78.3	62.3	4931.3
28	[Li(crypt)][Cp' <sub>4</sub> Y]	13.13	14.17	16.77	101.2	91.96	111.96	2820.5
29	Cp* <sub>2</sub> Yb(crypt)	26.38	9.3	31.55	90	90	90	7741
30	[Yb(crypt)][Cp' <sub>3</sub> Yb] <sub>2</sub>	15.6	25.42	23.89	90	94.89	90	9442.2
31	[K(crypt)][Cp'' <sub>2</sub> SmI]	11.06	15.73	16.61	92.33	91.04	100	2841.1
33	[Li(THF) <sub>4</sub> ][Cp'' <sub>3</sub> La]	11.48	18.87	27.56	90	92.4	90	5966
34	[U(crypt)I <sub>2</sub> ]I	11.48	26.77	12.28	90	101.2	90	3701

35	[Dy(crypt)(OTf)][OTf] <sub>2</sub>	16.81	10.89	21.46	90	108.8	90	3716.7
38	[Li(THF) <sub>4</sub> ][Cp'' <sub>3</sub> Ce]	11.44	18.91	27.5	90	92.605	90	5940.1
39	[Li(THF) <sub>4</sub> ][Cp'' <sub>3</sub> U]	11.41	18.92	27.44	90	92.568	90	5921
40	[La(crypt)Cl <sub>2</sub> ]Cl	13.83	16.25	13.16	90	106.06	90	2842.3
42	[Cs(THF) <sub>2</sub> Cp'' <sub>3</sub> La] <sub>n</sub>	12.49	16.84	12.91	90	106.76	90	2599.8
44	[Sm(crypt)(DMF) <sub>2</sub> ][BPh <sub>4</sub> ] <sub>2</sub>	11.53	13.8	21.98	85.48	84.36	89.9	3467.5
45	[Cp'' <sub>2</sub> M( <i>u</i> -I)] <sub>2</sub> M = La or U	10.72	11.52	13.29	72.77	83.26	78.93	1533.5
47	[K(crypt)][Cp <sup>Me</sup> <sub>3</sub> Dy]	10.16	28.86	13.45	90	104.3	90	3826.7
48	KCp(THF)	9.89	9.89	14.99	90	90	120	1269
49	[Cs(THF) <sub>2</sub> Cp'' <sub>3</sub> U] <sub>n</sub>	12.51	16.9	1271	90	106.10	90	2581.9
51	[(18-c-6)K( <i>u</i> -Cp <sup>Me</sup> )K(18-c-6)][Cp <sup>Me</sup> <sub>3</sub> Ho]	9.6	26.13	25.18	90	90.71	90	6316.7
52	[(18-c-6)K( <i>u</i> -Cp <sup>Me</sup> )K(18-c-6)][Cp <sup>Me</sup> <sub>3</sub> Er]	9.6	26.13	25.18	90	90.71	90	6316.7
53	[(18-c-6)K( <i>u</i> -Cp <sup>Me</sup> )K(18-c-6)][Cp <sup>Me</sup> <sub>3</sub> Tb]	9.6	26.14	25.2	90	90.77	90	6327
54	[U(crypt)I(OH <sub>2</sub> )] [BPh <sub>4</sub> ] [I]	20.14	9.63	26.98	90	107.30	90	4997
55	[K(18-c-6)][Cp <sup>Me</sup> <sub>3</sub> Gd] connectivity	14.89	12.04	17.43	90	102.26	90	3052.7
56	[H <sub>2</sub> crypt][BPh <sub>4</sub> ] <sub>2</sub>	19.47	19.47	37.47	90	90	120	12299
57	[Yb(DMF) <sub>6</sub> ][BPh <sub>4</sub> ] <sub>2</sub>	18.98	14.59	24.5	90	97.28	90	6732.7
58	[(18-c-6)K( <i>u</i> -Cp <sup>Me</sup> )K(18-c-6)][(Cp <sup>Me</sup> <sub>3</sub> Gd) <sub>2</sub> ( <i>u</i> -H)]	29.33	14.97 5	19.23 2	90	127.73	90	6681
59	[Na(crypt)][BPh <sub>4</sub> ]	17.96	19.22	22.16	90	90	90	7648.8
60	[Cs(THF)Cp' <sub>3</sub> Yb] <sub>n</sub>	9.44	16.87	21.02	90	92.07	90	3346.4
61	[Eu(crypt)(DMF) <sub>2</sub> ][I] <sub>2</sub>	8.48	36.55	10.83	90	92.34	90	3353.8
62	[Th(DMF) <sub>9</sub> ][Br] <sub>4</sub>	13.39	24.75	13.66	90	97.05	90	4465
63	[GdCl <sub>2</sub> (DMF) <sub>5</sub> ][GdCl <sub>4</sub> (DMF) <sub>2</sub> ]	8.94	15.7	16.26	63.44	82.51	77.183	1989.2
64	[Sm(crypt)(DMF) <sub>2</sub> ][BPh <sub>4</sub> ] <sub>2</sub>	11.53	13.8	21.98	85.48	84.36	89.9	3467.5
65	[K(crypt)][DyCl <sub>4</sub> (DMF) <sub>2</sub> ]	13.75	8.357	15.5	90	100.91	90	1749.2
66	[Yb(crypt)(DMF) <sub>2</sub> ] <sub>2</sub>	10.62	22.99	12.32	90	101.56	90	2954.5
67	[K(THF) <sub>5</sub> (Et <sub>2</sub> O)][ThOAr' <sub>4</sub> ]	27.65	31.52	9.6	90	90	90	8371
68	[Sm(crypt)(DMF) <sub>2</sub> ][I] <sub>2</sub>	8.48	36.55	10.83	90	92.34	90	3353.8
69	[K(18-c-6)][OAr']	31.59	13.78	14.85	90	90	90	6464.6
71	[Th(OAr') <sub>3</sub> ( <i>u</i> -OH)] <sub>2</sub>	14.76	17.33	23.59	90	91.8	90	6036
72	[Li(THF) <sub>4</sub> ][Th(OAr') <sub>4</sub> ]	20.99	19.88	39.09	90	95.36	90	16237
73	[Li(THF) <sub>4</sub> ] <sub>2</sub> {U(OAr') <sub>2</sub> ] <sub>2</sub> ( <i>u</i> -O)]	15.43	16.71	19.25	90	96.29	90	4930.2
74	[K(18-c-6)][Cp'' <sub>n</sub> ]	18.71	18.55	16.81	90	90.12	90	5836.4
75	[Nd(crypt)(DMF) <sub>2</sub> ][OTf] <sub>3</sub>	10.34	13.48	18.13	108.8	91.4	106.45	2277

76	[CoCp* <sub>2</sub> ][I]	10.42	23.02	11.62	90	90	90	2787.4
77	[Nd(DMF) <sub>8</sub> ][CoCp* <sub>2</sub> ][I] <sub>5</sub>	40.73	11.63	12.77	90	90	90	6048.7
78	[U(crypt)(OH <sub>2</sub> )(DMF)][I] <sub>3</sub>	17.76	11.3	17.8	90	111.15	90	3331.7
79	[Eu(crypt)(DMF) <sub>2</sub> ][BPh <sub>4</sub> ] <sub>2</sub>	11.54	43.81	22	85.45	84.46	89.33	3477.8
80	[K(crypt)][I][DMF]	11.15	11.61	12.05	115.3	92.43	94.67	1400.4
81	[Ba(crypt)(DMF) <sub>2</sub> ][I] <sub>2</sub>	35.71	18.21	18.04	90	104.67	90	11346.8
82	{BaCp* <sub>2</sub> (THF)} <sub>n</sub>	20.35	17.32	21.7	90	90	90	7644.5
83	[K(crypt)][Th(OAr') <sub>4</sub> ]	29.06	29.06	19.1	90	90	90	16130
86	KCp <sup>N</sup> (THF)	10.36	17.84	19.82	90	90	90	3660.3
87	[Nd(crypt)(OTf) <sub>2</sub> ]	16.89	9.88	17.96	90	92.42	90	2994
88	[U(crypt)(OH <sub>2</sub> ) <sub>2</sub> ][I] <sub>3</sub>	9.53	10.79	33.82	90	96.27	90	3458
89	[U(crypt)(MeCN)I][I] <sub>2</sub>	31.97	13.1	14.14	90	90	90	5918.8
90	[Ba(crypt)(OTf) <sub>2</sub> ]	17.14	9.76	18.29	90	92.46	90	3055.9